

10-10-83

(NASA-CR-195940) AIRBORNE
ASTRONOMY WITH A 150 MICROMETER -
500 MICROMETER HETERODYNE
SPECTROMETER Final Report, 1 Oct.
1983 - 30 Sep. 1991 (California
Univ.) 129 p

N94-34705

Unclass

G3/89 0010009

•
•••

11182
11182-1
11182-1
129P

FINAL REPORT

NASA GRANT NAG2-254

AIRBORNE ASTRONOMY WITH A 150 μ m - 500 μ m HETERODYNE SPECTROMETER

Period: October 1, 1983 through September 30, 1991

A. L. Betz, Principal Investigator

Space Sciences Laboratory, University of California, Berkeley

ABSTRACT

This report summarizes work done under NASA Grant NAG2-254 awarded to the University of California. The project goal was to build a far-infrared heterodyne spectrometer for NASA's Kuiper Airborne Observatory, and to use this instrument to observe atomic and molecular spectral lines from the interstellar medium. This goal was successfully achieved; the spectrometer is now in routine use aboard the KAO. Detections of particular note have been the 370 μ m line of neutral atomic carbon, the 158 μ m transition of ionized carbon, many of the high-J rotational lines of ^{12}CO and ^{13}CO between J=9-8 and J=22-21, the 119 μ m ground-state rotational line of OH, and the 219 μ m ground-state rotational line of H_2D^+ . All of these lines were observed at spectral resolutions exceeding 1 part in 10^6 , thereby allowing accurate line shapes and Doppler velocities to be measured.

I. Introduction

The following synopsis relies on the detailed presentations available from cited publications included here as Appendices. A list of corresponding publications is included on page 13. References to individual entries are noted in the text by a number in brackets (e.g., [1]). The text below begins with a technical review of the spectrometer and then details the specific astronomical observations accomplished with this instrument.

II. Technical Overview

Our FIR heterodyne spectrometer has the 4 basic subsystems characteristic of most heterodyne instruments: a local oscillator (LO), a mixer, an intermediate-frequency (IF) amplifier, and a multi-channel radio-frequency signal analyzer (either a filter bank or an acousto-optic spectrometer: AOS).

The LO is an optically-pumped laser [1], and the mixer is a cooled Schottky-diode in a special mount [6]. These components, together with the IF amplifier, are the critical "front-end" components of the spectrometer, and they are the only ones actually mounted on the telescope. The "back-end" components such as the filter bank are mounted in the experimenters' rack. They are non-critical in that they affect the resolution but not the sensitivity of the spectrometer. For this reason, a heterodyne spectrometer has a very

practical advantage over an incoherent instrument for high resolution spectroscopy. A heterodyne spectrometer does its spectral analysis *after* "detection" whereas a spectrometer using incoherent detection does its resolving *before* detection. In this latter case, the inevitable losses and extraneous emissions of the spectrometer reduce the signal-to-noise ratio from that obtainable with a perfect instrument. On the other hand, the coherent (heterodyne) spectrometer does have an additional but fundamental source of noise from quantum fluctuations. Realistically however, the quantum-noise level of a heterodyne receiver even at $\lambda = 100 \mu\text{m}$ is only $T_Q = 140 \text{ K}$, or about $10^{-21} \text{ W Hz}^{-1/2}$, and thus is negligible compared to the non-fundamental noise of current receivers. Perhaps the most obvious advantage of heterodyne spectroscopy is its capability for ultra-high resolution. A velocity resolution $< 1 \text{ km/s}$ can easily be achieved with a velocity-scale accuracy limited only by the knowledge of the laser and source line-frequencies.

The front-end components of our airborne spectrometer weigh 200 lbs. and have a moment of 800 ft-lbs. measured from the center of the air bearing on the KAO. The size of the laser-frame dictates the overall size of the front-end hardware. The frame is 40" L x 13.5" W x 8" H and consists of four 1-inch O.D. invar rods that separate 2 insulating granite end-plates. A 40" x 13.5" aluminum plate is attached to the top of the laser frame, and on it are positioned all the optical components of the spectrometer. The entire assembly fits halfway into the instrument cavity at the Naysmith focus position. The other half of the spectrometer protrudes beyond the position of the standard instrument flange, but is braced to the instrument cavity. The standard instrument-mounting flange is removed, of course.

The layout of the spectrometer is illustrated in Figure 1 of Appendix A (also reference [1]), which also contains other details of the instrument's configuration and operation.

III. Scientific Program

(1) FY85 Results

At the time of the instrument's observational debut in 1985, there were no high resolution spectrometers aboard the KAO that operated at wavelengths between 200 μm and 500 μm . Consequently, this unexplored spectral region was ripe for the detection of many new and important lines. Ground-based observations are for the most part impossible because of obscuration by water vapor in the Earth's atmosphere. The new instrument was successfully inaugurated during two flights in July, 1985, when the 373 μm fine structure line of atomic carbon was detected in four sources [2]. The results, presented in detail in Appendix B, allow us to derive useful estimates for the excitation and abundance of neutral carbon in dense molecular clouds. Since these first observations, the sensitivity and wavelength coverage of the instrument have been continually improved.

(2) FY86 Results

Neutral Atomic Carbon: The 373 μm Fine Structure Line

In FY86, our second year on the KAO, we continued our survey of the 810 GHz (373 μm) $^3\text{P}_2 - ^3\text{P}_1$ fine structure line of neutral atomic carbon in dense molecular clouds. Our J = 2-1 results from a year earlier indicated that neutral carbon is very abundant, as originally shown by the Caltech group from observations of the 610 μm CI J=1-0 line.

Our analysis, however, indicated that while carbon was abundant, it was probably not optically thick in the fine structure lines, since excitation temperatures between 30 and 60 K were indicated by the observed line intensity ratios. Observations of the $J = 2-1$ line in additional sources previously detected in the CI $J=1-0$ line, especially Orion, were needed to confirm the general validity of our conclusions. Three flights were scheduled for the end of the 1986 observing season for this purpose. (Earlier winter flights were not available.) The flights in September, 1986, went very well, and new data on the $J=2-1$ CI line at selected locations in M42, NGC 2024, S140, DR21, and W3 were obtained to complement our earlier results [4]. Figure 1 in Appendix D shows new $J=2-1$ spectra in 4 of the above mentioned sources. The 1986 results show a factor of 3 improvement in sensitivity over our 1985 detections. In addition a limited amount of mapping of $J=2-1$ CI distribution was done for each of the new sources. Our 1986 results on CI generally confirm our earlier analysis but with improved limits, and the updated conclusions were reported at the January, 1987, AAS meeting in Pasadena. The observations and analysis of the CI data from 1985 and 1986 formed a major part of the Ph.D. thesis dissertation of Jonas Zmuidzinas [17].

(3) FY87 Results

Singly Ionized Carbon: the 158 μm Fine Structure Line

In FY87 our work concentrated on observations of the 158 μm fine structure line of C II at the edges of dense molecular clouds. Our purpose is to study the excitation, abundance, and dynamics of gas in photodissociation regions which lie between neutral molecular clouds and the H II regions surrounding nearby O- and B-type stars. In early February 1987, we observed the C II fine structure line in M42, NGC 2024, and W3. These observations were the first to resolve the narrow C II line completely, and to open up the short wavelength ($\lambda < 200 \mu m$) part of the FIR spectrum to heterodyne spectroscopy. Our results on M42, in particular, at 0.8 km s^{-1} resolution showed that the C II emission has multiple velocity components at some positions, and noticeable changes in line shape and velocity between the BN and Trapezium regions [3]. Several C II components correlate with C^+ recombination line features observed at microwave frequencies, while others appear at known velocities of molecular material such as CO. The results, partially presented in Appendices C, I, and K, allow us to derive useful estimates for the excitation, abundance, and velocity distribution of ionized carbon that can be readily compared with similarly accurate microwave data. Following these first heterodyne observations, we have gone on to detect C II emission from more than 100 positions in over 40 sources observed.

A thorough analysis requires a detailed comparison with carbon recombination line data (when available) and isotopic CO data from microwave observations. Such a comparison can readily be made because our C II line profiles are measured at the same high spectral resolution (0.8 km s^{-1}) as the microwave data. In general we find that the C II line profiles are very similar to those of $J=1-0$ and $J=2-1$ ^{12}CO . These CO lines are usually optically thick in the clouds observed and thus only provide information on the near-side cloud boundary. The C II lines are thought to arise from photodissociation regions at these same cloud boundaries. The intensity of C II appears to correlate with the UV flux impinging on the peripheral molecular material. The C II emission is seen to peak on the cloud boundary close to the adjacent H II region whenever the geometry permits a view

perpendicular to the direction of UV illumination (e.g., NGC 7538, Cep B, S140, M17) [11]. Also for a given source, the velocities of the stronger C II line components (when there are several) agree with those of the carbon recombination lines, which in general have velocities similar to the molecular material (CO) rather than the hydrogen recombination lines. This fact is additional evidence for locating the C II in the molecular cloud/H II interface region, as expected.

An interesting phenomenon observed in a number of sources is the presence of apparent "self-reversal" in the C II line emission. As shown in Appendix I, the spectra of W49 and W51 appear to show two velocity components, when in fact some of the emission near line center has been absorbed by foreground C⁺ in the ground state. Similar "self-reversed" profiles are seen in the low-J CO lines for these sources. Other sources showing C II self-reversals are W3, NGC 2024, and to a lesser extent Mon R2 and M17. We cannot give a complete explanation here, but the general conclusion is that ionized carbon in a foreground cloud or cloud periphery exists in low density regions ($n_{\text{H}_2} < 10^3 \text{ cm}^{-3}$) where the collisional excitation rate is insufficient to maintain the population of the upper energy level in LTE. Consequently, when the velocity dispersion of the foreground material is less than that of the background emitting gas, we see absorption. We know that there is cooler foreground material in the sources mentioned from microwave data on CO and H₂CO.

The absorption centers of self-reversed lines are frequently optically thick. This fact is self-evident from the absorption depths. For W51, the minimum optical depth of C II in absorption is ~ 2.0 , and the maximum excitation temperature of the absorbing foreground gas is 29 K. The gas kinetic temperature is higher, and our preliminary calculations indicate that in the absorbing cloud $T_{\text{kin}} > 40 \text{ K}$, if $n_{\text{H}_2} < 500 \text{ cm}^{-3}$. In W51 the pathlength through the absorbing foreground cloud is ~ 2 parsecs, given the C II column density of 10^{18} cm^{-2} we calculate from the integrated strength of the absorption. In such diffuse regions, C II line radiation is thought to be the dominant cooling mechanism; however, when the line is optically thick, then the cloud temperature must rise and CO emission becomes more significant.

The fact that all C II sources do not show self-reversals indicates that morphological effects must be taken into consideration. For example, if there is a sufficient velocity gradient (1 linewidth) between the background C II emitter and the foreground gas, then no absorption can occur. Note that the sources for which self-absorption is seen generally have relatively wide emission lines $> 10 \text{ km s}^{-1}$, which makes a larger "quasi-continuum" available for subsequent absorption. In front- and side-UV-illuminated sources we don't see much evidence for self-absorption; whereas in the interior- or back-illuminated sources we see absorption just like that seen in $J=1-0 \text{ }^{12}\text{CO}$. The profiles of the C II lines generally follow those of CO; however, from the ^{12}C II emission profiles alone we cannot conclude with certainty whether C II is itself optically thick like CO. Other fine structure lines, such as those from neutral oxygen, need to be observed at similarly high spectral resolution before we can make definitive statements on the relative importance of various cooling processes in photodissociation regions.

(4) FY88 Results

Shock-excited CO: the 153 μ m J=17-16 Line

In January 1988, we observed the 153 μ m (1956.018 GHz) J=17–16 transition of ^{12}CO at 5 positions in the IRc2 region of the Orion molecular cloud. The results, shown as Figure 2 of Appendix E, are the first spectra of a far-infrared CO line taken with sufficient resolution to not only show the lineshape, but also to provide an accurately calibrated Doppler velocity scale. The far-infrared CO lines can now be compared directly with millimeter and submillimeter CO data taken at similarly high resolution of $<1 \text{ km s}^{-1}$. A full account of the work has now been published [5] and is reproduced here as Appendix E. We'll just summarize the two principal conclusions here.

At 0.8 km s^{-1} resolution we can distinguish 2 velocity components in the spectra: a broad component with FWHM $\sim 30 \text{ km s}^{-1}$ which is very similar to the plateau component seen in millimeter-wave lines, plus a second narrower component with FWHM $< 10 \text{ km s}^{-1}$ that seems dynamically and spatially characteristic of the quiescent molecular cloud. The narrow component is strongest at the Trapezium and suggests that UV-heating may provide some of the excitation for high-J CO emission. The existence of such hot quiescent gas is quite interesting, and heretofore unknown. We also see weak narrow line emission (2 km s^{-1} (FWHM)) of this kind in our CO J=17–16 spectra of AFGL 490. Appendix J is another reference to this work that we presented at the International Conference on Millimeter and Submillimeter-wave Astronomy, held in Kona, HI [10]. Figure 2 of this latter paper shows a comparison of the peak brightness temperatures of CO emission in the plateau component measured with heterodyne instruments all the way up to J = 17-16. A single-component fit to the data indicates that essentially all of the CO plateau emission can be characterized by an excitation temperature of $180 \pm 50 \text{ K}$ over this range of J-values. The question remains, however, whether even higher-J CO emission seen in Orion has a plateau component which can be similarly represented, and whether it is dynamically related to the low-J emission. In addition, we need to understand the significance of the narrow component CO emission we see in Orion.

During the CO observations we also made a brief search for shock-excited emission from H_2O . The $9_{54} - 8_{63}$ line of H_2O at 1969.223 GHz was searched for in Orion without success. This transition, predicted to be a very weak maser in the calculations of Neufeld and Melnick in 1987, was nevertheless close enough to the CO J=17-16 line that we could do it at the same time. The failure to detect it places no strong constraints on either the abundance or excitation of H_2O .

(5) FY89 Results

(A) Shock-Excited CO: the 119 μ m J = 22-21 Line

In January 1989 we observed the J=22-21 line of ^{12}CO at 2528 GHz (118.8 μ m) with our heterodyne spectrometer. The spectra obtained on the IRc2 region of Orion are the highest frequency heterodyne data obtained so far on the KAO. The high 0.6 km s^{-1} resolution of the spectra allow us to resolve the line clearly. We distinguish 2 velocity components in the high-J CO emission: a broad component with a 35 km s^{-1} line width (FWHM), and a narrow component with an 8 km s^{-1} width (FWHM).

The 2 components can be unambiguously associated with those seen at millimeter wavelengths - the wide one with the outflow gas from IRc2 and the narrow with the

quiescent molecular cloud. These results are the first to demonstrate that the high-J infrared emission of CO comes from the same kinematic components of gas as the low-J emission, which is thought to arise principally from much cooler material.

By comparing these observations with data on lower-J transitions, including the J=17-16 line which we observed at similarly high resolution in KAO observations of January 1988, we see that the J=22-21 emission comes from the shock-heated interface between the outflowing and quiescent gas components. While this effect has been predicted by magnetohydrodynamic models of interstellar shocks, the new data provide the only direct evidence for the predicted heating of quiescent gas to temperatures near 600 K just before it is swept into the stream of outflowing gas. A reprint of the Ap. J. Letters publication [7] describing this work is included as Appendix G.

(B) OH Fundamental Line at 119 μ m in the Orion-IRc2 Region

On our second flight in January 1989 we observed the 2514 GHz (119.2 μ m) line of OH at 0.6 km s⁻¹ resolution in the same region of Orion. From observations at the IRc2, H₂ peak-1 and H₂ peak-2 positions, we find the emission to be quite compact, with a size <25". The relatively small size means that the OH emission, although associated with the outflow from IRc2, is not primarily produced in the gas immediately behind the shock-front interface, which has a ~60" diameter. Most theoretical models of the shock region associate both the far-infrared OH and high-J CO emission with the shock-front. However, we see now that only the CO emission is sufficiently extended for this association to be valid.

Another interesting aspect of the OH emission at the IRc2 position is that apparently the entire blue-shifted half of the emission line profile for this ground-state OH transition is absorbed by less excited foreground gas. An additional sharp absorber is present at 5.5 km s⁻¹ VLSR, the characteristic velocity of the "hot core" source. This is the first time the "hot core" has been seen in absorption, and naturally implies that a significant part of the "hot core" lies in the foreground of a more compact OH emission region, and in fact in front of the dust responsible for the FIR continuum. Our analysis places most of the OH emitting region within 5" of IRc2, and most of the absorbing gas more than 5 times further away.

The "self-absorption" of half the 119 μ m line intensity explains an apparent discrepancy noticed between the relative intensities of the fundamental and various excited-state lines: namely, that the OH 163 μ m/119 μ m integrated intensity ratio was more than a factor of 2 larger than allowed even by gas at infinite temperature. Now we see that is not the case, and something near LTE likely prevails. Here again high resolution makes a big difference to the interpretation of data; new phenomena are visible when you have the ability to see them. A full account of the observations and analysis may be found in reference [8], reproduced here as Appendix H.

(C) ¹²CO and ¹³CO J=9-8 Observations

In August 1989 we observed the ¹²CO and ¹³CO J=9-8 lines (at 1037 and 991 GHz, respectively) in a variety of galactic molecular clouds that have been extensively studied in lower-J transitions. The purpose of these 300 μ m CO observations was to look for high excitation, probably low optical depth, gas that would not be evident in the low-J data. Any such gas would be a likely indicator of UV-excitation from embedded young

stars. What we found was something quite different - averaged over our 1.4' beam much of the emission in the J=9-8 transitions of ^{12}CO and ^{13}CO appears to originate in the dense regions of the molecular cloud with the same moderate excitation temperatures ($T_{\text{ex}} \sim 50$ K) seen in the low-J ($J \leq 3$) CO lines.

Our ^{13}CO observations are the first detections of this line in any source, and the first detection of a resolved ^{13}CO line above J=2-1. With J=9-8 data from both the ^{12}CO and ^{13}CO isotopic species taken under identical conditions, we are able to deduce the optical depth of the ^{12}CO J=9-8 line independently of the excitation conditions. We find the latter line to be significantly optically thick in most of the sources observed. This result is a somewhat surprising given the relatively low line intensities that were observed: $T_{\text{a}}^* \sim 10-20$ K. The gas must be either cold, significantly clumped, or more likely both.

A non-LTE analysis (including line opacity effects) of the ^{12}CO and ^{13}CO J=9-8 data in the context of previous observations of lower-J lines suggests that much of the high-J CO emission arises from the bulk of the molecular cloud material. However, most of the emitting region is clumped, with beam filling factors < 1 for the high density gas producing the ^{13}CO emission. Although some additional emission from warmer gas near 100 K is also evident in the ^{12}CO data, it is optically thin and very beam diluted. It is interesting to note that in some sources the J=9-8 lines of ^{12}CO and ^{13}CO are probably produced under quite different physical conditions, as a consequence of the high densities or radiation levels required to maintain level populations at high-J. In the J=9-8 ^{12}CO line we do not see the intense extended emission reported by other observers for the J=7-6 ^{12}CO line. More details on the J=9-8 results are to be found in reference [13] included here as Appendix M.

(D) C II Data Analysis

In January 1988 we completed our initial survey of 158 μm C II line emission in 22 galactic molecular clouds. C II was detected from 40 positions in 17 sources, and the line profiles observed at 0.8 km s^{-1} resolution were compared with available CO J=2-1 and 1-0 data. The results on the dynamics of photodissociated gas have been divided into three categories, which are being analyzed separately. The first, on C II emission from side-illuminated molecular clouds, has been completed [11], and is included here as Appendix K. The reprint of the second manuscript [9], on sources which show "self-reversed" C II line profiles, is included here as Appendix I.

(6) FY90 Results

(A) C II in the Large Magellanic Cloud

In May, 1990, we participated in the FY90 Southern Skies Expedition of the KAO. The primary goal of our successful 2-flight series was to observe the 158 μm C II fine structure line near a number of identifiable H II regions in the LMC, and to correlate any observed emission with low-J CO emission available from ground-based observations. Because we are interested in dynamical as well as intensity correlations, the high spectral resolution of the infrared heterodyne receiver, comparable to that of a millimeter wave receiver, is essential.

The LMC is known to have a low metallicity relative to the Galaxy. Therefore, the UV flux from newly formed stars can penetrate far deeper into molecular clouds before being attenuated by dust. The previously observed low intensity of millimeter-wave CO

radiation from the LMC has been attributed both to the relatively low abundance of C and O, and also to the enhanced photodestruction of unshielded CO by UV radiation. Conversely, the C II radiation could be expected to be relatively more intense because of the greater penetration depth of ionizing radiation, and hence, the column density of C II should be higher around a hot star in the LMC than in our galaxy.

Our observations showed that the C II emitting regions are widespread in the LMC, as would be expected from the relative paucity of dust, and that the intensity of radiation in a given region is comparable to (or slightly less than) that which would be observed from a Galactic giant molecular cloud at the same distance [14]. This comparison suggests that C^+ is either colder or less abundant in the LMC than in our own galaxy, on average; or that C II is marginally optically thick or partially self-absorbed, in contrast to current predictions of photodissociation regions. The spectra illustrated in Figure 2 of Appendix N show examples of our C II results from the 30 Doradus region, one of numerous positions we observed in the LMC. Here C II emission is strong at the positions of the two far-infrared continuum peaks that straddle the central excitation source R136. CO emission from these regions of UV-heated dust is relatively weak. However, no C II emission was detected at the locations which show the strongest CO millimeter emission in several LMC molecular cloud regions, in contrast to the usual case in our own Galaxy. The anticorrelation provides direct evidence for the hypothesis that UV-photodestruction of CO is the major reason why CO lines are weak in the LMC. The anticorrelation does not support a current model of CO radiation from galaxies which argues that most CO emission, even from low-J lines, arises from the warm gas around photodissociation regions. In the case of the LMC, the low dust abundance appears to be the most significant determinant of both CO and C II radiation. This conclusion could be tested with future observations of C II and CO in the SMC, a companion galaxy with even lower metallicity.

(B) C II in G333.6-0.2

The other major C II source observed during the Southern Hemisphere deployment was the immense RCW 106 complex, which includes the giant H II region G333.6-0.2, which is the most intense C II and H_2 source in the sky. A total of 11 positions in RCW 106 were observed to provide an overall assessment of the correlation of C II and molecular gas dynamics and excitation. The relatively large line width of the emission makes self-absorption from less excited foreground material readily apparent. Similar self-absorption is seen in just about all the wide-line ($>15 \text{ km s}^{-1}$ FWHM) sources we have observed so far in the galaxy. The ability of the spectrometer to resolve line profiles allows us to detect absorption components of significant column density (and optical depth) that would otherwise be missed. There are interesting changes in line shapes with position, presumably because of "self-absorption" effects at the $1'$ offset position. The complex spectra observed at various positions will take some time to analyze fully, but a manuscript detailing the initial results is currently in preparation. It also includes data taken in subsequent years on the J=9-8, 12-11, and 14-13 transitions of CO.

(C) Guest Investigator Flights

During FY90 two flights were scheduled for guest investigators. Because of the aircraft delays of March 1990 both flights were carried-over to FY91. Problems with the aircraft cavity-wall in Oct., 1990, and with the OSM (chopper) mechanism in Dec., 1990

caused further delays. One flight for J. Keene was finally flown successfully in Dec., 1990, and one for G. Melnick was completed successfully in late Feb., 1991.

(7) FY91 Results

During FY91 the spectrometer was flown in four flight series: 1 G.I. flight in February, 1991 and 1 5-hr flight for us, 3 flights in March 1991 in NZ, 2 flights and 1 G.I. flight in August 1991, and 3 G.I. flights in Oct. 91.

(A) Detection of the H_2D^+ fundamental at 1370 GHz

The molecular ion H_3^+ is perhaps the most critical component in ion-molecule theories of interstellar chemistry. Its pivotal role is to initiate the formation of most molecular ions which in turn produce the more complicated neutral species. Unfortunately the observation of H_3^+ is hampered in dense molecular clouds because the ion has no permanent dipole moment and hence no allowed dipole transitions. The deuterated variant, H_2D^+ , however, does have a moment of 0.6 D and permitted transitions. H_2D^+ also has a special chemical significance, because it is thought to be the source of the enhanced deuterium fractionation of molecules seen in cold clouds.

In Dec., 1990, and February, 1991, we searched for the $1_{01} - 0_{00}$ rotational transition of H_2D^+ at 1370 GHz (219 μ m) in several galactic molecular clouds. Since this para-species transition is linked to the ground state, H_2D^+ could be detected in absorption against strong continuum sources as well as in emission from gas with densities near the $\sim 2 \times 10^8 \text{ cm}^{-3}$ required to thermalize the $J=1$ rotational level. H_2D^+ could exist in such dense regions, as its formation is thought to be a product of cosmic ray ionization of molecular hydrogen followed by a proton exchange reaction.

The results on M42/IRc2 are shown in Figure 1 of Appendix P, which is a reprint of the Ap. J. (Letters) publication [16]. The absorption line is a 7- σ detection, centered at a V_{LSR} of $3.8 \pm 1.3 \text{ km s}^{-1}$. If we interpret it as the 1370 GHz $1_{01} - 0_{00}$ transition of para- H_2D^+ , then the velocity is close to the 5 km s^{-1} V_{LSR} of the "hot core" source near and in front of IRc2. The linewidth (FWHM) of $17 \pm 3.5 \text{ km s}^{-1}$ is also similar to the 10-15 km s^{-1} values noted for the "hot core". We have already seen OH at 119 μ m in absorption against the continuum of IRc2 at a similar velocity [8].

From the measured linewidth and the line center optical depth of 0.19, we calculate the column density of ground-state H_2D^+ to be $2.3 \times 10^{13} \text{ cm}^{-2}$. This relatively large column density compared to the expected abundance of H_3^+ , given the cosmic D/H ratio, suggests significant enhancement of H_2D^+ . Since chemical fractionation processes for deuterium enhancement in molecules are effective only in cold ($T < 30 \text{ K}$) gas, it may be that H_2D^+ results from cold mantle material ablated from grains by the hot wind from IRc2. Such an argument has been put forward by other observers to explain the high abundance of deuterated molecules in the IRc2 "hot core".

We also searched unsuccessfully for H_2D^+ in NGC 2264, a comparatively cold source for which Phillips and coworkers in 1985 reported the detection of a weak line at 372 GHz, the frequency of the lowest ortho-species transition of H_2D^+ . Subsequently, more sensitive observations of the 372 GHz transition by van Dishoeck and coworkers in 1992 from the CSO and Pagani, Wannier, and Frerking in 1992 from the KAO have failed to confirm the initial tentative detection of the 372 GHz line. Consequently, our

detection of a 1370 GHz absorption line in M42/IRc2 is now the only viable candidate for H_2D^+ in the interstellar medium. Given the difficulty of detecting the higher excitation 372 GHz line (because proton exchange likely keeps the ortho- and para-species energetically coupled), the next best way of "confirming" our line is to look for similar absorptions in the spectra of other strong continuum sources embedded in dense molecular clouds.

(B) Search for the H_3O^+ Fundamental at 984 GHz

A search for the 984 GHz transition of the hydronium ion, H_3O^+ , was finally completed in a carry-over flight in Dec., 1990. The Orion/IRc2 region and W3 were the principal sources observed. Emission from the IRc2 region had earlier been reported from the the lowest lying para-state transition at 307 GHz and more recently from the next highest para-transition at 364 GHz. In our observations no emission from the ortho-state fundamental at 984 GHz was detected, with an upper limit to the integrated intensity of $\sim 1 \times 10^{-5}$ ergs cm^{-2} s^{-1} sr^{-1} (assuming a 10 km s^{-1} linewidth as seen in the other transitions). Considering the fact that the H_3O^+ line is near a strong atmospheric water vapor line, this is a good limit for a line at 984 GHz with state-of-the-art receiver noise temperatures of 8000 K (SSB). The significance of our non-detection is now being evaluated in light of some very recent measurements on the spatial distribution of the higher excitation lines done by Caltech investigators at the CSO. Although the non-detection of the 984 GHz line might help constrain the density in the H_3O^+ line formation region, any limit must be relaxed because of the uncertain effects of beam dilution for this particular transition. As a guide, recent observations of the 307 GHz and 364 GHz lines show that the emission is confined to a $\sim 20''$ region, whereas the KAO beam at 984 GHz is closer to $80''$ (FWHM).

(C) CO J=9-8 Line Radiation in Southern Sources

In March, 1991, we participated in the Southern Skies Expedition of the Kuiper Observatory to Christchurch, New Zealand. The primary goal of our flight program was to observe the J=9-8 rotational line of ^{12}CO and ^{13}CO in the Large Magellanic Cloud and selected high density molecular clouds observable only from the Southern Hemisphere. The high spectral resolution of our infrared heterodyne spectrometer is comparable to that of the millimeter-wave line receivers, which allows us to make specific comparisons with lower-J CO line profiles.

The LMC is known to have a low metallicity relative to the galaxy, and therefore the ultraviolet flux from newly formed stars can penetrate far deeper before being attenuated by dust than is the case in our own galaxy. The previously observed low intensity of CO radiation from the LMC has been attributed both to the relatively lower abundance of C and O, and also to the enhanced photodestruction of this molecule by UV radiation. Our upper limit to the J=9-8 intensity in N159 in the LMC shows that the beamfilling factor of dense molecular gas is much less than that in equivalent clouds in our own galaxy, consistent with this scenario. The J=9-8 CO observations of the LMC were analyzed and published with the C II work from the year previous [14] (see Appendix N).

Our observations of the J=9-8 lines of ^{12}CO and ^{13}CO were more fruitful in the dense clouds G333.6-0.2, RCW 57, M42, and NGC 2024. We find the ^{12}CO line to be significantly optically thick in all the detected sources. In G333.6-0.2 it's at least a τ of

10, if the $^{12}\text{C}/^{13}\text{C}$ isotopic ratio is ≥ 30 . A similar result was seen previously in the Northern Hemisphere sources W3, M17, DR 21, and W51 [13]. Note that only a modest detection of the ^{13}CO line is needed to establish the ^{12}CO optical depth. The ^{13}CO J=9-8 line is more difficult to detect than some of the higher-J ^{13}CO lines, because it falls in the wing of a strong atmospheric water line where the transmission is at best only 50%.

The relatively high ^{12}CO optical depth may seem somewhat surprising, given the relatively low line intensities that were observed: $T_{\text{A}}^* \sim 10\text{--}20$ K. The gas must be either cold, significantly clumped, or more likely both. A full analysis of the Southern CO data is now in progress in concert with subsequent observations off higher J. The main import seems evident already: when averaged over our $1.4'$ beam, much of the emission in the J=9-8 transitions of ^{12}CO and ^{13}CO appears to originate in the dense regions of the clouds with the same moderate excitation temperatures ($T_{\text{ex}} \sim 50$ K) seen in the low-J transitions. Although the J=9-8 data suggest that up to $\sim 20\%$ of the observed emission may originate in hotter material, there is no strong evidence for large scale distributions of hot gas ($T > 200$ K) from observations of CO lines at wavelengths $> 280 \mu\text{m}$. This conclusion is at variance with the interpretation of the ^{12}CO J=7-6 line observed by other investigators, who suggested that the J=7-6 line is an adequate indicator for the PDR component. To unambiguously detect the hotter gas thought to be a significant component of photodissociation regions, we must re-observe these sources in CO lines with $J \geq 11$. That is what we did in subsequent observations of some Northern Hemisphere clouds in August, 1991 (see following section).

(D) CO 12-11 and CO 14-13 Line Radiation

In August, 1991, we observed the J=12-11 and J=14-13 rotational lines of ^{12}CO in W3, M17, W51, DR 21, and W49. We had previously observed the ^{12}CO J=9-8 line in all these sources and the ^{13}CO J=9-8 line in all but W49 [13]. The linewidths of the J=12-11 and J=14-13 lines are typical of those seen in lower-J observations, and identify the emission as emanating from gas which is not likely shock excited, and therefore presumably the photodissociation component. For W51 our J=14-13 and J=12-11 spectra showed similarly narrow lines, about 10 km s^{-1} (FWHM). No evidence was seen for a broad component of 70 km s^{-1} linewidth in W51 IRS 2 or 90 km s^{-1} linewidth in W51 Main, as reported by Jaffe and others in 1987 from Fabry-Perot observations of the J=16-15 transition. The discrepancy is significant, because of the inference of shock activity that broad profiles suggest.

For the 5 sources we observe, the (J=14-13)/(J=12-11) line intensity ratios indicate excitation temperatures ≥ 150 K. The lower limit applies to LTE excitation, which is most likely not the case for high-J CO in these sources. Detailed statistical equilibrium calculations are in progress to define the excitation temperature and density of the gas more accurately. Regardless, the temperatures indicated are consistent with the values of 200-300 K predicted for the PDR component by Tielens & Hollenbach in 1985. It would be very helpful to have additional data on the weaker ^{13}CO lines in order to estimate column densities of hot gas and to pin down the ^{12}CO optical depths. Supporting observations of this type were planned for FY92 so that sufficient constraints will be in place to make a definitive interpretation of the data.

(E) Guest Investigator's Flights

There were four guest investigator flights flown in FY91, and all four flights were successful. The first was flown in August, 1991 for J. Keene and collaborators during which the 158 μm fine structure line of ionized carbon was mapped across a number of ionization fronts in selected galactic molecular clouds. In October, 1992, three more flights of a similar nature were flown for Dr. Keene, and enough C II data were collected to keep her team busy for a while.

IV. Status and Conclusions

Although a great deal of information has been gathered on the abundance, excitation, and dynamics of atomic and molecular material in interstellar molecular clouds, the capabilities of the spectrometer have by no means been exhausted. Since FY91 we have continued to work on the project at the University of Colorado, Boulder, under NASA Grant NAG2-753. New enhancements to the sensitivity and wavelength coverage of the instrument continue to be made so that it remains at the forefront of high resolution far-infrared spectroscopy. The success of our KAO flight program has been aided by the considerable efforts of the technical staff at NASA Ames Research Center, and we are grateful for their help in this program.

Publications from NAG2-254

1. "A 150 μm to 500 μm Heterodyne Spectrometer for Airborne Astronomy", A. L. Betz and J. Zmuidzinas, *Proceedings of the Airborne Astronomy Symposium*, 11-13 July 1984, pp. 320-329, (NASA Conf. Publ. 2353).
2. "Observations of Neutral Atomic Carbon at 809 GHz", J. Zmuidzinas, A. L. Betz, and D. M. Goldhaber, *Ap. J. (Letters)*, **307**, L75-L79 (1986).
3. "Heterodyne Spectroscopy of the 158 μm C II Line in M42", R. T. Boreiko, A. L. Betz, and J. Zmuidzinas, *Ap. J. (Letters)*, **325**, L47-L51 (1988).
4. "Neutral Atomic Carbon in Dense Molecular Clouds", J. Zmuidzinas, A. L. Betz, R. T. Boreiko, and D. M. Goldhaber. *Ap. J.*, **335**, 774-785 (1988).
5. "Heterodyne Spectroscopy of the J=17-16 CO line in Orion", R. T. Boreiko, A. L. Betz, and J. Zmuidzinas, *Ap. J.*, **337**, 332-341 (1989).
6. "A Corner Reflector Mixer Mount for Far Infrared Wavelengths", J. Zmuidzinas, A. L. Betz, and R. T. Boreiko. *Infrared Physics*, **29**, 119-131 (1989).
7. "Heterodyne Spectroscopy of the J=22-21 CO Line in Orion", R.T. Boreiko and A.L. Betz, *Ap. J. (Letters)*, **346**, L97-L100 (1989).
8. "Reversed Far-Infrared Line Emission from OH in Orion", A.L. Betz and R.T. Boreiko, *Ap. J. (Letters)*, **346**, L101-L104 (1989).
9. "Heterodyne Spectroscopy of C II in Molecular Clouds", A.L. Betz, R.T. Boreiko, and J. Zmuidzinas, in *Submillimetre Astronomy*, G.D. Watt and A.S. Webster (eds.), pp. 117-121 (Kluwer Acad. Publ. 1990).
10. "Plateau Emission from Orion in the CO J=17-16 Line", R.T. Boreiko, A.L. Betz, and J. Zmuidzinas, in *Submillimetre Astronomy*, G.D. Watt and A.S. Webster (eds.), pp. 167-168 (Kluwer Acad. Publ. 1990).
11. "Ionized Carbon in Side-Illuminated Molecular Clouds", R. T. Boreiko, A. L. Betz, and J. Zmuidzinas, *Ap. J.*, **353**, 181-192 (1990).
12. "Far-Infrared Heterodyne Technology". A.L. Betz and R.T. Boreiko, in *Proc. 29th Liège International Astrophysical Colloquium: From Ground-Based to Space-Borne Sub-mm Astronomy*, Liège, Belgium, 3-5 July 1990, ESA SP-314 (December 1990), pp. 205-210.
13. "Observations of ^{12}CO and ^{13}CO J=9-8 in Galactic Molecular Clouds", R.T. Boreiko and A.L. Betz, *Ap. J.*, **369**, 382-394 (1991).
14. "Ionized Carbon in the Large Magellanic Cloud", R.T. Boreiko and A.L. Betz, *Ap. J. (Letters)*, **380**, L27-L30 (1991).
15. "High Resolution Far-Infrared Spectroscopy", A.L. Betz and R.T. Boreiko (1993), in *Astronomical Infrared Spectroscopy*, ed. S. Kwok, Astron. Soc. of Pacific Conf. Series, V. 41, pp. 349-356.
16. "A Search for the Rotational Transitions of H_2D^+ at 1370 GHz and H_3O^+ at 985 GHz", R.T. Boreiko and A.L. Betz, *Ap. J. (Letters)*, **405**, L39-L42 (1993).
17. "Far-Infrared Spectroscopy of Neutral and Ionized Carbon in the Interstellar Medium", J. Zmuidzinas, Ph.D. Thesis, University of California, Berkeley (1987).

A 150 μ m TO 500 μ m HETERODYNE SPECTROMETER FOR AIRBORNE ASTRONOMY*

A. Betz and J. Zmuidzinas

Space Sciences Laboratory, University of California, Berkeley

I. Introduction

The advantages of heterodyne detection for high resolution spectroscopy have long been apparent to radio astronomers. Heterodyne spectroscopy has also been productive at submillimeter wavelengths $> 500 \mu\text{m}$ for airborne observations [e.g., Keene et al, 1983], but its extension to shorter submillimeter and far-infrared (FIR) wavelengths has until recently been hampered by inadequate mixers and local oscillators (LO's). A significant advance in FIR receiver technology was demonstrated by Goldsmith et al (1981), who used an optically-pumped FIR laser and a Schottky-diode mixer to detect the J=6-5 line of CO at 434 μm . The 8000 K noise temperature of that ground-based receiver was low enough to detect the CO line without difficulty, but the sheer bulk of the instrumentation limited the observing effort to the coude room of the IRTF on Mauna Kea. Any similar spectrometer intended for airborne observations at shorter wavelengths (i.e., 150-500 μm) must of course be designed from the start to be compatible with the more restrictive aircraft environment. The instrument must at least maintain the sensitivity of the ground-based system and yet fit into a volume $< 1/2 \text{ m}^3$ and weigh $< 350 \text{ lbs}$. These constraints have been overcome to the extent necessary in our design for a FIR heterodyne spectrometer. The effectiveness of the design has been verified in ground-based observations with a prototype version of the instrument. The prototype spectrometer was used at the Cassegrain focus of the MKO 88-inch telescope in January, 1984, to make the first detection of the 809 GHz $^3\text{P}_2 - ^3\text{P}_1$ line of C I in OMC-1 [Jaffe et al, 1984]. The airborne successor to this ground-based spectrometer is even more compact, and in addition has a much broader spectral coverage. First flights with the new instrument are scheduled for the coming year.

II. Spectrometer Overview

Our FIR heterodyne spectrometer has the 4 basic subsystems characteristic of most heterodyne instruments: a local oscillator (LO), a mixer, an intermediate-frequency (IF) amplifier, and a multi-channel radio-frequency (RF) filter bank.

* work supported in part by NASA grant NAG 2-254 and NSF grant AST-8211520.

The LO is an optically-pumped laser, and the mixer is a cooled Schottky-diode. These components, together with the IF amplifier, are the critical "front-end" components of the spectrometer, and they are the only ones actually mounted on the telescope. The "back-end" components such as the filter bank are mounted in the experimenters' rack. They are non-critical in that they affect the resolution but not the sensitivity of the spectrometer. For this reason, a heterodyne spectrometer has a very practical advantage over an incoherent instrument for high resolution spectroscopy. A heterodyne spectrometer does its spectral analysis after "detection" whereas a spectrometer using incoherent detection does its resolving before detection. In this latter case, the inevitable losses and extraneous emissions of the spectrometer reduce the signal-to-noise ratio from that obtainable with a perfect instrument. On the other hand, the coherent (heterodyne) spectrometer does have an additional but fundamental source of noise from quantum fluctuations. Realistically however, the quantum-noise level of a heterodyne receiver even at $\lambda=100\mu\text{m}$ is only $T_Q=140\text{ K}$, or about $10^{-21}\text{ WHz}^{-1/2}$, and thus is negligible compared to the non-fundamental noise of current receivers. Perhaps the most obvious advantage of heterodyne spectroscopy is its capability for ultra-high resolution. A velocity resolution $<1\text{ km/s}$ can easily be achieved with a velocity-scale accuracy limited only by the knowledge of the laser and source line-frequencies.

The front-end components of our airborne spectrometer weigh 200 lbs. and have a moment of 800 ft-lbs. measured from the center of the air bearing on the KAO. The size of the laser-frame dictates the overall size of the front-end hardware. The frame is 40" L x 13.5" W x 8" H and consists of four 1-inch O.D. invar rods that separate 2 insulating granite end-plates. A 40" x 13.5" aluminum plate is attached to the top of the laser frame, and on it are positioned all the optical components of the spectrometer. The entire assembly fits halfway into the instrument cavity at the Naysmith focus position. The other half of the spectrometer protrudes beyond the position of the standard instrument flange, but is braced to the instrument cavity. The standard instrument-mounting flange is removed, of course.

The layout of the spectrometer is illustrated in Figure 1. The LO beam generated by an optically-pumped FIR laser and the signal collected by the telescope are combined in an optical diplexer and focussed onto a cooled diode mixer. The IF signals out of the mixer are amplified by a low-noise FET amplifier and then sent by coaxial cable to the multichannel filterbank located in the experimenter's rack. Because the LO frequencies available from the FIR laser are discrete and essentially untunable, the center frequency of the IF amplifier must be selected to match the difference frequency between the laser LO and the astronomical line of interest. Changes in the Doppler shift of the source due to the orbital and rotational motions of the Earth must be tracked in the IF if a spectral resolution of 1 part in 10^6 is to be maintained. A description of the individual components and factors influencing the chosen optical configuration are detailed in the sections that follow.

III. Component Descriptions

(1) Local Oscillator

For submillimeter wavelengths much shorter than $500\ \mu\text{m}$, the only reasonable choice for the LO at present is the optically-pumped molecular gas laser. Fixed-frequency gas lasers are sometimes dismissed as being too bulky, too limited in frequency coverage, and too unstable in output power for effective use as local oscillators "in the field". Even though such criticisms may have been valid for simple laboratory lasers in years past, problems of this type are not any more endemic to lasers than they are to klystrons, BWO's, or any other oscillator. Steady development and good engineering practice generally lead to useful devices, and such is now the case for optically-pumped lasers. The operation of the FIR laser is illustrated in Figure 2. Pump radiation from a CO_2 laser is absorbed by a vibrational transition in a polar gas molecule. A population inversion is produced between rotational levels in the excited vibrational state, and, if the gas is enclosed by an optical cavity tuned to the rotational transition frequency, FIR laser action can occur. The CO_2 laser serves only as an "optical power supply" for the FIR laser.

The comparative advantages of FIR lasers as local oscillators have been discussed by Danielowicz (1980). As far as airborne use is concerned, the only serious drawback heretofore has been that of size and weight. The compact laser developed for this project overcomes these limitations adequately enough so that the spectrometer can be mounted at the Naysmith focus of the KAO telescope. The laser system is 1-m long and has the following necessary characteristics:

- (a) LO power levels of 1 to 40 mW can be generated on selected FIR-laser lines with pump powers $< 15\ \text{W}$ from a CO_2 laser. Our measurements on GaAs-diode mixers in the far-infrared indicate that $\sim 4\ \text{mW}$ of LO power is needed to drive a room-temperature mixer and $\sim 1.5\ \text{mW}$ is required to drive a cooled mixer for minimum noise temperature (best sensitivity). The high efficiency of this laser is achieved by pumping on-axis and by using an output coupler mirror with a transmission optimized for high gain laser lines ($T \sim 40\%$). The output coupler is a silicon etalon of the type described in detail by Chiou (1983).
- (b) Instabilities sometimes encountered with on-axis pumping are not a problem in this system because: (1) the FIR laser uses gases that are good absorbers of the pump radiation, (2) the CO_2 laser is undercoupled ($T = 10\%$) to make it less sensitive to unabsorbed pump radiation reflected from the FIR cavity, and (3) a single rigid frame defines the length of both FIR and pump cavities.
- (c) The FIR and CO_2 lasers are both run with sealed and not flowing gas fills. Sealed operation allows the use of isotopic gases in either laser, and consequently far more high-power laser lines are available from the best FIR laser gases. In addition, the bulky high-pressure gas cylinder required by a flowing CO_2 laser is not needed aboard the aircraft.

- (d) Selection of the LO frequency is precisely controlled by the FIR laser gas and the selected pumping transition. Selection of the pump line is done by a grating control on the CO₂ laser.
- (e) The LO frequency is inherently stable because it is determined by a specific molecular transition. Stabilization of the FIR-laser-cavity on the molecular resonance is done both passively by invar-rod spacers and actively by a motor-controlled end-mirror to yield a 1 part in 10⁷ accuracy. The FIR laser frequency can also be measured with respect to high-order harmonics of a microwave reference oscillator.

(2) Diplexer and Optics

Signals from the telescope and the LO are combined optically in a device called a diplexer. Although there are many functional variants of these devices (Miles, 1982), they usually have the same purpose: to combine two beams with almost 100% efficiency. Diplexers are also sometimes used as filters to reject LO noise at the sideband frequencies: $f_{LO} \pm f_{IF}$. Optically-pumped lasers are essentially monochromatic, however, and do not require such sideband filtering. "Phase-noise" is more of a problem with electrically-tunable oscillators such as Impatts and carcinotrons.

The type of diplexer illustrated in Figure 1 is called a polarization diplexer. A wire-grid polarizer is used as a lossless beam combiner for the LO and telescope beams. The signals out of the beam-combiner are cross-polarized as they enter the diplexer. Most of the visible radiation passes through the grid to the fiber-optic pickup for the focal-plane camera. The LO beam has previously been focussed by a polyethylene lens so that it has the same f/17 convergence as the telescope beam. Actually, the beams must properly be discussed in terms of Gaussian optics (Goldsmith, 1982), but this point will not be dwelt on here. The collinear beams travel into the diplexer where they encounter another polarizing grid at 45° incidence. The axis of this second grid is also oriented at 45° with respect to each beam's polarization vector, and so splits the combined input beam into equal amplitude halves. The halves are separately reflected from roof mirrors and recombined at the wire grid. For certain displacement differences of the roof mirrors from the grid, all the input power is transmitted in a linearly polarized output beam toward the mixer. This is possible without violating the conservation of brightness because the two input beams are at different frequencies. If the frequency offset between the LO and signal beams is kept > 2 GHz, then the displacement difference is < 7.5 cm and can be easily accommodated in the space available. The bandwidth of the telescope signal transmitted by the diplexer is about 20% of the IF center frequency. Consequently, IF frequencies > 5 GHz are necessary in order to get an IF bandwidth of 1 GHz (i.e., 500 km/s at $\lambda=500$ μ m, 100 km/s at $\lambda=100$ μ m).

Certain factors favored the selection of a polarization diplexer for the airborne spectrometer:

- (1) broad bandwidth--a single grid (unlike a dielectric-film) covers the entire wavelength range,
- (2) low loss--no dielectric films in the beam (more important at wavelengths $< 150 \mu\text{m}$),
- (3) compact form--beams are redirected along a single beam-axis and not translated as in amplitude diplexers using dielectric films,
- (4) compatible with FIR laser polarization (vertical or horizontal depending on LO line) --polarizing beam-combiner can be simply rotated 90° to pass laser polarization,
- (5) low susceptibility to vibration--wire grids are not as acoustically perturbed as are dielectric films in the noisy aircraft environment.

The beam out of the diplexer is focussed onto the mixer by a polyethylene lens that has a focal ratio matched to the mixer's antenna pattern ($-f/2.6$). Reflection losses from the 2 surfaces of the lens decrease the system sensitivity by 8%. The 8% loss could be eliminated by coating or grooving the lens surfaces. Absorption losses are $< 2\%$ at $\lambda=500 \mu\text{m}$ and $\sim 16\%$ at $\lambda=100 \mu\text{m}$. A crystal-quartz lens would have lower loss at short wavelengths but would need AR-coating.

Advantages of a lens over an off-axis mirror are easier alignment, more compact structure, and a symmetric Gaussian "illumination pattern" on the telescope's primary mirror. This last point refers to the efficiency of the mixer's optical coupling to the telescope. It is important to optimize the coupling efficiency (hopefully $\sim 60\%$) and the receiver's intrinsic sensitivity together for best performance. A low receiver-noise-temperature by itself is not necessarily the best measure of a spectrometer's performance on the telescope.

(3) Mixer and Amplifier

The mixer is a GaAs Schottky-diode mounted in a corner-reflector mount. The diode-chips are made at the U. Va. Semiconductor Device Laboratory and have $1 \mu\text{m}$ contact metallizations; they are also optimized for use in cooled receivers at submillimeter wavelengths (Mattauch, 1984). The FIR bandwidth of a pre-adjusted mixer is $\sim 20\%$, and a number of separate mixer-mounts are available to cover the lines of interest during a flight series. This approach was chosen over a single adjustable mixer in order to permit rapid wavelength changes between flight legs, if desired. The availability of separate pre-cooled mixers also gives a backup capability in case the primary mixer fails during observations. Open-resonator mixers with corner reflectors ("cube-corner mixers") have been shown to be effective and relatively easy to fabricate for submillimeter wavelengths [Kräutle et al, 1977; Fetterman et al, 1978]. The sensitivity of the receiver, stated as the single-sideband (SSB) system-noise-temperature, T_N , is given in figure

3. The quoted noise temperatures are for room-temperature devices and can be improved somewhat by cooling. The improvement with cooling is not as dramatic in submillimeter mixers as in millimeter-wave devices, however. Nonthermal noise due to "tunneling currents" becomes significant relative to thermal noise at high frequencies, and tunneling noise is not reduced by cooling. The net improvement by cooling to temperatures < 80 K is currently about a factor of 2 at the longer wavelengths of interest. More importantly, however, is that cooling reduces the LO power needed to drive the mixer to the minimum conversion loss (i.e., best sensitivity). At submillimeter wavelengths LO power is often at a premium. A larger number of laser lines can be used with a cooled mixer because only 1 to 2 mW of LO power is needed. One final point on cooling is that the IF amplifier should be cooled regardless of the mixer so that the IF contribution to the total system noise is $< 10\%$. Since the IF amplifier is best mounted in close proximity to the mixer, the simplest and most effective procedure is to cool both mixer and amplifier together.

The IF amplifiers are dual-stage GaAs-FET amplifiers with gains of ~ 20 dB and ~ 3 dB bandwidths of $\sim 30\%$ of the IF center frequency (e.g., 2.0 GHz bandwidth for a 6.3 GHz IF amplifier). These reactively-tuned amplifiers are designed in our laboratory to have the broadest possible bandwidths consistent with an IF noise temperature < 50 K when cooled to physical temperatures < 80 K. Optimizing for lower amplifier noise would restrict the usable IF bandwidth without appreciably improving the overall system sensitivity. A 50 K amplifier contributes less than 10% to the overall system noise level. This is true only because of the relatively high 9000 K noise temperature and 12 dB conversion loss of the mixer itself (room-temperature values at $\lambda=370\mu\text{m}$). As better cooled mixers are developed, lower IF noise temperatures will also be required. Currently we are still emphasizing bandwidth over noise by developing an ultra-broadband IF amplifier for 2-8 GHz. This amplifier will give us more frequency coverage for each cooled mixer-amplifier and eliminate the need to change IF amplifiers within the cryostat during a flight series. With narrow-band amplifiers, the highest IF being considered is about 15 GHz. Above this frequency the noise-contribution of the amplifier increases above the $0.1 T_N$ limit we have imposed. Of course, in special situations where a close LO coincidence is not available, IF bands as high as ~ 26 GHz could be used with a penalty on T_N .

IV. Scientific Program

Currently there are no high resolution spectrometers aboard the KAO that operate at wavelengths between $200\ \mu\text{m}$ and $500\ \mu\text{m}$. Consequently, this unexplored spectral region is ripe for the detection of many new and important lines. Ground-based observations are for the most part impossible because of obscuration by water vapor in the Earth's atmosphere. Some of the more promising candidate lines are listed in Tables I, II, and III. The tables show the intended source line, the FIR laser gas, and the IF center frequency in the rest frame. Table I demonstrates that a single laser line can be in good (accidental) frequency coincidence with many important spectral lines. Of particular note is that the ^{12}C I line and the 3 lines of ^{13}C I can all be observed simultaneously because of the wide

1 GHz IF bandwidth of the spectrometer. Even a room-temperature mixer with a 10000 K noise temperature can detect ^{13}C I after a 1-hr flight leg when the optical depth of ^{12}C is > 5 and the gas-excitation temperature exceeds 30 K. Planned reductions of the system noise to < 5000 K in the current year will allow ^{13}C to be detected whenever $\tau_{^{12}\text{C}} > 2$. Observations of the $^3\text{P}_2$ - $^3\text{P}_1$ lines of ^{13}C I at $370 \mu\text{m}$ are the only way atomic ^{13}C is going to be detected in dense clouds impenetrable by interstellar UV.

Table II lists the frequency coincidences between high-J lines of $^{12}\text{C}^{16}\text{O}$ and strong laser lines. CO lines up to $J = 8$ are likely to be thermalized in dense clouds where the H_2 density is greater than 10 cm^{-3} and the excitation temperature exceeds 80 K. Rotational transitions from thermalized levels are likely to be optically thick because of the high abundance of CO. Transitions from unthermalized levels are more likely to be optically thin and thus better indicators of the physical conditions in the interior of the cloud [McKee et al, 1982]. Of particular interest are the 9-8, 11-10, and 17-16 transitions. These lines all have a 5 GHz IF and can be observed using our favorite laser gases: $^{15}\text{NH}_3$ and CH_2F_2 . The $153 \mu\text{m}$ line of $^{15}\text{NH}_3$ is the strongest known FIR laser line. Also of interest for future work is the coincidence between the well-known $118 \mu\text{m}$ laser line of CH_3OH and the $J = 22$ -21 line of $^{12}\text{C}^{16}\text{O}$.

Table III concludes the list of coincidences. Listed are the principal fine-structure lines for wavelengths longer than $150 \mu\text{m}$ with allowance for the O I line. Once again we see that the astronomically important lines can all be matched with good laser coincidences. In the case of O I the coincidence is too good. Proper operation of the diplexer requires a frequency offset between the laser and the source line. High resolution observations of the $145 \mu\text{m}$ O I line may be better done with a heterodyne spectrometer that does not require a diplexer. For example, a receiver that uses a photoconductive mixer and a beamsplitter for LO injection might well do O I for a start. The sample coincidences given in these tables should be ample evidence that a heterodyne spectrometer with a fixed-frequency laser-LO has the potential to be scientifically productive. The observations possible with just the listed lines will take many years to complete with normal flight scheduling for the spectrometer. No mention was made of the numerous far-infrared transitions of light molecules such as the hydrides which also will be observable. The number of useable laser lines should continue to grow over the next few years as more laboratory measurements are made of the isotopic variants of known good laser molecules. Furthermore, receiver sensitivities should also steadily improve as well-engineered mixers replace the current first-generation devices. Sensitivities of existing mixers are more than 2 orders of magnitude worse than the limits placed by quantum-noise.

References

Chiou, A. (1983), Ph.D. Thesis, Caltech.

Danielowicz, E.J. (1980), Proc. Heterodyne Systems and Technology Conference, Williamsburg, VA., NASA CP-2138, p. 417.

Fetterman, H.R., Tannenwald, P.E., Clifton, B.J., Parker, C.D., Fitzgerald, W.D., and Erickson, N.R. (1978), Appl. Phys. Lett., 35, 151.

Goldsmith, P.F., Erickson, N.R., Fetterman, H.R., Clifton, B.J., Peck, D.D., Tannenwald, P.E., Koepf, G.A., Buhl, E., and McAvoy, N. (1981), Ap. J. (Lett.), 243, L79.

Goldsmith, P.F., (1982), in Infrared and Millimeter Waves, Vol.6, K.J. Button, ed., Academic Press, N.Y, N.Y.

Jaffe, D., Harris, A., Silber, M., Genzel, R., and Betz, A. (1984), to be published.

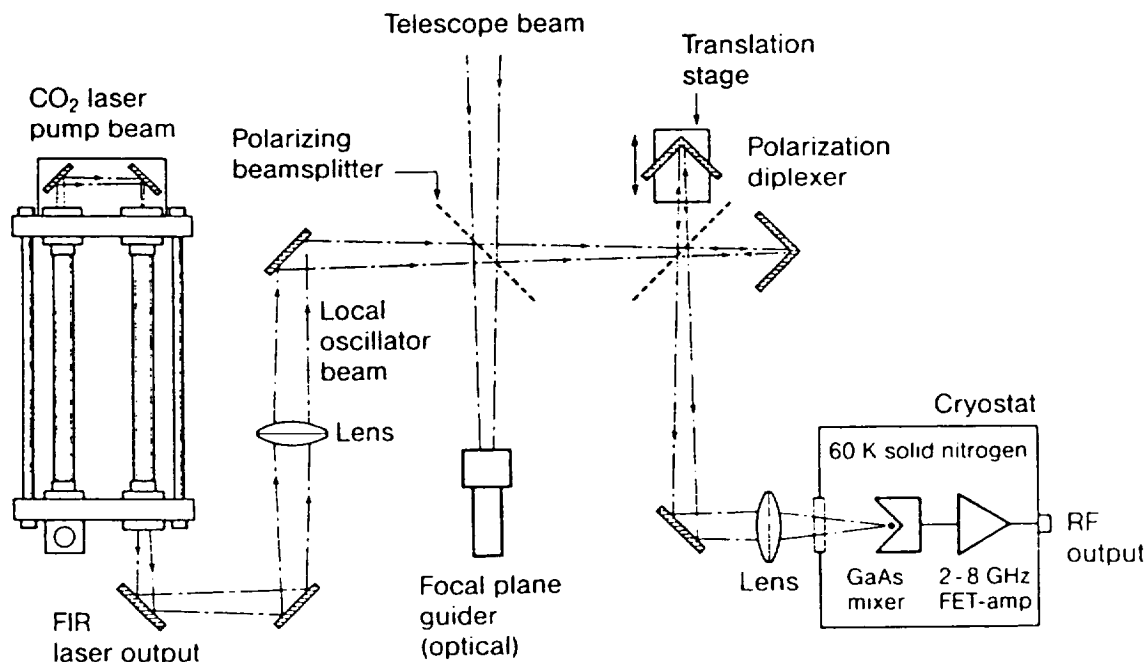
Keene, J., Blake, G.A., and Phillips, T.G. (1983), Ap. J. (Lett.), 271, L27.

Krättele, H., Sauter, E., and Schultz, G.V. (1977), Infrared Physics, 17, 477.

Mattauch, R. (1984), private communication.

McKee, C.F., Storey, J.W.V., Watson, D.M., and Green, S. (1982), Ap. J., 259, 647.

Miles, P. (1982), Appl. Optics, 21, 1367.



Airborne Far-Infrared Heterodyne Spectrometer

Figure 1

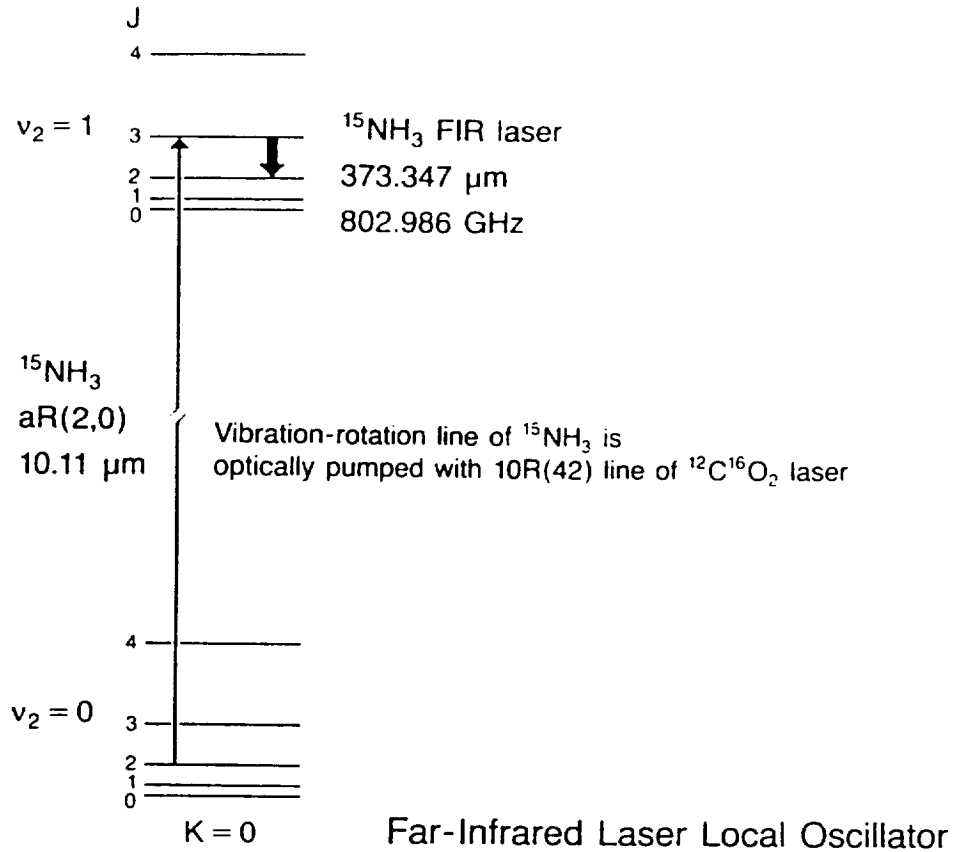


Figure 2

SPECIFICATIONS*

Frequency Coverage:	600-1500 (2000) GHz
Wavelength Range:	500-200 (150) μm
Resolution:	1.2 MHz \times 50 Channels 5.0 MHz \times 40 Channels 20.0 MHz \times 128 Channels (2.0 MHz \times 512 Channel-AOS)
Sensitivity (uncooled):	T_N [SSB] = 10000 K NEP = 4×10^{-16} W \cdot Hz $^{-1/2}$ at $\lambda = 400 \mu\text{m}^\ddagger$ (T_N [SSB] \sim 25000 K NEP $\sim 2 \times 10^{-15}$ W \cdot Hz $^{-1/2}$ at $\lambda = 150 \mu\text{m}$)
Beamsize on KAO:	Diffraction-limited 2.2 arcmin at $\lambda = 500 \mu\text{m}$ 0.9 arcmin at $\lambda = 200 \mu\text{m}$
Dimensions:	14" H \times 14" W \times 54" L
Weight:	200 lbs., installed

* Specifications in parentheses are planned improvements

† Per channel at 0.4 km/s (1.2 MHz) resolution, includes chopping and telescope-coupling losses

Figure 3

LINE COINCIDENCES

Laser Line (LO)	Frequency (GHz)	Source Line	Frequency (GHz)	IF (GHz)
$^{15}\text{NH}_3$	802.986	$^{12}\text{C } 1^3\text{P}_2 - ^3\text{P}_1$	809.345	-6.359
		$^{13}\text{C } 1^3\text{P}_2 - ^3\text{P}_1$		
		$\frac{5}{2} - \frac{3}{2}$	809.494	-6.508
		$\frac{3}{2} - \frac{1}{2}$	809.125	-6.139
		$\frac{3}{2} - \frac{3}{2}$	809.121	-6.135
		CO J = 7-6	806.652	-3.666
		HCN J = 9-8	797.433	5.553
		HCO ⁺ J = 9-8	802.445	0.541

Table 1

$^{12}\text{C}^{16}\text{O}$ COINCIDENCES

λ (μm)	CO Line	Laser Gas	I.F. (GHz)
371.6504	7-6	$^{15}\text{NH}_3$	3.666
325.2252	8-7	$\text{C}_2\text{H}_2\text{F}_2$	3.840
289.1204	9-8	CH_2F_2	-5.238
260.2399	10-9	$\text{C}_2\text{H}_2\text{F}_2$	1.085
236.6134	11-10	CH_2F_2	-5.157
162.8118	16-15	CH_3OH	2.504
153.2669	17-16	$^{15}\text{NH}_3$	4.990
124.1937	21-20	CH_2DOH	4.618
118.5811	22-21	CH_3OH	5.383

Table 2

FINE STRUCTURE LINES

λ (μm)	Species	Laser Gas	IF (GHz)
370.4139	C I	$^{15}\text{NH}_3$	-6.359
203.9	N II	CH_2F_2	10.42
		$^{13}\text{CH}_3\text{OH}$	1.91
157.737	C II	CH_2F_2	-9.310
		$^{13}\text{CH}_3\text{OH}$	-2.305
145.526	O I	CH_3OH	0.0

Table 3

OBSERVATIONS OF NEUTRAL ATOMIC CARBON AT 809 GHz

J. ZMUIDZINAS, A. L. BETZ, AND D. M. GOLDBABER

Space Sciences Laboratory, University of California, Berkeley

Received 1986 May 13; accepted 1986 May 23

ABSTRACT

We have detected the 809 GHz $^3P_2-^3P_1$ fine-structure line of neutral atomic carbon in four dense molecular clouds: M17, W51, W3, and DR 21(OH). These observations complement the published observations of the 492 GHz $^3P_1-^3P_0$ line and allow the excitation temperature of the 3P levels along with the line optical depths to be determined. The results indicate excitation temperatures $T_x \approx 30-60$ K and optical depths of $\tau_{10} \leq 1$. This implies that the $\sim 10^{18}$ cm $^{-2}$ lower limit to the C I abundance derived from 492 GHz observations is probably the actual abundance, which gives C I/CO ≈ 0.1 in dense molecular clouds.

Subject headings: interstellar: abundances — interstellar: matter — nebulae: abundances

I. INTRODUCTION

The 3P ground state of neutral atomic carbon is split by spin-orbit coupling into the $J = 0, 1,$ and 2 levels which have energies of 0 K, 23.6 K, and 62.4 K, respectively. Magnetic dipole transitions are allowed between adjacent levels; these lead to the $^3P_2-^3P_1$ transition at 809.3432 GHz (370.4145 μm) and the $^3P_1-^3P_0$ transition at 492.1612 GHz (609.1347 μm) (Cooksy *et al.* 1986). The $^3P_1-^3P_0$ line has been observed in many dense molecular clouds by Phillips and Huggins (1981), and the spatial distribution of intensity in two clouds has also been presented (Keene *et al.* 1985). The large observed $^3P_1-^3P_0$ intensities implied lower limits to the C I column densities ($N_{C\ I} \approx 0.1 N_{CO}$) which were much larger than the column densities predicted by steady state models of cloud chemistry (Langer 1976*a*), although time-dependent models predicted a large C I abundance for the first 10^6 yr of cloud evolution (Langer 1976*b*). Several other models have since been proposed to explain the high observed abundance (e.g., Tarafdar *et al.* 1985; Tielens and Hollenbach 1985). A good review of the current situation is presented by Keene *et al.* (1985). Phillips and Huggins (1981) have further argued that comparisons between CO and C I line widths imply that the $^3P_1-^3P_0$ lines are optically thick, and that the abundance of carbon could be as large as $N_{C\ I} \approx 0.7 N_{CO}$ in some cases. The largest optical depth derived by this comparison was $\tau_{10} \approx 25$ for OMC-1. The comparison was only carried out for a few clouds which had well-defined CO line width-opacity relationships, but the implication was that the C I lines were possibly optically thick in other clouds as well. A more direct approach for estimating the C I abundance would have been to observe both of the C I fine-structure lines (the $^3P_1-^3P_0$ line at 492 GHz and the $^3P_2-^3P_1$ line at 809 GHz) and compare the results, but observations at the higher frequency were not possible at the time. The first detection of the $^3P_2-^3P_1$ line was subsequently presented by Jaffe *et al.* (1985), who detected it in OMC-1. Although their data favor optically thin C I lines, the result is not firm due to large systematic uncertainties. We have recently observed the $^3P_2-^3P_1$ line in

four dense molecular clouds: M17, W51, W3, and DR 21(OH). In this *Letter* we present our data, compare them to existing $^3P_1-^3P_0$ data, and derive estimates for the excitation temperature and column density of neutral carbon.

II. OBSERVATIONS

Since the transmission of the atmosphere at 370 μm is at best rather poor from the ground, we observed the $^3P_2-^3P_1$ transition from the NASA Kuiper Airborne Observatory (KAO) at an altitude of 41,000 feet. The observations were completed in 1985 July using an airborne far-infrared heterodyne receiver (Betz and Zmuidzinas 1984). This is the first laser spectrometer to be used aboard the KAO, although similar (but larger) instruments have been used at ground-based observatories (e.g., Koepf *et al.* 1982; Jaffe *et al.* 1985). Briefly, it consists of a CO $_2$ laser-pumped far-infrared laser local oscillator (LO), a polarization diplexer to combine telescope and LO beams, and a GaAs Schottky diode mixer in an open structure mount. A velocity resolution of 1.85 km s $^{-1}$ over an interval of 74 km s $^{-1}$ was achieved by using a filter bank with 40 5 MHz channels to analyze the intermediate frequency (IF) signal. The room-temperature receiver had a 20,000 K (SSB) noise temperature.

We used the chopping secondary of the telescope to switch between two beams that were alternately placed on the source. At the chopping frequency of 21 Hz the maximum chopper-throw consistent with a reasonable waveform efficiency was 5', which in some cases may not have been sufficient to place the off-source beam in a region free of emission (see § IV). The absolute flux calibration was derived from raster scans of the telescope beam across Jupiter. The calibration uncertainty is dominated by source coupling effects, as will be discussed in § IV. These measurements, corrected for the finite size of Jupiter, also provided the beam size (80" FWHM), the main beam efficiency ($\sim 30\%$ including chopper waveform inefficiency), and the instrument boresight (to $\pm 15''$). We assumed that Jupiter had an uniform elliptical intensity distribution with major and minor axes of 48" and 45", respec-

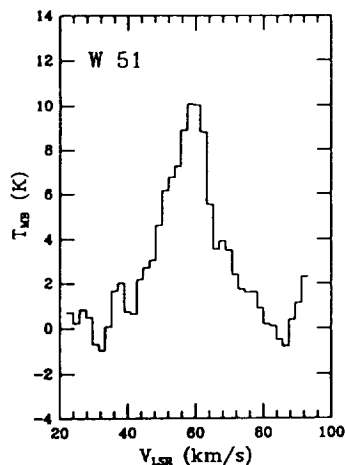


FIG. 1a

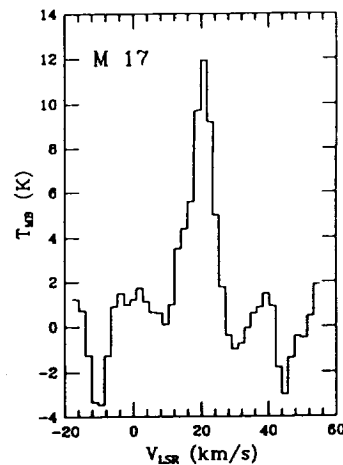


FIG. 1b

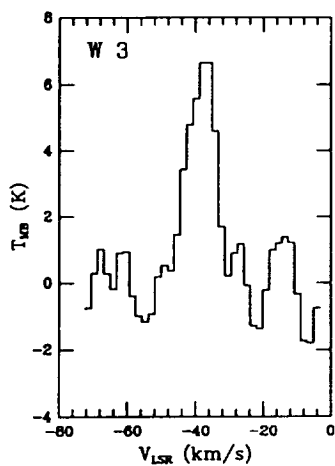


FIG. 1c

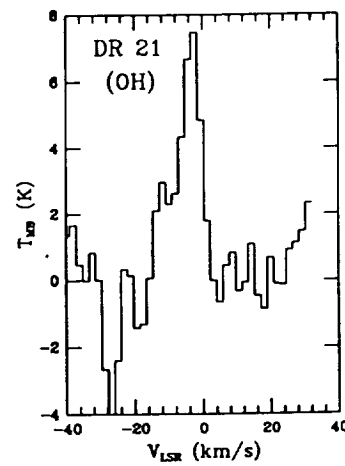


FIG. 1d

FIG. 1.—809 GHz $C\ I\ ^3P_2-^3P_1$ emission observed toward (a) W51, integration time = 32 minutes; (b) M17, integration time = 44 minutes; (c) W3, integration time = 58 minutes; and (d) DR 21(OH), integration time = 23 minutes.

tively, and a brightness temperature of 160 K at $370\ \mu\text{m}$ (Hildebrand *et al.* 1985). The Moon, which was used to calibrate the $^3P_1-^3P_0$ data (Phillips and Huggins 1981), was not available at the time of these observations. The overall pointing accuracy is estimated to be between $20''$ and $30''$.

III. RESULTS

Figures 1a–1d show the $^3P_2-^3P_1$ spectra measured for four dense clouds: M17, W51, W3, and DR 21(OH). The observed positions were chosen to match locations where $^3P_1-^3P_0$ emission had been measured previously. We also observed S140 but failed to detect a line. The $^3P_1-^3P_0$ emission in S140 has been shown to have a spatial extent of over $10'$ in a direction similar to our misoriented chop direction (Keene *et al.* 1985). Consequently, emission in the reference beam may have canceled equivalent emission in the “on-source” beam to produce a zero differential signal. If this is so, then the $^3P_2-^3P_1$ emission and the $^3P_1-^3P_0$ emission have similar spatial distributions.

The spectra in Figure 1 have been Hanning smoothed to an effective resolution of $3.7\ \text{km s}^{-1}$, and small linear baselines have been subtracted. Table 1 shows the measured peak intensities, line widths, line centers, and their uncertainties. These parameters were determined by fitting a Gaussian profile degraded by the instrumental resolution to the unsmoothed data, in order to correct these parameters for the finite resolution of the spectrometer. The χ^2 values of the fits were consistent with independent measurements of the receiver noise, although the line profiles are not necessarily expected to be Gaussian (the S/N ratio is not large enough to show the fine details of the line profile). Also shown in Table 1 are $^3P_1-^3P_0$ line parameters. The center velocities agree well, while the line widths agree well only for M17 and DR 21(OH). We expect the line widths to be similar if the gas is optically thin, while the $^3P_1-^3P_0$ line should be somewhat wider than the $^3P_2-^3P_1$ line if the gas were cool and optically thick since the optical depth of the $^3P_1-^3P_0$ line would be ~ 2 times larger than the depth of the $^3P_2-^3P_1$ line (for

TABLE 1
 C I LINE PARAMETERS

Source	$T_{MB}(2-1)$ (K)	$\Delta V(2-1)$ (km s ⁻¹)	$V_{center}(2-1)$ (km s ⁻¹)	$T_A^*(1-0)$ (K)	$\Delta V(1-0)$ (km s ⁻¹)	$V_{center}(1-0)$ (km s ⁻¹)
M17 ^a	12.9 ± 1.3	6.7 ± 0.8	19.6 ± 0.7	11.0	6.4	20.5
W51 ^b	8.9 ± 1.0	16.0 ± 2.2	57.5 ± 1.0	8.0	20.5	60.0
W3 ^{b,c}	7.3 ± 0.9	9.1 ± 1.5	-38.8 ± 0.8	6.0	5.0	-38.0
DR 21(OH) ^d	8.5 ± 1.9	5.7 ± 1.5	-4.0 ± 0.8	4.0	5.0	...

NOTE.—The quoted uncertainties are ±1 σ .

^a1-0 data from Keene *et al.* 1985.

^b1-0 data from Phillips and Huggins 1981.

^cThe value shown in Table 1 of Phillips and Huggins 1981 for the 1-0 line width is 6.5 km s⁻¹. However, their published spectrum shows a line width of 5 km s⁻¹ (FWHM). We believe the larger value to be a typographical error.

^d1-0 data from J. Keene 1986, private communication.

$T_x \approx 20$ K). However, the line width variations are probably best explained by the fact that the two different beams (80'' at 809 GHz versus 180'' at 492 GHz) sample different spatial regions of sources with a complex velocity structure (Phillips *et al.* 1981; Brackmann and Scoville 1980 [W3]; Mufson and Liszt 1979 [W51]).

IV. INTENSITY CALIBRATION AND SOURCE COUPLING EFFECTS

A comparison of the intensities of the $^3P_2-^3P_1$ and $^3P_1-^3P_0$ transitions can provide useful information about the abundance and excitation of carbon. However, the comparison of intensities is not straightforward since the beam size of the $^3P_1-^3P_0$ observations (3') is a factor of 2 larger than that of the $^3P_2-^3P_1$ observations, and so the source coupling differs. Furthermore, the calibration procedures (and sources) differ. These details are important in interpreting the data since the $^3P_2-^3P_1/^3P_1-^3P_0$ line intensity ratio for optically thin gas is at most only a factor of 2 larger than the same ratio for optically thick gas. In fact, the source-coupling corrections change the line intensities by ~30% or more; hence, the statistical uncertainties in the data (~15%) are small compared to the uncertainties in the source coupling.

The $^3P_1-^3P_0$ data were calibrated in such a manner that a source of uniform intensity $T_R(1-0)$ filling the entire diffraction pattern of the telescope, including sidelobes, would give a measured intensity of $T_A^*(1-0) = T_R(1-0)$. A source not large enough to fill all of the sidelobes completely would give $T_A^*(1-0) = \eta_{1-0} T_R(1-0)$, where $\eta_{1-0} < 1$ (Kutner and Ulich 1981). On the other hand, the $^3P_2-^3P_1$ data were calibrated in such a manner that a source of uniform intensity $T_R(2-1)$ filling only the main lobe of the diffraction pattern and not filling any sidelobes would give a measured intensity of $T_{MB}(2-1) = T_R(2-1)$. If the source were smaller than the main lobe the measured intensity would be $T_{MB}(2-1) = \eta_{2-1} T_R(2-1)$ with $\eta_{2-1} < 1$, while if the source were larger than the main lobe and started filling the sidelobes as well, we would have $\eta_{2-1} > 1$. We calculated both of these source coupling coefficients, η_{1-0} and η_{2-1} , assuming a Gaussian source intensity distribution with a peak intensity T_R and a theoretically calculated telescope diffraction pattern. The re-

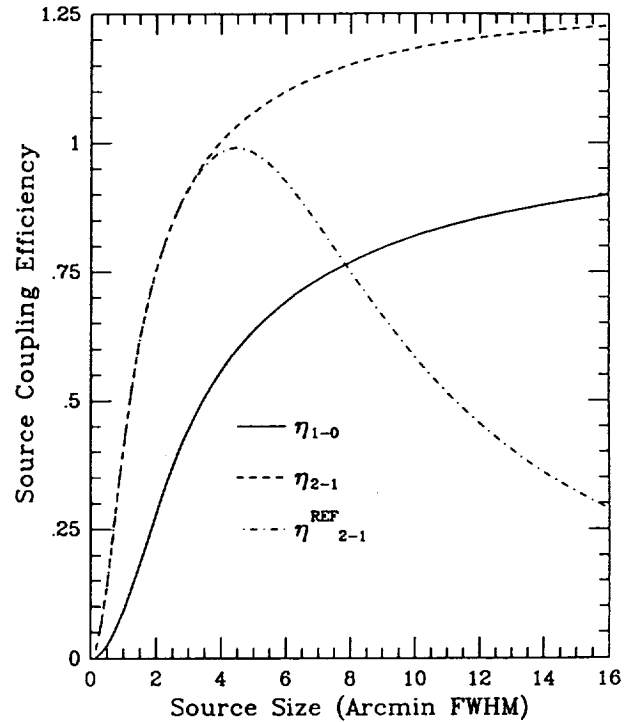


FIG. 2.—Solid line: source coupling efficiency η_{1-0} for the $^3P_1-^3P_0$ observations as a function of source size. Dashed line: source coupling efficiency η_{2-1} for the $^3P_2-^3P_1$ observations. Dot-dashed line: η_{2-1} corrected for emission in the reference beam.

sults are plotted in Figure 2 as a function of assumed source size.

The difference between the two calibrations is easily understood by considering the calibration sources used. The $^3P_1-^3P_0$ data were calibrated by using the Moon, which fills the entire telescope diffraction pattern, while the $^3P_2-^3P_1$ data were calibrated using Jupiter, which fills only a small fraction of the main lobe of the diffraction pattern. The main lobe was scanned across Jupiter in order to deduce the strength of the signal that would have been measured on a source large enough to fill the main lobe. We could not directly deduce the

TABLE 2
 OPTICAL DEPTHS AND EXCITATION TEMPERATURES

SOURCE	A: UNCORRECTED ^a				B: CORRECTED ^b				C: CORRECTED ^c				θ_{SOURCE}^f
	T_x	T_{LL}^d	τ_{10}	τ_{UL}^e	T_x	T_{LL}^d	τ_{10}	τ_{UL}^e	T_x	T_{LL}^d	τ_{10}	τ_{UL}^e	
M17	72.	53.	0.20	0.31	36.	26.	0.95	> 2	48.	36.	0.56	0.91	6.2
W51	64.	47.	0.17	0.25	37.	21.	0.51	0.81	64.	46.	0.22	0.37	7.8
W3	74.	51.	0.10	0.17	31.	22.	0.87	> 2	31.	22.	0.83	> 2	3.5
DR 21(OH).....	> 200.	89.	< 0.03	0.09	98.	44.	0.07	0.20	147.	55.	0.04	0.15	6.0

^a Derived from measured line intensities with no correction for source coupling effects.

^b Corrected for source coupling only using a source size of θ_{SOURCE} .

^c Corrected for source coupling and reference beam emission using a source size of θ_{SOURCE} .

^d Lower limit for T_x (95% confidence level; based on statistical uncertainty of 2-1 intensity only).

^e Upper limit for τ_{10} (95% confidence level; based on statistical uncertainty of 2-1 intensity only).

^f θ_{SOURCE} is the $^{12}\text{CO}(1-0)$ source size (FWHM). The CO source sizes are taken from Thronson and Lada 1983, see also Keene *et al.* 1985 (M17); Mufson and Liszt 1979 (W51); Brackmann and Scoville 1980 (W3); Dickel *et al.* 1978 [DR 21(OH)].

signal that a source filling the entire telescope pattern would have produced because the signal-to-noise ratio was not large enough to allow the sidelobes to be mapped in the available time.

Another important consideration for the $^3P_2-^3P_1$ data is the possibility that the 5' chopper throw was not large enough, and that there was emission from the source in the reference beam, which would cause the differential signal to be smaller. This effect obviously depends on source size. We define η_{2-1}^{REF} to be the ratio $T_{\text{MB}}(2-1)/T_R(2-1)$ corrected for reference beam emission, again assuming a Gaussian source intensity distribution, and we plot it in Figure 2 as a function of source size.

V. DISCUSSION

We model the measured C I line intensities with an emission region of uniform temperature in which the 3P levels are fully thermalized [$n(\text{H}_2) \geq 10^4 \text{ cm}^{-3}$]. We also assume that the velocity distribution of the gas sampled with the 180'' beam at 492 GHz is similar to the velocity distribution of the gas sampled with the 80'' beam at 809 GHz, although this assumption probably breaks down for W3, as shown by the line widths in Table 1. Only two unknown quantities, the $^3P_1-^3P_0$ line optical depth at the center velocity $\tau_{10}(V_{\text{center}})$ and the excitation temperature T_x , determine the line intensities in this model, so a measurement of the two intensities allows us to fully determine these parameters. Other parameters of interest, namely the $^3P_2-^3P_1$ optical depth τ_{21} and the C I column density $N_{\text{C I}}$, can be derived assuming thermal equilibrium. Under such circumstances, the ratio of optical depths τ_{21}/τ_{10} is larger than 1 for $T_x > 50$ K and asymptotically approaches the value of 2.1 as T_x is increased, while τ_{21}/τ_{10} is less than 1 for $T_x < 50$ K.

We derive T_x and τ_{10} for three sets of line intensities. The first set A is given by $T_R(1-0) = T_A^*(1-0)$ and $T_R(2-1) = T_{\text{MB}}(2-1)$; here we take the line intensities "as is" and perform no corrections. The second set B is given by $T_R(1-0) = T_A^*(1-0)/\eta_{1-0}$ and $T_R(2-1) = T_{\text{MB}}(2-1)/\eta_{2-1}$. The source sizes used in estimating the source coupling coefficients are listed in Table 2 (see Fig. 2 also) and are derived from maps

of $J = 1 \rightarrow 0$ ^{12}CO emission. Scans of the C I $^3P_1-^3P_0$ emission in OMC-1 (Phillips and Huggins 1981), and M17 and S140 (Keene *et al.* 1985), indicate that the C I emission region is similar in extent to the CO emission region, and, as mentioned in § III, our nondetection of $^3P_2-^3P_1$ emission in S140 may provide evidence that the $^3P_2-^3P_1$ emission and the $^3P_1-^3P_0$ emission have similar spatial distributions. The third set C of intensities for which we calculate T_x and τ_{10} is the same as the second set with η_{2-1} replaced by η_{2-1}^{REF} ; this attempts to correct for possible emission in the reference beam. The corresponding values of T_x and τ_{10} are listed in Table 2. The results show that $\tau_{10} < 1$ in all cases, and that T_x is typically 30-60 K. M17 and W3 show the largest corrected optical depths; for M17 this is due to the large observed $^3P_1-^3P_0$ intensity, while for W3 this is due to the large upward correction to the observed $^3P_1-^3P_0$ intensity necessitated by its small 3.5 source size. Both W51 and DR 21(OH) appear to be optically thin regardless of the assumed correction. In the case of DR 21(OH) the excitation temperatures seem anomalously high. However, the $^3P_2-^3P_1$ intensity has a large uncertainty, as indicated by the considerably smaller lower limits for T_x shown in Table 2.

Since the lines seem to be optically thin, the lower limits to the column densities of C I ($\sim 10^{18} \text{ cm}^{-2}$), derived by Phillips and Huggins (1981) using an optically thin approximation with $T_x = 20$ K, are likely to be the actual column densities. The column densities derived in this approximation are very insensitive to the assumed excitation temperature, changing by only 25% over the range $15 \text{ K} \leq T_x \leq 200 \text{ K}$. The minimum column densities are calculated by assuming $T_x = 30$ K, while the column densities calculated by assuming $T_x = 20$ K are only 6% larger. After correction for source coupling (case B above), we derive the following column densities (in units of 10^{18} cm^{-2}): 2.1 for M17, 2.8 for W51, 2.1 for W3, and 0.5 for DR 21(OH). Note that these are the peak column densities; the column densities averaged over the source or averaged over a beam would be smaller.

If we compare the parameters derived from the uncorrected line intensities to the parameters derived from the intensities corrected for source coupling, we see that the source-corrected excitation temperatures drop typically by a factor of 2, while

the optical depths increase by an even larger factor. This demonstrates the sensitivity of the results to the assumed source-coupling coefficients, especially to the large upward corrections of the ${}^3P_1-{}^3P_0$ intensities. However, the source-coupling coefficients are derived with the aid of several assumptions and are not known precisely. Hence, it is difficult to put strict upper limits on the derived values of τ_{10} or lower limits on T_x , especially for M17 and W3. The solution to this problem, of course, is to use beam sizes that are much smaller than the source size (such as would be obtained from a larger telescope), and to make sure that the source positions and reference positions are well separated. Even with a 30%

relative uncertainty between the two intensities, firm limits could be placed on the model parameters. Future observations of isotopic C I may also help to reduce uncertainties in the estimates of the optical depths.

We thank the staff of the Kuiper Airborne Observatory for their expert assistance with this new project. We are grateful to J. Keene for communicating C I ${}^3P_1-{}^3P_0$ results prior to publication, and to her and D. Jaffe for many helpful discussions. This work was supported in part by NASA grant NAG 2-254.

REFERENCES

- Betz, A., and Zmuidzinas, J. 1984, in *Proc. Airborne Astronomy Symposium* (NASA CP-2353), p. 320.
 Brackmann, E., and Scoville, N. 1980, *Ap. J.*, **242**, 112.
 Cooksy, A. L., Saykally, R. J., Brown, J. M., and Evenson, K. M. 1986, *Ap. J.*, in press.
 Dickel, J. R., Dickel, H. R., and Wilson, W. J. 1978, *Ap. J.*, **223**, 840.
 Hildebrand, R. H., Lowenstein, R. F., Harper, D. A., Orton, G. S., Keene, J., and Whitcomb, S. E. 1985, *Icarus*, **64**, 64.
 Jaffe, D. T., Harris, A. I., Silber, M., Genzel, R., and Betz, A. L. 1985, *Ap. J. (Letters)*, **290**, L59.
 Keene, J., Blake, G. A., Phillips, T. G., Huggins, P. J., and Beichman, C. A. 1985, *Ap. J.*, **299**, 967.
 Koepf, G. A., Buhl, D., Chin, G., Peck, D. D., Fetterman, H. R., Clifton, B. J., and Tannenwald, P. E. 1982, *Ap. J.*, **260**, 584.
 Kutner, M. L., and Ulich, B. L. 1981, *Ap. J.*, **250**, 341.
 Langer, W. 1976a, *Ap. J.*, **206**, 699.
 . 1976b, *Ap. J.*, **210**, 328.
 Mufson, S. L., and Liszt, H. S. 1979, *Ap. J.*, **232**, 451.
 Phillips, T. G., and Huggins, P. J. 1981, *Ap. J.*, **251**, 533.
 Phillips, T. G., Knapp, G. R., Huggins, P. J., Werner, M. W., Wannier, P. G., Neugebauer, G., and Ennis, D. 1981, *Ap. J.*, **245**, 512.
 Tarafdar, S. P., Prasad, S. S., Huntress, W. T., Villere, K. R., and Black, D. C. 1985, *Ap. J.*, **289**, 220.
 Thronson, H. A., and Lada, C. J. 1983, *Ap. J.*, **269**, 175.
 Tielens, A. G. G. M., and Hollenbach, D. 1985, *Icarus*, **61**, 40.

Note added in proof.—An analysis of recent observations of the ${}^3P_1-{}^3P_0$ line in DR 21(OH) (J. Keene 1986, private communication) indicates a peak antenna temperature T_A^* (1-0) of 6.5 K, which is 50% higher than the preliminary value given in Table 1. This larger intensity results in excitation temperatures T_x of 86, 41, and 52 K for cases A, B, and C in Table 2, along with optical depths τ_{10} of 0.09, 0.36, and 0.26, respectively. The upper limit to the optical depth of the ${}^3P_1-{}^3P_0$ line is $\tau_{UL} = 0.95$ for case B. The new values are similar to those derived for the other three observed sources.

A. L. BETZ, D. M. GOLDBABER, and J. ZMUIDZINAS: Space Sciences Laboratory, University of California, Berkeley, CA 94720

HETERODYNE SPECTROSCOPY OF THE 158 MICRON C II LINE IN M42

R. T. BOREIKO, A. L. BETZ, AND J. ZMUIDZINAS
Space Sciences Laboratory, University of California, Berkeley
Received 1987 October 5; accepted 1987 November 23

ABSTRACT

We have obtained velocity-resolved spectra of the $^{12}\text{C II } 157.8 \mu\text{m } ^2P_{3/2}-^2P_{1/2}$ fine-structure line in the M42 region of Orion. Observations at 0.8 km s^{-1} resolution with a laser heterodyne spectrometer show multiple velocity components in some locations, with typical linewidths of $3\text{--}5 \text{ km s}^{-1}$. Spectra of $\theta^1\text{C}$ and BN-KL also show weak emission from the $F = 2\text{--}1$ hyperfine component of the equivalent $^{13}\text{C II}$ line. From the observed $^{12}\text{C II}/^{13}\text{C II}$ line intensity ratios, we deduce that the $^{12}\text{C II}$ emission is optically thick with $\tau \approx 5$ at both positions. Excitation temperatures of 128 K and 90 K, together with column densities of $\sim 1 \times 10^{19} \text{ cm}^{-2}$ and $\sim 4 \times 10^{18} \text{ cm}^{-2}$, are derived for $\theta^1\text{C}$ and BN-KL, respectively.

Subject headings: infrared: spectra — interstellar: matter — nebulae: Orion Nebula

I. INTRODUCTION

Line emission from the $\text{C II } ^2P_{3/2}-^2P_{1/2}$ fine-structure transition at $157.8 \mu\text{m}$ (1900 GHz) is well recognized as a major coolant for the diffuse neutral regions of interstellar gas clouds (Dalgarno and McCray 1972). Observations with airborne telescopes have shown C II emission to be strong and pervasive in molecular cloud regions exposed to ultraviolet radiation (Russell *et al.* 1980, 1981; Kurtz *et al.* 1983; Crawford *et al.* 1986; Melnick *et al.* 1986). Heretofore, interpretation of the C II data for galactic clouds has been hampered by inadequate resolution of line profiles. Typically, only integrated intensities have been obtained, and other physical parameters, such as optical depth, temperature, column density, and velocity structure, have not been determined uniquely (Watson 1984; Stacey 1985). The observed C II emission has generally been interpreted as optically thin, which then leads to an estimated gas temperature $> 200 \text{ K}$. A quantitative estimate of the C II optical depth would require the detection of at least two line components with different intrinsic line strengths. The $157.8 \mu\text{m}$ line of $^{12}\text{C II}$ has only one spectral component, but the $^{13}\text{C II}$ line could serve as the other, given a known $^{12}\text{C}/^{13}\text{C}$ isotopic ratio. If the optical depth of the $^{12}\text{C II}$ emission could be determined and the line profile resolved, then the line intensity could be used to derive both the excitation temperature and abundance of C^+ . The M42 region of Orion is probably the best source for initial observations of this kind.

This Letter describes the first observations of the $157.8 \mu\text{m}$ C II line with a heterodyne spectrometer capable of providing 0.8 km s^{-1} resolution. Several positions in the Orion molecular cloud have been observed, and the results provide some significant new insights on the abundance and excitation of ionized carbon in this region.

II. INSTRUMENTATION AND CALIBRATION

The instrument used for the observations discussed here is an airborne far-infrared heterodyne receiver (Betz and Zmuidzinas 1984). The local oscillator (LO) is a CH_2F_2 optically pumped laser at 1891.2743 GHz (Petersen, Scalabrin, and Evenson 1980), which is 9.3 GHz away from the rest frequency of the $^{12}\text{C II}$ transition at 1900.5369 GHz (Cooksey *et al.* 1986). The mixer is a GaAs Schottky diode (University of Virginia

type 1E7A) in a corner-reflector mount. The system noise temperature, with the mixer at ambient temperature and the 9.3 GHz IF amplifier cooled to 77 K, was measured to be 32,000 K (SSB) during the observations. The IF signal is analyzed by a 40 channel bank of 5 MHz filters which provides 0.8 km s^{-1} resolution over a range of 32 km s^{-1} , and a 64 channel bank of 20 MHz filters which gives 3 km s^{-1} resolution spanning 200 km s^{-1} . The narrow filters provide good resolution for the C II line, while the wide filters give a broader view of the spectrum that facilitates the measurement of continuum levels.

At $158 \mu\text{m}$ the transmission of a 1 m path at sea level is typically less than 0.5 because of water vapor absorption, so it is essential to observe the C II line from a high altitude. The instrument was therefore flown aboard the NASA Kuiper Airborne Observatory (KAO) at an altitude of 12.5 km, where the line-of-sight transmission is ~ 0.94 . From scans of the lunar limb, the telescope beamwidth was measured to be approximately $43''$ and the coupling efficiency ~ 0.6 . Pointing accuracy is estimated to be $15''$. The chopping secondary mirror was used with an 8° E-W throw to alternate between on-source and off-source positions at 2 Hz. The lack of significant distortion in the measured profiles, such as would be produced by strong emission in the reference beam from different velocity or linewidth components, indicates that the throw was adequate.

Absolute flux calibration was obtained from measurements of the Moon, for which a physical temperature of 394 K and an emissivity of 0.98 were assumed (Linsky 1973). The double-sideband measurement was corrected to a corresponding single-sideband value by using the unequal, but known, transmissions of both the aircraft pressure window and the atmosphere in the signal and image sidebands. The Moon is an appropriate source for intensity calibration for observations such as these where the spatial extent of the line emission encompasses both the main beam and inner sidelobes. A black-body source was used as a secondary standard throughout the observations to maintain the initial lunar calibration. The statistical and systematic uncertainty in the calibration arising from all sources except the unknown spatial distribution of the radiation within our beam is estimated to be no greater than 10%. The velocity scale is determined from the known line and LO frequencies, and is accurate to better than 0.4 km s^{-1} .

III. OBSERVATIONS

The data were obtained on the night of 1987 February 9, at four locations within the Orion complex: $15''$ west of $\theta^1\text{C}$ (hereafter referred to simply as $\theta^1\text{C}$), BN-KL, and $2'$ and $4'$ east of $\theta^1\text{C}$. Figure 1 shows the spectra obtained in the 40×5 MHz filterbank, with the position of the strongest hyperfine component of the ^{13}C II line indicated. The $^{13}\text{C}^+$ ion has nuclear-spin splitting of the fine-structure levels which leads to three emission components at velocities of 11.2, 63.2, and -65.2 km s $^{-1}$ relative to the ^{12}C II line center (Cooksy *et al.* 1986). The relative intensities of the three components are 0.44, 0.20, and 0.36, respectively. Table 1 lists various parameters measured from the spectra.

The continuum temperature was obtained from an average of the data in the 64×20 MHz filterbank excluding the channels containing the line and has been corrected to a SSB value. Previous measurements of the continuum by Werner *et al.*

(1976) show a maximum near (but not at) BN-KL, with $T_A^* = 4.5 \pm 1$ K (interpolated for $158 \mu\text{m}$) within a $1'$ beam. The continuum drops off sharply from the peak, and consequently the $10''$ - $15''$ uncertainty in our viewing direction may be responsible for the lower continuum temperature measured near BN-KL in the present set of observations. In the vicinity of $\theta^1\text{C}$, there is no corresponding discrepancy, probably because the emission is more uniform over a spatially extended ($> 1'$) region. Slight offsets in pointing will not materially affect the observed intensity of the C II line, since the fine-structure emission is much more extended than the continuum emission. However, because of this difference in spatial distributions, the line intensity estimates would not necessarily be accurate if they were derived solely from the line-to-continuum ratios, especially if the continuum intensity is derived from data obtained at a different spatial resolution.

The integrated line intensity has previously been measured at low spectral resolution to be $\sim 3.5 \times 10^{-3}$ ergs s $^{-1}$ cm $^{-2}$ sr $^{-1}$

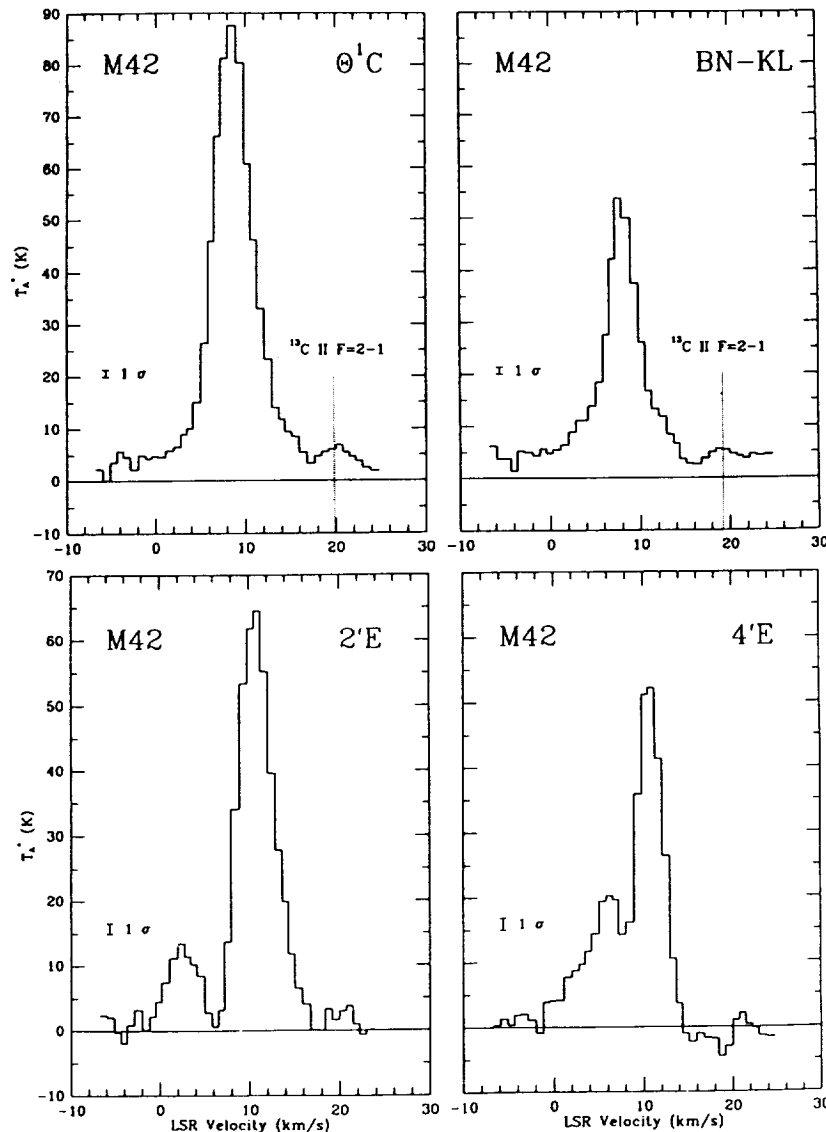


FIG. 1.—Spectra of the $^2P_{3/2} - ^2P_{1/2}$ line of C II at 0.8 km s $^{-1}$ resolution from four positions in M42. Integration times are 16 minutes for $\theta^1\text{C}$ and BN-KL, 12 minutes for $2'E$, and 8 minutes for $4'E$.

TABLE 1
OBSERVED C II LINE PARAMETERS

Position	V_{LSR} (km s^{-1})	Line Width (km s^{-1} , FWHM)	T_A^* (K)	T_b (K)	Integrated Intensity ($\text{ergs s}^{-1} \text{cm}^{-2} \text{sr}^{-1}$)	Continuum (K)
$^{12}\text{C II}$						
$\theta^1\text{C}$	8.59(0.05)	5.0(0.1)	87.7(1.2)	127.9(1.3)	$3.26(0.04) \times 10^{-3}$	1.70(0.08)
BN-KL	8.05(0.05) 8.01(0.15)	2.7(0.2) 7.5(0.6)	51.2(1.1)	89.2(1.2)	$1.64(0.05) \times 10^{-3}$	2.40(0.08)
2'E	10.79(0.05) 2.45(0.24)	4.5(0.1) 3.8(0.6)	64.1(1.8) 13.1(1.8)	103.1(1.9) 44.0(2.6)	$2.20(0.04) \times 10^{-3}$ $0.43(0.04) \times 10^{-3}$	0.39(0.10)
4'E	10.87(0.07) 5.76(0.42)	3.0(0.2) 6.7(0.9)	51.8(2.3) 19.9(2.3)	89.8(2.5) 53.0(2.9)	$2.03(0.05) \times 10^{-3}$	0.33(0.10)
$^{13}\text{C II } F = 2-1$						
$\theta^1\text{C}$	8.8(0.5)	3.3(1.2)	3.6(1.1)	27.9(2.7)	$7.6(2.5) \times 10^{-5}$	1.70(0.08)
BN-KL	8.0(0.8)	1.9(1.8)	1.8(1.6)	23.1(8.2)	$3.4(2.5) \times 10^{-5}$	2.40(0.08)

NOTES.—(1) T_A^* is corrected for the continuum. (2) The continuum values listed are corrected for transmission of the pressure window in each of the two infrared sidebands and represent the antenna temperature T_A^* of the continuum in each sideband. (3) Values in parentheses represent 1σ statistical uncertainties.

(Russell *et al.* 1980), for an assumed uniform beam over the $4' \times 8'$ field of view centered on the continuum peak. This value is larger than that derivable from the present data over an equivalent beamsize, if the C II line has its maximum intensity at the position of $\theta^1\text{C}$. Recently, Crawford *et al.* (1986) have reported an integrated intensity at the Trapezium of $5.5 \times 10^{-3} \text{ ergs s}^{-1} \text{ cm}^{-2} \text{ sr}^{-1}$. The data, shown by Lugten (1987), were obtained at 25 km s^{-1} resolution and calibrated using the line-to-continuum ratio. After deconvolving the instrumental response function from the C II data, Crawford *et al.* (1986) estimated the intrinsic linewidth to be $7 \pm 2 \text{ km s}^{-1}$, which is in reasonable agreement with the more precise value of $5.0 \pm 0.1 \text{ km s}^{-1}$ presented here.

The rest of the parameters given in Table 1 for $\theta^1\text{C}$ and BN-KL are derived from least-squares fitting of one or more Gaussian profiles to the data. The $^{12}\text{C II}$ profile in BN-KL shows clear evidence for two components with significantly different widths. These two components fit the data to within statistical uncertainties. The velocity and width for the two components are tabulated separately, but the amplitude and integrated intensity represent the combined values. Similarly, two components are evident in the spectra obtained 2' and 4' east of $\theta^1\text{C}$. For these data, the component centers and widths were obtained from the fits, while the T_A^* values represent measured peak values.

All of the parameters for the $F = 2-1$ $^{13}\text{C II}$ lines, with the exception of integrated intensity, were obtained from a fit to a Gaussian. The statistical significance of the lines was conservatively found to be 4σ and 1.3σ for $\theta^1\text{C}$ and BN-KL, respectively, from the ratio of signal to noise within a Gaussian filter having the same width and V_{LSR} as the $^{12}\text{C II}$ line, but centered at the expected location of a $^{13}\text{C II}$ component. The weaker $F = 1-1$ and $F = 1-0$ hyperfine components of the $^{13}\text{C II}$ line are not within the bandpass of the high-resolution filterbank, and were not detected in the wideband filterbank because of insufficient resolution and signal-to-noise ratio.

The identification of the weak detected features with $^{13}\text{C II}$ rests on several points. First, the location of the features relative to the $^{12}\text{C II}$ lines is correct and is fixed relative to the main lines rather than being at a common velocity for $\theta^1\text{C}$ and

BN-KL, as would be the case if they were due to a separate velocity component within the gas. Second, the width of the small line is approximately proportional to that of the associated $^{12}\text{C II}$ line, but is always less, as would be expected if the two lines were produced in the same gas, but one was broadened as a result of having significantly greater optical depth. Finally, the integrated intensity of the feature in the BN-KL spectrum is smaller than that in $\theta^1\text{C}$, following the behavior of the $^{12}\text{C II}$ line, which is consistent with the two regions having similar optical depths.

IV. ANALYSIS AND CONCLUSIONS

a) Optical Depth

The detection of $^{13}\text{C II}$ allows the optical depth in the $^{12}\text{C II}$ line to be determined, provided that the $F = 2-1$ $^{13}\text{C II}$ line is optically thin, and the $^{12}\text{C}/^{13}\text{C}$ isotopic ratio is known. The line center optical depths for the $\theta^1\text{C}$ and BN-KL positions are given in Table 2. The derived parameters are obtained from the data in Table 1 by using a value of 60 for the $^{12}\text{C}/^{13}\text{C}$ isotopic ratio (Wannier 1980), and 0.444 for the fractional intensity of the $F = 2-1$ $^{13}\text{C II}$ hyperfine component (Cooksey *et al.* 1986). The conclusion from our data is that the $^{12}\text{C II}$ line is definitely optically thick ($\tau = 5.6 \pm 1.7$) at line center for $\theta^1\text{C}$ and is likely to be thick for BN-KL as well. Our deduced values are somewhat higher than the previous upper limit ($\tau < 2$ [Crawford *et al.* 1986], revised to $\tau < 3[1\sigma]$ [Lugten 1987]) derived from the nondetection of either of the two most separated $^{13}\text{C II}$ hyperfine components. The optical depths quoted here, based on the detection of the $F = 2-1$ $^{13}\text{C II}$ hyperfine component, depend only on the ratio of observed antenna temperatures, and hence are insensitive to systematic

TABLE 2
DERIVED PHYSICAL PARAMETERS

Position	$\tau_{^{12}\text{C II}}$	T_{ex} (K)	N (cm^{-2})
$\theta^1\text{C}$	5.6	128	1×10^{19}
BN-KL	4.8	90	4×10^{18}

errors in calibration. The derived values for optical depth and column density depend approximately linearly on the isotopic ratio, while the excitation temperature is insensitive to this parameter.

Supporting evidence for our comparatively high value for the optical depth is provided by the relative linewidths of the $^{12}\text{C II}$ and $^{13}\text{C II}$ lines. The ratio of the apparent FWHM of a line with $\tau \approx 5$ to its intrinsic width is 1.7 for a Gaussian line originating in a homogeneous medium. This is comparable to the ratio of measured half-widths of the $^{12}\text{C II}$ and $^{13}\text{C II}$ lines (1.5 for $\theta^1\text{C}$ and 1.4 for BN-KL), as would be expected if the two lines originate in the same gas.

b) Excitation Temperature

Theoretical models of the Orion photodissociation region (e.g., Tielens and Hollenbach 1985) have generally concluded that the C II line is optically thin with an excitation temperature of at least 250 K. These two parameters are coupled, however, and cannot be determined simultaneously from measurements of a single C II line. However, because we estimate the line optical depth independently of the line intensity, the line excitation temperature can be calculated directly. In addition, because the critical density for the $^2P_{3/2} - ^2P_{1/2}$ transition is only $\sim 10^3 \text{ cm}^{-3}$, the level populations will likely have their equilibrium values, and the derived excitation temperature can be interpreted as the gas kinetic temperature. Our deduced values are listed in Table 2 for the positions noted. Because the $^{12}\text{C II}$ lines are optically thick, the uncertainty in excitation temperature is less than $\sim 10\%$ determined from the calibration accuracy. The temperatures are considerably lower than those previously assumed and appear to indicate that C II is more in equilibrium with the cooler molecular component than the warmer atomic gas in the ionization interface region. For comparison, Stacey (1985) calculates that the gas temperature in the photodissociation region is $\sim 350 \text{ K}$, based on the intensities of the $145 \mu\text{m O I}$ and $158 \mu\text{m C II}$ lines. However, the calculation assumed that both lines were optically thin. A lower gas temperature would be indicated if C II were taken to be optically thick. Perhaps a better estimate for the atomic gas temperature can be derived from the integrated intensity and estimated linewidth of the $63 \mu\text{m O I}$ line observed by Crawford *et al.* (1986). If the line is optically thick as suggested by Stacey (1985), then an excitation temperature of $180 \pm 40 \text{ K}$ is indicated, which is reasonably consistent with the C II results presented here.

Our analysis assumes that the C II emission fills the beam uniformly. Should the emission arise from discrete clumps that do not fill the beam, then the derived excitation temperature would represent only a lower limit. The optical depth within the clumps, however, would not change significantly since the beam filling factor would be expected to be the same for both the $^{12}\text{C II}$ and $^{13}\text{C II}$ lines.

c) Column Densities

Column densities for C II toward the $\theta^1\text{C}$ and BN-KL positions are listed in Table 2. For the $\theta^1\text{C}$ region, the value quoted is accurate to within 30%, limited by the statistical accuracy of T_A^* for the $^{13}\text{C II}$ line. Our C II column density of

$1 \times 10^{19} \text{ cm}^{-2}$ for $\theta^1\text{C}$ is about a factor of 3 higher than that obtained by Tielens and Hollenbach (1985) from simple physical considerations. In their calculation, photodissociation of CO and ionization of C to C^+ within the cloud proceed only to the UV penetration depth ($A_v \approx 4$), which is limited primarily by absorption by dust. For a standard H I column density of $1.9 \times 10^{21} \text{ cm}^{-2}$ per magnitude of extinction, and an assumed carbon fractional abundance of 4×10^{-4} , their calculated C II column density is $3 \times 10^{18} \text{ cm}^{-2}$. This value can be increased by changing the extinction properties of the dust or the dust-to-gas ratio. Also, the C II column density derived from observations will generally be higher, since the line of sight into a plane-parallel region will not necessarily be in the direction to the ionizing star, as assumed in the calculation.

d) Spatial and Velocity Structure

Our observations at four locations within the Orion complex are too few to provide much information on the spatial structure, other than to confirm the known fact that C II emission is extended over more than $4'$. Our high spectral resolution does give new data on the C II velocity structure, however. The spectra show evidence for four velocity components: 2.5, 5.8, 8.3, and 10.8 km s^{-1} . Our three strongest velocity components in C II are clearly seen in C^+ recombination lines at 6.1, 8.4, and 10.8 km s^{-1} , with widths of 4–5 km s^{-1} , comparable to those in the $^{12}\text{C II}$ line (Jaffe and Pankonin 1978). The much larger beamsize of 2.6 for the recombination line work, however, precludes making detailed lineshape or spatial comparisons. Nevertheless, the general agreement in component velocities supports the expectation that the recombination lines and the C II radiation arise from similar regions.

Another point of significance is that the spectrum of C II emission from BN-KL at $V_{\text{LSR}} = 8 \text{ km s}^{-1}$ shows evidence for a broad component with a linewidth of $\sim 7.5 \text{ km s}^{-1}$ in addition to the narrow 3.0 km s^{-1} linewidth component. This broad emission does not arise from the "hot core" component seen in NH_3 (Morris, Palmer, and Zuckerman 1980), although the linewidth is comparable, because the V_{LSR} of the ammonia emission is 5.2 km s^{-1} . Nor is it likely to arise from the shocked gas which is thought to produce the CO plateau emission and the broad (30–40 km s^{-1}) component of lines such as O I, since this C-type shock is nonionizing. Also, the profiles of lines produced by the shock generally show a blue asymmetry, while the present data show no asymmetry and only moderate wings. Nevertheless, the spectrum of BN-KL shows a different character than the other spectra obtained, and it would be informative to observe the emission from the wings of the C II line in more detail, and in particular to examine variations with position near BN-KL.

Our observations were made possible by the concerted effort of the operations staff of the Kuiper Airborne Observatory, and we thank them for their technical assistance. We also thank D. Goldhaber for help with the observations. R. T. B. acknowledges her postdoctoral fellowship award from the Natural Sciences and Engineering Research Council of Canada. These observations were supported by NASA grant NAG 2-254.

25
at
si-
of
to
ly
of
ed
II
ed
st-
r-
a
to

REFERENCES

Betz, A., and Zmuidzinis, J. 1984, in *Proc. Airborne Astronomy Symposium*, (NASA CP-2353), p. 320.
Cooksy, A. L., Blake, G. A., and Saykally, R. J. 1986, *Ap. J. (Letters)*, **305**, L89.
Crawford, M. K., Lugten, J. B., Fitelson, W., Genzel, R., and Melnick, G. 1986, *Ap. J. (Letters)*, **303**, L57.
Dalgarno, A., and McCray, R. A. 1972, *Ann. Rev. Astr. Ap.*, **10**, 375.
Jaffe, D. T., and Pankonin, V. 1978, *Ap. J.*, **226**, 869.
Kurtz, N. T., Smyers, S. D., Russell, R. W., Harwit, M., and Melnick, G. 1983, *Ap. J.*, **264**, 538.
Linsky, J. L. 1973, *Ap. J. Suppl.*, **25**, 163.
Lugten, J. B. 1987, Ph.D. thesis, University of California, Berkeley.
Melnick, G., Stacey, G. J., Viscuso, P. J., and Fuller, C. E. 1986, *Ap. J.*, **303**, 638.
Morris, M., Palmer, P., and Zuckerman, B. 1980, *Ap. J.*, **237**, 1.
Petersen, F. R., Scalabrin, A., and Evenson, K. M. 1980, *Int. J. Infrared Millimeter Waves*, **1**, 111.
Russell, R. W., Melnick, G., Gull, G. E., and Harwit, M. 1980, *Ap. J. (Letters)*, **240**, L99.
Russell, R. W., Melnick, G., Smyers, S. D., Kurtz, N. T., Gosnell, T. R., Harwit, M., and Werner, M. W. 1981, *Ap. J. (Letters)*, **250**, L35.
Stacey, G. J. 1985, Ph.D. thesis, Cornell University.
Tielens, A. G. G. M., and Hollenbach, D. 1985, *Ap. J.*, **291**, 747.
Wannier, P. G. 1980, *Ann. Rev. Astr. Ap.*, **18**, 399.
Watson, D. M. 1984, in *Galactic and Extragalactic Infrared Spectroscopy*, ed. M. F. Kessler and J. P. Phillips (Dordrecht: Reidel), p. 195.
Werner, M. W., Gatley, I., Harper, D. A., Becklin, E. E., Loewenstein, R. F., Telesco, C. M., and Thronson, H. A. 1976, *Ap. J.*, **204**, 420.

A. L. BETZ, R. T. BOREIKO, and J. ZMUIDZINAS: Space Sciences Laboratory, University of California, Berkeley, CA 94720

on
he
at
al
re,
n-
st
si-
m
in
on
or
in
n-
s.
II
or
li-
uis
nt
gh
ia
he
is-
as
of
y,
te
nt
be
II
ns

ort
cy,
so
B.
he
of
nt

NEUTRAL ATOMIC CARBON IN DENSE MOLECULAR CLOUDS

J. ZMUIDZINAS, A. L. BETZ, R. T. BOREIKO, AND D. M. GOLDBABER

Space Sciences Laboratory, University of California

Received 1988 March 21; accepted 1988 June 7

ABSTRACT

We have detected the $370 \mu\text{m } ^3P_2-^3P_1$ fine-structure line of neutral carbon (C I) in seven sources: OMC 1, NGC 2024, S140, W3, DR 21, M17, and W51. Simultaneous analysis of our $J = 2-1$ data and available observations of the $J = 1-0$ line allow us to deduce optical depths and excitation temperatures for these lines. These data indicate that both C I lines are likely to be optically thin, and that the ratio of C I to CO column densities in these clouds is typically ~ 0.1 . The $J = 2-1$ [C I] line in the Orion BN/KL region shows no definite signs of emission from broad high-velocity line wings, such as those seen in CO. A comparison of $J = 2-1$ [C I] and CO(2-1) spectra provides an upper limit of 0.12 for the C I/CO column density ratio in the high-velocity gas. This limit, while more restrictive than those previously derived, does not indicate a depletion of C I relative to CO in the high-velocity gas, given the results of our observations of quiescent clouds.

Subject headings: infrared: spectra — interstellar: abundances — interstellar: molecules — nebulae: general

1. INTRODUCTION

Neutral atomic carbon (C I) has two fine-structure transitions in its electronic ground state: the $^3P_2-^3P_1$ transition at 809.3432 GHz ($370.4145 \mu\text{m}$) and the $^3P_1-^3P_0$ transition at 492.1612 GHz ($609.1347 \mu\text{m}$) (Cooksy *et al.* 1986). Recent advances in receiver technology have made it possible to observe these lines, allowing the abundance and excitation of C I in dense portions of the interstellar medium to be studied. The detection of the $J = 1-0$ line in dense molecular clouds was first reported by Phillips *et al.* (1980); additional observations were presented by Phillips and Huggins (1981). This line has also been mapped in one dimension across two clouds (M17 and S140) which have edge-on H II region-molecular cloud interfaces (Keene *et al.* 1985), and in the Orion molecular cloud (OMC 1) which has a face-on interface (Phillips and Huggins 1981). The observed $J = 1-0$ intensities implied large lower limits to the C I column densities ($N_{\text{C I}} \sim 10^{18} \text{ cm}^{-2} \sim 0.1 N_{\text{CO}}$). Cloud chemistry models (Langer 1976a) predicted that C I should be abundant near the cloud surface due to the photodissociation of CO by interstellar ultraviolet radiation, but the predicted column densities were about one order of magnitude lower than those observed. In addition, the early time-dependent chemical models (Langer 1976b) predicted that all but a small fraction ($< 10^{-3}$) of C I initially present in the cloud interior would be converted to CO within 10^6 yr, a time scale which is short compared to cloud lifetime estimates. Later models were able to predict abundances more in line with C I observations (Graedel, Langer, and Frerking 1982; Tarafdar *et al.* 1985).

The $J = 1-0$ C I observations stimulated work on a number of models aimed at increasing the predicted amount of C I. A good review of these proposals is contained in Keene *et al.* (1985). As discussed in this review, the models fall into two general categories: (1) those which increase the C I produced in the photodissociation region near the cloud surfaces, such as the model described by Tielens and Hollenbach (1985a, b), and (2) those which increase the amount of carbon in the cloud interior, either through changes in the chemical network, through the production of UV photons in the cloud interior, through the sputtering of carbon from dust grains due to the

passage of shock waves, or through an increase in the assumed C/O abundance. The observations of Keene *et al.* (1985) seem to rule out case (1) models, since the 492 GHz [C I] emission appears to be widespread throughout the clouds M17 and S140, and not localized near the interfaces between the molecular clouds and their associated H II regions (the interfaces are nearly perpendicular to the plane of the sky). On the other hand, UV photodissociation may be responsible for C I emission throughout the clouds if interior sources of UV radiation are available. For example, Stutzki *et al.* (1988) observe widespread low-level $158 \mu\text{m}$ [C II] emission in M17, as well as a peak near the interface region. In one interpretation, the extended [C II] emission component is a result of the UV radiation produced by a number of B-stars embedded in a clumpy cloud. The presence of C II directly demonstrates the presence of UV radiation, regardless of its source, and Stutzki *et al.* conclude that this UV could also be responsible for the extended [C I] emission observed.

Only lower limits to the C I column densities can be derived from [C I] 492 GHz observations alone, since the optical depth (and hence the excitation temperature) of the line is unknown, unless other assumptions are made. Phillips and Huggins (1981) have suggested that the optical depth of the $1-0$ line for OMC-1 is $\tau_{10} \sim 25$, based on a comparison of [C I] and CO line widths, which implies that the C I excitation temperature is $T_x \sim 21$ K if the emission is spatially uniform. The resulting column density is $N_{\text{C I}} \sim 3.5 \times 10^{19} \text{ cm}^{-2}$ which gives $N_{\text{C I}}/N_{\text{CO}} \sim 0.7$. This large value is very difficult to understand theoretically, and almost certainly rules out models in which the C I is produced only in photodissociation regions. Alternatively, the C I column density and excitation temperature may be obtained directly by combining observations of both the $J = 2-1$ and $J = 1-0$ transitions, if the C I emission region does not have substantial temperature gradients.

The $^3P_2-^3P_1$ line was first detected by Jaffe *et al.* (1985) from ground-based observations of OMC 1. Unfortunately, large systematic and statistical uncertainties prevented Jaffe *et al.* from drawing firm conclusions from their data. To improve this situation, we have observed the $2-1$ line with higher sensitivity in OMC 1 and six other clouds for which $1-0$ data were

available, and have used the results from both lines to derive estimates for the line excitation temperatures and optical depths. Some of our results have already been presented (Zmuidzinas, Betz, and Goldhaber 1986, hereafter ZBG); here we extend that preliminary effort with an analysis of new $J = 2-1$ data for the sources OMC 1, NGC 2024, and S140, together with improved data for W3 and DR 21. In the tables that follow we have included our earlier results on W51 and M17 for completeness.

II. 809 GHz OBSERVATIONS

a) Procedure

Observations of the 809 GHz $^3P_2-^3P_1$ line of C I were performed over two flight series on the NASA Kuiper Airborne Observatory (KAO) at an altitude of 41,000 feet using our laser heterodyne spectrometer. The observational procedure and technical details of the 1985 flights have been described by ZBG. For the second series in 1986 September, both the mixer and the intermediate-frequency (IF) amplifier were cooled to 77 K, which reduced the system noise temperature to 10,000 K (SSB). The mixer is a GaAs Schottky-diode in a corner-reflector mount, and the local oscillator (LO) is an optically pumped $^{15}\text{NH}_3$ laser. The fixed LO frequency is 802.986 GHz, which is offset 6.3 GHz from the $J = 2-1$ C I line.

A filterbank with 40 5-MHz channels provided a velocity resolution of 1.85 km s^{-1} over an interval of 74 km s^{-1} . For the 1986 flights, a 64×20 MHz filterbank was used simultaneously to provide a wide view of the spectrum over 474 km s^{-1} at a resolution of 7.4 km s^{-1} . The chopping secondary of the telescope was switched at 2 Hz with a 7' throw. The absolute calibration was derived from raster scans of the telescope beam across Jupiter (see § III). These measurements also provided the beam size ($80''$ FWHM; corrected for the partially resolved Jupiter), the net main beam coupling efficiency ($\eta_{\text{MB}} = 0.3$), and the instrument boresight (to $15''$). The net coupling efficiency includes losses due to spillover, the central blockage, sidelobes, the pressure-window transmission (80%), and the deviation of the chopper waveform from a square wave. These individual contributions to the measured net coupling efficiency are common to observations of all the sources, and are not separable in the data presented here. Jupiter was assumed to have a uniform elliptical intensity distribution with major and minor axes of $45'' \times 48''$ for the 1985 flights, and $46'' \times 49''$ for the 1986 flights. The brightness temperature of Jupiter at $370 \mu\text{m}$ was taken to be 160 K (Hildebrand *et al.* 1985).

b) Sources of Systematic Uncertainty

The largest source of uncertainty for airborne observations is the source coupling, which quantifies how well the astronomical source fills the telescope antenna pattern. The source coupling differs for the $J = 2-1$ and $J = 1-0$ observations, because the telescope beamwidth is 3' for the 492 GHz observations and 1.5' for the 809 GHz observations, and the sources are usually comparable in size ($3'-10'$) to the beams. Furthermore, a calculation of the source coupling efficiency requires knowledge of the entire telescope antenna pattern, including sidelobes, as well the spatial intensity distribution of the astronomical source. This information is generally not available, so educated guesses must be made, as is discussed in § III. The source coupling uncertainty can be removed if both telescope beams are small enough that the source can be reason-

ably assumed to have a uniform intensity over the beam areas, but this will require larger airborne or space-based telescopes.

Atmospheric transmission is not a source of systematic uncertainty in airborne observations of C I, because the transmission in both sidebands is essentially perfect. This is in contrast to the situation for ground-based observations at both 492 and 809 GHz. Even at the 4.2 km altitude of the best mountain sites such as Mauna Kea, the transmission at these frequencies is usually less than 30%, and variability on the time scale of hours can be large. Consequently, calibration is more difficult than it is in airborne work. The 492 GHz C I observations of Phillips and Huggins (1981) with which we compare our 809 GHz data were performed on the KAO and likewise do not suffer from atmospheric transmission uncertainties.

c) Results

Figures 1a through 1d show our results on the C I $^3P_2-^3P_1$ line from observations of OMC 1, NGC 2024, W3, and S140 done in 1986 September. For comparison, spectra of the corresponding 1-0 line at 492 GHz taken from Phillips and Huggins (1981) are also plotted. Three positions in DR21 were also observed, and the results are shown in Figure 2, along with a map of the $^{12}\text{C}^{16}\text{O}(1-0)$ integrated intensity labeled with the observed positions. No baseline corrections or smoothing were applied to the 1986 data. Whenever possible, the positions observed were chosen to match those of the 1-0 observations. Our 1985 July results on the 2-1 line in W51, M17, W3, and DR21 are shown in ZBG. The C I line centers, widths (FWHM), peak temperatures and their uncertainties are listed in Table 1 for both transitions. In most cases, these parameters were deduced from Gaussian fits to the data for both transitions. For W3 and DR 21(OH) (position 1 in Fig. 2), we list the 1986 results only since these data are of higher quality, although the 1985 data are consistent within the uncertainties. The velocity scale for the [C I] 1-0 data presented by Phillips and Huggins (1981) was based on a transition frequency of 492.1623 GHz, as measured by Saykally and Evenson (1980). Since then, this frequency has been revised to 492.1612 GHz by Cooksy *et al.* (1986), which corresponds to a velocity shift of 0.7 km s^{-1} . A discrepancy between CO and [C I] velocities in astronomical sources of about this magnitude was also noticed by Phillips *et al.* (1980). Therefore, we have shifted the spectra of Phillips and Huggins (1981) by -0.7 km s^{-1} . This shift is incorporated in the line parameters presented in Table 1 as well as in the spectra plotted in Figures 1 and 2. Data taken from Keene *et al.* (1985) were not shifted because they already incorporate a velocity correction. In most cases, the line centers and widths agree reasonably well. The substantially different line widths for W3 may be due to beamsize effects since CO maps show that W3 has a complex velocity structure (Brackmann and Scoville 1980).

The accuracy of the Doppler velocity scale for our $J = 2-1$ data depends on both the laboratory measurement of the C I line and our knowledge of the laser LO frequency. The statistical accuracy of the $^3P_2-^3P_1$ rest frequency measurement is 1 MHz at the 99.95% (3.5σ) confidence limit (A. Cooksy 1988, private communication), and the systematic uncertainty is 0.3 MHz at the same confidence level (K. Evenson 1988, private communication). Our laboratory measurement of the $^{15}\text{NH}_3$ laser frequency is $802.9860 \pm 0.0005 \text{ GHz}$. Were the laser to be mistuned, its output frequency could differ by as much as 2 or 3 MHz from the value quoted above. We are careful, however, to

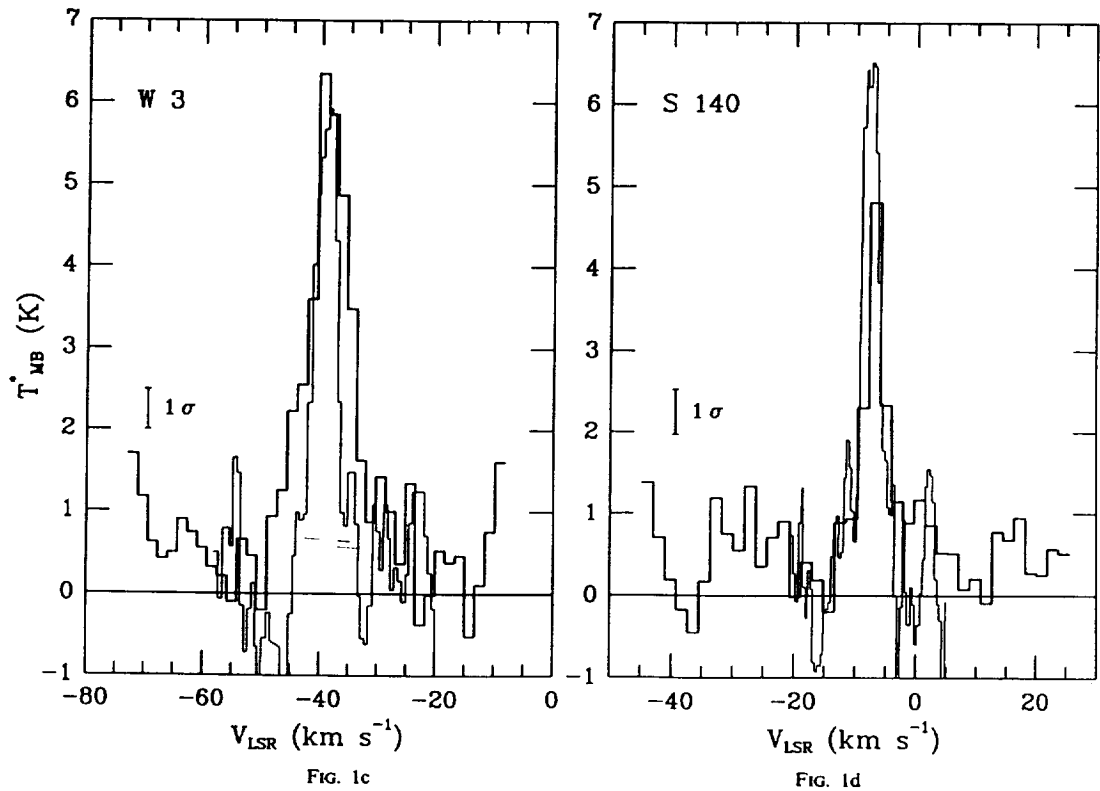
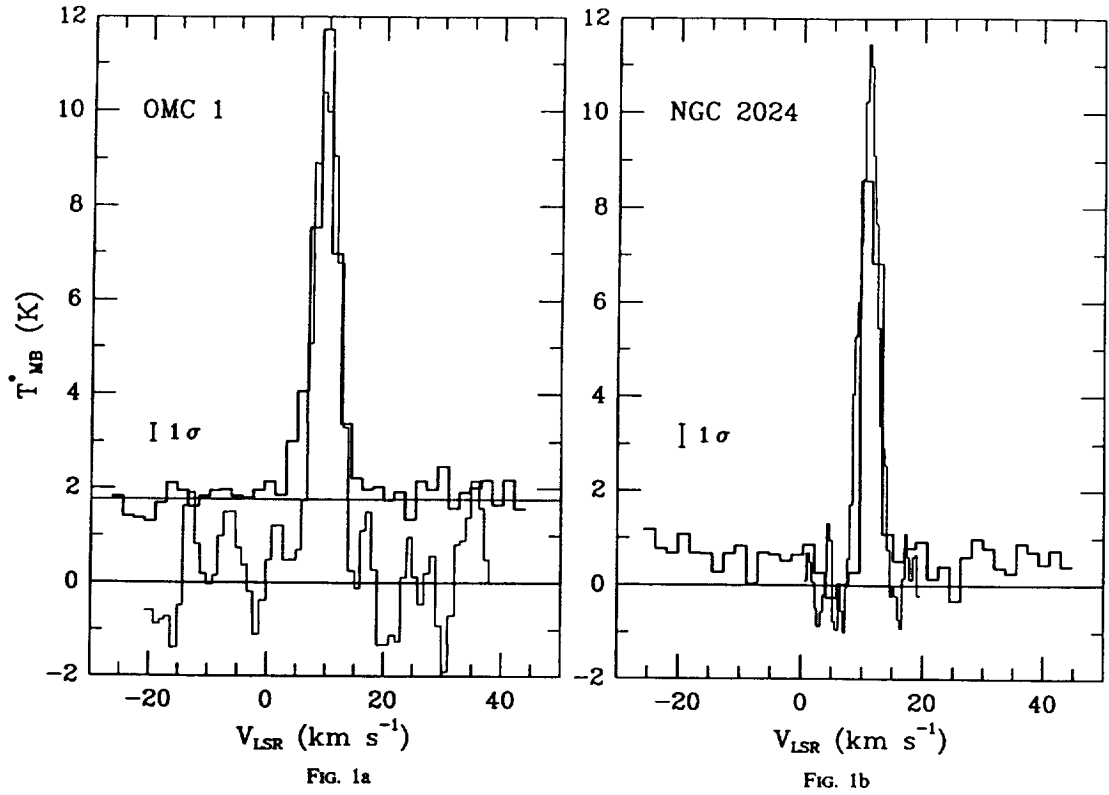


FIG. 1.—809 GHz $[C\ I] \ ^3P_2-^3P_1$ emission (*heavy line*) observed toward (a) OMC 1, integration time of 60 minutes; (b) NGC 2024, integration time of 32 minutes; (c) W3, integration time of 32 minutes; and (d) S140, integration time of 26 minutes. The $^3P_1-^3P_0$ data (*light line*) of Phillips and Huggins (1981) are also shown. The 2-1 data were obtained in 1986 September. The dotted line in (a) shows the expected $370\ \mu\text{m}$ continuum emission in a $90''$ beam (Keene, Hildebrand, and Whitcomb 1982) corrected for the dewar window transmission in each sideband. Statistical uncertainties of $1\ \sigma$ are shown for the $^3P_2-^3P_1$ data only.

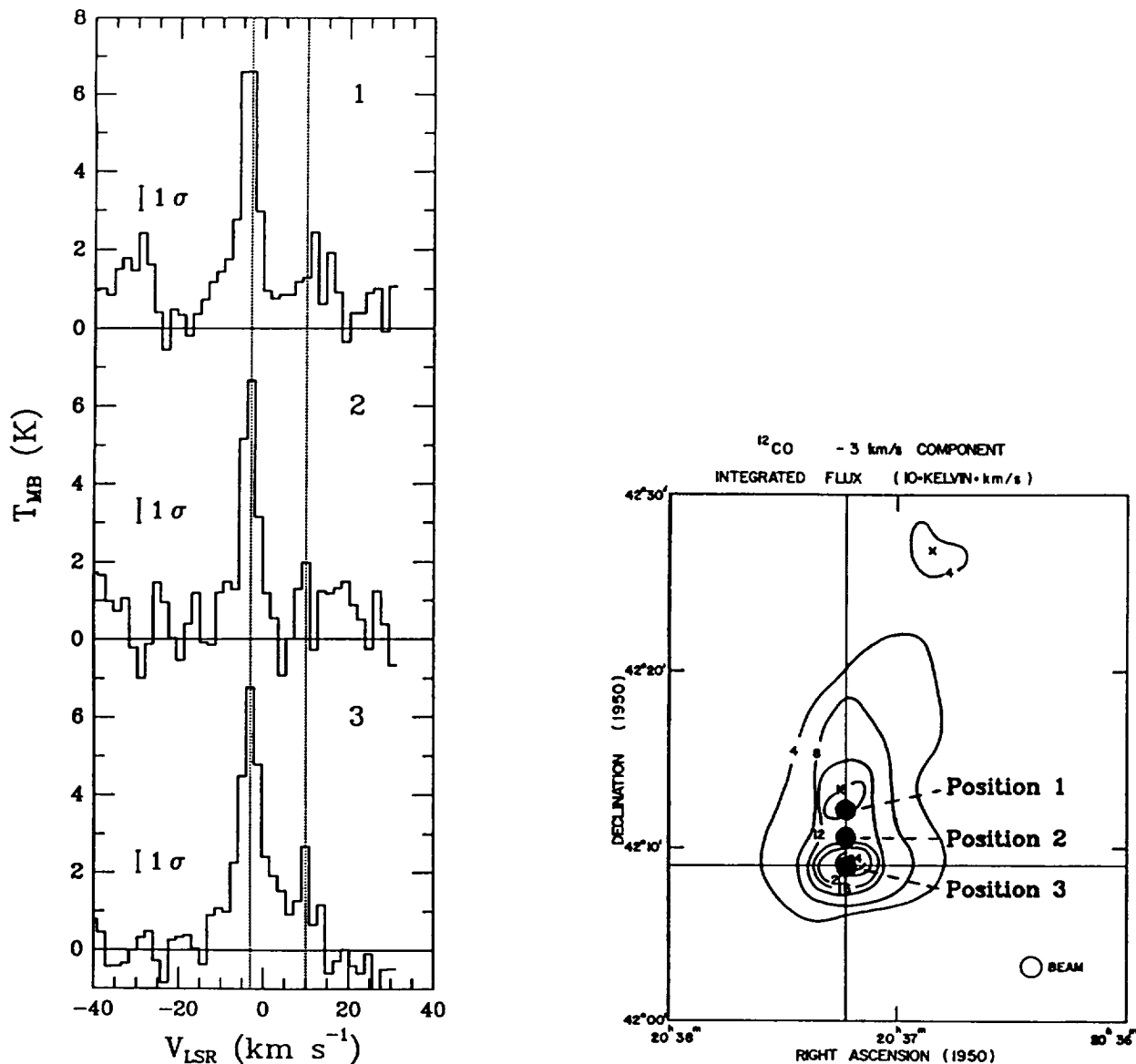


FIG. 2.—809 GHz [C I] $^3P_2-^3P_1$ emission observed toward three locations in DR21. Integration times are 20 minutes for position 1 [DR21(OH)] and position 2 and 24 minutes for position 3. Also shown is a map of the CO(1-0) integrated intensity (Dickel, Dickel, and Wilson 1978) labeled at the observed positions with dark circles, which indicate the beam size of the [C I] 2-1 observations. Dotted lines are drawn at -3 and $+10$ km s^{-1} where microwave emission from CO is observed.

keep the laser cavity tuned to the peak of the power output curve, and consequently our uncertainty is the 0.5 MHz value quoted above. The total 2σ uncertainty in the frequency accuracy of our C I observations is 1.7 MHz, which corresponds to a conservative velocity scale accuracy of 0.65 km s^{-1} . From the difference between the C I and LO frequencies, we get an IF center frequency of 6.3 GHz.

III. CALIBRATION AND SOURCE COUPLING

If the [C I] emitting region is hot ($kT_x \gg h\nu_{21}$; here T_x is the [C I] excitation temperature), optically thin, and sufficiently dense for the transitions to be thermalized, then the 2-1 line will be twice as bright (in temperature units) as the 1-0 line. If the gas is cool ($T_x \sim 20$ K) and optically thick, the 2-1 line will be about half as bright. Given this limited dynamic range, it is important to consider the effects of systematic calibration errors (such as source coupling) on the line intensities prior to

deriving excitation temperatures and optical depths. For this reason, we will present a detailed discussion of calibration procedures and their implications for source coupling.

In general, we can express the signal power per unit bandwidth incident on the receiver in one polarization from the astronomical source as (Kutner and Ulich 1981):

$$S_r = \eta_c k T_R \frac{\int d\Omega P_n(\Omega) B(\Omega)}{\Omega_A}, \quad (1)$$

where $P_n(\Omega)$ is the normalized telescope beam pattern [$P_n(0) = 1$], $B(\Omega)$ is the normalized spatial intensity distribution of the source [$B(0) = 1$], T_R is the peak Rayleigh-Jeans radiation temperature of the source ($I = 2kT_R/\lambda^2$ is the peak specific intensity), η_c is the net telescope coupling efficiency, and Ω_A is the antenna solid angle $\int d\Omega P_n(\Omega)$. The beam pattern $P_n(\Omega)$ is usually axially symmetric and consists of a central main beam

TABLE 1
C I LINE PARAMETERS

Source	$T_{MB}(2-1)$ (K)	$T_A^*(1-0)$ (K)	$V_{LSR}(2-1)$ (km s ⁻¹)	$V_{LSR}(1-0)$ (km s ⁻¹)	$\Delta V(2-1)$ (km s ⁻¹)	$\Delta V(1-0)$ (km s ⁻¹)
OMC 1	9.7 ± 0.4	11.7 ± 0.7	9.6 ± 0.1	9.9 ± 0.1	4.3 ± 0.2	4.6 ± 0.4
NGC 2024 ^a	8.8 ± 0.5	11.1 ± 0.3	11.3 ± 0.1	10.5 ± 0.1	3.4	3.4 ± 0.1
W3	5.5 ± 0.4	6.2 ± 0.4	-38.5 ± 0.3	-39.7 ± 0.1	8.0 ± 0.6	4.3 ± 0.3
S140 ^b	4.5 ± 0.5	4.1	-6.8 ± 0.2	-7.2	3.3 ± 0.4	2.6
W51	8.9 ± 1.0	8.0 ± 0.2	57.5 ± 1.0	58.5 ± 0.3	16.0 ± 2.2	18.8 ± 0.8
M17 ^b	12.9 ± 1.3	11.0	19.6 ± 0.7	20.5	6.7 ± 0.8	6.4
DR 21(OH) ^c	6.7 ± 0.7	6.5	-3.9 ± 0.2	...	4.1 ± 0.5	5.0

^a The 2-1 line width cannot be determined unambiguously since emission was observed in two channels only; hence, the 1-0 width was assumed.

^b The 1-0 line parameters were taken from Keene *et al.* 1985 and were *not* deduced from the fit, so no uncertainties are listed. This more recent data for the 1-0 line in S140 supercedes the earlier results of Phillips and Huggins shown in Fig. 1. In reference to the Keene *et al.* 1985 observations, the position for S140 corresponds to the one labeled 0.0, while that for M17 is labeled -1.3

^c 1-0 parameters from J. Keene (1986, private communication).

NOTE.—The quoted uncertainties are ± 1 σ. These uncertainties represent receiver noise only; systematic errors in the intensity calibrations and the velocity scales are not included. In most cases, 1-0 line parameters were derived from our fits to the data presented by Phillips and Huggins 1981, taking into account the Hanning smoothing of their spectra. These spectra were shifted by -0.7 km s⁻¹ prior to fitting (*see text*).

and concentric sidelobes, and can be calculated if the telescope illumination is known (Goldsmith 1987). These calculations show that for reasonable choices of illumination of the KAO telescope, the main beam solid angle Ω_M is typically 80%–85% of the total, or

$$\frac{\Omega_M}{\Omega_A} = \frac{\int_{\text{main beam}} d\Omega P_n(\Omega)}{\int_{\text{all lobes}} d\Omega P_n(\Omega)} \sim 0.8. \quad (2)$$

Measurements of the Moon (to obtain Ω_M) and Jupiter (to obtain Ω_M) at 492 GHz (J. Keene 1986, private communication) give reasonable agreement with equation (2). At 809 GHz we only have measurements on Jupiter and so cannot calculate the main-beam efficiency independently of our other coupling factors. It should be emphasized that the KAO telescope is of optical quality, so that calculated beam shapes are expected to be accurate.

Calibration involves measuring the signal power received from a source for which both T_R and $B(\Omega)$ are known, and then using the results to estimate T_A^* for an astronomical source from the signal power received. For example, the 1-0 data are calibrated using the Moon. The intensity distribution of the Moon is fairly constant over the entire telescope beam [$B(\Omega) = 1$], so $S_A(\text{Moon}) = \eta_c k T_R(\text{Moon})$. The antenna temperature T_A^* is then defined in terms of known quantities as the ratio of the power received from the astronomical source to the power received from the Moon, multiplied by the radiation temperature of the Moon:

$$T_A^* = \frac{S_r}{S_A(\text{Moon})} T_R(\text{Moon}) = \frac{\int d\Omega P_n(\Omega) B(\Omega)}{\Omega_A} T_R \equiv \eta_{1-0} T_R, \quad (3)$$

where the source coupling efficiency η_{1-0} for the 1-0 observations has been defined as

$$\eta_{1-0} = \frac{\int d\Omega P_{1-0}(\Omega) B(\Omega)}{\Omega_A}. \quad (4)$$

If the source is large enough to fill the telescope beam including all sidelobes uniformly, then $\eta_{1-0} = 1$. In the usual case, the source does not fill the beam completely, and $\eta_{1-0} < 1$.

The 2-1 data were calibrated using Jupiter. Since Jupiter is not large enough to fill the main lobe of the telescope beam, the telescope beam must be mapped on Jupiter to deduce the signal that would have been measured on a source large enough to fill the main lobe. Measuring sidelobe patterns with this technique is not feasible given the signal-to-noise ratio and the limited flight time. The beam was mapped on a 7 × 6 grid with a spacing of 20" and an integration time of 15 s per point. The data are corrected using an optimal filtering technique for the finite settling time of the lock-in amplifier which measures the signal and are then fitted to a two-dimensional Gaussian profile whose center, amplitude S_0 , major and minor 1/e widths w_1 and w_2 , and orientation of the principal axes are free parameters. The statistical uncertainty in these parameters is less than a few percent and is a negligible source of error in the calibration procedure. The results indicate that the beam is asymmetric, with one width ~20% less than the other. Since the direction of the chop coincides almost exactly with the direction in which the beam is broadened, "ringing" of the chopping secondary is most likely the source of this asymmetry. The beam asymmetry does not affect the calibration since the total power in the beam is unchanged. It does, however, affect the source coupling to some degree, but is not likely to be important since the sources are at least a factor of 2 larger than our beam.

The main lobe solid angle is determined from the measured scan using

$$\eta_c k \frac{\Omega_M}{\Omega_A} = \frac{S_0 w_1 w_2}{T_R(\text{Jup}) ab}, \quad (5)$$

where a and b are the major and minor semidiameters of Jupiter (Zmuidzinas 1987). $T_R(\text{Jup})$ is calculated to be 141 K by assuming that Jupiter radiates like a 160 K blackbody at 370 μm (Hildebrand *et al.* 1985).

Calibration of the $J = 2-1$ main beam line intensities consists of dividing the power received (eq. [1]) by $\eta_c k \Omega_M / \Omega_A$ (eq. [5]):

$$T_{MB} = T_R \frac{\int d\Omega P_{2-1}(\Omega) B(\Omega)}{\Omega_M} \equiv \eta_{2-1} T_R. \quad (6)$$

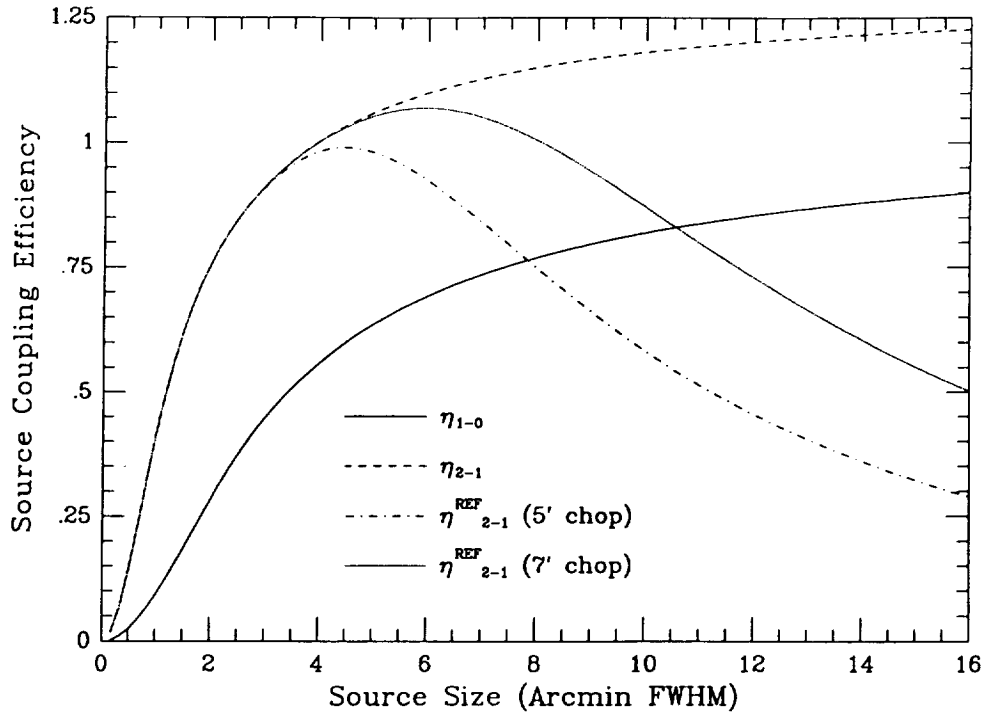


FIG. 3.—Solid line: source coupling efficiency η_{1-0} for the 1-0 observations as a function of source size. Dashed line: source coupling efficiency η_{2-1} for the 2-1 observations. Dot-dashed line: η_{2-1} corrected for emission in the reference beam for a 5' chopper throw. Dotted line: η_{2-1} corrected for a 7' throw.

The last equality defines the source coupling efficiency for the 2-1 observations, η_{2-1} . For a source which completely fills the main beam uniformly but does not fill any sidelobes $\eta_{2-1} = 1$. For a source which fills the main beam as well as some sidelobes, $\eta_{2-1} > 1$, since only the power in the main beam is used in the calibration. Both η_{1-0} and η_{2-1} were calculated using theoretical telescope beam patterns and sources with a Gaussian intensity distribution. The results are plotted in Figure 3 as a function of source size. As can be seen in this figure, the chosen illumination produces a main beam containing 80% of the total radiated power ($\eta_{2-1} \rightarrow 1.25$ for large sources). For large source sizes, emission in the reference beams of the 2-1 observations must also be considered, since this emission reduces the apparent line intensity. Therefore, we calculate η_{2-1} corrected for emission in the reference beams (again assuming a Gaussian intensity distribution) and plot the results in Figure 3 for the 5' and 7' chopper throws used in the 1985 and 1986 observations, respectively.

IV. MODEL CALCULATIONS: UNIFORM EMISSION REGION

a) Density Required for Thermal Equilibrium

The A-coefficients and collisional de-excitation rates ($\gamma_{ji} = \langle \sigma_{ji} v \rangle$ for collisions with H atoms) for the 3P transitions of C I are listed in Table 2, along with the critical densities (the densities for which collisional and radiative rates are equal: $n_{cr} = A_{ji}/\gamma_{ji}$). The line intensities produced from a uniform emission region in which the levels are populated according to thermal equilibrium are easily calculated. These intensities depend only on the temperature and the C I abundance, so a measurement of both line intensities in principle provides sufficient information to determine these parameters. The assumption of equilibrium implies that we are considering regions with densities of $n(H_2) \geq 10^4 \text{ cm}^{-3}$, larger than the critical density of either transition. Zmuidzinas (1987) discusses this point in more

detail, including the suggestion of Monteiro and Flower (1987) that the collision rate of the 1-0 transition could be smaller by more than one order of magnitude as compared to the 2-1 and 2-0 transitions for collisions involving He or H₂. The conclusion is that deviations from thermal equilibrium line intensity ratios only become significant for densities less than $2-3 \times 10^4 \text{ cm}^{-3}$.

Densities greater than 10^4 cm^{-3} are not considered to be large for the regions we observed near the dense cores of molecular clouds. Studies of CS rotational transitions in M17, S140, and NGC 2024 (Snell *et al.* 1984a) have shown that average H₂ densities of $5 \times 10^5 - 10^6 \text{ cm}^{-3}$ are common in the cores of molecular clouds. These densities are derived from LVG (large velocity gradient) excitation models and are quite uniform over regions with sizes of 4'-6'. The CS column densities, on the other hand, are smaller by one order of magnitude at the edges than at the centers of the regions observed. This suggests that the clouds consist of high-density clumps interspersed with lower density gas, and that the beam filling factor of these clumps varies from ~ 1 near the centers to ~ 0.1 at the edges, for the 1' beam used in these observations. Similar multi-

TABLE 2
C I TRANSITION DATA

LEVEL		A_{ji} (s^{-1})	$\gamma_{ji} = aT^b \text{ cm}^3 \text{ s}^{-1}$		$n_{cr}(T = 50 \text{ K})$ (cm^{-3})
<i>j</i>	<i>i</i>		<i>a</i>	<i>b</i>	
3P_1	3P_0	7.93×10^{-8}	1.3×10^{-10}	0.045	5.1×10^2
3P_2	3P_1	2.68×10^{-7}	7.8×10^{-11}	0.035	3.0×10^3
3P_2	3P_0	2.0×10^{-14}	2.0×10^{-10}	0.084	...

NOTE.—A-coefficients are from Nussbaumer 1971. The collisional rates are due to Launay and Roueff 1977, as parameterized by Tielens and Hollenbach 1985a.

transition studies of H_2CO (Mundy *et al.* 1987) indicate the presence of an additional component of gas with a density of $\geq 10^4 \text{ cm}^{-3}$, which is likely to be foreground or interclump gas. These conclusions are supported by submillimeter dust continuum measurements, which indicate average core densities of $\geq 10^5 \text{ cm}^{-3}$ (OMC 1: Keene, Hildebrand, and Whitcomb 1982; W3: Jaffe *et al.* 1983; W51: Jaffe, Becklin, and Hildebrand 1984; see also Schloerb, Snell, and Schwartz 1987).

Large densities are also likely if the $[\text{C I}]$ emission arises in photodissociation regions, given the strong $[\text{O I}]$ 63 μm and 145 μm lines observed in the photodissociation regions of several clouds (Crawford *et al.* 1986; Genzel and Stacey 1985). The large critical densities of these lines ($> 10^5 \text{ cm}^{-3}$) combined with their large intensities indicate hydrogen densities of $\sim 10^5 \text{ cm}^{-3}$ for these regions (Stacey 1985), provided that the optical depths are not too large.

b) Methodology

The line radiation temperature emitted by a region of uniform excitation temperature is given by the usual formula:

$$T_{\text{R}}(j-i) = \frac{hv/k}{e^{hv/kT_x} - 1} (1 - e^{-\tau_{ij}}). \quad (7)$$

Under the assumption that the levels are thermally populated with an excitation temperature T_x , the ratio of the 1-0 and 2-1 optical depths is given by

$$\rho(T_x) = \frac{\tau_{21}}{\tau_{10}} = 1.28 \exp\left(\frac{-23.6}{T_x}\right) \frac{1 - \exp(-38.8/T_x)}{1 - \exp(-23.6/T_x)}. \quad (8)$$

This ratio is plotted in Figure 4. From this figure, we can see that $\tau_{21} \leq \tau_{10}$ for $T_x \leq 50 \text{ K}$, while $\tau_{21} \geq \tau_{10}$ for $T_x \geq 50 \text{ K}$. This ratio approaches the limiting value of 2.1 for large temperatures. Thus, given T_x and τ_{10} , we can calculate τ_{21} from

equation (8) and both line intensities from equation (7). In most cases, this procedure is invertible. That is, if we are given the intensities $T_{\text{R}}(1-0)$ and $T_{\text{R}}(2-1)$ at the line center velocity V_0 , we can find the corresponding values of T_x and τ_{10} . However, there are cases for which two solutions (T_x, τ_{10}) exist, as well as cases for which no solutions exist. These situations as well as the effects of finite measurement uncertainties are discussed in depth by Zmuidzinas (1987). If T_x and τ_{10} are known, the column density can be calculated from

$$N_{\text{C I}} = 0.47\tau_{10}(V_0)\Delta V \frac{f(T_x)}{1 - \exp(-23.6/kT_x)}, \quad (9)$$

where $N_{\text{C I}}$ is in units of 10^{17} cm^{-2} and ΔV is the equivalent width of the velocity distribution in km s^{-1} . For a Gaussian profile, the equivalent width ΔV is given in terms of the full width to half-maximum ΔV_{FWHM} by $\Delta V = [\pi/(4 \ln 2)]^{1/2} \Delta V_{\text{FWHM}} = 1.06 \Delta V_{\text{FWHM}}$. We will generally ignore the distinction between ΔV and ΔV_{FWHM} . Also, we do not perform opacity corrections on the measured line widths, since such corrections are generally small.

V. EXCITATION TEMPERATURES AND OPTICAL DEPTHS

As in ZBG, we derive T_x and τ_{10} for three sets of line intensities. The first set (A) is given by $T_{\text{R}}(1-0) = T_x^*(1-0)$ and $T_{\text{R}}(2-1) = T_{\text{MB}}(2-1)$. For this oversimplified case, we use the line intensities exactly as they are given in Table 1 and perform no corrections for beam filling effects. The resulting values of T_x and τ_{10} are listed in Table 3, along with 95% confidence lower limits for T_x and upper limits for τ_{10} . These limits are based on the statistical uncertainties of the line intensities as listed in Table 1. The method with which these confidence limits were derived is discussed by Zmuidzinas (1987). In cases for which

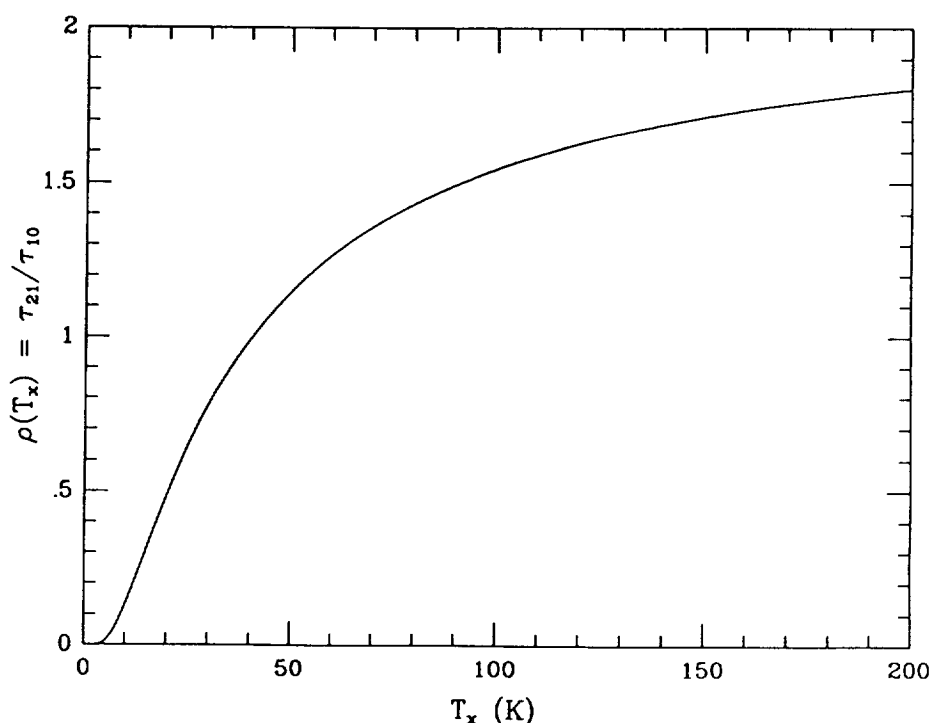


FIG. 4.—Ratio of $[\text{C I}]$ optical depths as a function of excitation temperature

TABLE 3
 OPTICAL DEPTHS AND EXCITATION TEMPERATURES

Source	(A) UNCORRECTED ^a				(B) CORRECTED ^b				(C) CORRECTED ^c				θ_s^f
	T_x	T_{LL}^d	τ_{10}	τ_{UL}^e	T_x	T_{LL}^d	τ_{10}	τ_{UL}^e	T_x	T_{LL}^d	τ_{10}	τ_{UL}^e	
OMC 1	42.	36.	0.47	0.69	27.	22.	1.6	>2	77.	62.	0.23	0.33	14.
NGC 2024	40.	35.	0.48	0.63	25.	22.	1.3	>2	71.	59.	0.24	0.32	~14
W3	45.	38.	0.11	0.16	25.	21.	1.25	>2	25.	21.	1.25	>2	3.5
S140	61.	42.	0.09	0.17
W51	64.	47.	0.17	0.25	37.	21.	0.51	0.81	64.	46.	0.22	0.37	7.8
M17	72.	53.	0.20	0.31	36.	26.	0.95	>2	48.	36.	0.56	0.91	6.2
DR 21(OH)	56.	40.	0.16	0.29	29.	19.	0.60	1.7	32.	19.	0.55	1.4	6.

^a Derived from measured line intensities with no correction for source coupling effects.

^b Corrected for source coupling only using a source size of θ_s .

^c Corrected for source coupling and reference beam emission using a source size of θ_s .

^d Lower limit for T_x (95% confidence level).

^e Upper limit for τ_{10} (95% confidence level).

^f θ_s is either the [C I] or $^{12}\text{CO}(1-0)$ source size (FWHM arcmin). The sizes are from Phillips and Huggins 1981 ([C I] in OMC 1); Kutner *et al.* 1977 (CO in NGC 2024); Brackman and Scoville 1980 (CO in W3); Mufson and Liszt 1979 (CO in W51); Keene *et al.* 1985 ([C I] in M17); and Dickel, Dickel, and Wilson 1978 (CO in DR 21).

the 1-0 uncertainty was not available, the 2-1 and 1-0 intensities were assumed to have equal uncertainty.

The second set (B) is given by $T_R(1-0) = T_x^*(1-0)/\eta_{1-0}$ and $T_R(2-1) = T_{MB}(2-1)/\eta_{2-1}$. The resulting values of T_x and τ_{10} , as well as the source sizes used in estimating the source coupling coefficients, are listed in Table 3 (see also Fig. 3) and are derived from maps of $J = 1-0$ ^{12}CO emission, except in cases for which the [C I] source size is known (OMC1; M17). Scans of the [C I] 1-0 emission in OMC 1 (Phillips and Huggins 1981) and M17 and S140 (Keene *et al.* 1985) indicate that the C I emission region is similar in extent to the CO emission region. Furthermore, the [C I] 2-1 emission is also likely to have a similar spatial distribution judging from the constant intensities measured at three positions separated by 4' in DR 21. Additional evidence for extended 2-1 emission is provided by our observations of S140. Keene *et al.* (1985) have shown the 1-0 emission to be extended over more than 10' in S140. Our data indicate that the 2-1 emission in S140 is also spread over at least 7' in the NE-SW direction of the Keene *et al.* scan, because chopping in the direction of the scan fails to show any differential emission in the $J = 2-1$ line, while chopping perpendicular to this direction yields the line shown in Figure 1. Unfortunately, the position we observed in S140 was quite near the ionization front, and it is difficult to estimate a reliable source coupling efficiency for this position given the size and pointing uncertainty of the 1-0 beam; thus, S140 is not listed in Table 3.

The third set of intensities (C) for which we calculated T_x and τ_{10} is the same as the second set (B) but with η_{2-1} replaced by η_{2-1}^{REF} . This extra correction accounts for possible emission in the "off-source" reference beam because of the large source size. The results are listed in Table 3.

As can be seen from Table 3, the derived excitation temperatures and optical depths are sensitive to the source correction applied, especially to the large upward corrections of the 1-0 intensity. In contrast, the statistical uncertainties are in most cases negligible. For case C, which is probably the most realistic given the evidence for extended 2-1 emission, the results show that $\tau_{10} < 1$ in most cases, and that the excitation temperatures are typically 30-80 K. However, the sensitivity of the results to the source coupling corrections precludes putting strict limits on the optical depths and excitation temperatures.

VI. COMPARISON WITH CO ABUNDANCE

Since our evidence points to optically thin [C I] lines, the lower limits to the C I column densities derived by Phillips and Huggins (1981) using an optically thin approximation with $T_x = 20$ K are likely to be the actual column densities. The column densities derived in this approximation depend mainly on the measured line integrated intensity and are very insensitive to the assumed excitation temperature, varying by only 25% over the range $15 \text{ K} \leq T_x \leq 200 \text{ K}$. Thus, the column density estimates can be expected to be valid even if variations in the excitation temperature exist along the line of sight or within the beam, as long as the line is optically thin. On the other hand, the CO column density estimates are more uncertain. The standard method for estimating the CO column density involves measuring the intensity of the optically thick $^{12}\text{CO}(1-0)$ line to deduce the excitation temperature, and using this temperature in conjunction with the intensity of an optically thin isotopic line such as $^{13}\text{CO}(1-0)$ or $^{12}\text{C}^{18}\text{O}(1-0)$ to derive the column density of the isotopic species, which is then used along with an assumed relative abundance to calculate the ^{12}CO column density. The sensitivity of the result to the assumption that the optically thick ^{12}CO line measures the average excitation temperature within the cloud is easily demonstrated. The intensity of the isotopic CO line essentially measures the column density of CO in the $J = 1$ state. The fraction of CO in the $J = 1$ state is inversely proportional to the partition function $f(T_x)$ and consequently the total derived CO column density is proportional to $f(T_x)$. Since $f(T_x) \propto T_x$ in the classical limit, the derived column densities are directly proportional to the assumed excitation temperatures. In this case, line of sight variations in the excitation temperature will lead to errors, particularly when the temperature of the foreground gas preferentially sampled by the optically thick ^{12}CO line is not representative of the average temperature throughout the cloud. Other sources of error are the possible non-LTE level populations for high- J states and the uncertainties in the relative abundances of the isotopic species of CO.

With these warnings in mind, we present a comparison of CO and C I abundances in Table 4. The CO column density estimates generally agree with those presented by Phillips and Huggins (1981) although in most cases they were derived from

TABLE 4
COMPARISON OF C I AND CO ABUNDANCES

Source	$T_{\text{ex}}(\text{C I})$ (K)	$T_{\text{ex}}(\text{CO})$ (K)	T_{dust} (K)	$N_{\text{C I}}$ (10^{17} cm^{-2})	N_{CO} (10^{18} cm^{-2})	$N_{\text{C I}}/N_{\text{CO}}$
OMC 1	77.	70.	70.	9.5	21.	0.05
NGC 2024	71.	38.	40.	7.0	15.	0.05
W3	25.	36.	50.	10.6	11.	0.10
W51	64.	30.	45.	31.0	21.	0.15
M17	48.	35.	50.	18.0	23.	0.08
DR 21(OH)	32.	27.	40.	6.3	12.	0.05

NOTE.—The CO column densities and excitation temperatures were taken from or derived from data in: Schloerb *et al.* 1987 (OMC 1, W51); Phillips and Huggins 1981 (NGC 2024); Loren *et al.* 1981 (NGC 2024); D. T. Jaffe 1987, private communication (W3, W51, DR 21); Thronson and Lada 1983 (M17); Dickel, Dickel, and Wilson 1978 (DR 21). The dust temperatures were taken from Werner *et al.* 1976 (OMC 1); Thronson *et al.* 1984 (NGC 2024); Werner *et al.* 1980 (W3); Harvey *et al.* 1986 (W51, DR 21); and Gatley *et al.* 1979 (M17).

independent data. The column densities of C I are derived from the case C optical depths and excitation temperatures listed in Table 3. It is important to remember that these are peak column densities since they were derived from intensities corrected for source coupling; beam-averaged column densities would be smaller. The C I (Table 3) and CO excitation temperatures as well as dust temperatures are also listed in Table 4 for comparison. The CO temperatures were not corrected for possible self-absorption, although there is some evidence that doing so results in temperatures which more closely match those measured from the thermal dust emission (Phillips *et al.* 1981).

VII. EFFECTS OF SUBCRITICAL DENSITIES

While there seems to be no doubt that significant amounts of high-density gas are present in the clouds we have observed, what is not certain is whether the [C I] emission arises in these high-density regions or in the lower density gas which envelops the dense cores. It is therefore important to examine the effects of subcritical densities on our conclusions, which are derived on the basis of thermal equilibrium. Obviously, a unique solution for all three parameters (i.e., kinetic temperature, H_2 density, and C I column density) is not possible with just two [C I] line intensities, so additional assumptions are needed. We proceed by assuming that the brightness temperature of the (optically thick) ^{12}CO line measures the kinetic temperature of the [C I] emission region. The two [C I] lines may then be used to deduce or constrain the two remaining parameters: $n(\text{H}_2)$ and $N_{\text{C I}}$. Our C I excitation models incorporating the escape probability approximation in a plane-parallel region (Scoville and Solomon 1974) show that if $T_{\text{kin}} \geq 30$ K, $T_{\text{ex}}^*(1-0) \leq 12$ K, and $T_{\text{MB}}(2-1)/T_{\text{ex}}^*(1-0) \geq 0.5$, then $\tau_{10} < 1$. Tables 1 and 4 show that these inequalities are satisfied by all of the sources observed, so the [C I] lines are optically thin in this model as well. If the [C I] lines are optically thin, then the observed ratio of the 2-1 and 1-0 intensities may be used to constrain the density of the [C I] emission region. For instance, if the radiation temperatures of the two lines are equal, the density must be larger than $\sim 10^3 \text{ cm}^{-3}$. Also, the excitation calculations indicate that the intensity of the 1-0 line still measures essentially only the C I column density if the H_2 density is $\geq 500 \text{ cm}^{-3}$, for kinetic temperatures of 30 K or larger, since such temperatures and densities result in 1-0 excitation temperatures of at least 15 K (see § VI). We conclude that the column density estimates are not likely to be affected by subcritical densities. Densities lower than 10^4 cm^{-3} will

mainly cause the kinetic temperature and the C I excitation temperature to differ. [C I] emission region densities lower than $\sim 10^3 \text{ cm}^{-3}$ are excluded by the data.

VIII. LINE WIDTH ARGUMENTS

To date, the only evidence offered in support of large [C I] optical depths is the line width comparison of Phillips and Huggins (1981). In this comparison, an empirical relationship between opacity and line width is established with observations of the 1-0 and 2-1 transitions of the various isotopic forms of CO. The optical depth of the [C I] 1-0 line is then deduced from its line width. The deduced values are $\tau_{10} \sim 25$ for OMC 1 and $\tau_{10} \sim 4$ for NGC 2024, which are based on line widths of $\Delta V = 5.0 \text{ km s}^{-1}$ for OMC 1 and $\Delta V = 4.0 \text{ km s}^{-1}$ for NGC 2024. For comparison, the [$^{12}\text{CO}(1-0)$, $^{13}\text{CO}(1-0)$] line widths listed by Phillips and Huggins for these sources are [5.9, 3.9] km s^{-1} for OMC 1 and [5.1, 3.0] km s^{-1} for NGC 2024. The line widths that we deduce from least-squares fits to the [C I] data in Phillips and Huggins are generally smaller than the values listed in their tables. In our fitting program, the model profile is first degraded by the spectrometer resolution and is then Hanning smoothed, since the $J = 1-0$ [C I] data are also smoothed. Our fits indicate that the finite resolution and smoothing result in a significant broadening of the line profile, which should be considered prior to a comparison of line widths. The line widths deduced from our fits to the Phillips and Huggins 1-0 [C I] data (see Table 1) are $4.6 \pm 0.4 \text{ km s}^{-1}$ for OMC 1 and $3.4 \pm 0.1 \text{ km s}^{-1}$ for NGC 2024, which are consistent with those of our 2-1 line profiles. The optical depths deduced from the corrected line widths, if we follow the original arguments of Phillips and Huggins, are $\tau_{10} \sim 5$ for OMC 1 and $\tau_{10} \sim 0.8$ for NGC 2024. For these lower optical depths, the ratio of column densities $N_{\text{C I}}/N_{\text{CO}}$ in these two clouds is reduced from ~ 0.7 to ~ 0.14 . Moreover, this ratio is subject to the uncertainties in the CO abundance estimates, the uncertainties in the construction of the line width versus opacity relationship, and the strength of the argument that line-width variations are principally due to optical depth effects. Thus, at this point, there seems to be little evidence in favor of optically thick ($\tau \gg 1$) [C I] lines, while evidence to the contrary is provided by the fact that the Planck-corrected [C I] brightness temperatures are substantially smaller than temperatures measured from optically thick ^{12}CO lines or thermal emission from dust. It may be that the [C I] lines become optically thick in more localized regions within specific

clouds, but such a conclusion cannot be deduced from the data currently available with beam sizes greater than $90''$.

IX. AN UPPER LIMIT TO HIGH-VELOCITY C I IN OMC 1

a) Review

Extended high-velocity ($\pm 100 \text{ km s}^{-1}$) wings on numerous molecular lines, particularly CO, are observed toward the BN/KL region of OMC 1. Maps of the high-velocity wings of the CO emission (Masson *et al.* 1987; Erickson *et al.* 1982) indicate a bipolar outflow from a central source, perhaps IRC2, extending over a region $\sim 30''$ in diameter. The "hot core" is a $10''$ region near the center of the outflow (Morris, Palmer, and Zuckerman 1980), and consists of hot ($\geq 150 \text{ K}$), dense ($> 10^6 \text{ cm}^{-3}$) gas with a relatively low velocity dispersion (10 km s^{-1}). Lobes of H_2 vibrational emission are observed at about $\pm 20''$ along the direction of the outflow from the center and are thought to arise from shocked gas at the interface between the high-velocity ($\pm 100 \text{ km s}^{-1}$) flow and the ambient gas. Velocity-resolved observations of far-infrared CO, OH, and [O I] emission (Crawford *et al.* 1986) arising in the shocked or postshock gas show that these line profiles have widths of $30\text{--}50 \text{ km s}^{-1}$, consistent with the H_2 profiles (Nadeau, Geballe, and Neugebauer 1982).

A search for high-velocity [C I] 492 GHz emission was reported by Beichman *et al.* (1982). The primary motivation for this search was to study the effects of shocks or elevated temperatures and densities on the chemistry of CO and C I. For example, Williams and Hartquist (1984) have suggested that shocks may be responsible for the large abundances of C I in molecular clouds. They propose that in dense clouds, mantles are accreted onto dust grains from the gas, and that these mantles are removed by periodically recurring shock waves. If a significant fraction of the mantle material is returned to gas phase in atomic form, and if shocks occur every 10^6 yr , then large C I abundances (C I/CO ~ 0.1) can be maintained. The negative result of Beichman *et al.* in the 1-0 [C I] line has been interpreted as evidence that shocks do not enhance the C I abundance, or that any C I produced in shocks is rapidly converted to CO in the hot, dense postshock gas (e.g., by reactions with H_2). Our high signal-to-noise spectrum (Fig. 5) of the [C I] 2-1 line in OMC 1 allows us to place improved limits on the high-velocity C I abundance. There are two advantages to observing at the higher frequency: (1) for hot gas, the 2-1 line is twice as bright as the 1-0 line; and (2) the beam size on a given telescope is narrower, so beam dilution is less important.

b) Emission Regions

As already discussed, there are several components in the broad-line emission from BN/KL: the hot core, the outflow, and the shock/postshock region. In general, the relative contribution from each component to the total emission will depend heavily upon the line observed. For example, millimeter-wave CO lines are not very sensitive to the shocked component since the large (750 K) excitation temperature implies that only a small fraction of CO is in low- J states. Conversely, far-infrared CO ($J > 20$) emission does not arise in the hot-core or outflow regions since the excitation is inadequate. C I emission would not necessarily be restricted to any one of these three regions, since each has sufficient excitation to populate substantially all three C I levels. Rather, the emission from a given region depends primarily on the product of C I column density and the beam filling factor of the region, unless the line is optically

thick, in which case it depends on the temperature and the filling factor.

c) Hot Core

The mass of the hot core has been estimated to be $9 M_{\odot}$ based on interferometric maps of the $^{13}\text{CO}(1-0)$ emission (Masson *et al.* 1987). Working backwards, we deduce that the average ^{12}CO column density in the hot core is $N_{\text{CO}} = 1.3 \times 10^{20} \text{ cm}^{-2}$ based on their assumed relative CO abundance of $[\text{CO}]/[\text{H}_2] = 1.3 \times 10^{-4}$ and a linear size of $7 \times 10^{16} \text{ cm}$ ($10''$). In turn, this allows an estimate of the [C I] 2-1 optical depth:

$$\tau_{21} \sim 10(N_{\text{C I}}/N_{\text{CO}}) \quad (10)$$

based on an assumed excitation temperature of 150 K and a velocity width of 10 km s^{-1} (FWHM; Genzel *et al.* 1982). Typically, $N_{\text{C I}}/N_{\text{CO}} \sim 0.1$, so $\tau_{21} \sim 1$. From equation (7), we deduce that $T_{\text{R}}(2-1) \sim 83 \text{ K}$. The beam dilution factor for a $10''$ disk observed by a $90''$ FWHM Gaussian beam is $\eta_{2-1} = 8.5 \times 10^{-3}$, so the expected intensity would be $T_{\text{MB}} \sim 0.71 \text{ K}$. Since the noise per 1.85 km s^{-1} channel in the [C I] spectrum shown in Figure 5 is 0.28 K (1σ), this intensity would have been detectable, especially since it would have covered about five channels. Unfortunately, the presence of the strong emission component from the quiescent molecular cloud overwhelms any such emission over more than half of the expected velocity interval (the hot core is centered at 5.5 km s^{-1} ; Genzel *et al.* 1982), making it difficult to set limits on the C I abundance in the hot core. Even so, attempts to fit two Gaussian profiles to the data with the center of one of the components fixed at 5.5 km s^{-1} and its width fixed at 10 km s^{-1} resulted in an amplitude for this component of 0.77 K , while the χ^2 of the fit was reduced by an amount which was almost statistically significant. Thus, a hot core emission component may be present in our data. The emission from the hot core could easily be detected unambiguously with a 3 m airborne telescope if $N_{\text{C I}}/N_{\text{CO}} \sim 0.1$. Higher velocity resolution would also be useful in distinguishing the hot core component from the emission due to the quiescent cloud.

d) The "Plateau" or High-Velocity Flow

The column density of CO in the high-velocity flow can be estimated from the integrated intensity of the CO(2-1) line wings (see Fig. 5). Assuming that the wings are optically thin,

$$I_{ji} = \int T_{\text{R}}(j-i) dV = \frac{hc}{k} \frac{\lambda_{ji}^2}{8\pi} A_{ji} N_j \quad (11)$$

The column densities N_j for C I and CO are related to the total column densities by

$$N_{\text{C I}}(J=2) = N_{\text{C I}} \frac{5 \exp(-62.4/T_x)}{f_{\text{C I}}(T_x)} \quad (12)$$

and

$$N_{\text{CO}}(J=2) = N_{\text{CO}} \frac{5 \exp(-16.6/T_x)}{f_{\text{CO}}(T_x)} \quad (13)$$

The partition function f_{CO} can be approximated by

$$f_{\text{CO}} \sim \frac{2T_x}{5.5 \text{ K}} \quad (14)$$

The ratio of C I and CO integrated intensities is given by

$$\frac{I_{\text{C I}}}{I_{\text{CO}}} = \left[\frac{\lambda_{\text{C I}}}{\lambda_{\text{CO}}} \right]^2 \frac{A_{\text{C I}} N_{\text{C I}} f_{\text{CO}}(T_x)}{A_{\text{CO}} N_{\text{CO}} f_{\text{C I}}(T_x)} \exp\left(\frac{-45.8}{T_x}\right). \quad (15)$$

For $T_x \sim 100$ K (Plambeck, Snell, and Loren 1983; Richardson *et al.* 1985), this gives

$$I_{\text{C I}}/I_{\text{CO}} = 0.12 N_{\text{C I}}/N_{\text{CO}}. \quad (16)$$

We estimate the CO integrated intensity (see Fig. 5) in the velocity range $V \geq 18.8$ km s⁻¹ and $V \leq -0.8$ km s⁻¹ to be $I_{\text{CO}} = 247$ K km s⁻¹, which corresponds to an average column density of 3×10^{17} cm⁻² over a 75" beam. The peak column density is much higher, since the size of the high-velocity flow is $\leq 40''$ (Erickson *et al.* 1982). However, using CO and C I data obtained with similar beam sizes reduces the relative filling factor uncertainty. The omitted velocity interval -0.8 km s⁻¹ $\leq V \leq 18.8$ km s⁻¹ is estimated to contribute a similar integrated intensity; thus, the column densities we quote are representative of only half of the CO in the flow. If the line wings are optically thick (Plambeck, Snell, and Loren 1983; Richardson *et al.* 1985) with $\tau \sim 3$ then $N_{\text{CO}} \sim 10^{18}$ cm⁻². These estimates are consistent with others appearing in the literature. For example, Snell *et al.* (1984b) give $8.2M_{\odot}$ for the total mass in the flow, which gives $\sim 2 \times 10^{18}$ cm⁻² for the average column density in the 75" CO beam.

We estimate from our data that the 3σ upper limit to the [C I] intensity in the same velocity interval (out to the limits of our filterbank) is $I_{\text{C I}} \leq 8.14$ K km s⁻¹, which gives a limit on the average column density over a 90" beam of 8.7×10^{16} cm⁻². This estimate was obtained by using the observed CO line wings as a weighting factor to give higher weight to the lower velocity channels which would be expected to have more signal, which results in a minimum uncertainty estimate. Since

the C I beam is somewhat larger than the CO beam, we apply a correction factor of 1.4 to the C I column densities and intensities, as is appropriate for a source which is small compared to either beam. Equation (16) gives the limits $N_{\text{C I}}/N_{\text{CO}} \leq 0.38$ for optically thin CO wings and ≤ 0.12 (3σ) for optically thick wings. These limits are not restrictive enough to indicate any depletion of C I relative to the quiescent molecular cloud, given the results of §§ VI and VIII.

e) Shocked Gas

From far-infrared observations of CO rotational emission lines, Watson *et al.* (1985) estimate that the CO column density in the shocked gas is 4×10^{17} cm⁻², averaged over a 1' diameter area. After correcting for beam filling (0.27, for a 1' disk observed by a 90" FWHM Gaussian beam) and velocity coverage (0.6; based on 30 km s⁻¹ FWHM for the line profiles [Crawford *et al.* 1986]), we obtain a limit to the C I column density in this gas of $N_{\text{C I}} \leq 5 \times 10^{17}$ cm⁻². Thus $N_{\text{C I}}/N_{\text{CO}} \leq 1.3$ for the shocked gas, which again is not a severe limit.

f) Comparison to the Results of Beichman *et al.*

Beichman *et al.* (1982) quote a 3σ upper limit of 6.9×10^{17} cm⁻² to the column density of C I in a 40" diameter disk in the velocity intervals -5 km s⁻¹ $\leq V \leq 5$ km s⁻¹ and 13 km s⁻¹ $\leq V \leq 20$ km s⁻¹. Our limit for the equivalent velocity interval and source size is 3.9×10^{17} cm⁻², for $T_x = 100$ K. Thus, we are more sensitive by a factor of 1.8 to high-velocity C I emission, but still have not detected any. Even so, our limit of $N_{\text{C I}}/N_{\text{CO}} \leq 0.12$ for the case of optically thick line wings is similar to the limit of ≤ 0.13 quoted by Beichman *et al.* This coincidence can be understood as the result of several factors: (1) the limit quoted by Beichman *et al.* is a factor of 4 lower than justified by their data, because their calculation represents

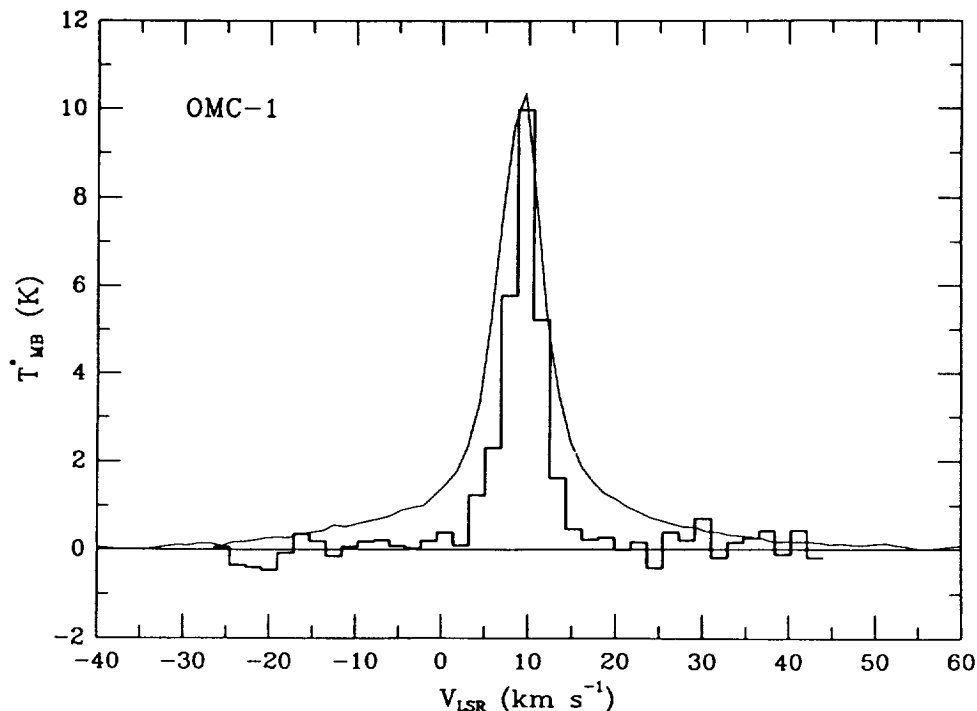


FIG. 5.— ${}^3P_1-{}^3P_1$ [C I] (heavy line) and ${}^{12}\text{C}^{16}\text{O}(2-1)$ (light line; $\times \frac{1}{3}$) emission toward OMC 1/BN/KL. CO data from Plambeck, Snell, and Loren (1983).

a comparison of the column density of C I in a selected velocity interval with that of CO over the *entire* line profile; (2) our observations have about twice the sensitivity; and (3) our chosen CO column density for the case of optically thick CO line wings is about twice that chosen by Beichman *et al.* The factors of 2 downward (2, 3) cancel the factor of 4 upward (1), resulting in similar numerical values for the abundance ratio.

g) Summary

The ratio of C I to CO in quiescent molecular clouds derived in § VI (see Table 4) is significantly less than that deduced previously, and therefore the upper limit to this ratio in the BN/KL high-velocity flow does not indicate a relative depletion of C I. Thus, models invoking periodic shocks to explain high C I abundances are not contradicted by the existing experimental data. It may be that C I is depleted in these

regions; all that we can say is that it is not enhanced substantially. [C I] emission from the hot core may be present in our data but cannot be separated unambiguously from emission produced by the quiescent cloud. Future studies utilizing larger airborne or space-based telescopes will be more sensitive to such emission by at least one order of magnitude.

The staff of the Kuiper Airborne Observatory was very helpful in providing technical assistance during our flight series, and we thank them for their effort. We also thank J. Keene for access to data prior to publication and for valuable discussions. R. T. B. is grateful to the Natural Sciences and Engineering Research Council of Canada for her postdoctoral fellowship. These observations were supported by NASA grant NAG 2-254.

REFERENCES

- Beichman, C. A., Phillips, T. G., Wootten, H. A., and Frerking, M. A. 1982, in *Regions of Recent Star Formation*, ed. R. S. Roger and P. E. Dewdney (Dordrecht: Reidel), p. 445.
- Brackmann, E., and Scoville, N. 1980, *Ap. J.*, **242**, 112.
- Cooksy, A. L., Saykally, R. J., Brown, J. M., and Evenson, K. M. 1986, *Ap. J.*, **309**, 828.
- Crawford, M. K., Lugten, J. B., Fitelson, W., Genzel, R., and Melnick, G. 1986, *Ap. J. (Letters)*, **303**, L57.
- Dickel, J. R., Dickel, H. R., and Wilson, W. J. 1978, *Ap. J.*, **223**, 840.
- Erickson, N. R., Goldsmith, P. F., Snell, R. L., Berson, R. L., Huguenin, G. R., Ulich, B. L., and Lada, C. J. 1982, *Ap. J. (Letters)*, **261**, L103.
- Gatley, I., Becklin, E. E., Sellgren, K., and Werner, M. W. 1979, *Ap. J.*, **233**, 575.
- Genzel, R., Downes, D., Ho, P. T. P., and Bieging, J. 1982, *Ap. J. (Letters)*, **259**, L103.
- Genzel, R., and Stacey, G. J. 1985, *Mitt. Astr. Ges.*, **63**, 215.
- Goldsmith, P. F. 1987, *Internat. J. Infrared Millimeter Waves*, **8**, 771.
- Graedel, T. E., Langer, W. D., and Frerking, M. A. 1982, *Ap. J. Suppl.*, **48**, 321.
- Harvey, P. F., Joy, M., Lester, D. F., and Wilking, B. A. 1986, *Ap. J.*, **300**, 737.
- Hildebrand, R. H., Loewenstein, R. F., Harper, D. A., Orton, G. S., Keene, J., and Whitcomb, S. E. 1985, *Icarus*, **64**, 64.
- Jaffe, D. T., Becklin, E. E., and Hildebrand, R. H. 1984, *Ap. J. (Letters)*, **279**, L51.
- Jaffe, D. T., Harris, A. I., Silber, M., Genzel, R., and Betz, A. L. 1985, *Ap. J. (Letters)*, **290**, L59.
- Jaffe, D. T., Hildebrand, R. H., Keene, J., and Whitcomb, S. E. 1983, *Ap. J. (Letters)*, **273**, L89.
- Keene, J., Blake, G. A., Phillips, T. G., Huggins, P. J., and Beichman, C. A. 1985, *Ap. J.*, **299**, 967.
- Keene, J., Hildebrand, R. H., and Whitcomb, S. E. 1982, *Ap. J. (Letters)*, **252**, L11.
- Kutner, M. L., Tucker, K. D., Chin, G., and Thaddeus, P. 1977, *Ap. J.*, **215**, 521.
- Kutner, M. L., and Ulich, B. L. 1981, *Ap. J.*, **250**, 341.
- Langer, W. 1976a, *Ap. J.*, **206**, 699.
- . 1976b, *Ap. J.*, **210**, 328.
- Launay, J. M., and Roueff, E. 1977, *Astr. Ap.*, **56**, 289.
- Loren, R. B., Plambeck, R. L., Davis, J. H., and Snell, R. L. 1981, *Ap. J.*, **245**, 495.
- Mason, C. M., Lo, K. Y., Phillips, T. G., Sargent, A. I., Scoville, N. Z., and Woody, D. P. 1987, *Ap. J.*, **319**, 446.
- Monteiro, T. S., and Flower, D. R. 1987, *M.N.R.A.S.*, **228**, 101.
- Morris, M., Palmer, P., and Zuckerman, B. 1980, *Ap. J.*, **237**, 1.
- Mufson, S. L., and Liszt, H. S. 1979, *Ap. J.*, **232**, 451.
- Mundy, L. G., Evans, N. J., Snell, R. L., and Goldsmith, P. F. 1987, *Ap. J.*, **318**, 392.
- Nadeau, D., Geballe, T. R., and Neugebauer, G. 1982, **253**, 154.
- Nussbaumer, H. 1971, *Ap. J.*, **206**, 411.
- Phillips, T. G., and Huggins, P. J. 1981, *Ap. J.*, **251**, 533.
- Phillips, T. G., Huggins, P. J., Kuiper, T. B. H., and Miller, R. E. 1980, *Ap. J. (Letters)*, **238**, L103.
- Phillips, T. G., Knapp, G. R., Huggins, P. J., Werner, M. W., Wannier, P. G., Neugebauer, G., and Ennis, D. 1981, *Ap. J.*, **245**, 512.
- Plambeck, R. L., Snell, R. L., and Loren, R. B. 1983, *Ap. J.*, **266**, 321.
- Richardson, K. J., White, G. J., Avery, L. W., Lesurf, J. C. G., and Harten, R. H. 1985, *Ap. J.*, **290**, 637.
- Saykally, R. J., and Evenson, K. M. 1980, *Ap. J. (Letters)*, **238**, L107.
- Schloerb, F. P., Snell, R. L., and Schwartz, P. R. 1987, *Ap. J.*, **319**, 426.
- Scoville, N. Z., and Solomon, P. M. 1974, *Ap. J. (Letters)*, **187**, L67.
- Snell, R. L., Mundy, L. G., Goldsmith, P. F., Evans II, N. J., and Erickson, N. R. 1984a, *Ap. J.*, **276**, 625.
- Snell, R. L., Scoville, N. Z., Sanders, D. B., and Erickson, N. R. 1984b, *Ap. J.*, **284**, 176.
- Stacey, G. J. 1985, Ph.D. thesis, Cornell University.
- Stutzki, J., Stacey, G. J., Genzel, R., Harris, A. I., Jaffe, D. T., and Lugten, J. B. 1988, *Ap. J.*, submitted.
- Tarafdar, S. P., Prasad, S. S., Huntress, W. T. Jr., Villere, K. R., and Black, D. C. 1985, *Ap. J.*, **289**, 220.
- Thronson Jr., H. A., and Lada, C. J. 1983, *Ap. J.*, **269**, 175.
- Thronson Jr., H. A., Lada, C. J., Schwartz, P. R., Smith, H. A., Smith, J., Glaucum, W., Harper, D. A., and Loewenstein, R. C. 1984, *Ap. J.*, **280**, 154.
- Tielens, A. G. G. M., and Hollenbach, D. 1985a, *Ap. J.*, **291**, 722.
- . 1985b, *Ap. J.*, **291**, 747.
- Watson, D. M., Genzel, R., Townes, C. H., and Storey, J. W. V. 1985, *Ap. J.*, **298**, 316.
- Werner, M. W., Becklin, E. E., Gatley, I., Neugebauer, G., Sellgren, K., Thronson Jr., H. A., Harper, D. A., Loewenstein, R., and Moseley, S. H. 1980, *Ap. J.*, **242**, 601.
- Werner, M. W., Gatley, I., Harper, D. A., Becklin, E. E., Loewenstein, R. F., Telesco, C. M., and Thronson, H. A. 1976, *Ap. J.*, **204**, 420.
- Williams, D. A., and Hartquist, T. W. 1984, *M.N.R.A.S.*, **210**, 141.
- Zmuidzinas, J. 1987, Ph.D. thesis, University of California, Berkeley.
- Zmuidzinas, J., Betz, A. L., and Goldhaber, D. M. 1986, *Ap. J. (Letters)*, **307**, L75 (ZBG).

A. L. BETZ, R. T. BOREIKO, and D. M. GOLDBER: Space Sciences Laboratory, University of California, Berkeley, CA 94720

J. ZMUIDZINAS: Astronomy Department, University of Illinois, 1011 West Springfield Avenue, Urbana, IL 61801

HETERODYNE SPECTROSCOPY OF THE $J = 17-16$ CO LINE IN ORION

R. T. BOREIKO AND A. L. BETZ

Space Sciences Laboratory, University of California, Berkeley

AND

J. ZMUIDZINAS

Department of Astronomy, University of Illinois

Received 1988 May 20; accepted 1988 July 11

ABSTRACT

We have obtained high-resolution spectra of the $153 \mu\text{m}$ $J = 17-16$ CO line in the BN-KL region of Orion using a laser heterodyne spectrometer. The line shows broad wings (30 km s^{-1} FWHM at BN) characteristic of the plateau emission as well as a narrower component probably associated with the quiescent gas in the molecular ridge. From an analysis of the plateau emission together with that observed in lower J CO transitions, we derive an excitation temperature of $180 \pm 50 \text{ K}$ and minimum column density of $1 \times 10^{18} \text{ cm}^{-2}$ for CO in this component, which constitutes 80% of the total integrated intensity of the $J = 17-16$ line near BN. The peak intensity of the narrower component observed at 0.8 km s^{-1} resolution increases relative to that of the plateau component toward $\theta^1\text{C}$ and away from BN, while the width decreases from 10 to 4 km s^{-1} (FWHM).

Subject headings: interstellar: molecules — nebulae: internal motions — nebulae: Orion Nebula

I. INTRODUCTION

The core of the Orion molecular cloud has been extensively studied in many molecular transitions, and the data have been interpreted to show the existence of three main components in this region. The ambient molecular cloud (ridge) is spatially extended, and produces relatively narrow lines (FWHM $3-7 \text{ km s}^{-1}$) at a V_{LSR} near 9 km s^{-1} . The outflow source or plateau emission region is characterized by broad lines ($\sim 30 \text{ km s}^{-1}$ FWHM) with V_{LSR} of $7-9 \text{ km s}^{-1}$. Part of the plateau emission originates from a somewhat compact region ($25''-40''$ in low-excitation lines), but there is some indication that this size increases with excitation. Finally, the "hot core" component is a hot ($T > 200 \text{ K}$) and dense ($n_{\text{H}} > 10^6 \text{ cm}^{-3}$) region which is spatially compact ($\sim 10''$) and gives rise to lines of $\sim 8-15 \text{ km s}^{-1}$ width, with a V_{LSR} of $\sim 5 \text{ km s}^{-1}$.

High-excitation molecular emission from the BN-KL region has been attributed to the interaction of the high-velocity outflow material with the ambient molecular cloud, thereby producing a shock which heats the gas (Draine and Roberge 1982; Chernoff, Hollenbach, and McKee 1982). The observed vibrational emission from H_2 (Beckwith *et al.* 1978; Nadeau, Geballe, and Neugebauer 1982; Scoville *et al.* 1982; Geballe *et al.* 1986) has been interpreted as originating from shock-excited gas at temperatures near 2000 K , although some contribution from ultraviolet-excited H_2 cannot be excluded (Hayashi *et al.* 1985). However, detailed modeling on the basis of these data is hampered by the uncertain, but probably significant, effect of extinction. Observations in transitions of the next most abundant molecule, CO, reveal evidence of disturbed gas originating from the plateau source. The low- J ($J < 4$) transitions show very extended wing emission (Plambeck, Snell, and Loren 1983; Richardson *et al.* 1985), but the bulk of the intensity arises from relatively cool ($T < 100 \text{ K}$) quiescent gas from the ridge. High- J ($J > 10$) transitions, on the other hand, should be sensitive primarily to much hotter gas, originating in either the "plateau" gas or the "hot core," with less confusion from emission by the quiescent cloud.

These components can in most cases be distinguished by their differing V_{LSR} , spatial characteristics, and line widths. The BN-KL region has been observed in several higher J CO lines (Crawford *et al.* 1986; Storey *et al.* 1981; Watson *et al.* 1980, 1985), but unfortunately the instrumental resolution was insufficient to measure line profiles. While integrated intensities provide significant information for interpreting conditions in the high-excitation gas, accurate line profiles and velocities provide greater constraints for the hot gas kinematics.

The work presented here describes the first high-resolution observations of the $153 \mu\text{m}$ $^{12}\text{C}^{16}\text{O}$ $J = 17-16$ line obtained with a heterodyne spectrometer. The results from five positions near BN show that the emission originates primarily from the "plateau" gas, with no discernible contribution from the "hot core," but that a narrower emission component which is more identifiable with warm quiescent ridge gas also exists.

II. INSTRUMENTATION AND CALIBRATION

The far-infrared heterodyne receiver used for these observations is described in detail by Betz and Zmuidzinas (1984). The local oscillator is an optically pumped $^{15}\text{NH}_3$ laser, and the mixer is a cooled GaAs Schottky diode in a corner-reflector mount. The system noise temperature was measured during the observations to be $21,000 \text{ K}$ (SSB). The "back end" consists of two filterbanks in parallel, one consisting of 64 channels of 20 MHz (3 km s^{-1}) resolution, and the other of 40 channels of 5 MHz (0.8 km s^{-1}) resolution. For a wide line such as that expected from the high-velocity plateau region, the wide bandwidth filterbank is essential to determine the shape of the wings, while the higher resolution filterbank gives a more detailed look at the shape near line center, where asymmetries may be most prominent.

Observations in the $100-200 \mu\text{m}$ range need to be made at aircraft altitudes or higher, since water vapor in Earth's atmosphere renders this band essentially opaque from the ground. The spectrometer was flown aboard the Kuiper Airborne Observatory at an altitude of 12.5 km , where the atmospheric

transmission at the source-corrected CO frequency is approximately 0.97. The CO $J = 17-16$ line at 1956.0181 ± 0.0001 GHz (Nolt *et al.* 1987) falls less than 50 MHz from a weak H₂O line in Earth's atmosphere. Fortunately, the Doppler shift of Orion at the time of these observations was approximately 36 km s^{-1} and that, along with the intrinsic source V_{LSR} of $\sim 9 \text{ km s}^{-1}$, shifted the frequency of the observed CO line 250 MHz (36 km s^{-1}) from the atmospheric H₂O line, and even further from the atmospheric CO line. Scans of the lunar limb were used to measure the beam size to be $\sim 43''$ (FWHM), and the coupling efficiency ~ 0.5 . Pointing accuracy is estimated to be better than $15''$. The data were obtained with the chopping secondary of the telescope operated at 2 Hz with a throw of 6.3 E-W . This throw amplitude should be sufficient to avoid confusion from possible emission in the reference beam because of the relatively compact nature of the plateau source.

Absolute flux calibration was obtained from spectra of the Moon, for which we assume a physical temperature of 394 K and emissivity of 0.98 (Linsky 1973). The single-sideband line intensity was derived from the measurement by using the unequal (but known) transmission of the quartz aircraft pressure window and the atmosphere in the two receiver sidebands. The lunar calibration was maintained throughout the flight by frequent observations of an internal blackbody source used as a secondary standard. The uncertainty in the absolute calibration from all contributions apart from the unknown source coupling is estimated to be no greater than 10%.

The velocity scale accuracy of the data is determined both by the CO line and $^{15}\text{NH}_3$ laser frequencies. The former has recently been measured to better than $\pm 0.1 \text{ MHz}$ (2σ) by Nolt *et al.* (1987), but the latter frequency was previously not known with comparable accuracy. Therefore we measured the difference in frequency between the laser and the CO $J = 17-16$ transition by using our heterodyne spectrometer in its flight configuration. Radiation from a blackbody source was passed through a sample cell containing CO at room temperature, and the absorption line was analyzed in the filterbanks. The frequency difference was found to be $6731.0 \pm 0.5 \text{ MHz}$, which establishes the $^{15}\text{NH}_3$ laser frequency at $1962.7491 \pm 0.0005 \text{ GHz}$. The overall 1σ velocity scale accuracy of our spectra is thus $\pm 0.1 \text{ km s}^{-1}$.

III. OBSERVATIONS

The data were obtained on the night of 1988 January 26 at five locations within the Orion complex: BN, H₂ peak 1, H₂ peak 2, $30''$ SE of H₂ peak 2 along the line joining peaks 1 and 2, and at $\theta^1\text{C}$. These positions are shown in Figure 1, superposed upon a map of the $v = 1-0 \text{ S}(1)$ H₂ emission (Beckwith *et al.* 1978). As can be seen from this figure, our beam size of $43''$ is sufficiently large that several localized sources such as BN, IRc2, and the hot core lie within a single beam. For convenience we refer to this position simply as BN without implying that this specific object is the origin for the observed radiation. Figure 2 shows the spectra obtained at each position, from

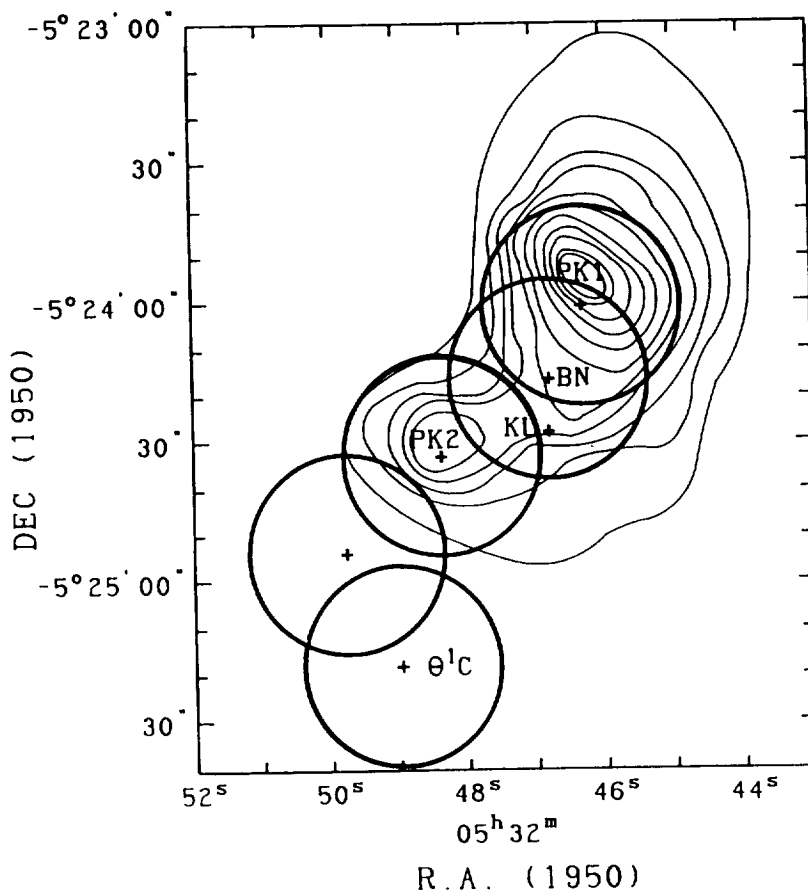


FIG. 1.—Location of the positions observed, superposed upon a map of H₂ vibrational emission from Beckwith *et al.* (1978). The outermost contour represents the limits of the map. The circle size indicates the beam size used for the observations.

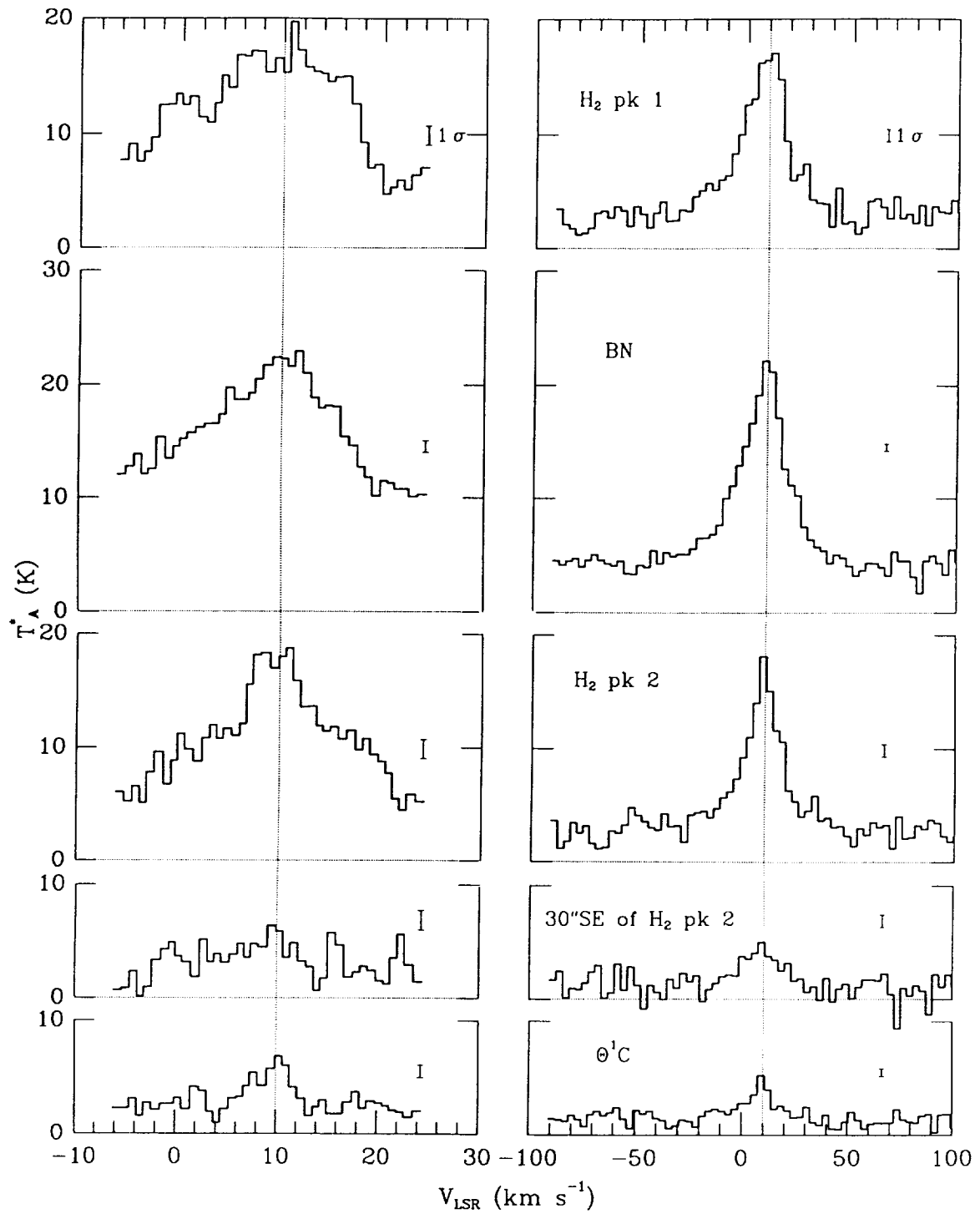


FIG. 2.—Spectra of the $J = 17-16$ line of CO at 0.8 km s^{-1} (left panel) and 3.0 km s^{-1} (right panel) resolution from five positions in Orion. Integration times are 24 minutes for BN, 20 minutes for $\theta^1\text{C}$, and 8 minutes for each of the three remaining positions. The dotted vertical line is at 10 km s^{-1} .

TABLE 1
153 MICRON CO $J = 17 \rightarrow 16$ RESULTS

Source	T_A^{**} (K)	V_{LSR} (km s ⁻¹)	Line Width (km s ⁻¹ , FWHM)	Integrated Intensity (ergs s ⁻¹ cm ⁻² sr ⁻¹)	Continuum ^b (K)
H ₂ peak 1	9.1 (1.1) 6.8 (1.3)	4.6 (1.4) 11.4 (0.5)	26.4 (2.0) 10.7 (1.7)	2.81 (0.16) × 10 ⁻³	1.74 (0.10)
BN	6.6 (0.5)	10.6 (0.2)	8.3 (0.7)		
H ₂ peak 2	10.0 (0.6) 5.8 (0.7)	9.4 (0.3) 9.6 (0.2)	22.2 (1.2) 4.4 (0.7)	2.26 (0.16) × 10 ⁻³	1.74 (0.09)
30° SE of H ₂ peak 2	3.3 (0.3)	8.9 (0.9)	20.8 (2.7)		
θ ¹ C	1.4 (0.2) 3.5 (0.4)	6.9 (1.8) 9.7 (0.2)	30.8 (6.3) 3.8 (0.5)	3.60 (0.10) × 10 ⁻⁴	0.80 (0.10)
Average BN, peak 1, peak 2	10.3 (0.4) 6.7 (0.4)	6.6 (0.4) 10.6 (0.2)	30.8 (0.6) 9.3 (0.6)		

NOTE.—Quantities in parentheses are 1 σ statistical uncertainties.
^a T_A^* is corrected for the continuum.
^b The continuum temperatures are single-sideband values.

both the 40 × 5 MHz filterbank (*left panel*) and 64 × 20 MHz filterbank (*right panel*). The positions are approximately uniformly spaced in a NE-SW direction. No continuum or slope has been subtracted from the data, and no smoothing has been applied. Table 1 summarizes various parameters deduced from the spectra.

All of the parameters in Table 1, with the exception of integrated intensity, were obtained from fits of the continuum plus one or two Gaussian profiles to the data. In the fitting procedure, the calculated Gaussian was degraded to the resolution of the individual filterbanks, thus permitting a simultaneous fit to both sets of data. All of the fits were found to be good representations of the data, with residuals consistent with those expected from statistical uncertainty (i.e., system noise). Only one Gaussian profile was fitted to the data 30° SE of H₂ peak 2 because of the lower signal-to-noise ratio of this spectrum; the existence of two components cannot, however, be ruled out. Figure 3 shows the average of spectra from BN and H₂ peaks 1 and 2 (which have similar characteristics) together with the calculated two-Gaussian profile and the wide component of the fit alone. The quality of the fit, which reproduces the wide wings as well as the asymmetry seen most clearly in the higher resolution data, lends support to the interpretation of the line profile in terms of two distinct components, although this interpretation is not unique. A possible physical basis for the two components is discussed in IV.

The antenna temperature of the continuum obtained from the fit was corrected to a single-sideband value by using the different (but known) transmissions of the pressure window and the atmosphere in the two sidebands. Comparison of these continuum values with those interpolated from the data of Werner *et al.* (1976) indicates that our measurements are about a factor of 1.7 lower. This discrepancy is unlikely to be attributable to pointing errors, since the proportionality between the continuum intensity of Werner *et al.* (1976) and that of the present data remains approximately constant for each location. Nor can it arise from incorrect determination of the pressure window or atmospheric transmission, since these factors are common to the continuum and the calibration, which are both intrinsically double-sideband. Our continuum temperature for BN of 2.49 ± 0.06 K at 153 μ m is in good agreement with the 2.40 ± 0.08 K measured at 157 μ m by Boreiko, Betz, and Zmuidzinas (1988) using totally independent data

and calibration. It should be noted that our continuum measurement does not influence our calibration of the CO line intensity, but is mentioned mainly for comparison with other observations which rely on line-to-continuum estimates for calibration.

The integrated intensity in the $J = 17-16$ line at BN has previously been measured by Stacey *et al.* (1982) to be 8.0 ± 2.5 × 10⁻³ erg s⁻¹ cm⁻² sr⁻¹. This intensity estimate was calibrated with respect to the continuum measurement of Werner *et al.* (1976). If our lower continuum temperature is adopted, however, the two determinations for the CO $J = 17-16$ integrated intensity agree to within the statistical uncertainties.

The uncertainties associated with the parameters of Table 1 are derived only from statistical fluctuations (1 σ), as determined from the rms noise in spectra of sources for which no CO $J = 17-16$ emission was seen. The noise per channel was found to correspond to that expected from a system noise temperature of 21,000 K (SSB) which was measured as such independently. Furthermore, the effective noise decreased with integration time as expected for a random process, showing that system instabilities or standing wave problems do not contribute significantly to the uncertainties in the results.

IV. ANALYSIS AND CONCLUSIONS

In general, CO line emission could have contributions from several distinct regions such as the quiescent ridge, the plateau, and the hot core. Distinction among these contributions usually requires additional information on the characteristics of each emission component, and the resolution and sensitivity to distinguish between these characteristics. This is certainly true in the case of low- J lines, where the temperature of the quiescent cloud is such that the low- J levels are substantially populated, which leads to optically thick emission that dominates other possible contributions except in the line wings. The shape of the wing profile and its intensity as a function of rotational level provides information on the temperature, optical depth, and velocity structure of the high-velocity gas. However, the range of J of observed lines must be large so that systematic uncertainties in source coupling and calibration do not overwhelm the real dependence of intensity on J . Heretofore, resolved line profiles for CO have been obtained only up to the $J = 7-6$ transition. We choose to exclude profiles

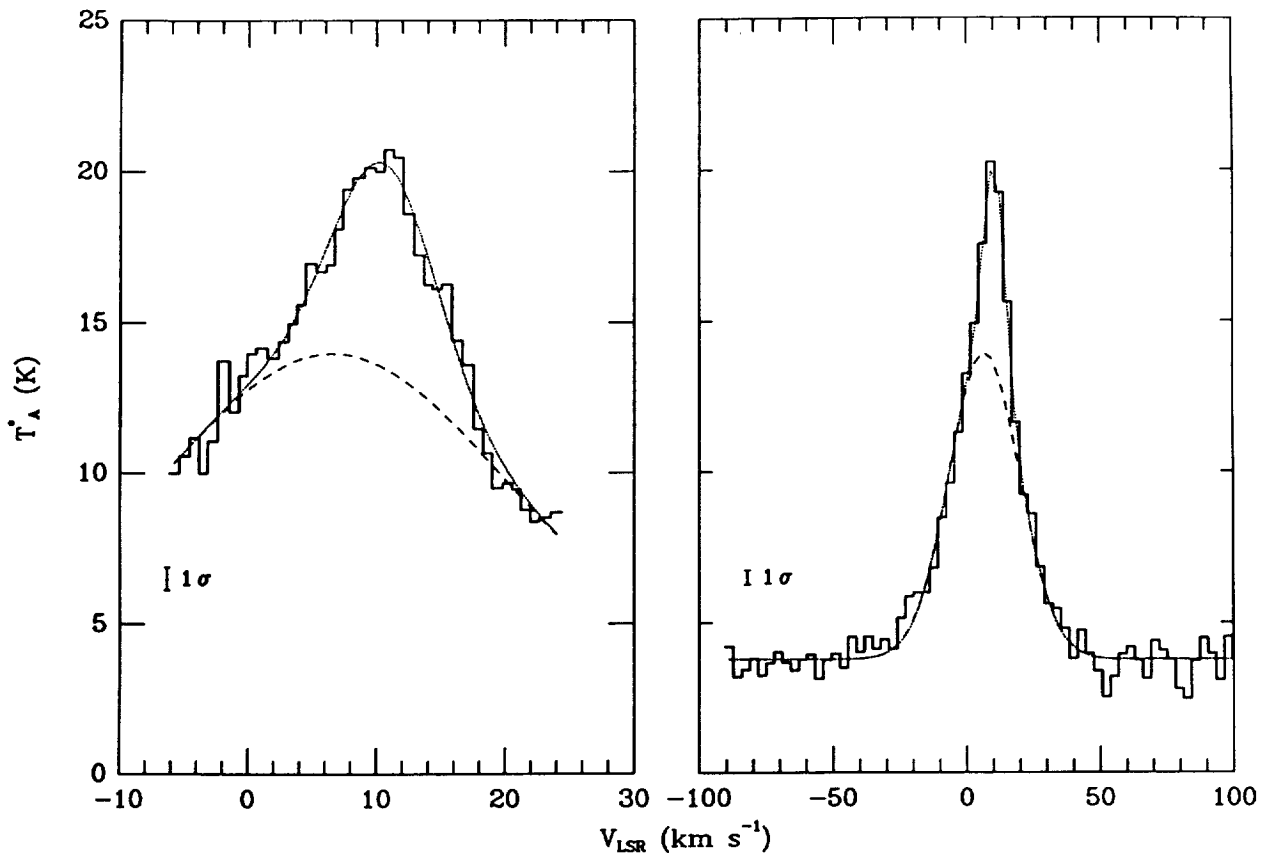


FIG. 3.—The averaged spectrum of the $J = 17-16$ line of CO from the BN, H_2 peak 1, and H_2 peak 2 positions. Total integration time is 40 minutes. The dotted line shows the two-component Gaussian fit to the data, while the dashed line shows only the wide component of the fit.

obtained from deconvolution, since these are more susceptible to systematic uncertainties resulting from incomplete knowledge of the instrumental response. The range of energy levels over which the plateau emission is well resolved is increased by more than a factor of 5 by the $J = 17-16$ data presented here, and consequently the constraints on deduced properties of the high-velocity gas are more stringent.

a) Fitting Procedure—Broad Emission Component

The optical depth at a frequency ν in a CO transition $J + 1 \rightarrow J$, assuming all level populations are thermalized, is given by

$$\tau(\nu) = \frac{8\pi^3 \mu^2 (J+1) e^{-E_l/kT_x}}{3h Q_r(T_x)} (1 - e^{-h\nu/kT_x}) \int n\phi(\nu) ds, \quad (1)$$

where μ is the dipole moment (0.112 Debye; Lang 1980), Q_r is the rotational partition function, E_l is the energy of the lower level involved in the transition, n is the number density of CO, $\phi(\nu)$ is the line profile function (in velocity units) which also includes a beam filling factor due to possible clumpiness, and the integral is performed along the path from the observer through the molecular cloud. For convenience, the integral can be replaced by $N\phi(\nu)$, where N is an equivalent column density, and $\phi(\nu)$ is redefined for this relationship to hold. The LVG (large velocity gradient) condition is assumed, so that radiation from all values of J arises in an equivalent manner from different velocity components of the gas. With this assumption, $\phi(\nu)$ does not depend upon rotational level, and therefore compari-

sons of intensities in the wings of lines with various J can meaningfully be made at the same absolute velocities. In the limit of small optical depth, equation (1) can be rearranged to show the dependence of intensity on J :

$$\ln \left(\frac{(J+1)h\nu}{kT_{\lambda}^*} \right) = \frac{E_u}{kT_x} + \ln \left(\frac{3hQ_r(T_x)}{8\pi^3 \mu^2 N\phi(\nu)} \right). \quad (2)$$

Therefore, a least-squares fitting of the quantity on the left-hand side of the equation to E_u , the energy of the upper level involved in the transition, yields a slope of $1/kT_x$ and an intercept related to $N\phi(\nu)$. Note that this relationship underscores the need to have as large a range of E_u as possible. This fitting procedure was carried out using the line profiles for the BN region for $J = 1-0$ and $J = 2-1$ from Plambeck, Snell, and Loren (1983), $J = 3-2$ from Richardson *et al.* (1985), $J = 6-5$ from Koepf *et al.* (1982), $J = 7-6$ from Schultz *et al.* (1985), and the present data for $J = 17-16$. For each line, a baseline (and for the case of the $J = 6-5$ data also a slope) was determined from a one-component or two-component Gaussian fit, and subtracted from the data. Beam sizes for the $J = 1-0$ through $J = 17-16$ observations were $64''$, $75''$, $55''$, $35''$, $35''$, and $43''$, respectively.

b) Assumptions in the Fitting Procedure

The assumptions implicit in the fitting procedure are that (1) a single temperature characterizes all the transitions, (2) the source coupling correction is similar for all the observations

and relatively small, (3) all the levels are in LTE, and (4) the radiation in the wings of all the transitions is optically thin.

The first assumption cannot be addressed by the present limited set of observations. While there is evidence that a range of excitations exists in the plateau region (Blake *et al.* 1987), a single-temperature interpretation will be used as a preliminary approach. The derived temperature will then represent a "level-averaged" temperature for the wing radiation.

The relative constancy of the CO $J = 17-16$ emission at BN and H₂ peaks 1 and 2 suggests that the source is extended over more than 1', consistent with the value of 1.5 (FWHM) deduced by Storey *et al.* (1981) from $J = 21-20$ data. If the source distribution is similar in lower J transitions, then the magnitude of individual corrections for source coupling is expected to be small. Interferometric mapping in CO $J = 1-0$ (Masson *et al.* 1987) shows that approximately 25% of the plateau emission originates from a source slightly larger than 25" in extent, while the remainder is smoothly distributed on a scale of $\sim 1'$ or more. Our data have insufficient spatial resolution to determine whether this small-scale structure exists in the $J = 17-16$ line, and therefore we proceed on the assumption that most of the wing emission comes from an extended region so that individual source coupling values do not greatly affect the data. There is some evidence that the source size is $\leq 40''$ in other low- J CO transitions (e.g., Erickson *et al.* 1982). If the source size increases with excitation and is spatially unresolved in the low- J lines, then there will be a systematic error in our procedure which leads to an estimate of the excitation temperature that is too high and of the column density that is too low. For example, the inclusion of a source coupling correction consisting of the ratio of the solid angle of the beam to that of a 45" source lowers the estimate of the excitation temperature by about 25% and raises the column density by about a factor of 3. The unknown source distribution produces the greatest uncertainty in our procedure, even though the beam sizes of all the observations are similar.

Densities within the plateau region are known to be fairly high ($n > 10^6 \text{ cm}^{-3}$) from observations of several transitions of molecules with high dipole moments (e.g., Keene, Blake, and Phillips 1983; Loren and Wootten 1986; Padman *et al.* 1985; Moore, Langer, and Huguenin 1986; White *et al.* 1986; Blake *et al.* 1987). The critical density for a rotational transition in CO increases with J , reaching approximately $2 \times 10^6 \text{ cm}^{-3}$ at 180 K for the $J = 17-16$ transition (McKee *et al.* 1982). Thus, available evidence indicates that all the levels used in the present analysis are thermalized, or nearly so. The effect of sub-thermal excitation, which would be seen mainly in the $J = 17-16$ data, would be to lower the measured value of T_A^* compared to its thermal value, which would lead to a temperature estimate that is too low and a column density that is too high. This latter effect is opposite in sense to that produced by a source whose size appears to increase with excitation.

The fourth assumption is the most difficult to address. Plambeck, Snell, and Loren (1983) in their analysis of $J = 2-1$ and $1-0$ data suggest that the line wings are moderately optically thick over a large range of velocities, since the ratio of the intensities in the two lines is smaller than that expected for optically thin gas. Richardson *et al.* (1985) subsequently deduced from their observations of the $J = 3-2$ line in concert with available $J = 2-1$ and $1-0$ data that the plateau emission was thin in the $J = 1-0$ line but moderately thick in the $J = 3-2$ transition. These various estimates of optical depth depend upon an assumed excitation temperature (usually

70–90 K), source coupling corrections for individual telescopes to an assumed source size (typically $\sim 40''$), proper correction for spike emission, and accurate knowledge of the baseline. Most likely the $J = 1-0$ line wings are optically thin, and the $J = 17-16$ wings almost certainly will also be thin, and therefore our fitting procedure could be followed with just these two sets of data. Should the wings in intermediate- J lines be optically thick, as suggested by the ratios of the $J = 3-2$ and $J = 1-0$ data, the effect would be to saturate the value of T_A^* for these transitions, with adverse effects on the quality of the fit; specifically, the column density would be underestimated. The derived excitation temperature, however, would be relatively unaffected.

c) Results and Interpretation

The fitting was performed at velocity intervals of 5 km s^{-1} from -25 to 0 km s^{-1} and 20 to 45 km s^{-1} V_{LSR} , with the individual spectra degraded to 5 km s^{-1} resolution. The excitation temperature T_x derived from least-squares fits to equation (2) over these intervals is $180 \pm 35 \text{ K}$, with no significant variation in T_x with wing velocity. Including an estimate of possible systematic effects raises the 1σ uncertainty to $\pm 50 \text{ K}$. The values of $N\phi(v)$ range from $0.09 \times 10^{16} \text{ cm}^{-2} (\text{km s}^{-1})^{-1}$ in the far wings to $2.2 \times 10^{16} \text{ cm}^{-2} (\text{km s}^{-1})^{-1}$ closer to line center, and have uncertainties of 30%.

The fitting procedure depends critically on the existence of the $J = 17-16$ data, which arise from an energy level a factor of 5 higher than those of transitions previously observed with equivalently high spectral resolution. The intensities of wing emission in lower J data ($J \leq 7$) are not mutually consistent with either optically thin or thick emission from a source of any size, to within the reported uncertainties of the individual measurements. These inconsistencies mask any true dependence of wing emission intensity on J over the much smaller range of J sampled by low- J observations alone.

The relative constancy of the derived excitation temperature with velocity is interesting, in that an outflow source might be expected to have a temperature gradient, which would be translated into a dependence of T_x on V_{LSR} by the relationship between distance from the source and velocity. The absence of this effect implies that the outflow is not a smooth one, and suggests the presence of clumps, as pointed out by Plambeck, Snell, and Loren (1983) and Padman *et al.* (1985). Provided that the beam filling factor of the clumps is not so low as to make optical depths within a single clump large, the effect on the derived temperature will be negligible.

The derived parameters are relatively insensitive to the data at any given J because of the range in J available. For example, a 20% change in T_A^* of the $J = 1-0$ line results in a 6% change in $N\phi(v)$, with very little change in T_x , while the equivalent change in the $J = 17-16$ line changes T_x by 5%, with little effect on $N\phi(v)$. Intermediate- J lines have comparable effects on a combination of the two parameters. Therefore, provided that no significant common systematic effects exist in the data, these parameters characterize the gas giving rise to the extended wing emission in CO.

If the assumption is made that the line shape function is a Gaussian, then a fitting procedure can be used to determine the value of $N\phi(v)$ at the peak, and the total value of N . This procedure indicates that $N\phi(v)$ is well-represented by a Gaussian, at least in the wings, centered at $V_{\text{LSR}} = 6.5 \pm 0.5 \text{ km s}^{-1}$ with a FWHM of $35.7 \pm 1.5 \text{ km s}^{-1}$ and amplitude $(2.65 \pm 0.16) \times 10^{16} \text{ cm}^{-2} (\text{km s}^{-1})^{-1}$. Integrating over the

fitted line profile then gives a total column density for CO in this component of the gas of $(1.0 \pm 0.1) \times 10^{18} \text{ cm}^{-2}$, where the formal error represents solely the uncertainty in the parameters of the fit to the derived $N\phi(v)$ profile. An assumed CO fractional abundance of $[\text{CO}]/[\text{H}_2] = 1.2 \times 10^{-4}$ (Watson 1982) thus gives $N_{\text{H}_2} \sim 8 \times 10^{21} \text{ cm}^{-2}$, which is consistent with the limit derived by Blake *et al.* (1987) of $N_{\text{H}_2} \leq 1 \times 10^{23} \text{ cm}^{-2}$.

The optical depth at line center for the high-velocity component with $T_x = 180 \text{ K}$ peaks at $J = 8-7$ with a value of $0.5/\Omega$, where Ω is the beamfilling factor ($0 < \Omega < 1$). The corresponding optical depth for the $J = 17-16$ CO line at line center is 0.07. This result confirms that our procedure is at least self-consistent, and that the emission in the wings of the $J = 17-16$ line is optically thin for reasonable values of the filling factor.

d) Comparison with Other Observations

Our estimate of $180 \pm 50 \text{ K}$ for the excitation temperature of CO in the plateau emission source is consistent with values deduced from other emission lines thought to arise in the same region. For example, Masson *et al.* (1984) find a brightness temperature of 160 K for the CO $J = 1-0$ line originating from the compact ($\sim 25''$ FWHM) component of the plateau emission. Schloerb *et al.* (1983) have observed a number of SO_2 transitions of varying excitation, and found that $T_x \sim 150 \text{ K}$ is most consistent with the intensities observed in the higher excitation lines. Blake *et al.* (1987) also show that a range of temperatures up to $\sim 200 \text{ K}$ characterizes the excitation of many other molecules in the plateau source.

An excitation temperature as low as 180 K is insufficient to produce significant radiation in transitions with $J > 20$. For example, at line center the expected antenna temperature and integrated intensity are about 2 K and $1.1 \times 10^{-3} \text{ ergs cm}^{-2} \text{ s}^{-1} \text{ sr}^{-1}$ in the $J = 21-20$ transition, with further decrease at higher J . This estimate is inconsistent with the measured integrated intensities of high- J lines which are about an order of magnitude or more larger than the values expected from this 180 K component (Watson *et al.* 1980; Storey *et al.* 1981; Watson *et al.* 1985). However, as discussed by these authors, the radiation at higher J is well described by a single-component model of "warm," postshock gas at $T \sim 750 \text{ K}$. This single-component model incorporates an earlier measurement of the $J = 17-16$ integrated intensity (Stacey *et al.* 1982), which, as discussed previously, is already somewhat higher than our measured value. Furthermore, if one accepts the similarity of line shape in the wings of the $J = 17-16$ line with that in the lower J lines (see Figs. 4a and 4b) as evidence that the same component gives rise to the wing radiation in all of these transitions, then the discrepancy with the 750 K model increases, since only approximately 20% of our observed $J = 17-16$ intensity is left unaccounted for by the 180 K gas component.

The two approaches are complementary, in that Storey *et al.* (1981) and Watson *et al.* (1985) make a model based on data from the higher J lines, which should be sensitive predominantly to the higher temperature post shock gas. Their model, however, does not address the origin of the "excess" emission in low- J lines formed in cooler gas. We, on the other hand, attempt to describe the cooler high-velocity gas that is seen in the wings of low- J and intermediate- J lines. At the intermediate- J values, both gas components can be expected to contribute significantly to the line intensity, and neither description alone suffices. The high resolution available in the

present observations allows us to separate these contributions to some extent, with the conclusion that up to $J = 17-16$ most of the radiation can be explained as arising from the cooler gas. Reconciling this conclusion with the model of Storey *et al.* (1981) and Watson *et al.* (1985) requires an increase in T_x in their model to decrease the expected contribution from hot gas to the intensities of the $J = 17-16$ and $16-15$ lines, and a change in the H_2 density to fit the modified data. It would be informative to observe a high-excitation line ($J > 20$) at resolution similar to that of the present observations to confirm the expected decrease in intensity of the high-velocity, cool component of the line, and to compare a line profile typical of the $> 750 \text{ K}$ gas with that of the narrower component seen in our $J = 17-16$ data.

There is no similarity of the observed $J = 17-16$ line with that of the H_2 vibrational emission in the central region, as shown in Figure 4c. In particular, the marked asymmetry seen in the H_2 profile is absent in the CO data. This is not unexpected, since the vibrational emission is thought to arise from 2000 K gas (Beckwith *et al.* 1978), which is not expected to produce a noticeable contribution to any of the CO rotational lines (Storey *et al.* 1981; Watson *et al.* 1985). However, Scoville *et al.* (1982) conclude from their H_2 vibrational emission data that the asymmetry of the profile results at least partially from the superposition of two distinct emission components, the stronger of which has a V_{LSR} near that of OMC 1 and a FWHM of less than 50 km s^{-1} . If that is indeed the case, then it is possible that the line profiles of the CO and H_2 emission from this component are more similar than indicated by Figure 4c.

As evidence that the high- J infrared CO line emission has a common origin with some high-excitation millimeter-wave spectral lines, Figure 4d shows a comparison of our CO $J = 17-16$ spectrum with that of the SO 7_8-6_7 transition (Loren and Wootten 1986), which arises from an energy level approximately 65 K above the ground, and is associated with the plateau source. As can be seen, the agreement in line profiles is very good, suggesting strongly that emission seen in both lines arises from the same gas. The SO observations were done with a beam size of $1' \times 1.2'$. Although some CO $J = 17-16$ radiation is expected to arise from the hot core, it is likely optically thin since it was not detected. Any optically thick emission would have been seen, even with the beam dilution expected for this compact source.

e) Narrow Component Emission

The narrower component that we observe does not arise in the "hot core," because its V_{LSR} of $9-11 \text{ km s}^{-1}$ is higher than that attributed to hot core emission but typical of the value characteristic of the ridge emission, and in addition it is spatially extended. If our narrow emission represents a contribution that increases with higher J , then it could perhaps be identified with a shock-heated component of the ridge. More observations at good spatial and spectral resolution are needed to clarify this point.

Figure 5a shows the spatial behavior of the two components of the CO $J = 17-16$ spectra. As can be seen from this figure, the intensity of the narrower component is strongest at H_2 peak 1 and decreases monotonically fairly steeply to the southeast in a manner consistent with the change in H_2 vibrational emission (see Fig. 1 and Fig. 5a), while the wider component is strongest at BN and has approximately equal integrated intensities at H_2 peak 1 and peak 2 positions. It

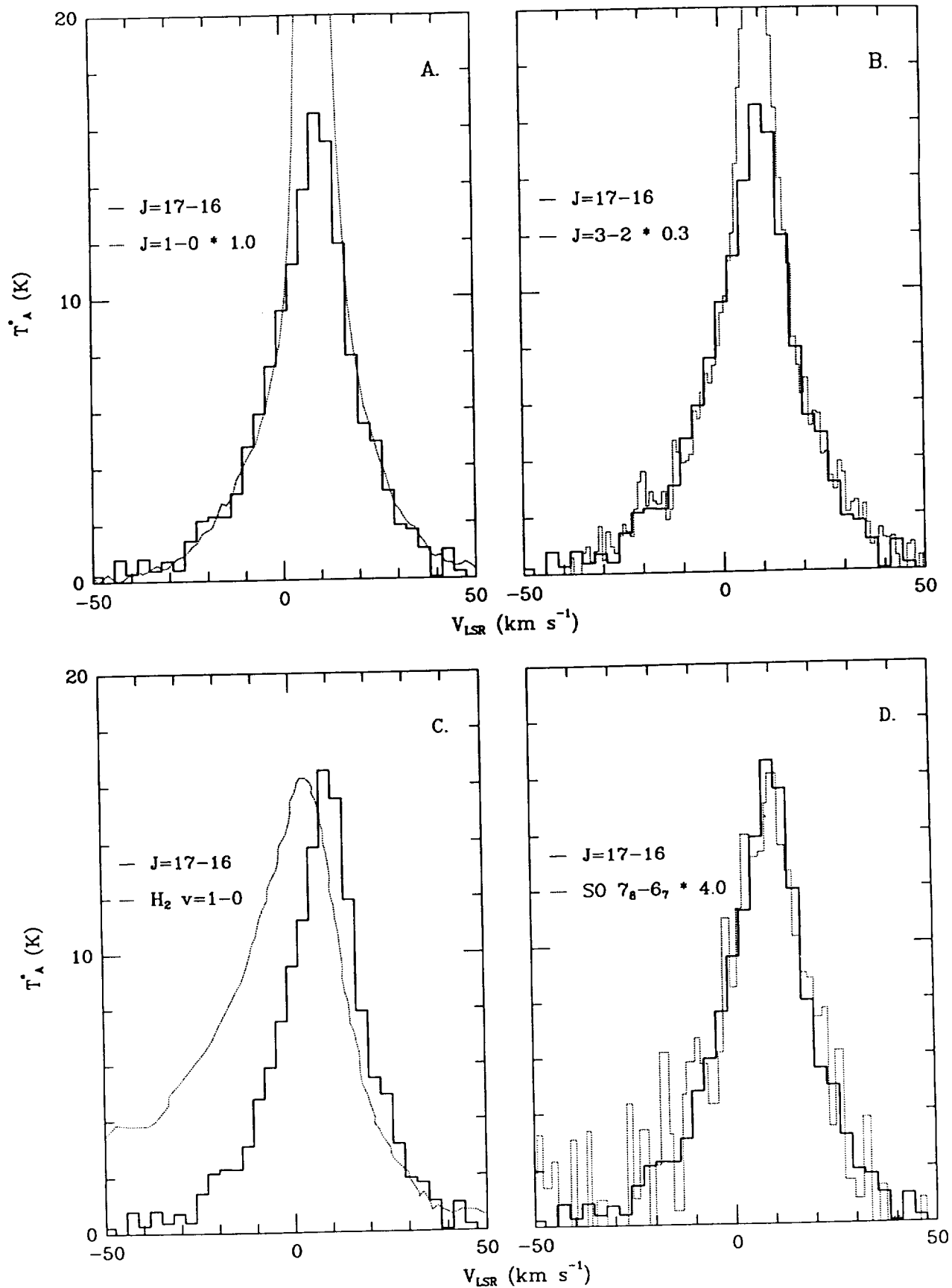


FIG. 4.—The averaged spectrum of the $J = 17-16$ line of CO (solid line), compared with spectra of (a) CO $J = 1-0$ (Plambeck *et al.* 1983); (b) CO $J = 3-2$ (Richardson *et al.* 1985); (c) $\text{H}_2 v = 1-0 S(1)$ (Nadeau, Geballe, and Neugebauer 1982); and (d) $\text{SO } 7_8-6_7$ transition (Loren and Wootten 1986). The continuum has been subtracted from all spectra.

should be noted that this intensity decrease is solely due to a reduction in the component line width. The peak temperatures at the three positions are quite similar. It would be possible by increasing the relative contribution of the narrow component to the line to obtain a spatial distribution similar to that seen in the $J = 21-20$ data of Storey *et al.* (1981), which is also shown in Figure 5a for comparison.

The existence of the narrow line component in the $J = 17-16$ line, especially at θ^1C , suggests that phenomena other than shocks may contribute to the excitation of high- J CO lines. It has been shown by Hayashi *et al.* (1985) that some vibrational emission from H_2 is produced from UV-excited gas. Tielens and Hollenbach (1985) state that production of CO at the edges of photodissociation regions is initiated by reactions of vibrationally excited H_2 . CO produced in an excited state can lead to high- J rotational emission. If CO is self-shielding, then a substantial amount of CO emission would be expected from UV-heated gas, as is suggested by observa-

tions of CO $J = 7-6$ in M17 and S106 (Harris *et al.* 1987). Further evidence for UV-heated CO is provided by the strong, narrow lines of CO $J = 6-5$ emission seen in OMC 1 away from the BN-KL region (Koepl *et al.* 1982). The line width and V_{LSR} of the narrow component in the $J = 17-16$ data are similar to those of other species such as C II known to be produced in the photodissociation region (Boreiko, Betz, and Zmuidzinas 1988). Dual production mechanisms of shocks and ultraviolet photoelectric heating at different spatial locations within the Orion complex are also seen in the O I line at $63 \mu m$ (Werner *et al.* 1984). This latter line shows distinct spatial peaks near θ^1C and BN, but with different widths, being unresolved at θ^1C and with FWHM $\sim 50 \text{ km s}^{-1}$ near BN. The θ^1C region is an interesting candidate for further high-resolution observations in other high- J CO transitions to investigate the excitation mechanism for this narrow emission.

Finally, it is interesting to note the different spatial dependences of the V_{LSR} of the CO line components deduced from

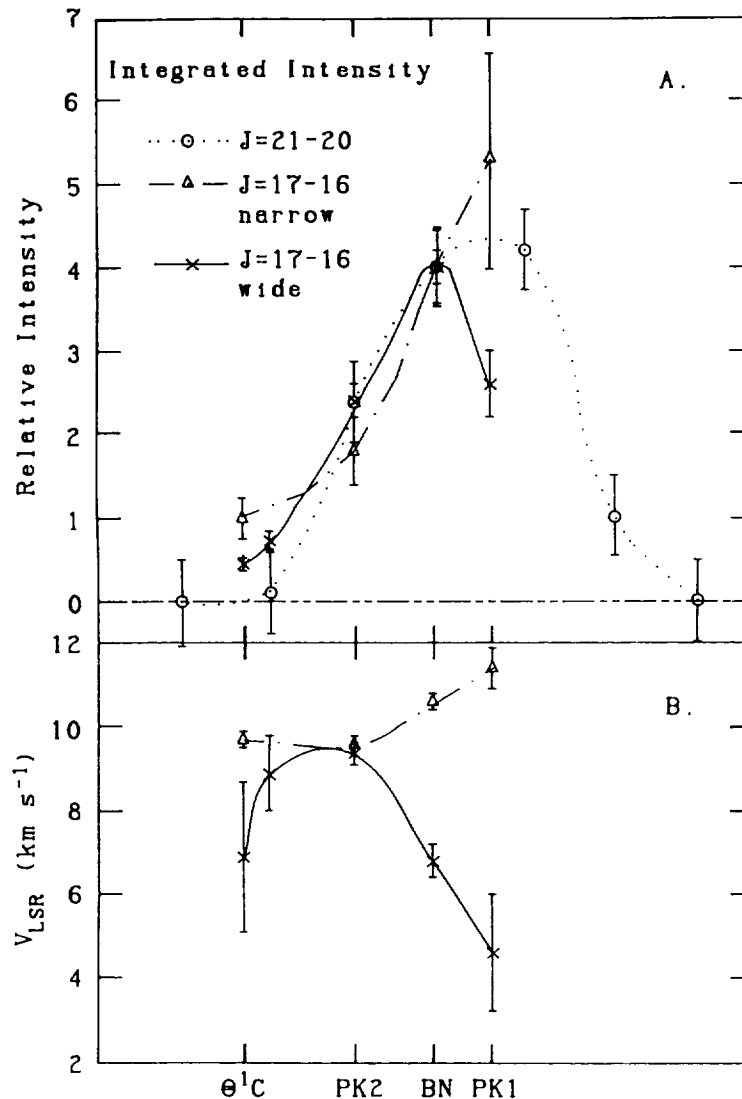


FIG. 5.—Spatial dependence of (a) the integrated intensity of the two components of the CO $J = 17-16$ emission compared with that of the $J = 21-20$ line observed by Storey *et al.* (1981), normalized at BN; and (b) the V_{LSR} of each of the two components of the $J = 17-16$ emission.

our fits. As shown in Figure 5b, the V_{LSR} of the wide component generally decreases from SE to NW, and is always less than that of the narrow component, which increases from SE to NW, although more slowly. This strongly suggests that the narrow component does not originate from the hot core, which is characterized by $V_{\text{LSR}} \sim 5.5 \text{ km s}^{-1}$, but rather from the molecular material in the ridge, which shows a general decrease in V_{LSR} from NE to SW and a V_{LSR} in the range between 8 and 10 km s^{-1} (Bastien *et al.* 1981). The velocity trend in the wide component is similar to that seen in the

high-velocity emission in lower J transitions (Snell *et al.* 1984), further confirming the plateau as the source of the wide component of the $J = 17-16$ CO emission.

We are grateful to the staff of the Kuiper Airborne Observatory for their consistent effort and helpfulness during all phases of our flight operations. We thank R. Plambeck for providing us with tabulated copies of his $J = 2-1$ and $J = 1-0$ CO spectra. These observations were supported by NASA grant NAG 2-254.

REFERENCES

- Bastien, P., Bieging, J., Henkel, C., Martin, R. N., Pauls, T., Walmsley, C. M., and Ziurys, L. M. 1981, *Astr. Ap.*, **98**, L4.
- Beckwith, S., Persson, S. E., Neugebauer, G., and Becklin, E. E. 1978, *Ap. J.*, **223**, 464.
- Betz, A., and Zmuidzinas, J. 1984, in *Proc. Airborne Astronomy Symposium*, (NASA Conf. Pub. CP-2353), pp. 320-329.
- Blake, G. A., Sutton, E. C., Masson, C. R., and Phillips, T. G. 1987, *Ap. J.*, **315**, 621.
- Boreiko, R. T., Betz, A. L., and Zmuidzinas, J. 1988, *Ap. J. (Letters)*, **325**, L47.
- Chernoff, D. F., Hollenbach, D. J., and McKee, C. F. 1982, *Ap. J. (Letters)*, **259**, L97.
- Crawford, M. K., Lugten, J. B., Fitelson, W., Genzel, R., and Melnick, G. 1986, *Ap. J. (Letters)*, **303**, L57.
- Draine, B. T., and Roberge, W. G. 1982, *Ap. J. (Letters)*, **259**, L91.
- Erickson, N. R., Goldsmith, P. F., Snell, R. L., Berson, R. L., Huguenin, G. R., Ulich, B. L., and Lada, C. J. 1982, *Ap. J. (Letters)*, **261**, L103.
- Geballe, T. R., Persson, S. E., Simon, T., Lonsdale, C. J., and McGregor, P. J. 1986, *Ap. J.*, **302**, 693.
- Harris, A. I., Stutzki, J., Genzel, R., Lugten, J. B., Stacey, G. J., and Jaffe, D. T. 1987, *Ap. J. (Letters)*, **322**, L49.
- Hayashi, M., Hasegawa, T., Gatley, I., Garden, R., and Kaifu, N. 1985, *M.N.R.A.S.*, **215**, 31P.
- Keene, J., Blake, G. A., and Phillips, T. G. 1983, *Ap. J. (Letters)*, **271**, L27.
- Koepf, G. A., Buhl, D., Chin, G., Peck, D. D., Fetterman, H. R., Clifton, B. J., and Tannenwald, P. E. 1982, *Ap. J.*, **260**, 584.
- Lang, K. R. 1980, *Astrophysical Formulae* (New York: Springer).
- Linsky, J. L. 1973, *Ap. J. Suppl.*, **25**, 163.
- Loren, R. B., and Wootten, A. 1986, *Ap. J.*, **310**, 889.
- Masson, C. R., *et al.* 1984, *Ap. J. (Letters)*, **283**, L37.
- Masson, C. R., Lo, K. Y., Phillips, T. G., Sargent, A. I., Scoville, N. Z., and Woody, D. P. 1987, *Ap. J.*, **319**, 446.
- McKee, C. F., Storey, J. W. V., Watson, D. M., and Green, S. 1982, *Ap. J.*, **259**, 647.
- Moore, E. L., Langer, W. D., and Huguenin, G. R. 1986, *Ap. J.*, **306**, 682.
- Nadeau, D., Geballe, T. R., and Neugebauer, G. 1982, *Ap. J.*, **253**, 154.
- Nolt, I. G., *et al.* 1987, *J. Molec. Spectrosc.*, **125**, 274.
- Padman, R., Scott, P. F., Vizard, D. R., and Webster, A. S. 1985, *M.N.R.A.S.*, **214**, 251.
- Plambeck, R. L., Snell, R. L., and Loren, R. B. 1983, *Ap. J.*, **266**, 321.
- Richardson, K. J., White, G. J., Avery, L. W., Lesurf, J. C. G., and Harten, R. H. 1985, *Ap. J.*, **290**, 637.
- Schloerb, F. P., Friberg, P., Hjalmarsen, A., Höglund, B., and Irvine, W. M. 1983, *Ap. J.*, **264**, 161.
- Schultz, G. V., Durwen, E. J., Röser, H. P., Sherwood, W. A., and Wattenbach, R. 1985, *Ap. J. (Letters)*, **291**, L59.
- Scoville, N. Z., Hall, D. N. B., Kleinmann, S. G., and Ridgway, S. T. 1982, *Ap. J.*, **253**, 136.
- Snell, R. L., Scoville, N. Z., Sanders, D. B., and Erickson, N. R. 1984, *Ap. J.*, **284**, 176.
- Stacey, G. J., Kurtz, N. T., Smyers, S. D., Harwit, M., Russell, R. W., and Melnick, G. 1982, *Ap. J. (Letters)*, **257**, L37.
- Storey, J. W. V., Watson, D. M., Townes, C. H., Haller, E. E., and Hansen, W. L. 1981, *Ap. J.*, **247**, 136.
- Tielens, A. G. G. M., and Hollenbach, D. 1985, *Ap. J.*, **291**, 722.
- Watson, D. M. 1982, in *Symposium on the Orion Nebula to Honor Henry Draper*, ed. A. E. Glassgold, P. J. Huggins, and E. L. Schucking (*Ann. NY Acad. Sci.*, **395**, 136).
- Watson, D. M., Genzel, R., Townes, C. H., and Storey, J. W. V. 1985, *Ap. J.*, **298**, 316.
- Watson, D. M., Storey, J. W. V., Townes, C. H., Haller, E. E., and Hansen, W. L. 1980, *Ap. J. (Letters)*, **239**, L129.
- Werner, M. W., Crawford, M. K., Genzel, R., Hollenbach, D. J., Townes, C. H., and Watson, D. M. 1984, *Ap. J. (Letters)*, **282**, L81.
- Werner, M. W., Gatley, I., Harper, D. A., Becklin, E. E., Loewenstein, R. F., Telesco, C. M., and Thronson, H. A. 1976, *Ap. J.*, **204**, 420.
- White, G. J., Avery, L. W., Richardson, K. J., and Lesurf, J. C. G. 1986, *Ap. J.*, **302**, 701.

A. L. BETZ and R. T. BOREIKO: Space Sciences Laboratory, University of California, Berkeley, CA 94720

J. ZMUIDZINAS: Astronomy Department, University of Illinois, 1011 West Springfield Avenue, Urbana, IL 61801

A CORNER-REFLECTOR MIXER MOUNT FOR FAR INFRARED WAVELENGTHS

J. ZMUIDZINAS,* A. L. BETZ and R. T. BOREIKO

Space Sciences Laboratory, University of California, Berkeley, CA 94720, U.S.A.

(Received 22 July 1988)

Abstract—A new type of corner-reflector mixer mount, which has the advantages of ease of fabrication and assembly as well as frequency versatility, has been designed and constructed. The mixer works with arbitrary antenna lengths $\geq 4\lambda$ with the reflector to antenna spacing adjusted to give a strong and symmetric central lobe. The predicted response patterns have been experimentally verified for various antenna lengths and operating frequencies between 800 and 2000 GHz. An important design feature is the incorporation of a microstrip matching network which eliminates IF impedance mismatch and provides mechanical isolation for the whisker antenna.

1. INTRODUCTION

The most sensitive mixers using Schottky diodes at frequencies > 100 GHz are currently whisker-contacted devices. At millimeter wavelengths where waveguide structures are generally used, the whisker serves to couple radiation from the waveguide into the diode with an efficiency exceeding 90%. At far-infrared (FIR) wavelengths ($\lambda < 300 \mu\text{m}$), however, waveguide structures are excessively lossy and exceedingly difficult to fabricate. The most evident solution to this problem is to use the contacting whisker as a free-space antenna. In the FIR, fabrication difficulties make it preferable to use whiskers which are long compared to a wavelength ($L \gg \lambda$), even though multi-wavelength antennas do not lead to optimum main beam efficiencies. The radiation pattern of such a long-wire antenna is symmetric about the wire axis and has a main beam in the shape of a hollow cone, however, which is difficult to couple efficiently to other optical systems such as a telescope. This situation can be improved by placing a corner reflector behind the long-wire antenna. Kräutle, Sauter, and Schultz⁽¹⁾ investigated the beam patterns of a 4λ antenna used with corner reflectors of various opening angles (45° , 60° , 75° , 90° , 120° and 180°) as a function of the antenna-reflector spacing s . They found that for a 4λ antenna, a 90° corner reflector whose apex is spaced $s = 1.2\lambda$ from the antenna produces a main beam which peaks at an angle of $\theta_{\text{max}} = 25^\circ$ from the wire axis and whose E-plane and H-plane widths are 14° and 17° , respectively. Since this beam is approximately circularly symmetric, it can be easily matched to a telescope using simple optical elements such as lenses or off-axis mirrors. Although this has proved to be a popular configuration for corner-reflector mixers, it is not the only one which produces an approximately circular main beam. For our application where we must ease the fabrication problem at shorter FIR wavelengths, it is desirable to use antenna lengths larger than 4λ . Although working with longer antennas would optimally require a smaller corner reflector angle as well as a larger spacing between the antenna and the reflector apex, we shall show that keeping a 90° corner angle but increasing the antenna-reflector spacing results in acceptable main beam patterns and coupling efficiencies.

Several corner-reflector mixer mount design variations now exist, each with its own advantages and shortcomings. Fetterman *et al.*⁽²⁾ describe mounts which are compact, but are not tunable and are moderately difficult to fabricate and assemble. Sauter, Schultz and Wohlleben⁽³⁾ describe a mount in which the position of the corner reflector is tuned by a 3-axis translator. While this arrangement is useful for optimizing the reflector position, it is bulky and complicated, and not well suited for high intermediate frequencies (IF) or cryogenic operation. Our application in FIR airborne astronomy required mixers which were simple, compact, easy to fabricate, adjustable and

*Now at Astronomy Department, University of Illinois, 1011 West Springfield Avenue, Urbana, IL 61801, U.S.A.

stable under cryogenic cooling. In addition, the microwave design of the IF port needed attention since the mixer would have to operate at IF frequencies up to at least 10 GHz. These considerations led to our present design. These mixers have been successfully used for airborne observations over the last few years at frequencies between 800 and 2000 GHz.^(4,5)

2. MECHANICAL DESIGN

The configuration of our corner-reflector mixer mount is shown in Fig. 1. The mount is simple, involving only three machined pieces, none requiring difficult tolerances. The mount is tunable in the sense that the reflector position relative to the antenna can be easily adjusted during the final assembly step, and can be repositioned later to accommodate a change in the operating wavelength. An integral microstrip IF matching network allows the IF output impedance of the diode to be easily matched to an external 50 Ω circuit over large bandwidths and at high IF frequencies, and also provides mechanical isolation between the whisker and the IF connector. The mount is rugged and is quite stable upon cryogenic cooling. A novel feature of our mount is that the antenna wire bends away from the apex of the corner reflector. In several previous designs^(2,6) the antenna wire passes through a hole in the reflector apex. The chief advantage of our approach is simplified assembly and adjustment. The antenna can be installed and contacted to the diode prior to the installation of the reflector. Furthermore, the position of the reflector can be adjusted (with the aid of translation stages) without disturbing the antenna. Another advantage of this approach is that the reflector apex does not have any discontinuities, such as a hole⁽²⁾ or a groove⁽³⁾ for the whisker. Although no current flows at the apex, discontinuities near the apex should be kept to a minimum since the surface currents induced by the antenna on the reflector rise rapidly at points away from the apex.⁽⁷⁾ Bending the whisker away from the reflector does not have an adverse effect on the antenna pattern, as will be shown in a later section.

The mount consists of 3 pieces: a base and a reflector, which are machined from tellurium copper and gold plated, and an IF matching network. The assembly procedure is as follows: first, the

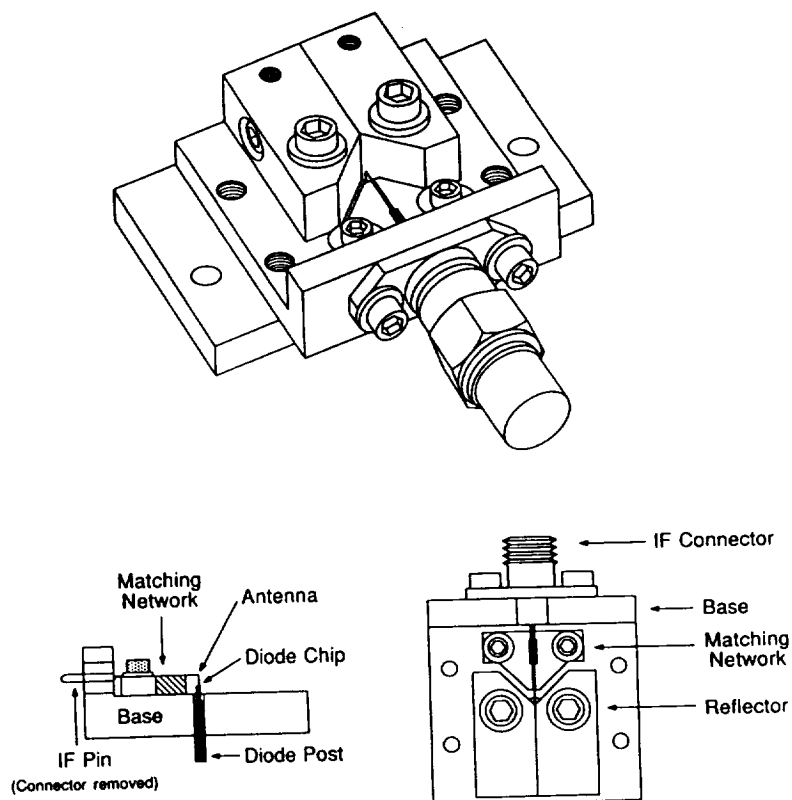


Fig. 1. Our simple corner reflector mixer mount. The side view at lower left omits the reflectors for clarity.

antenna wire (82% Au, 18% Ni, 25 μm dia; obtained from California Fine Wire Co.) is bent to a right angle, one end is cut to the proper antenna length, and the other end is soldered to a microstrip transmission line at one end of the matching network. The matching network is fabricated from aluminum-backed high dielectric constant ($\epsilon = 10.3$) microwave circuit board material (Keene Corp., Laminates Div.). The tip of the whisker-antenna is electrochemically etched to a sharp point in a KCN-K₄Fe(CN)₆ solution. The matching network is set on the base, and its position is adjusted until the pointed antenna hangs over the diode chip, and is then fastened to the base with two screws. At this point, the center pin of an SMA coaxial-to-microstrip IF connector is soldered to the input transmission line of the matching network. The diode chip (100 \times 100 μm , University of Virginia type 1E7A or 1I7) is indium-soldered onto a post consisting of a gold-plated 0.063" dia brass rod reduced at the "diode" end to a diameter of 0.016". The post is held in the base with a set-screw. Diode chips are usually soldered toward the edge of the post to allow small antenna-reflector spacings. The diode post is then raised with a differential-screw micrometer (with the set-screw loose) until the antenna whisker contacts one of the $< 1 \mu\text{m}$ diode anodes on the chip. Each chip has numerous anode metallizations arranged on a square grid, and the exact anode contacted cannot be predetermined. Once a proper contact is made, the differential screw is advanced to provide holding pressure, the diode post set-screw is tightened, and the differential screw is removed. The final step is reflector installation. The reflector consists of two pieces split at the apex to simplify polishing of the reflecting surfaces. These surfaces are polished to near-optical quality to aid the adjustment of the reflector position relative to the antenna. For alignment the reflector is mounted on an X - Y - Z translation stage and then carefully positioned by measuring the antenna to image spacing under a microscope. Once the position is correct, the reflector is fastened to the base, and the X - Y - Z stage is detached and removed.

3. ANTENNA PATTERNS

(a) Introduction

Although the beam patterns of corner reflector mixers have been previously derived in the literature,^(1,2) we will examine the underlying assumptions in more detail, and give a clear derivation of the proper reflector spacing for arbitrary-length antennas. Contour plots of the beam patterns of corner reflector configurations with antenna lengths $L \geq 4\lambda$ will be presented, and the main-beam efficiencies of such configurations will be calculated. In addition, our method can be extended to derive beam patterns for arbitrary-angle corner reflectors,⁽⁹⁾ as well as other reflector shapes, since it does not rely on the method of images.

Our starting point is an expression for the power received by an antenna from an incident electric field. First, let $\mathbf{J}_t(\mathbf{r})$ be the current density on the antenna when *transmitting* and let $\mathbf{E}_{\text{inc}}(\mathbf{r})$ be the electric field incident on the antenna when *receiving* [fields produced by currents induced on the antenna are not included in $\mathbf{E}_{\text{inc}}(\mathbf{r})$]. Harmonic time dependence is assumed. The power received is given by:

$$P_{\text{rec}} \propto \left| \int d^3r \mathbf{J}_t(\mathbf{r}) \cdot \mathbf{E}_{\text{inc}}(\mathbf{r}) \right|^2. \quad (1)$$

This is a result of the well-known reciprocity theorem. If the transmitting current distribution on the antenna is known or can be approximated, this equation permits us to calculate the relative amount of power received by the antenna from any incident radiation field. This relationship will be used to calculate the beam patterns of corner-reflector mixers, and to illustrate the well-known result that optimum coupling is obtained by matching the incident radiation field to the antenna pattern.

(b) Current distribution

Our first task in calculating beam patterns of corner-reflector mixers is to estimate the current distribution on the wire antenna in the transmitting case. Although the characteristics of wire antennas have been the subject of intensive investigation,⁽¹⁰⁾ the category of very long ($> 4\lambda$), extremely thick ($2a > 0.1\lambda$; a = wire radius) antennas is computationally difficult and rarely occurs in other applications, and so therefore has not received much attention. Hallén⁽¹¹⁾ has derived an

exact expression for the outgoing current wave on a cylindrical antenna of infinite length. If the antenna radius is very small ($a \ll 0.01\lambda$), the transmitting current distribution has the form of a wave which travels along the antenna away from the feed point. We can write this as $I(z) = I_0 \exp(ik|z|)$, where $k = \omega/c$ is the free-space wavevector, the z -axis is chosen along the antenna, and $z = 0$ is the feed point. For thick ($a > 0.01\lambda$) antennas, the amplitude of this outgoing wave falls sharply at small distances from the feeding point and remains fairly constant thereafter. On antennas of finite length, the outgoing waves are reflected at the end of the antenna, producing incoming waves. The incoming and outgoing waves interfere to produce standing waves on the antenna. Pickett and Boyd⁽⁷⁾ argue that this effect should be small for thick antennas, reasoning that the amplitude of the reflected current wave should experience a rapid fall-off similar to that experienced by the original outgoing wave. They conclude that the current on a long, electrically thick wire antenna should be well approximated over most of its length by an outgoing traveling wave of constant amplitude, at least for the purposes of determining the antenna pattern. Pickett and Boyd⁽⁷⁾ support this conclusion by noting that the performance of their mixer was unchanged when the conducting "floor" of their cube-corner mount was covered with an absorbing material, which would absorb most of the radiation produced by an incoming current wave instead of reflecting it into the direction of the radiation produced by the outgoing wave. Harris⁽⁶⁾ also reports that tilting the floor of a cube-corner mount by 5° did not change the beam pattern or the mixer conversion loss.

In this paper, we shall assume the current distribution to be an outgoing traveling wave, and we will neglect the effects of currents on the horizontal section of the whisker. These assumptions simplify the beam-pattern and design calculations and allow us to easily evaluate the *general* characteristics of mixers with arbitrary-length antennas. In addition, our predicted main beam patterns give good agreement with the experimental data. Vowinkel⁽⁸⁾ has presented results of beam-pattern and main-beam efficiency calculations of 4λ mixers based on a more complicated ad-hoc current distribution, including currents on the horizontal section of the whisker. Of critical importance for the efficiency calculations is the magnitude of the current on the horizontal section, since this current generally produces larger sidelobe levels, reducing the efficiency. Vowinkel's approach is to treat the horizontal and vertical sections as transmission lines, ignoring mutual impedance effects at the bend where the two sections meet. The transmission-line approximation is particularly suspect, since many propagation modes are allowed for typical whisker-reflector spacings ($s \geq \lambda$). Nevertheless, Vowinkel was able to obtain improved agreement with experimental scale-model antenna patterns. However, it is not clear that Vowinkel's model would accurately predict the characteristics of mixers with our geometry, in which the whisker bends away from the reflector, since the transmission-line approximation would be even more questionable in this case. Clearly, an accurate theoretical description of the current distribution will require a rigorous solution of the antenna boundary-value problem. The detailed antenna characteristics of our mixers are perhaps best evaluated experimentally by careful scale-model measurements.

(c) Beam patterns

Consider a wire antenna of length L oriented along the z -axis of a coordinate system and placed with its center at the origin. The current on the (transmitting) antenna is assumed to be:

$$\begin{aligned} I(z) &= I_0 \exp(ikz) \quad \text{for } |z| < L/2, \\ &= 0 \quad \text{for } |z| > L/2. \end{aligned} \quad (2)$$

This current distribution should be adequate for the calculation of beam patterns. Calculations of the antenna impedance, however, would require the exact current distribution. The power received from a plane wave incident from direction \mathbf{u} with polarization \mathbf{a} ($\mathbf{a} \cdot \mathbf{a} = \mathbf{u} \cdot \mathbf{u} = 1$; $\mathbf{a} \cdot \mathbf{u} = 0$) is given by [see equation (1)]:

$$P_{\text{rec}}(\mathbf{u}, \mathbf{a}) \propto \left| \int_{-L/2}^{L/2} dz I_0 \exp(ikz) a_z \exp(-ikz u_z) \right|^2, \quad (3)$$

where a_z and u_z are the z -components of \mathbf{a} and \mathbf{u} , respectively. Expressing \mathbf{u} in polar coordinates

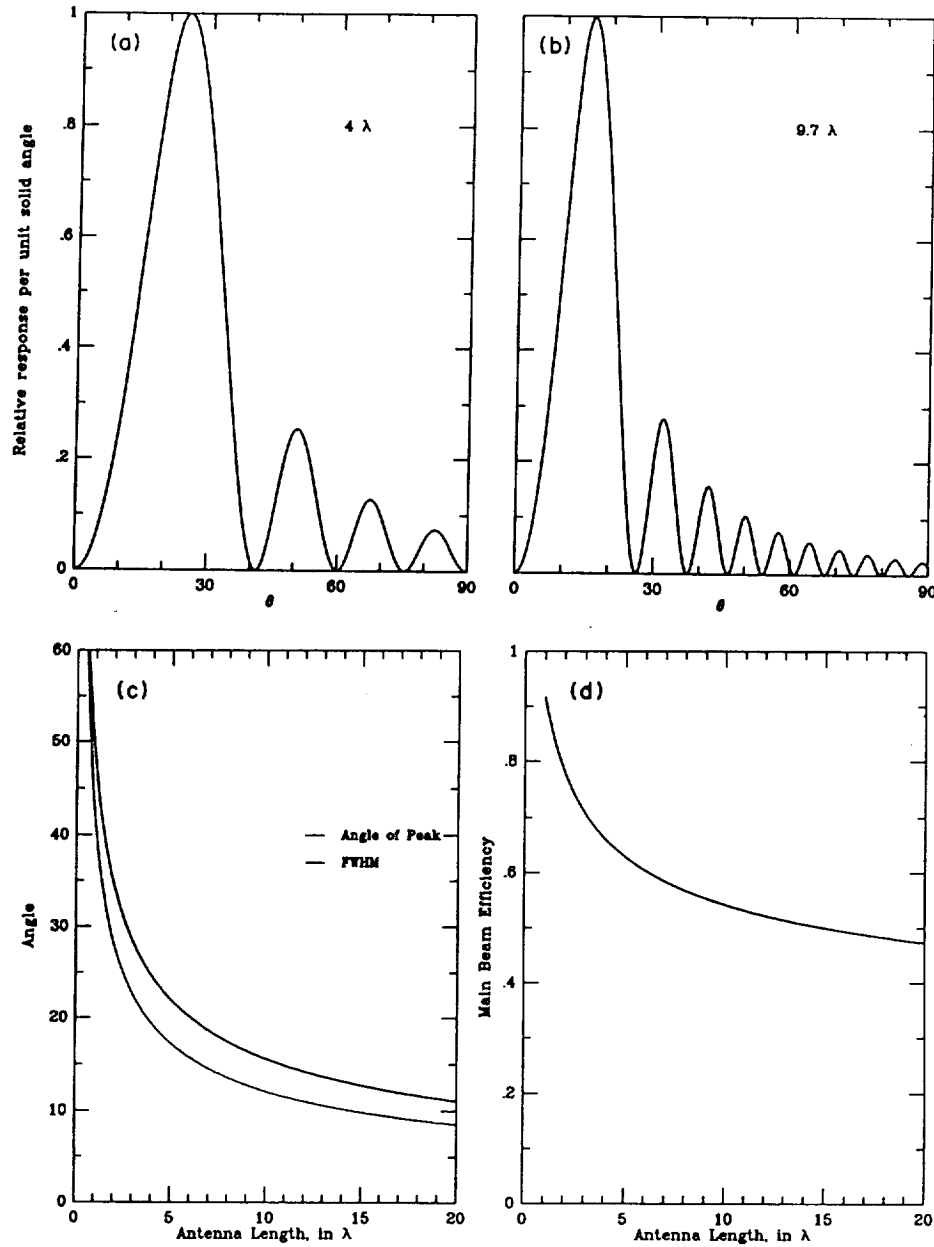


Fig. 2. (a) Beam pattern of a 4λ wire antenna. (b) Beam pattern of a 9.7λ wire antenna. (c) Main beam angle (solid) and FWHM (dotted) vs antenna length. (d) Main beam efficiency vs antenna length.

and choosing the polarization a which maximizes a_z leads to:

$$P_{\text{rec}}(\theta) \propto \left| \sin \theta \int_{-L/2}^{L/2} dz \exp[ikz(1 - \cos \theta)] \right|^2 = L^2 \sin^2 \theta \text{sinc}^2 \left[\frac{L\pi}{\lambda} (1 - \cos \theta) \right]. \quad (4)$$

The first term measures the degree of polarization matching between the antenna current and the incident wave and is maximized at normal incidence ($\theta = \pi/2$), while the second term measures the degree of phase matching, and is maximized for a wave incident along the antenna axis ($\theta = 0$). For long antennas ($L > \lambda$), the angle θ_{max} at which equation (4) is maximized is given approximately by:

$$\theta_{\text{max}} \approx \cos^{-1} [1 - 0.37101\lambda/L]. \quad (5)$$

Figures 2(a) and (b) show the resulting patterns for $L = 4\lambda$ and $L = 9.7\lambda$ (chosen because

$4 \times 370 \mu\text{m} = 9.7 \times 153 \mu\text{m}$; the wavelengths correspond to two strong $^{15}\text{NH}_3$ FIR laser lines which were used to test mixers). The patterns consist of a main lobe and several smaller sidelobes. The main lobe becomes narrower and peaks at smaller angles when the antenna length is increased, and the number of sidelobes increases. This can also be seen from Fig. 2(c), which plots θ_{max} and the full width to half maximum (FWHM) of the main lobe as a function of antenna length. The main lobe efficiency is defined as the ratio of the power radiated into the main lobe to the total power radiated into all lobes, and is plotted in Fig. 2(d) as a function of antenna length. The efficiency decreases gradually with increasing antenna length because the main lobe becomes narrower and the number of sidelobes increases.

We are now in a position to calculate the beam patterns of long-wire antennas inside corner reflectors. We begin by expanding the incident field in terms of plane waves:

$$\mathbf{E}_{\text{inc}}(\mathbf{r}) = \int \sin \theta \, d\theta \, d\phi \, g(\theta, \phi) \mathbf{a}(\theta, \phi) \exp[-ik\mathbf{r} \cdot \mathbf{u}(\theta, \phi)]. \quad (6)$$

Here $\mathbf{u}(\theta, \phi)$ is a unit vector in the direction given by the polar angles θ and ϕ :

$$\mathbf{u}(\theta, \phi) = \cos \theta \, \mathbf{z} + \sin \theta (\cos \phi \, \mathbf{x} + \sin \phi \, \mathbf{y}), \quad (7)$$

$\mathbf{a}(\theta, \phi)$ is the unit vector perpendicular to \mathbf{u} which maximizes its z -component:

$$\mathbf{a}(\theta, \phi) = \sin \theta \, \mathbf{z} - \cos \theta (\cos \phi \, \mathbf{x} + \sin \phi \, \mathbf{y}), \quad (8)$$

and $g(\theta, \phi)$ gives the amplitude of the plane wave incident from direction $\mathbf{u}(\theta, \phi)$. The power carried by this field can be obtained by calculating the Poynting vector flux through the x - y plane; the result is

$$P_{\text{inc}} \propto \int \sin \theta \, d\theta \, d\phi \, |g(\theta, \phi)|^2. \quad (9)$$

We place a 90° corner reflector with its apex along the z -axis and its reflecting surfaces along the x - z and y - z planes. When the incident wave encounters the reflector, four waves of equal amplitude are produced: the incident wave, reflected waves from each of the two surfaces, and one doubly-reflected wave. These waves add to produce the following z -component of the electric field in the vicinity of the reflector:

$$E_z(\mathbf{r}) \propto \int \sin \theta \, d\theta \, d\phi \, g(\theta, \phi) \sin \theta \exp(-ikz \cos \theta) \sin(kx u_x) \sin(ky u_y), \quad (10)$$

which shows that E_z is composed of standing waves which vanish on the reflecting surfaces $x = 0$ and $y = 0$. Equations analogous to equation (10) for more complicated reflector geometries may be obtained by solving a boundary-value problem for the field inside the reflector, and relating the asymptotic behavior of the solution to the plane-wave expression given by equation (6).⁽⁹⁾ Next, consider a long-wire antenna placed near the reflector, at the position (x_a, y_a) . The (transmitting) current on the antenna should not change substantially due to the presence of the reflector, since in practical circumstances the distance to the reflector will be at least one wavelength. The power received by the antenna from the incident field is calculated from equations (1) and (10):

$$P_{\text{rec}} \propto \left| \int \sin \theta \, d\theta \, d\phi \, g(\theta, \phi) h^*(\theta, \phi) \right|^2, \quad (11)$$

where $h(\theta, \phi)$ is given by:

$$h(\theta, \phi) = \sin \theta \, \text{sinc} \left[\frac{\pi L}{\lambda} (1 - \cos \theta) \right] \sin(kx_a u_x) \sin(ky_a u_y). \quad (12)$$

The antenna pattern is given by $|h(\theta, \phi)|^2$, as can be seen by choosing $g(\theta, \phi)$ to be highly peaked in one direction. Equation (11) is a general result applicable to any antenna. Applying the Cauchy-Schwartz inequality to equations (9) and (11) shows that P_{rec} is maximized for a fixed incident power when $g(\theta, \phi) \propto h(\theta, \phi)$. This means that the incident radiation should be matched to the antenna pattern for optimal coupling, a familiar result. When this is not the case, the power

received by the antenna is reduced by:

$$\eta_{\text{antenna}} = \frac{|(g, h)|^2}{(g, g)(h, h)}, \quad (13)$$

where the inner product (g, h) is given by:

$$(g, h) = \int \sin \theta \, d\theta \, d\phi \, g(\theta, \phi) h^*(\theta, \phi). \quad (14)$$

Equations (13) and (14) are also expressions which apply generally to all antennas.

(d) Antenna-reflector spacing

We have already seen that a long-wire antenna is most sensitive to radiation incident at an angle of θ_{max} with respect to the wire axis [see equation (5)]. The presence of a reflector will produce standing waves; the positions of the standing-wave peaks depend on the direction (θ, ϕ) of the incoming radiation. The power received by the antenna from radiation incident at (θ, ϕ) will be maximized if the antenna is located at the position of a standing-wave peak. For optimum coupling, the antenna should be placed at a standing-wave peak produced by a plane wave which is on-axis ($\phi = \pi/4$) and is incident at $\theta = \theta_{\text{max}}$. This is a general principle useful for finding the optimum location of the antenna with respect to reflectors of *arbitrary shape*, including corner reflectors of *any* opening angle (not just those which produce a finite number of image antennas), as well as parabolic, cylindrical, or elliptical reflectors. Applying this principle to the case of 90° corner reflectors gives, from equations (7) and (12):

$$kx_a \sin \theta_{\text{max}} \cos(\pi/4) = \pi/2 \quad \text{and} \quad ky_a \sin \theta_{\text{max}} \sin(\pi/4) = \pi/2, \quad (15)$$

which gives $x_a = y_a$ and:

$$s = \sqrt{x_a^2 + y_a^2} = \frac{\lambda}{2 \sin \theta_{\text{max}}}. \quad (16)$$

For example, an antenna with $L = 4\lambda$ has $\theta_{\text{max}} \approx 25^\circ$ and so the optimal spacing is predicted from equation (16) to be $s = 1.2\lambda$. Notice that the standing-wave peak nearest to the reflector apex has been chosen. This choice results in good coupling over the broadest possible range of incidence angles, and thus gives the best main-beam efficiency.

(e) E-plane and H-plane angles

Beam patterns for corner-reflector mixers are usually presented in terms of E-plane and H-plane angles. Figure 3 shows the definition of these angles as well as the definition of the usual polar angles. From the figure, we can see that the unit vector \mathbf{u} [see equation (7)] can be expressed in terms of the E-plane angle θ' and the H-plane angle Γ :

$$\mathbf{u}(\theta', \Gamma) = (\mathbf{z} \cos \theta' + \mathbf{n} \sin \theta') \cos \Gamma + \mathbf{m} \sin \Gamma, \quad (17)$$

where the unit vectors \mathbf{n} and \mathbf{m} are:

$$\mathbf{n} = \frac{1}{\sqrt{2}}(\mathbf{x} + \mathbf{y}) \quad (18)$$

$$\mathbf{m} = \frac{1}{\sqrt{2}}(-\mathbf{x} + \mathbf{y}). \quad (19)$$

The beam pattern can be calculated in terms of θ' and Γ from equation (12) by using:

$$\cos \theta = \cos \theta' \cos \Gamma \quad (20)$$

$$u_x = \frac{1}{\sqrt{2}}(\sin \theta' \cos \Gamma - \sin \Gamma) \quad (21)$$

$$u_y = \frac{1}{\sqrt{2}}(\sin \theta' \cos \Gamma + \sin \Gamma). \quad (22)$$

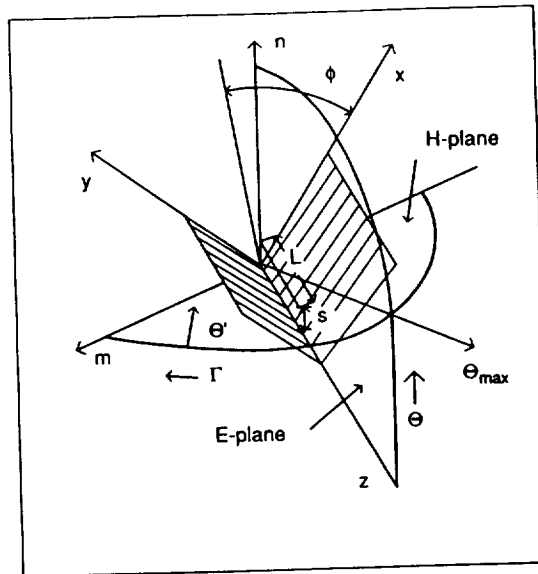


Fig. 3. Diagram showing the definition of the polar angles (θ , ϕ) and the E-plane and H-plane angles (θ' , Γ). Adapted from Vowinkel.⁽⁶⁾

We note that for a 90° corner reflector, the azimuthal angle ϕ is restricted to $0 \leq \phi \leq \pi/2$; otherwise, the reflector shadows the antenna from the incident radiation. This results in a restriction on the H-plane angle Γ , given by:

$$\cos^2 \Gamma \geq \frac{1}{1 + \sin^2 \theta'} \quad (23)$$

(f) *Mixers with arbitrary-length antennas*

Equation (16) can be used to design 90° corner reflector mixers with arbitrary antenna lengths. For practical reasons, the antenna length will usually be between 4λ and 10λ . Given the antenna length L , one calculates θ_{\max} from equation (5), and the proper spacing from equation (16). However, the symmetry of the main beam is of concern. The width of the beam in the E-plane direction is reduced as the antenna length is increased (see Fig. 2(c)), and it would seem that a symmetric beam (equal H-plane and E-plane widths) could only be obtained for a unique antenna length. Fortunately, longer antennas have a smaller θ_{\max} , and the corner reflector is more effective in confining the H-plane width of the beam at steeper incidence angles [see equation (23)], and so approximate symmetry can be maintained over a large range of antenna lengths. Figure 4 shows a contour plot of the antenna pattern of a 4λ antenna at a spacing of 1.2λ (the usual configuration), while Fig. 5 shows the pattern of a 9.7λ antenna at a spacing of 1.7λ . Also drawn are the reflector boundaries in E- and H-plane coordinates [equation (23)]. Both patterns have fairly symmetric main beams, and the effect of the reflector in confining the H-plane extent of the patterns is clearly seen. The E-plane widths (FWHM) are 13.7° and 8.8° , and the H-plane widths are 17.2° and 11.8° , for the 4λ and 9.7λ antennas, respectively. The relative asymmetry (ratio of H- to E-plane width) is 1.26 for the 4λ antenna and 1.35 for the 9.7λ antenna.

Longer antennas do offer some practical advantages, especially at the shorter FIR wavelengths ($\lambda < 200 \mu\text{m}$). First, fabrication is easier since the antenna is longer and spaced farther from the reflector. Also, the narrower main beam can be coupled more efficiently to the telescope, especially when off-axis reflective optics (which produce amplitude distortions for beams of large opening angle⁽¹²⁾) are used. The disadvantage of longer antennas is the somewhat reduced main-beam efficiency.

(g) *Main-beam efficiency of mixers with arbitrary-length antennas*

The main-beam efficiency of long-wire antennas without reflectors has been presented in Fig. 2(d). A corner reflector modifies the main-beam efficiency somewhat, because it affects the main

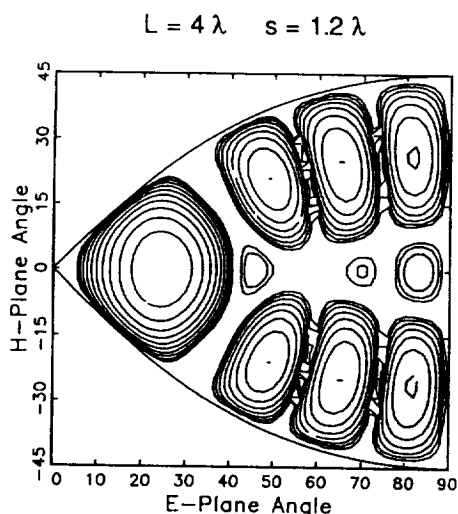


Fig. 4. Antenna pattern of a 4λ antenna spaced 1.2λ from the apex of a 90° corner reflector. Contour spacing is 3 dB. Also plotted is the reflector boundary [equation (23)].

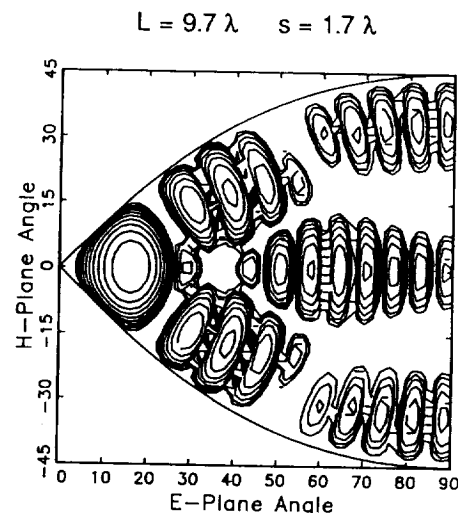


Fig. 5. Same as Fig. 4 except for a 9.7λ antenna spaced 1.7λ from the apex of a 90° corner reflector.

beam and sidelobes differently. In general, the corner reflector *increases* the efficiency. This occurs because the antenna-reflector spacing is chosen to be resonant at the main-beam angle θ_{\max} , and (on average) is not resonant at the sidelobe angles. Thus, the reflector suppresses the sidelobes relative to the main lobe.

The main-beam efficiency is defined as $\eta_{\text{MB}} \equiv \eta_{\text{antenna}}$ [see equation (13)] for the case in which the incident field $g(\theta, \phi)$ matches the antenna pattern $h(\theta, \phi)$ over the main beam and is zero otherwise, and gives the fraction of the power in such an incident field which is received by the antenna (if it has an impedance-matched load connected to its terminals). The incident field defined above is closely approximated in actual receiver systems, since the field incident on the mixer is usually a converging Gaussian beam (asymmetric if it need be) whose half-power beam width (HPBW) is matched to that of the mixer. Substituting $g(\theta, \phi)$ as defined above into equation (13) gives:

$$\eta_{\text{MB}} = \frac{\int_{\text{main beam}} \sin \theta \, d\theta \, d\phi |h(\theta, \phi)|^2}{\int_{\text{entire pattern}} \sin \theta \, d\theta \, d\phi |h(\theta, \phi)|^2} \quad (24)$$

The integrals over ϕ can be performed analytically:

$$\int_0^{\pi/2} d\phi |h(\theta, \phi)|^2 = \frac{\pi}{8} \sin^2 \theta \operatorname{sinc}^2 \left[\frac{\pi L}{\lambda} (1 - \cos \theta) \right] [1 - 2J_0(\sqrt{2}x) + J_0(2x)], \quad (25)$$

where:

$$x = \frac{2\pi s}{\lambda} \sin \theta,$$

and $J_0(x)$ is the ordinary Bessel function of order 0. The factor in equation (25) involving Bessel functions peaks at $x = 3.05$. This peak will correspond to the angle θ_{\max} if the spacing is given by:

$$s = \frac{0.97\lambda}{2 \sin \theta_{\max}},$$

which agrees well with equation (16). The integrals over θ in equation (24) must be performed numerically. The "main beam" is defined as $0 \leq \theta \leq \cos^{-1}(1 - \lambda/L)$ (i.e. to the first zero in the antenna pattern), while the "entire pattern" is defined as $0 \leq \theta \leq \pi$. These calculations assume that

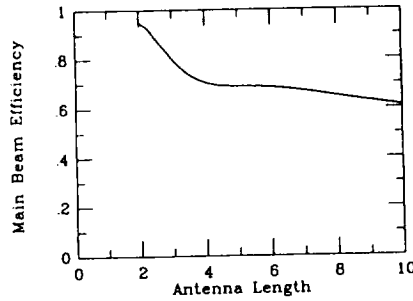


Fig. 6. The main-beam efficiency of corner reflector mixers as a function of antenna length.

no ground plane is present, so that the wave radiated by the antenna at an angle of $\pi - \theta$ (which is reflected by the ground plane into the angle θ) does not interfere with the wave radiated at angle θ . This should be a good approximation in our mixer design where the diode is usually several wavelengths above the ground plane, such that with the rapid phase variations between the direct and reflected waves with angle there should be little net interference between the two waves (i.e. there is little *spatial* overlap between the direct and reflected beams). Regardless, the fields radiated toward the ground plane by the antenna are small.

The resulting main-beam efficiency (η_{MB}) is plotted as a function of antenna length in Fig. 6. In the calculation, the antenna-reflector spacing for each value of antenna length was chosen according to equation (16). As can be seen, the reflector causes the efficiency to improve over that of a bare antenna (Fig. 2d), and to decrease more gradually for increasing antenna lengths. The efficiency of a $L = 4\lambda$ configuration is $\eta_{MB} = 0.71$, while the efficiency of a $L = 9.7\lambda$ configuration is $\eta_{MB} = 0.62$, which is only 13% worse. Naturally, these efficiencies may be somewhat overestimated if the current distribution is not ideal or the optical coupling does not accept an asymmetric Gaussian beam. Regardless, these calculations serve to show that the efficiency does not necessarily degrade rapidly with increasing antenna length.

(h) Experimental results

Comparison of Figs 4 and 5 with experimental results is not possible over the entire range of E- and H-plane angles, since our mixer mounts shadow the antenna from radiation at large E-plane angles. However, we note that the experimental pattern shown by Harris⁽⁶⁾ for a 4λ mixer of standard configuration agrees reasonably well with Fig. 4, and that the deviations are probably due to imperfect antenna alignment. Figure 7 shows the E-plane and H-plane cuts through the main

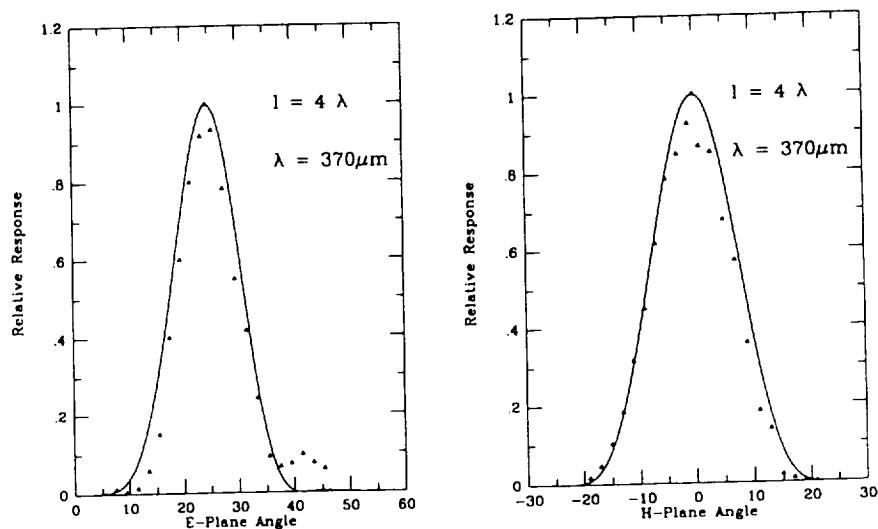


Fig. 7. Measured E- and H-plane patterns for a 4λ mixer.

beam measured with our 4λ mixer at $370\ \mu\text{m}$, along with the theoretical prediction. The results agree quite well, showing that the horizontal section of the wire does not affect the main beam. This is to be expected, since the horizontal section is poorly phase-matched to the incident radiation [see equation (4)]. Figure 8 shows the results measured for 9.7λ mixers, at 370 and $153\ \mu\text{m}$, which again agree well with the theoretical predictions with the exception of the H-plane pattern at $153\ \mu\text{m}$. The source of the discrepancy is unknown but perhaps due to alignment effects. System noise temperatures (SSB) measured with mixers cooled to $77\ \text{K}$ in our receiver⁽¹³⁾ are $8000\ \text{K}$ at $800\ \text{GHz}$ and $21,000\ \text{K}$ at $2000\ \text{GHz}$, for tests with IF center frequencies of 6.3 and $9.3\ \text{GHz}$, respectively.

4. MIXER MATCHING NETWORK

The IF resistance of the FIR mixer diode, under the d.c. bias and LO drive conditions which result in optimum heterodyne sensitivity, is in the range of $100\text{--}200\ \Omega$ (depending on the diode). This result was obtained from $200\ \text{MHz}$ RF network analyzer measurements, and (not surprisingly) agrees with resistances calculated from the pumped $I\text{--}V$ curve. In order to achieve optimum power transfer to the $50\ \Omega$ IF amplifier, and hence to minimize the effective noise contribution of the IF amplifier, an impedance matching network must be used. In addition, if an isolator is used to provide a stable source impedance for the amplifier, there is another important reason for ensuring good IF match. As can be seen in Fig. 9, the isolator termination radiates thermal (Johnson) noise towards the FIR mixer. If the mixer IF impedance is mismatched, this noise is partially reflected into the IF amplifier, which increases the effective IF noise temperature. Since the physical temperature of the isolator ($77\ \text{K}$) is significantly larger than the noise temperature of the IF amplifier, even moderate impedance mismatches can substantially increase the IF noise. Quantitatively, the total IF noise at the amplifier input is given by:

$$T_{\text{total}} = T_D (1 - |\Gamma|^2) + T_{\text{iso}} |\Gamma|^2 + T_a,$$

where T_D is the effective IF noise temperature of the diode, T_{iso} is the physical temperature of the isolator termination, T_a is the noise temperature of the amplifier, and Γ is the complex IF amplitude

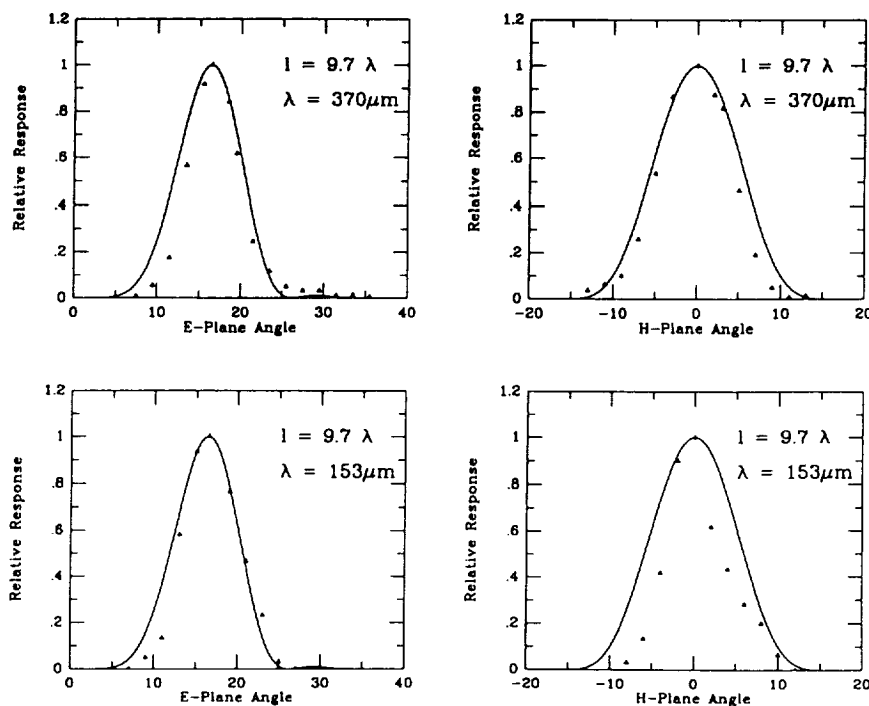


Fig. 8. Measured E- and H-plane patterns for 9.7λ mixers. The measurement wavelengths are labeled.

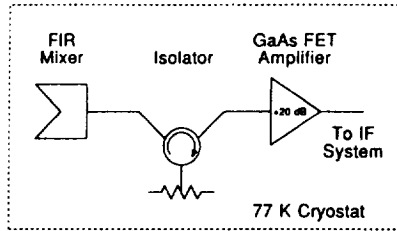


Fig. 9. First IF amplifier and isolator. The amplifier has an internal bias tee for d.c. bias of the mixer.

reflection coefficient of the mixer. If the mixer conversion loss L is known, the system noise temperature can be calculated in the usual way:

$$T_{\text{sys}} = \frac{L T_{\text{total}}}{1 - |\Gamma|^2} = T_N + L T_{\text{IF}},$$

where $T_N = L T_D$ is the noise temperature of the mixer and the effective IF noise temperature is given by:

$$T_{\text{IF}} = \frac{T_a + |\Gamma|^2 T_{\text{iso}}}{1 - |\Gamma|^2}.$$

For example, if $T_{\text{iso}} = 80$ K and $T_a = 40$ K, then a reflection coefficient of $|\Gamma| = 0.5$ (6 dB return loss) will result in an effective IF noise temperature which is double the amplifier noise temperature. This effect also makes it difficult to estimate the mixer conversion loss L when the impedance match is not known.

The microstrip matching networks used in our mixers for astronomical observations of the 1900 GHz line of ionized carbon⁽⁵⁾ are fabricated for an IF near 9.3 GHz, since a fixed-frequency laser is used as the local oscillator. The networks are designed to match a 100 Ω diode resistance, but will provide a reasonable match over the range of 50–200 Ω . Compensation is included for the stray circuit elements of the mixer mount, such as the inductance of the antenna wire. The design of the matching network started with the assembly of a mixer with a 50 Ω section of microstrip transmission line in place of the matching network. Next, the complex reflection coefficient of this mixer was measured with a microwave network analyzer over a broad range of frequencies and with varying diode dynamic resistances (controlled by d.c. bias). Subsequent modeling of these experimental results led to the equivalent circuit shown in Fig. 10. On the basis of this circuit, the desired transmission-line transformer was designed, and is shown in Fig. 11. This transformer was then assembled into a mixer and tested on a network analyzer. With the diode biased at 100 Ω dynamic resistance, the measured return loss was 22 dB at 9.3 GHz, and was better than 10 dB over the range 8.6–9.8 GHz. Similar networks have been built at lower IF frequencies with equivalent success.

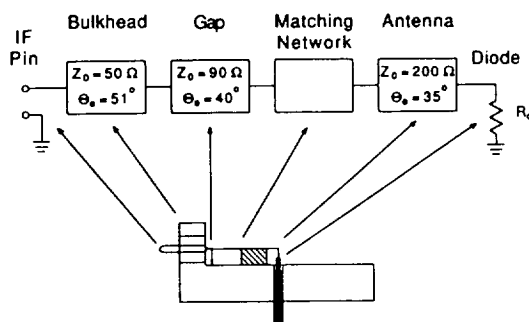


Fig. 10. Equivalent IF circuit of mixer mount. Electrical lengths θ_e given at 9.3 GHz.

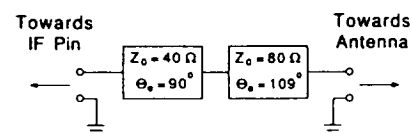


Fig. 11. Design of 9.3 GHz IF matching network. Electrical lengths θ_e given at 9.3 GHz.

5. SUMMARY

We have presented a design for a corner-reflector mixer which is suitable for use at FIR wavelengths. The design objectives required for our application in FIR airborne astronomy have all been met. The mixer is simple, rugged, adjustable and cryogenically coolable. A microstrip transmission-line transformer is used to match the mixer IF impedance to $50\ \Omega$ at IF frequencies as high as 9.3 GHz.

We have also investigated antenna length-reflector spacing configurations which differ from the usual $L = 4\lambda$, $s = 1.2\lambda$ prescription, and have presented a simple relation for calculating the optimum antenna-reflector spacing for antennas of arbitrary length. Theoretical beam patterns for $L = 4\lambda$ and $L = 9.7\lambda$ mixers have been presented, and have been shown to be in reasonable agreement with experimentally measured patterns. The degradation of mixer performance with increasing antenna length has been shown to be relatively gradual, both in terms of the symmetry and efficiency of the main beam. Therefore, the use of longer antennas and larger antenna-reflector spacings which eases mixer fabrication, especially at the shorter far-infrared wavelengths, does not necessitate a significant decrease in efficiency.

Acknowledgements—This work was supported by NASA under grant NAG 2-254. R. T. B. was supported in part through a postdoctoral fellowship award from the Natural Sciences and Engineering Research Council of Canada. We are grateful to R. Mattauch and T. Crowe of the University of Virginia Semiconductor Device Laboratory for supplying the GaAs diodes used in this work.

REFERENCES

1. H. Kräutle, E. Sauter and G. V. Schultz, *Infrared Phys.* **17**, 477 (1977).
2. H. R. Fetterman, P. E. Tannenwald, B. J. Clifton, C. D. Parker, W. D. Fitzgerald and N. R. Erickson, *Appl. Phys. Lett.* **33**, 151 (1978).
3. E. Sauter, G. V. Schultz and R. Wohlleben, *Int. J. infrared millimeter Waves* **5**, 451 (1984).
4. J. Zmuidzinas, A. L. Betz and D. M. Goldhaber, *Ap. J. Lett.* **307**, L75 (1986).
5. R. T. Boreiko, A. L. Betz and J. Zmuidzinas, *Ap. J. Lett.* **325**, L47 (1988).
6. A. I. Harris, Ph.D. thesis, U. C. Berkeley (1986).
7. H. M. Pickett and T. C. Boyd, *Proc. Eighth Ann. Int. Conf. on IR and MM Waves*, IEEE, New York (1983).
8. B. Vowinkel, *Int. J. infrared millimeter Waves* **7**, 155 (1986).
9. J. Zmuidzinas, Ph.D. thesis, U.C. Berkeley (1987).
10. R. W. P. King, *Tables of Antenna Characteristics*. Plenum, New York (1971).
11. E. Hallén, *Electromagnetic Theory*. Wiley, New York (1962).
12. J. A. Murphy, *Int. J. infrared millimeter Waves* **8**, 1165 (1987).
13. A. L. Betz and J. Zmuidzinas, in *Proc. Airborne Astronomy Symposium*, NASA Conf. Publ. 2353, pp. 320-329 (1984).

HETERODYNE SPECTROSCOPY OF THE $J = 22-21$ CO LINE IN ORION

R. T. BOREIKO AND A. L. BETZ

Space Sciences Laboratory, University of California

Received 1989 May 5; accepted 1989 August 23

ABSTRACT

We have observed the $J = 22-21$ line of ^{12}CO at 2528 GHz (118.8 μm) in the IRc2 region of Orion. The spectra at 0.6 km s^{-1} resolution show both plateau emission with FWHM $\sim 35 \text{ km s}^{-1}$ and a narrower component with FWHM $\sim 8 \text{ km s}^{-1}$. Comparison with heterodyne data of similar quality on the $J = 17-16$ line indicates that the broad and narrow components both originate in gas with an excitation temperature $T_{\text{ex}} \sim 600 \text{ K}$. The emission is consistent with the predictions of shock models in which the wide component arises from the heated outflow gas and postshock molecular material, while the narrow component comes from ambient material near the leading edge of the shock front where temperatures are high but significant acceleration has not yet occurred.

Subject headings: interstellar: molecules — nebulae: internal motions — nebulae: Orion Nebula

I. INTRODUCTION

The BN-KL/IRc2 region in Orion is an area of star formation where shock processes are thought to be important for the formation and excitation of molecular material (Draine and Roberge 1982; Chernoff, Hollenbach, and McKee 1982). The interaction of the supersonic outflow from the vicinity of IRc2 with the ambient molecular material can be readily studied through observations of high- J lines of CO which provide cooling for the postshock gas. Measurements of integrated intensities for various high- J lines have proved useful in constraining shock model parameters (Watson *et al.* 1980; Storey *et al.* 1981; Watson *et al.* 1985). High-resolution ($< 1 \text{ km s}^{-1}$) observations of the CO line profiles should provide complementary information on the dynamical behavior of the shock as it propagates into the ambient cloud.

This Letter presents the first observations of the 2528 GHz $J = 22-21$ line of ^{12}CO in which the line profile is clearly resolved. Comparison of these new heterodyne data with previous high-resolution spectra of the $J = 17-16$ line of CO (Boreiko, Betz, and Zmuidzinas 1989) allows us to deduce the temperature and column density of the emitting gas and to distinguish line emission at the leading edge of the shock front from the broader line profile produced by the heated outflow and swept-up material.

II. INSTRUMENTATION AND CALIBRATION

The data were obtained using a far-infrared heterodyne receiver (Betz and Zmuidzinas 1984). The local oscillator (LO) is an optically pumped laser operating on the 2522.7824 GHz line of CH_3OH (Inguscio *et al.* 1986), and the mixer is a GaAs Schottky diode (University of Virginia type 1T2) in a corner-reflector mount (Zmuidzinas, Betz, and Boreiko 1989) cooled to 77 K. The system noise temperature was measured to be 37,000 K (SSB) during the observations. The IF signal is analyzed by two parallel filterbanks, one with 0.6 km s^{-1} resolution spanning 24 km s^{-1} and the other with 2.4 km s^{-1} resolution over a 150 km s^{-1} range.

The spectrometer was flown aboard the Kuiper Airborne Observatory at an altitude of 12.5 km where the mean atmospheric transmission is better than 90% over the observed band. The diffraction-limited beam size was $\sim 33''$, and the

coupling efficiency was ~ 0.8 . The chopping frequency was 2 Hz, with a chop amplitude of $10'$ NE-SW. Pointing accuracy is estimated to be better than $10''$.

Absolute calibration is based on spectra of the Moon for which a physical temperature of 394 K and emissivity of 0.98 were assumed (Linsky 1973). The Orion spectra were corrected for five atmospheric features which affected only the continuum. The accuracy of the calibration, including all systematic effects apart from source coupling, is estimated to be 10%.

The velocity scale is determined from the known frequencies of the LO and of the $^{12}\text{C}^{16}\text{O}$ $J = 22-21$ transition ($2528.1720 \pm 0.0001 \text{ GHz}$; Nolt *et al.* 1987). The frequency stability of our LO was determined by laboratory measurements of CO in an absorption cell and set the 2σ accuracy of the V_{LSR} scale at better than $\pm 0.4 \text{ km s}^{-1}$.

III. OBSERVATIONS

Six positions within the Orion molecular complex were observed on the night of 1989 January 17: IRc2, H_2 peak 1, H_2 peak 2, $30''$ NW of H_2 peak 1 along a line joining peaks 1 and 2, θ^1 Ori C, and S6. Figure 1 shows the resulting spectra of the $J = 22-21$ line of CO in the wider bandwidth filterbank. The 0.6 km s^{-1} and 2.4 km s^{-1} resolution data were simultaneously fitted to a continuum plus one or two Gaussians degraded to the spectral resolution of the observations. The derived parameters given in Table 1 fit the data to within statistical uncertainties.

The peak continuum value in Table 1 of $T_c = 4.2 \pm 0.1 \text{ K}$ measured at IRc2 is in reasonable agreement with that interpolated from the relationship of Werner *et al.* (1976) of $T_c = 4.3 \text{ K}$ for a source uniformly filling a $1'$ beam. Since our data indicate a FWHM for the continuum of $35''-45''$, the correction for source size should not exceed 20%–30%.

IV. ANALYSIS AND INTERPRETATION

a) IRc2 Region

The spectrum at IRc2 can be fitted by two Gaussian components: one with FWHM of 35 km s^{-1} centered at 7.7 km s^{-1} V_{LSR} and the other with FWHM of 8 km s^{-1} centered at 7.3 km s^{-1} , as shown in Figure 1. The wide component is logically identified with the "plateau" emission seen in CO lines at all J

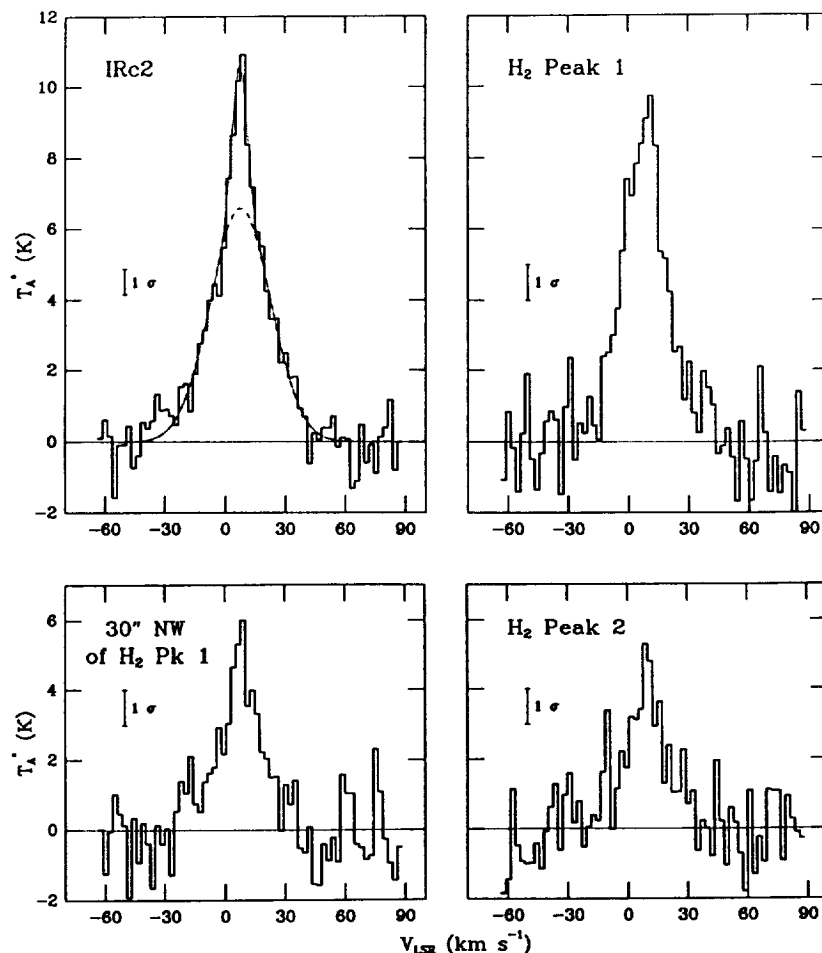


FIG. 1.—Spectra of the $J = 22-21$ line of CO at 2.4 km s^{-1} resolution from four locations in Orion. Integration times are 32 minutes for IRC2 and 16 minutes for each of the other locations. The continuum has been subtracted from all spectra. In the IRC2 spectrum, the dotted line shows the two-component Gaussian fit, while the dashed line shows the fit to the wide (plateau) component only.

for which high-resolution data are available. The narrower “spike” or “ridge” component seen in lower J CO lines is generally attributed to optically thick emission from the quiescent molecular cloud with $T_{\text{ex}} < 100 \text{ K}$. However, this same gas cannot be responsible for the narrow emission from the $J = 22-21$ line because the required column density at such a low temperature is far too high to be consistent with the measured intensity of the $J = 17-16$ line (Boreiko, Betz, and Zmuidzinas 1989, hereafter BBZ).

The profiles of the $J = 22-21$ line at IRC2 and $J = 17-16$ line at BN show very good agreement, aside from an apparent shift in the V_{LSR} of the narrow component between the two positions. This similarity strongly suggests that the gas volumes producing the narrow and wide components have similar temperature. The relative intensities of just these two lines suggest a temperature of 500–1000 K for both components. However, the similarity of the velocity and width of the wide component in both the $J = 22-21$ and $J = 17-16$ lines with those of the

TABLE 1
2528 GHz CO $J = 22 \rightarrow 21$ RESULTS

Source	T_A^{**} (K)	V_{LSR} (km s^{-1})	Line Width (km s^{-1} , FWHM)	Integrated Intensity ($\text{ergs s}^{-1} \text{cm}^{-2} \text{sr}^{-1}$)	Continuum ^b (K)
30" NW of H ₂ peak 1	5.1 (0.3)	8.0 (0.6)	20.4 (1.8)	$1.85 (0.32) \times 10^{-3}$	1.10 (0.09)
H ₂ peak 1	8.9 (0.3)	7.5 (0.4)	25.0 (1.2)	$3.97 (0.32) \times 10^{-3}$	3.01 (0.09)
IRC2	6.6 (0.4)	7.7 (0.6)	35.1 (2.2) } 8.1 (0.9) }	$4.64 (0.21) \times 10^{-3}$	4.15 (0.06)
H ₂ peak 2	4.0 (0.3)	9.1 (0.8)	24.3 (2.7)	$1.76 (0.32) \times 10^{-3}$	1.63 (0.09)
θ^1 Ori C	$0.07 (0.38) \times 10^{-3}$	0.45 (0.06)
S6	$0.38 (0.41) \times 10^{-3}$	0.65 (0.08)

NOTE.—Quantities in parentheses are 1σ statistical uncertainties.

^a T_A^* is corrected for the continuum.

^b Continuum temperatures are single-sideband values.

“plateau” component seen in lower J lines, together with the equivalent similarity between the narrow high- J component and the “spike” component of low- J lines, suggest that essentially all emission from CO near IRC2 up to $J = 22-21$ arises from the same interacting gas components, but under different physical conditions.

It was shown in BBZ that the CO plateau emission for all observed lines up to $J = 17-16$ could arise from a region characterized by $T_{\text{ex}} \sim 180$ K and $N_{\text{CO}} \sim 1 \times 10^{18} \text{ cm}^{-2}$. The new $J = 22-21$ data show that this simplified isothermal approximation is not suitable for either the plateau or the quiescent emission regions, and that the high-temperature region inferred from previous observations of far-infrared CO transitions to $J = 34-33$ (Watson *et al.* 1980; Storey *et al.* 1981; Watson *et al.* 1985) is intimately connected with both the outflow and the quiescent gas. We have fitted Gaussian components to published high spectral resolution ($\Delta V < 3 \text{ km s}^{-1}$) CO data between $J = 1-0$ and $J = 22-21$. The fits generally show clear evidence for a “plateau” component with $30-40 \text{ km s}^{-1}$ line width and a “ridge” component with $\sim 6 \text{ km s}^{-1}$ line width. Figure 2 shows the antenna temperatures derived for each component. Open circles in the plateau emission curve represent lower limits from data obtained with beam sizes larger than $45''$. Error bars include statistical uncertainties in the fits as well as the more dominant systematic calibration uncertainties (assumed to be 25% if not quoted).

The continuous curves in Figure 2 show the antenna temperatures expected from a two-component LTE model for the plateau and ridge emission. The curve for the plateau emission is obtained from gas at 130 K with CO column density of $N_{\text{CO}} = 1 \times 10^{18} \text{ cm}^{-2}$ together with gas at 600 K with $N_{\text{CO}} = 1 \times 10^{17} \text{ cm}^{-2}$. The ridge emission is modeled by a 67 K component with $N_{\text{CO}} = 1.6 \times 10^{19} \text{ cm}^{-2}$ and a 600 K component with $N_{\text{CO}} = 2 \times 10^{16} \text{ cm}^{-2}$. These values are representative only since there are insufficient constraints for a unique solution. The value of N_{CO} for the cooler ridge gas chosen for the

model is that given by Wilson *et al.* (1986). The excitation temperature of the quiescent gas is a lower limit since the fitting procedure underestimates T_{ex}^* for the narrow component if it is optically thick and absorbs some of the plateau emission in the same velocity range.

The temperature we deduce for the hot component agrees with that derived from observations of unresolved high- J CO lines by Storey *et al.* (1981) and Watson *et al.* (1985). This agreement should be expected if the CO profiles for $J > 22$ separate into wide and narrow components in a manner similar to that discussed here. However, the total column density for the high-temperature CO obtained here is a factor of 3 lower than the “best fit” value of Watson *et al.* (1985). This difference is related to the factor of 2.4 difference between our measured integrated intensity and that of Watson *et al.* (1985).

b) Shock-heated Gas

The CO $J = 22-21$ components which we associate with $T \sim 600$ K gas almost certainly arise from the shocked region where the outflow material collides with the quiescent ridge gas. We see strong emission in the hot plateau component from H_2 peak 2 to beyond H_2 peak 1, and therefore we identify the wide component with the shock-heated gas at the edge of the outflow and tentatively suggest that the narrow component is likely to be emission from associated warm gas in the ambient molecular cloud.

Models of MHD shock waves (e.g., Draine, Roberge, and Dalgarno 1983) predict that there is a region at the leading edge of the shock front, extending over almost half the shock-heated region, where the ambient gas has already been heated to temperatures near 1000 K but not yet accelerated to the outflow velocity. A typical width for the shock-heated region for a 25 km s^{-1} shock propagating into a cloud with a density of 10^6 cm^{-3} is $\sim 5 \times 10^{14} \text{ cm}$ (Draine, Roberge, and Dalgarno 1983). The narrow 600 K component of the $J = 22-21$ line has a column density of $\sim 2 \times 10^{16} \text{ cm}^{-2}$ and therefore arises from

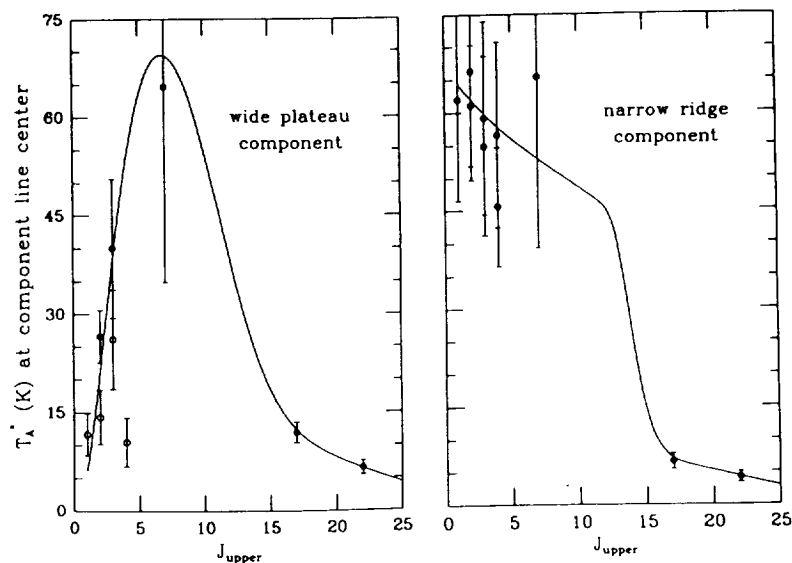


FIG. 2.—Antenna temperature as a function of J for the wide plateau component (left) and narrow ridge component (right). The data are from Plambeck, Snell, and Loren (1983; $J = 1-0$ and $2-1$), Sutton *et al.* (1985; $J = 2-1$), Erickson *et al.* (1982; $J = 3-2$), Richardson *et al.* (1985; $J = 3-2$), Phillips, Kwan, and Huggins (1980; $J = 4-3$, narrow component only because of the 2.9 beam size), Walker *et al.* (1988; $J = 4-3$), Schmid-Burgk *et al.* (1989; $J = 7-6$), BBZ ($J = 17-16$), and the present work ($J = 22-21$). The $J = 6-5$ data of Koepf *et al.* (1982) are not shown since it was not possible to derive two components from the published spectrum. Open circles are used for data with beam sizes greater than $45''$. The smooth curves come from a two-temperature model (see text).

a region of approximate thickness 2×10^{14} cm if the CO/H₂ ratio is 1.2×10^{-4} and the H₂ density is 10^6 cm⁻³. Therefore, it appears likely that the emission in the narrow velocity component comes from a thin sheet of gas at the leading edge of the shock front. The line width of the narrow component in the $J = 22-21$ and $J = 17-16$ CO lines is ~ 2 km s⁻¹ greater than values typical for $J \leq 3$, which could indicate some acceleration of the neutral gas toward the outflow velocity. A similar analysis of the wide 600 K component yields a thickness for the emitting region of $\sim 10^{15}$ cm. The emission most likely arises from the combination of the "swept-up" molecular cloud material behind the shock front and the warm outflow material itself.

c) Spatial and Velocity Characteristics

The integrated intensity of the $J = 22-21$ line probably peaks between IRC2 and H₂ peak 1, with a FWHM $\sim 1'$ as observed with our 33" beam. This distribution is similar to that observed in the $J = 17-16$ line (BBZ) but is narrower than the ~ 1.5 FWHM deduced by Storey *et al.* (1981) from an incremental strip scan in the $J = 21-20$ line.

While a single Gaussian fits the data at all positions except IRC2 to within statistical uncertainties, the addition of a second component noticeably improves the fits. The narrow components thus derived have a FWHM ~ 4 km s⁻¹, V_{LSR} of 9–10 km s⁻¹, and integrated intensities $\sim 5\%$ – 10% of those measured in the wide (plateau) component. The lower width for the

narrow component away from IRC2 is consistent with the expectation that the shock acceleration of the ambient material is more in the plane of the sky toward H₂ peaks 1 and 2 than at IRC2. However, spectra with higher signal-to-noise ratios are needed to confirm the existence of any narrow component at locations offset from IRC2.

The interpretation of the data presented here suggests that the angular size of the plateau emission observed in CO should change rather abruptly with J : for lower J (up to 10–15 in the simple two-component model illustrated in Fig. 2), the radiation originates from the bulk of the outflow material interior to the shocked region, while at higher J the CO emission comes from the shell of shocked material. This appears to be the case, with emission size being 25"–50" FWHM for $J \leq 3$ (Phillips, Kwan, and Huggins 1980; Knapp *et al.* 1981; Erickson *et al.* 1982; Masson *et al.* 1987) and $\geq 60''$ FWHM for $J \geq 17$ (Storey *et al.* 1981; Watson *et al.* 1985; BBZ; this work). The increase in size at high J is not simply related to the added angular thickness of the shell (which is very small) but rather depends upon the detailed geometry of the emitting region. Observations at much higher spatial resolution in the high- J transitions would be needed to delineate this effect.

We are grateful to the staff of the Kuiper Airborne Observatory for getting this flight off the ground at the last minute. This work was supported by NASA grant NAG 2-254.

REFERENCES

- Betz, A., and Zmuidzinas, J. 1984, in *Proc. Airborne Astronomy Symposium* (NASA Conf. Pub. CP-2353), p. 320.
 Boreiko, R. T., Betz, A. L., and Zmuidzinas, J. 1989, *Ap. J.*, **337**, 332 (BBZ).
 Chernoff, D. F., Hollenbach, D. J., and McKee, C. F. 1982, *Ap. J. (Letters)*, **259**, L97.
 Draine, B. T., and Roberge, W. G. 1982, *Ap. J. (Letters)*, **259**, L91.
 Draine, B. T., Roberge, W. G., and Dalgarno, A. 1983, *Ap. J.*, **264**, 485.
 Erickson, N. R., Goldsmith, P. F., Snell, R. L., Berson, R. L., Huguenin, G. R., Ulich, B. L., and Lada, C. J. 1982, *Ap. J. (Letters)*, **261**, L103.
 Knapp, G. R., Phillips, T. G., Huggins, P. J., and Redman, R. O. 1981, *Ap. J.*, **250**, 175.
 Inguscio, M., Moruzzi, G., Evenson, K., and Jennings, D. A. 1986, *J. Appl. Phys.*, **60**, R161.
 Koepf, G. A., Buhl, D., Chin, G., Peck, D. D., Fetterman, H. R., Clifton, B. J., and Tannenwald, P. E. 1982, *Ap. J.*, **260**, 584.
 Linsky, J. L. 1973, *Ap. J. Suppl.*, **25**, 163.
 Masson, C. R., Lo, K. Y., Phillips, T. G., Sargent, A. I., Scoville, N. Z., and Woody, D. P. 1987, *Ap. J.*, **319**, 446.
 Nolt, I. G., *et al.* 1987, *J. Molec. Spectrosc.*, **125**, 274.
 Phillips, T. G., Kwan, J., and Huggins, P. J. 1980, in *IAU Symposium 87, Interstellar Molecules*, ed. B. H. Andrew (Dordrecht: Reidel), p. 21.
 Plambeck, R. L., Snell, R. L., and Loren, R. B. 1983, *Ap. J.*, **266**, 321.
 Richardson, K. J., White, G. J., Avery, L. W., Lesurf J. C. G., and Harten, R. H. 1985, *Ap. J.*, **290**, 637.
 Schmid-Burgk, J., *et al.* 1989, *Astr. Ap.*, **215**, 150.
 Storey, J. W. V., Watson, D. M., Townes, C. H., Haller, E. E., and Hansen, W. L. 1981, *Ap. J.*, **247**, 136.
 Sutton, E. C., Blake, G. A., Masson, C. R., and Phillips, T. G. 1985, *Ap. J. Suppl.*, **58**, 341.
 Walker, C. K., Schulz, A., Krügel, E., and Gillespie, A. R. 1988, *Astr. Ap.*, **205**, 243.
 Watson, D. M., Genzel, R., Townes, C. H., and Storey, J. W. V. 1985, *Ap. J.*, **298**, 316.
 Watson, D. M., Storey, J. W. V., Townes, C. H., Haller, E. E., and Hansen, W. L. 1980, *Ap. J. (Letters)*, **239**, L129.
 Werner, M. W., Gatley, I., Harper, D. A., Becklin, E. E., Loewenstein, R. F., Telesco, C. M., and Thronson, H. A. 1976, *Ap. J.*, **204**, 420.
 Wilson, T. L., Serabyn, E., Henkel, C., and Walmsley, C. M. 1986, *Astr. Ap.*, **158**, L1.
 Zmuidzinas, J., Betz, A. L., and Boreiko, R. T. 1989, *Infrared Phys.*, **29**, 119.

REVERSED FAR-INFRARED LINE EMISSION FROM OH IN ORION

A. L. BETZ AND R. T. BOREIKO

Space Sciences Laboratory, University of California

Received 1989 May 5; accepted 1989 August 23

ABSTRACT

The fundamental OH rotational transition at 2514 GHz (119.2 μm) has been observed in the Orion IRc2 region at a spectral resolution of 0.6 km s^{-1} . The emission is spatially compact (<25" FWHM) and centered near IRc2. A comparison of the observed profile with spectra of other species known to exist in the region suggests that the entire blueshifted side of the OH profile has been "self-absorbed," leaving only a redshifted emission component. In addition, there is pronounced absorption near 5 km s^{-1} V_{LSR} indicative of the "hot core" source. The presence of the 119 μm absorption provides a straightforward explanation for the high ratio of 163/119 μm integrated line intensities which was previously considered anomalous.

Subject headings: interstellar: molecules — nebulae: internal motions — nebulae: Orion Nebula

I. INTRODUCTION

Emission from the far-infrared rotational lines of OH is an important indicator of high excitation phenomena in regions of star formation. Ever since the detection of the 119 μm transition in Orion (Storey, Watson, and Townes 1981), the OH lines have generally been interpreted as emission from shock-excited gas in the vicinity of IRc2. Theoretically a shock can provide both the high OH abundance and the high excitation required by the observations (Draine and Roberge 1982; Chernoff, Hollenbach, and McKee 1982). However, because some of the observed line intensity ratios seem anomalous, the usefulness of the data has been limited for constraining shock parameters. In particular, Viscuso *et al.* (1985) noted that the observed 163 μm /119 μm integrated intensity ratio appeared discrepant with the assumption of LTE, and suggested that the intensity observed for the 119 μm line was low because of collisional deexcitation effects. Melnick, Genzel, and Lugten (1987), on the other hand, suggested that processes other than collisions must enhance the 163 μm emission.

Heretofore, the far-infrared OH lines have not been observed with either a velocity resolution or a velocity scale accuracy adequate to match millimeter and submillimeter data available on other molecules. Since OH may have velocity structure on a scale of 1 km s^{-1} , similar to that observed for high-excitation lines of CO, HCN, SiO, SO, and HDO, we have reobserved the OH rotational fundamental at 119.2 μm with 0.6 km s^{-1} resolution.

II. INSTRUMENTATION AND CALIBRATION

A laser heterodyne spectrometer (Betz and Zmuidzinas 1984) was used aboard the NASA Kuiper Airborne Observatory to observe the $J^p = 5/2^- - 3/2^+$ OH hyperfine triplet centered near 2514.3 GHz (Farhoomand, Blake, and Pickett 1985). The local oscillator (LO) was the 2522.7824 GHz transition of a CH_3OH laser (Inguscio *et al.* 1986), and the mixer was a GaAs Schottky diode (University of Virginia type 117) in a corner-reflector mount (Zmuidzinas, Betz, and Boreiko 1989). The noise temperature of the cooled (77 K) receiver was measured to be 31,000 K (SSB) during the observations. The IF signals over a bandwidth of 1280 MHz (153 km s^{-1}) were analyzed in two parallel filter banks: 64 20-MHz filters and 40 5-MHz filters, yielding spectral resolutions of 2.4 km s^{-1} and

0.6 km s^{-1} , respectively. From measurements of the CO $J = 22-21$ line in a laboratory absorption cell, the long-term frequency stability of the LO is better than 2 MHz. The uncertainties in both the LO and OH line frequencies are sufficiently low that the Doppler velocity scale is accurate to 0.4 km s^{-1} (2σ).

The $^2\Pi_{3/2}$ OH rotational levels are split by lambda-doubling to yield a pair of fundamental rotational transitions at 2510 GHz ($J^p = 5/2^+ - 3/2^-$) and 2514 GHz ($J^p = 5/2^- - 3/2^+$). Each of the lambda-doubled levels is in turn split by hyperfine interactions to yield three components per rotational level. However, the velocity dispersion in IRc2 is generally high enough that the hyperfine components are blended. We observed the 2514 GHz (119.2 μm) triplet because of its more favorable atmospheric transmission of 0.95 at flight altitude of 12.5 km. The diffraction-limited beamwidth of the 91 cm telescope was $\sim 33''$ (FWHM), and a pointing accuracy $< 10''$ was maintained by frequent checks on the nearby star θ^1 Ori C. Beam-switching with a $10'$ throw (NE-SW) was done at 2 Hz. Calibration of the single-sideband OH line intensity was obtained from spectra of the Moon taken during the flight. The physical temperature of the Moon at the subsolar position was assumed to be 394 K and the emissivity 0.98 (Linsky 1973). Aside from the beam-filling factor, the overall statistical and systematic uncertainty in the intensity calibration is estimated to be less than 10%.

III. OBSERVATIONS

Spectra of the $J^p = 5/2^- - 3/2^+$ OH line were taken on the night of 1989 January 20 (UT), and results from IRc2 and the H_2 peak 1 and 2 positions of Beckwith *et al.* (1978) are shown in Figure 1. Also plotted for comparison in Figure 1a is a truncated spectrum of the ^{12}CO $J = 22-21$ line observed by Boreiko and Betz (1989) at IRc2. The CO line lies 14 GHz higher in frequency and was observed with the same spectral resolution and beam size 2 days earlier. The most notable point in the OH spectra is the large apparent redshift of the emission peak to a V_{LSR} near 20 km s^{-1} . No molecule observed in the Orion IRc2 region at radio wavelengths has thermal emission centered at this velocity. In fact, even OH itself, when observed in the $^2\Pi_{3/2}$ $J = 7/2$ lambda-doubled transition at 13 GHz, is centered at $V_{\text{LSR}} = 7 \pm 2$ km s^{-1} (Matthews *et al.*

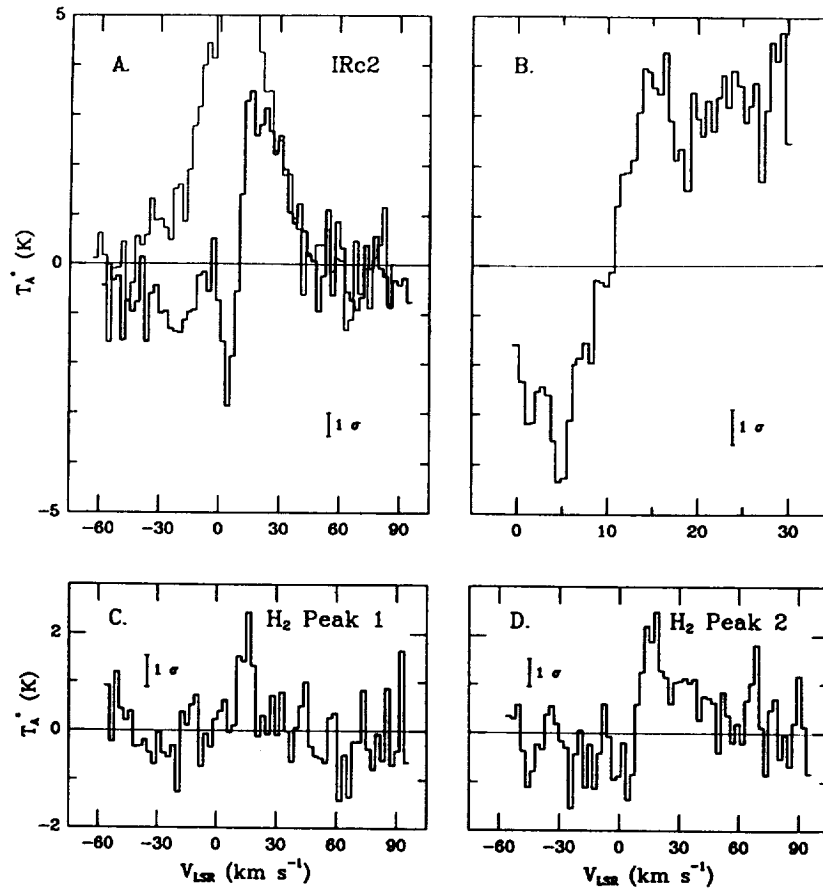


FIG. 1.—OH 2514 GHz (119.2 μm) line profiles observed at three positions in Orion. Panel (a) shows the spectra toward IRC2: the dark line shows the OH profile, while the light line is a truncated spectrum of the $J = 22-21$ spectrum of CO (Boreiko and Betz 1989). Panel (b) shows the central velocity section toward IRC2 at higher resolution (0.6 km s^{-1}). Integration times are 48 minutes for IRC2, 24 minutes for H_2 peak 1, and 32 minutes for H_2 peak 2. The continuum has been subtracted from all spectra.

1986), close to the $V_{\text{LSR}} \sim 8 \text{ km s}^{-1}$ usually ascribed to the “outflow” source.

The striking similarity of the redshifted edges of the CO and OH profiles in Figure 1a provides a strong visual clue to a likely explanation. Apparently, the entire blueshifted side of the OH line has been absorbed by unexcited foreground gas. Only emission redshifted from line center remains.

IV. ANALYSIS AND INTERPRETATION

a) OH Emission Component

The high excitation requirement for the OH rotational lines provides a significant constraint on the possible sources of emission. The upper level of the $J^P = 5/2^- - 3/2^+$ transition lies 120 K above the ground state. For this level to be maintained in LTE solely by collisions would require H_2 densities $> 10^{10} \text{ cm}^{-3}$ for gas in the 100–500 K range. Somewhat lower densities would suffice if OH is subthermally excited or optically thick. Regardless, densities $> 10^8 \text{ cm}^{-3}$ are likely only near the center of the outflow source. Figure 2 plots the integrated intensity of the 119.2 μm OH line at the three observed positions. For comparison, five-point scans of the $J = 22-21$ CO and continuum intensities (Boreiko and Betz 1989) are also plotted. We see that the OH emission peaks at IRC2 (within pointing uncertainties) and drops off markedly toward H_2 peak 1. This result differs from that of Watson *et al.* (1985), who reported that the OH integrated intensity at 119 μm peaked closer to H_2 peak 1. We find that the apparent angular size of the OH-emitting region is comparable to our $33''$ beam size

and noticeably less than the $45''-55''$ (FWHM) size we measure for the CO $J = 22-21$ emitting region or the $35''-45''$ (FWHM) extent of the 119 μm continuum. Allowing for uncertainties in pointing at the three observed positions, we deduce that the OH emission comes from a source $< 25''$ (FWHM) in diameter centered near IRC2.

Although the OH emission comes from a region significantly more compact than that responsible for the high- J CO lines, the similarity of the OH and CO line profiles in the red wing suggests that the OH emission is also likely associated with the high-velocity outflow. In the shock models of Draine and Roberge (1982), the abundance of OH is significantly enhanced over typical interstellar values by shock heating of the ambient cloud. Some OH is produced at high temperatures near the leading edge of the expanding shock front, but significantly more is left behind in the somewhat cooler postshock medium. The gas in this postshock medium has also been swept up to a high outflow velocity of $\sim 36 \text{ km s}^{-1}$. Comparatively little OH is expected to exist in cloud regions exterior to the front which have not yet been heated, and any which does exist will likely reside at the velocity of the quiescent cloud. The fact that only blueshifted OH absorption is seen means that the source of the 119 μm OH emission must lie interior to the absorbing gas in the “swept-up” postshock material. For these reasons, it is unlikely that the observed OH emission originates in the hotter gas near the shock front, as has previously been proposed. Rather, the OH emission region is compact, and in fact smaller than the continuum emitting region.

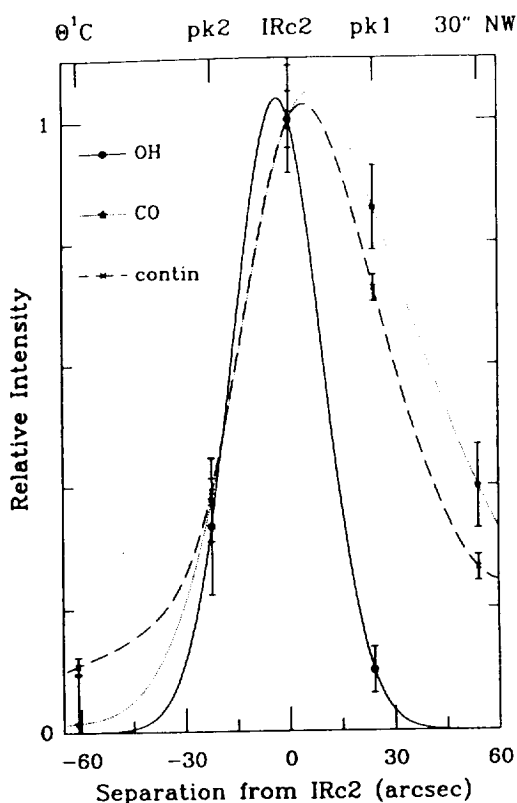


FIG. 2.—A strip scan of the OH $J^p = 5/2^- - 3/2^+$ integrated intensity along a line connecting H₂ peaks 1 and 2. For comparison, a scan of the integrated intensity of the ¹²CO $J = 22-21$ line and the relative continuum strength (Boreiko and Betz 1989) are also shown. The intensities are normalized at IRC2. The smooth curve through the OH measurements is a Gaussian (solid line), whereas the curves through the CO (dotted line) and continuum (dashed line) values are illustrative spline interpolations.

The compact nature of OH emission near IRC2 is similar to that of other molecules with high dipole moments and concomitant high-density excitation requirements. For example, interferometric maps of millimeter-wave lines of SO (Plambeck *et al.* 1982) and SiO (Wright *et al.* 1983) show that most of the emission is confined to a region within 10" of IRC2. For OH, however, the apparent source size may be misleading because only the redshifted emission is detected. We can derive a rough estimate for the temperature of the OH line-forming region if we speculate on the source size. The 1665 MHz OH masers clustered around IRC2 extend over a region $\sim 8'' \times 3''$ in size (Hansen and Johnston 1983), which defines a boundary for some moderately excited OH. Adopting this size for the 119 μm emission and taking the $T_{\text{rot}}^* = 3.5$ K as measured in our 33" beam, we derive a brightness temperature $T_B \sim 200$ K for the 119 μm line-forming region. This OH brightness temperature is close to the 230 K excitation temperature deduced independently for SiO in this region (Wright *et al.* 1983). If both species have the same excitation, then OH must be near LTE and the emission optically thick.

b) OH Emission Intensity and Optical Depth

Because much of the OH emission profile appears to be "self-absorbed" by foreground OH, we cannot calculate with

certainty the unobscured intensity of the $J^p = 5/2^- - 3/2^+$ fundamental. However, if the unobscured shape of the OH emission is similar to that observed for the broad component of the ¹²CO $J = 22-21$ line plotted in Figure 1a, we can estimate that the "intrinsic" intensity of the 119 μm line is a factor of 2-3 greater than observed. The "self-absorption" seen in the 119 μm profile explains the anomalously high ratio of 163 $\mu\text{m}/119 \mu\text{m}$ integrated intensities noted by Viscuso *et al.* (1985) and Melnick, Genzel, and Lugten (1987).

With our upward correction of a factor of 2-3 to the observed 119 μm intensity and provided the 163 μm and 84 μm lines are not also somewhat "self-absorbed," we find that the relative intensities of the OH rotational lines are consistent with optically thick LTE emission for the 119 μm fundamental. The inference that OH is optically thick in the 119 μm fundamental has already been drawn by Watson *et al.* (1985), Viscuso *et al.* (1985), and Melnick, Genzel, and Lugten (1987). However, these earlier observers generally associated the emitting OH with the more spatially extended postshock gas rather than the outflow gas near IRC2.

The integrated intensity we measure for the OH $J^p = 5/2^- - 3/2^+$ line at IRC2 (without correction for "self-absorption") is $1.61 \pm 0.14 \times 10^{-3}$ ergs s⁻¹ cm⁻² sr⁻¹ in a 33" beam. At H₂ peaks 1 and 2, the integrated intensities are $1.6 \pm 2.0 \times 10^{-4}$ ergs s⁻¹ cm⁻² sr⁻¹ and $5.4 \pm 1.8 \times 10^{-4}$ ergs s⁻¹ cm⁻² sr⁻¹, respectively. These intensities were calculated conservatively by integrating over the full 153 km s⁻¹ of observed bandwidth. For H₂ peak 1, the emission line width may be considerably narrower, and a lower statistical uncertainty could be quoted by restricting the velocity range. The earlier observations of Watson *et al.* (1985) for this same line at the position of BN, which is 7" from IRC2, yielded an intensity of $1.7 \pm 0.5 \times 10^{-3}$ ergs s⁻¹ cm⁻² sr⁻¹ in a 44" beam. Because the OH emission region is compact (<25"), the Watson *et al.* (1985) measurements correspond to a flux level a factor of 1.5-1.8 higher than what we observe.

A rough estimate of the line optical depth can be made by adopting an H₂ density of 10^8 cm⁻³, consistent with the minimum OH optical depth. For thermalized gas at $T \sim 200$ K and the line width observed, the OH column density need > 100 for LTE emission. However, radiative excitation near IRC2 or appreciably higher H₂ densities toward the center of the outflow would both lead to a lower estimate for the minimum OH optical depth. For thermalized gas at $T \sim 200$ K and the line width observed, the OH column density need only be $\sim 10^{15}$ cm⁻² for the 119 μm line to be optically thick ($\tau \geq 1$). If we assume a scale size of 3×10^{16} cm for the depth of the emission region in line with our adopted $3'' \times 8''$ estimate for the OH source size, then the average OH density in the emitting region is ~ 0.03 cm⁻³ per unit optical depth of the 119 μm line. For a moderately large optical depth of $\tau \sim 10$, which seems possible, the OH abundance would be relatively high for interstellar gas, but not for gas processed by endothermic reactions in the warm outflow close to IRC2.

It is still premature to attempt a detailed quantitative analysis of the far-infrared OH lines in Orion. Measurements of the 163 μm and 84 μm OH lines at a spectral and spatial resolution equivalent to that presented here are needed before postulating the relative importance of various excitation mechanisms. Given that the blueshifted OH absorption has a large optical depth in the 119 μm line, the 84 μm line might also be expected to show "self-absorption" effects if the absorbing foreground gas is moderately excited.

c) OH Absorption Component

The apparent absorption of the blueshifted OH emission in the 119 μm line is so complete for $V_{\text{LSR}} < 6 \text{ km s}^{-1}$, and yet so sharp near this limit, that we must consider at least two independent absorbers. The first is low-excitation gas expanding at an unimpeded outflow velocity of $\sim 36 \text{ km s}^{-1}$ relative to the $\sim 8 \text{ km s}^{-1}$ V_{LSR} velocity near IRC2. This component will need to be modeled in a spherically symmetric geometry, because no reasonably constructed plane-parallel approximation seems to fit the data. The second component is a sharp and very intense absorber centered near $V_{\text{LSR}} = 5.5 \text{ km s}^{-1}$ with an estimated line width of $\sim 10 \text{ km s}^{-1}$. However, some of the absorption near 9 km s^{-1} may come from OH in foreground ridge gas. Both the broad and sharp absorption components have high optical depths and OH column densities $\geq 10^{16} \text{ cm}^{-2}$. For the broader component, the absorber could be OH of enhanced abundance in the swept-up postshock gas. According to the shock model of Draine and Roberge (1982), almost all the OH in the fully accelerated postshock gas will be in the ground state, because gas temperatures and (more significantly) gas densities are too low to maintain significant upper state populations.

The LSR velocity and line width of the sharp absorber are very suggestive of the "hot core" source, which is thought to lie in the foreground of IRC2 (Wynn-Williams *et al.* 1984). This interpretation is strengthened by the fact that the narrow

absorption at $V_{\text{LSR}} = 5.5 \text{ km s}^{-1}$ is very intense toward IRC2, but not so evident toward H_2 peak 2, which is only $\sim 24''$ away. Densities in the hot core are thought to be a factor of 10^4 lower than the critical density of the observed transition (Sutton *et al.* 1986), so OH will likely be in the ground state and hence appear in absorption. Note that in the IRC2 spectrum the suggested "hot core" component absorbs essentially all of the continuum as well. A significant part of the absorbing OH at 5.5 km s^{-1} must therefore lie closer to us than the mean radius of the continuum source, in contrast to the case for the emitting OH. If we assume that the continuum-emitting region is spherically symmetric with our estimated $35''\text{--}45''$ (FWHM) diameter, then the distance between the center of this region and the absorbing part of the "hot core" OH is $\geq 1 \times 10^{17} \text{ cm}$. This lower limit on the distance between presumably IRC2 and the hot core is similar to the estimate of Wynn-Williams *et al.* (1984) based on infrared color temperature measurements, but somewhat higher than the value of $1\text{--}3 \times 10^{16} \text{ cm}$ deduced by Masson and Mundy (1988) from interferometric observations of HC_3N .

Our observations were made possible by the coordinated effort of many people in the KAO operations staff, and we thank them all for their assistance. This work is supported in part by NASA grant NAG 2-254.

REFERENCES

- Beckwith, S., Persson, S. E., Neugebauer, G., and Becklin, E. E. 1978, *Ap. J.*, **223**, 464.
 Betz, A., and Zmuidzinas, J. 1984, in *Proc. Airborne Astronomy Symposium* (NASA Conf. Pub. CP-2353), p. 320.
 Boreiko, R. T., and Betz, A. L. 1989, *Ap. J. (Letters)*, **347**, L97.
 Chernoff, D. F., Hollenbach, D. J., and McKee, C. F. 1982, *Ap. J. (Letters)*, **259**, L97.
 Draine, B. T., and Roberge, W. G. 1982, *Ap. J. (Letters)*, **259**, L91.
 Farhoomand, J., Blake, G. A., and Pickett, H. M. 1985, *Ap. J. (Letters)*, **291**, L19.
 Hansen, S. S., and Johnston, K. J. 1983, *Ap. J.*, **267**, 625.
 Inguccio, M., Moruzzi, G., Evenson, K. M., and Jennings, D. A. 1986, *J. Appl. Phys.*, **60**, R161.
 Linsky, J. L. 1973, *Ap. J. Suppl.*, **25**, 163.
 Masson, C. R., and Mundy, L. G. 1988, *Ap. J.*, **324**, 538.
 Matthews, H. E., Baudry, A., Guilloteau, S., and Winnberg, A. 1986, *Astr. Ap.*, **163**, 177.
 Melnick, G. J., Genzel, R., and Lugten, J. B. 1987, *Ap. J.*, **321**, 530.
 Plambeck, R. L., Wright, M. C. H., Welch, W. J., Bieging, J. H., Baud, B., Ho, P. T. P., and Vogel, S. N. 1982, *Ap. J.*, **259**, 617.
 Storey, J. W. V., Watson, D. W., and Townes, C. H. 1981, *Ap. J. (Letters)*, **244**, L27.
 Sutton, E. C., Blake, G. A., Genzel, R., Masson, C. R., and Phillips, T. G. 1986, *Ap. J.*, **311**, 921.
 Viscuso, P. J., Stacey, G. J., Fuller, C. E., Kurtz, N. T., and Harwit, M. 1985, *Ap. J.*, **296**, 142.
 Watson, D. M., Genzel, R., Townes, C. H., and Storey, J. W. V. 1985, *Ap. J.*, **298**, 316.
 Wright, M. C. H., Plambeck, R. L., Vogel, S. N., Ho, P. T. P., and Welch, W. J. 1983, *Ap. J. (Letters)*, **267**, L41.
 Wynn-Williams, C. G., Genzel, R., Becklin, E. E., and Downes, D. 1984, *Ap. J.*, **281**, 172.
 Zmuidzinas, J., Betz, A. L., and Boreiko, R. T. 1989, *Infrared Phys.*, **29**, 119.

HETERODYNE SPECTROSCOPY OF C II IN MOLECULAR CLOUDS

A.L. BETZ, R.T. BOREIKO, and J. ZMUIDZINAS[‡]
Space Sciences Laboratory, University of California
Berkeley, CA 94720

ABSTRACT. High-resolution spectra of the 158 μm fine-structure line of ionized carbon have been obtained with a heterodyne spectrometer toward a number of galactic molecular clouds. Strongly reversed C II line profiles are seen in sources noted for similar behavior in low-J ^{12}CO . The C^+ producing the optically thick ($\tau \geq 1$) absorption component is cool or subthermally excited, with excitation temperatures typically less than 25-50 K. Column densities for the absorption component are $\geq 10^{18} \text{ cm}^{-2}$, similar to values predicted by UV-photodissociation models for C II emitting gas. Thus the total C^+ column density in the vicinity of these molecular clouds is significantly greater than previously estimated from integrated intensity measurements.

1. Introduction

Line emission from the 158 μm fine-structure line of ionized carbon has long been recognized as a primary cooling mechanism for the low density gas at the boundaries of molecular clouds (Dalgarno and McCray 1972). Russell *et al.* (1980) first succeeded in detecting the C II line in Orion in observations with a cooled grating spectrometer at modest spectral resolution ($\delta\lambda/\lambda \sim 0.007$). This result confirmed the theoretical prediction that the line would be strong and therefore important for cooling diffuse molecular gas. Subsequently these researchers established the existence of large C II haloes surrounding galactic H II regions (Russell *et al.* 1981). The first observations of C II at a spectral resolution sufficient to measure the Doppler velocity (to a few km s^{-1} accuracy), and to resolve the line in a number of extragalactic sources, were done by Crawford *et al.* (1985) and Lugten (1987), who used a cooled Fabry-Perot spectrometer with a velocity resolution of $\sim 30 \text{ km s}^{-1}$ ($\delta\lambda/\lambda \sim 10^{-4}$). This resolution in itself, however, is not adequate to resolve the C II line in most galactic sources.

Since these pioneering efforts with incoherent spectrometers, the technology of heterodyne spectroscopy has advanced to the point that coherent receivers are now available at frequencies as high as 2000 GHz. Such instruments offer to the far-infrared the high spectral resolution and velocity-scale accuracy long enjoyed at radio wavelengths. We are now able to compare precisely the emission observed from

[‡] Now at Astronomy Department, University of Illinois, Urbana, IL 61801

neutral (CO) and partially ionized (C⁺) gas in UV-heated regions.

The first heterodyne observations of the C II line were reported by Boreiko *et al.* (1988). The spectra taken in Orion-Trapezium region at 0.8 km s⁻¹ (5 MHz) resolution revealed that the C II linewidth is 5 km s⁻¹ (FWHM), similar to that observed for millimeter wave CO lines. However, there were also significant variations in linewidth and velocity, and even evidence for multiple velocity components, in spectra observed from various nearby locations in Orion A.

2. C II Optical Depths

Current theoretical models of photodissociation regions generally predict low optical depths ($\tau < 1$) for C II line emission (e.g., Tielens and Hollenbach 1985). This conclusion proceeds from the argument that UV radiation will penetrate into a cloud to $\sim A_V = 4$, that this depth corresponds to a hydrogen column density of 10^{21} cm⁻², and therefore that the column density of ionized carbon will be $\sim 3 \times 10^{18}$ cm⁻². This column density will yield an optically thin line ($\tau < 1$) whenever the linewidth is > 6.9 km s⁻¹ for an excitation temperature $T_{ex} = 100$ K, or > 3.4 km s⁻¹ for $T_{ex} = 200$ K.

The question of the ¹²C II optical depth is important for evaluating the effectiveness of the line in cooling diffuse gas and also because many authors have suggested that the 158 μ m C II line should be good for measuring the ¹³C/¹²C isotopic abundance ratio without introducing the type of systematic errors implicit in multi-isotope CO comparisons. Given that we don't know the optical depths of C II lines *a priori*, the derivation of the ¹²C/¹³C isotopic ratio would require that all the C II lines are optically thin.

The J=3/2 upper level of the ¹²C II fine structure line is the lowest excited state in ionized carbon, and lies only 63 cm⁻¹ ($h\nu/k = 91$ K) above the J=1/2 ground state. The next highest state requires UV-excitation to a level 61,000 K above ground. Consequently, in the relatively cool molecular regions of interest here, ionized carbon is for all practical considerations just a two-level system. This makes calculations easy but interpretation hard. The reason is that with a two level system there are not enough observable quantities to separate questions of excitation from those of abundance in explaining a single observed emission line. Even if we assume LTE conditions, we still have two unknowns but only one observable. We need additional independent information on either the excitation or the abundance of the species. For example, observations of the isotopic ¹³C II lines can in principle aid us in interpreting the ¹²C II optical depth, *provided we already know the isotopic ratio accurately*. In the C II spectra taken by Boreiko *et al.* (1988), a weak feature was detected at the correct frequency for the strongest component of the ¹³C II triplet. If this feature is indeed ¹³C II, then from the apparent ¹²C II/¹³C II intensity ratio, the ¹²C II emission must be optically thick ($\tau > 1$) if the ¹²C/¹³C isotopic ratio is > 12 . For an *adopted* ratio of 60, the authors concluded that the ¹²C II line has an optical depth of $\tau \sim 5$ for two observed positions in Orion. It remains to be seen, however, if the weaker ¹³C II subcomponents can be detected for verification, and also what isotopic ratio is correct. For example, the lower ratio of 40 suggested by Blake *et al.* (1987) would correspondingly reduce the estimated ¹²C II optical depth to $\tau = 3 \pm 1$.

Generally speaking, if a spectral line can be observed in absorption, a lower limit to the optical depth can be determined without concern for the excitation. This gives us a tractable problem: one equation in one unknown. Of course, some knowledge of the

excitation is needed before any estimates of abundance can be made. With these points in mind we observed a number of molecular clouds with known strong reversals in the emission spectra of millimeter wave CO lines. The object was to look for "self"-absorption in C II, to compare the observed profiles with those of CO, and thereby to measure the column density of ionized carbon in such regions more accurately.

3. Receiver System

Because a detailed description of the spectrometer has been presented elsewhere (Betz and Zmuidzinas 1984), only a few highlights are repeated here. The receiver uses a cooled (77 K) Schottky diode (Univ. VA type 117) in a corner-reflector mixer mount (Zmuidzinas *et al.* 1988) and an optically pumped far-infrared (FIR) laser as the local oscillator. The laser oscillates on the 1891.2743 GHz line of CH₂F₂ (Petersen *et al.* 1980), which lies 9.3 GHz below the C II rest frequency of 1900.5369 GHz (Cooksy *et al.* 1986). The IF amplifier is centered at this offset frequency. The system noise temperature of the receiver mounted on the telescope is 26,000 K (SSB). Measured in units of $h\nu/k$, this system noise level is equivalent to that of a 115 GHz CO receiver with $T_{\text{sys}} = 1600$ K. Given that the frequency width of a 0.8 km s^{-1} channel corresponds to 5 MHz, one can integrate down to a few Kelvin post-detection noise level in a matter of minutes. Because the earth's atmosphere is completely opaque at the C II line frequency even at high mountain sites, observations are conducted from the Kuiper Airborne Observatory operated by NASA. The 91 cm telescope aboard the aircraft produces a 43 arcsec beam at $\lambda = 158 \mu\text{m}$. Calibrations of line intensities are relative to the brightness temperature of the Moon, which is reasonably well known. Most observations are done in sky-chopping mode with beam separations between 8 and 10 arcmin.

4. Observations and Analysis

Observations of 5 sources known for strong CO line reversals were done at various times in 1987 and 1988 as part of a larger survey of C II in galactic clouds. Figures 1 and 2 show observed spectra for particular positions in two of these sources: NGC 2024 and W51. For W51 we have also plotted the profile of the 230 GHz J=2-1 ¹²CO line taken by Stacey (1987) on the 12-m Kitt Peak telescope. The benefit of the higher resolution possible with heterodyne spectroscopy is immediately obvious. The linewidth (FWHM) of the apparently reversed component in the NGC 2024 spectrum is only 1.6 km s^{-1} . For all 5 of the observed sources (including W3, W49, and Mon R2 which are not shown here), the profiles of the ¹²C II lines follow the shapes of the optically thick ¹²CO lines remarkably well and are quite dissimilar to the shapes of the thinner isotopic CO lines. From this we conclude that the apparent reversals in the C II lines are real absorptions from ionized carbon in cooler or subthermally excited foreground gas, and are not just an artifact produced by multiple velocity components seen only in emission. While quantitatively we cannot do more than speculate on the optical depth of the emission (for reasons mentioned above), we are in a good position to place limits on the depth of the absorption component.

A lower limit for the optical depth of the absorption can be derived from inspection of the reversed profile. We have in this case:

$$\min \tau_{\text{abs}} = -\ln \left[\frac{T_{\Lambda}^*(\text{dip})}{T_{\Lambda}^*(\text{peak})} \right],$$

where we take the excitation temperature of the absorbing gas to be 3 K (or equivalently zero). This gives us $\tau_{\text{abs}} \geq 1.0$ for NGC 2024 and $\tau_{\text{abs}} \geq 2.2$ for W51-IRS2. With a more refined model using Gaussian absorption and emission components, we get $\tau_{\text{abs}} \geq 2.2 \pm 0.6$ for NGC 2024 and $\tau_{\text{abs}} \geq 4.4 \pm 2.7$ for W51-IRS2. The corresponding lower limits to the C⁺ column densities for the absorption component alone are $1 \times 10^{18} \text{ cm}^{-2}$ and $3 \times 10^{18} \text{ cm}^{-2}$ for NGC 2024 and W51-IRS2, respectively.

We see that in some sources there is likely as much ionized carbon in absorption as predicted by model calculations for the C⁺ emission component. It is possible some of this absorption is produced by gas previously identified from its spatially extended emission as the CII halo component in galactic HII regions (Russell *et al.* 1981). On the other hand, we see CII line reversals only in sources for which strong CO line reversals are noted, which suggests that the C⁺ seen in absorption is kinematically and probably energetically associated with molecular material rather than the extended atomic gas believed to give rise to the CII halo emission. These points and others are discussed in more detail in an upcoming manuscript on reversed CII line emission in galactic sources (Betz *et al.* 1988).

5. Conclusions

We have basically three simple conclusions we can draw from the analysis of all the reversed-line sources:

- (1) In dense molecular clouds the CII line profiles are generally similar to those of optically thick ¹²CO (and not ¹³CO), which suggests a common physical origin.
- (2) The optical depth of CII in absorption is typically ≥ 1 in reversed-line sources. The column density of this colder or subthermally excited CII typically exceeds $\sim 1 \times 10^{18} \text{ cm}^{-2}$; hence, the total abundance of ionized carbon is significantly higher than that estimated from observations of unresolved emission lines.
- (3) Excitation temperatures for photodissociation regions derived from the 158 μm CII/63 μm OI integrated intensity ratio should be viewed cautiously. Not only may the CII profiles be optically thick in emission, but they frequently show optically thick absorption reversals. Moreover, both these effects are likely to be even more significant in the 63 μm OI line.

This work was supported in part by NASA under grant NAG2-254 for research in airborne astronomy.

References

- Betz, A.L., and Zmuidzinas, J. (1984), 'A 150 to 500 μm Heterodyne Spectrometer for Airborne Astronomy', Airborne Astronomy Symposium, NASA Conference Publication 2353, 320-329.
- Betz, A.L., Boreiko, R.T., and Zmuidzinas, J. (1988), 'Reversed emission from ionized carbon in molecular clouds', (manuscript in preparation).
- Blake, G.A., Sutton, E.C., Masson, C.R., and Phillips, T.G. (1987), 'Molecular abundances in OMC-1: the chemical composition of interstellar molecular clouds and the influence of massive star formation', *Ap.J.*, **315**, 621-645.

- Boreiko, R.T., Betz, A.L., and Zmuidzinas, J. (1988), 'Heterodyne Spectroscopy of the 158 Micron C II Line in M42', *Ap. J. (Lett.)*, **325**, L47-L51.
- Cooksy, A.L., Blake, G.A., and Saykally, R.J. (1986), 'Direct measurement of the fine-structure interval and g_J factors of singly ionized atomic carbon by laser magnetic resonance', *Ap. J. (Letters)*, **305**, L89-L92.
- Crawford, M.K., Genzel, R., Townes, C.H., and Watson, D.M. (1985), 'Far-infrared spectroscopy of galaxies: the 158 micron C⁺ line and the energy balance of molecular clouds', *Ap. J.*, **291**, 755-771.
- Dalgarno, A., and McCray, R. (1972), 'Heating and ionization of HI regions', *Ann. Rev. Astron. Astrophys.*, **10**, 375-426.
- Lugten, J.B. (1987), 'Velocity resolved far-infrared spectroscopy of galactic sources', Ph.D. thesis, Univ. CA, Berkeley.
- Petersen, F.R., Scalabrin, A., and Evenson, K.M. (1980), 'Frequencies of cw FIR laser lines from optically pumped CH₂F₂', *Int. J. Infrared Millimeter Waves*, **1**, 111-115.
- Russell, R.W., Melnick, G., Gull, G.E., and Harwit, M. (1980), 'Detection of the 157 micron (1910 GHz) [CII] emission line from the interstellar gas complexes NGC 2024 and M42', *Ap. J. (Letters)*, **240**, L99-L103.
- Russell, R.W., Melnick, G., Smyers, S.D., Kurtz, N.T., Gosnell, T.R., Harwit, M., and Werner, M.W. (1981), 'Giant [CII] halos around HII regions', *Ap. J. (Letters)*, **250**, L35-L38.
- Stacey, G.J. (1987), private communication.
- Tielens, A.G.G.M., and Hollenbach, D. (1985), 'Photodissociation regions. I. Basic model', *Ap. J.*, **291**, 722-746.
- Zmuidzinas, J., Betz, A.L., and Boreiko, R.T. (1988), 'A Corner-Reflector Mixer Mount for Far-Infrared Wavelengths', *Infrared Physics*, (to be published).

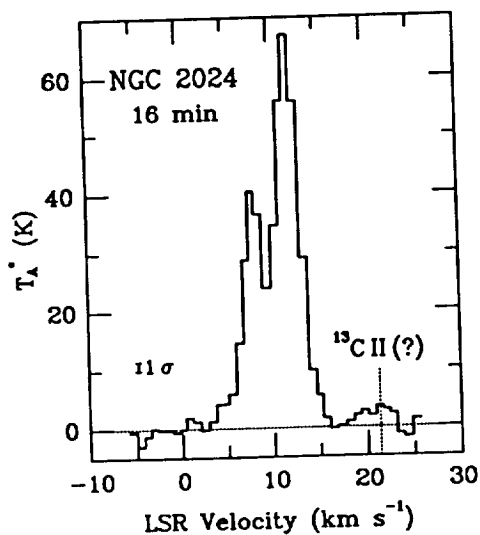


Fig. 1. C II in NGC 2024.

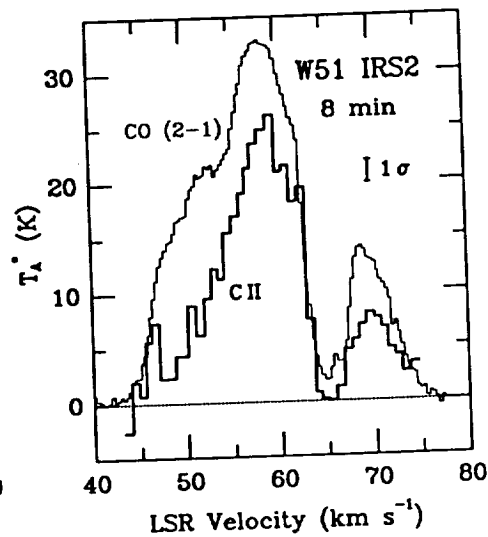


Fig. 2. C II and CO J=2-1 in W51.

PLATEAU EMISSION FROM ORION IN THE CO J=17-16 LINE

R.T. BOREIKO, A.L. BETZ
Space Sciences Laboratory, University of California
Berkeley, CA 94720
J. ZMUIDZINAS
Astronomy Department, University of Illinois
Urbana, IL 61801

ABSTRACT. High-resolution spectra of the J=17-16 CO line (1956 GHz) in the BN-KL region of Orion have been obtained with a heterodyne spectrometer. The profiles show a broad component with 30 km s^{-1} (FWHM) linewidth and a narrower 8 km s^{-1} component. The broader plateau emission detected over a range of transitions from J=1-0 to J=17-16 is analyzed under the assumptions of thermal equilibrium and optically thin wings to deduce an excitation temperature of $180 \pm 50 \text{ K}$ and minimum column density of $1 \times 10^{18} \text{ cm}^{-2}$ for CO in this component.

1. Procedure

The observation described here of the J=17-16 transition of CO at a resolution of 0.8 km s^{-1} extends the range of excitation covered by high-resolution CO data fivefold, allowing a more accurate determination of excitation temperature and column density. Comparison of CO spectra over a range of J shows that the emission in the wings is very likely to arise from the same source in all cases, and is optically thin. Available high-resolution spectra (J=1-0 and J=2-1 from Plambeck, Snell, and Loren 1983; J=3-2 from Richardson *et al.* 1985; J=7-6 from Schmid-Burgk *et al.* 1988; and J=17-16 from Boreiko, Betz, and Zmuidzinas 1989) were individually fitted to a linear combination of two Gaussians to isolate the plateau emission. The data and fit for the J=17-16 line are shown in Fig. 1. The plateau component with $\text{FWHM} \sim 30 \text{ km s}^{-1}$ contributes 80% of the integrated intensity of this line, while the remaining 20% arises from a component with $\text{FWHM} \sim 8 \text{ km s}^{-1}$. The fitted peak antenna temperatures for the plateau component were then used to determine the excitation temperature T_{ex} and column density, as discussed in detail by Boreiko, Betz, and Zmuidzinas (1989). The assumptions implicit in the procedure are that the line wings are optically thin, the levels are in LTE at a common excitation temperature, and source coupling corrections are similar for all data.

2. Results and Conclusions

The excitation temperature derived from the fitting procedure is $180 \pm 50 \text{ K}$, where the uncertainty reflects both statistical and systematic effects. The column density derived for the CO giving rise to the plateau emission is $\geq 1 \times 10^{18} \text{ cm}^{-2}$. Fig. 2

shows the data and the fit. The error bars represent uncertainties from calibration of the data and the Gaussian fitting. In cases where the errors are not quoted by the authors, a calibration uncertainty of 25% was assumed. As can be seen from Fig. 2, the low- J lines ($J < 5$) best define the CO column density in the plateau emission, since their intensities are relatively insensitive to T_{ex} in the range of interest. In contrast, lines with $J > 13$ are the most sensitive for determining T_{ex} once the column density is fixed. Lines with intermediate J are the strongest, and therefore the best indicators for optical depths effects at line center.

This work was performed as part of the KAO Airborne Astronomy Program under NASA Grant NAG 2-254.

References

- Boreiko, R.T., Betz, A.L., and Zmuidzinas, J. (1989) 'Heterodyne spectroscopy of the $J=17-16$ CO line in Orion', *Ap.J.* (to be published).
- Plambeck, R.L., Snell, R.L., and Loren, R.B. (1983) ' $J=2-1$ CO observations of molecular clouds with high-velocity gas: evidence for clumpy outflows', *Ap.J.* **266**, 321-330.
- Richardson, K.J., White, G.J., Avery, L.W., Lesurf, J.C.G., and Harten, R.H. (1985) 'CO $J=3-2$ observations of molecular line sources having high-velocity wings', *Ap.J.* **290**, 637-652.
- Schmid-Burgk, J. *et al.* (1988) 'Extended CO ($J=7-6$) emission from Orion Molecular Cloud 1: hot ambient gas, two hot-outflow sources', *Astron. Astrophys.* (to be published).

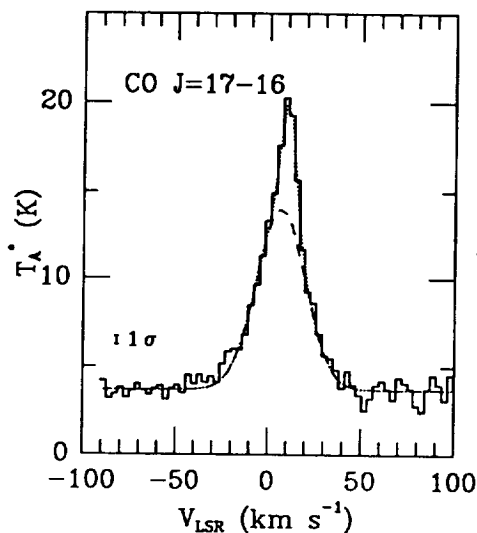


Fig. 1. $J=17-16$ line of CO. The dotted line shows the fit, and the dashed line shows only the plateau component of the fit.

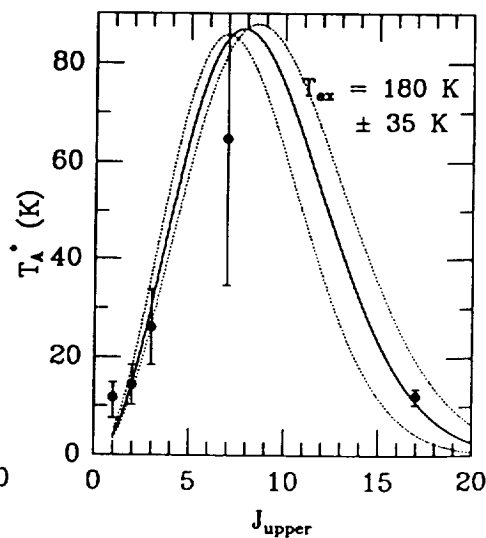


Fig 2. Fitted antenna temperatures and predicted values at line center for the plateau emission.

STRUCTURE

ABSTRACT.
from two you
have been co
which it is pe

1. G35.2N

The central s
an orthogonal
1985). It is
proposed disc
maps of this
which gives a
1100 μm . A
been assumed
 $Q_1 = 0.2 \times 10^{-4}$

The 1100
the detailed r
gas within the
cross-section
depletion in
optically thin
wavelengths w
with $n_d \propto r^{-2}$
depletion of [

An atten
plane, howev
wavelengths. l
wavelengths a
and 450 μm r
energy source
collisional hea

The "exc
(for $T_D = 40$
250 L_\odot . The

IONIZED CARBON IN SIDE-ILLUMINATED MOLECULAR CLOUDS

R. T. BOREIKO, A. L. BETZ, AND J. ZMUIDZINAS
Space Sciences Laboratory, University of California, Berkeley
Received 1989 June 12; accepted 1989 October 11

ABSTRACT

We have observed the ${}^2P_{3/2}-{}^2P_{1/2}$ fine-structure line of C II at 1900 GHz in five sources with ionization fronts nearly perpendicular to the plane of the sky. The LSR velocity of the C II emission is generally in good agreement with that observed for molecular species such as CO. However, the observed line widths of 3-14 km s⁻¹ are typically wider than those of molecular lines and often show rapid spatial variations in the regions observed. In some sources this may indicate that part of the C II emanates from an ionized gas component, while for others it suggests an association between C II emission and an outflow. The C II brightness temperatures are typically equal to or slightly higher than the dust temperature at all locations observed. In the optically thin approximation, C II excitation temperatures are ≥ 100 K and column densities are $\leq 10^{18}$ cm⁻² for all sources except M17, which has a more intense and complicated line profile with a larger spatial extent than any other source observed. The quoted column density estimates derived in the optically thin limit appear to be somewhat lower than those predicted by models of photodissociation regions for sources with a side-illuminated geometry, but uncertainties in the UV flux and geometry of the ionization front preclude a definitive comparison. The estimated column densities would be higher if the C II emission were somewhat optically thick, in which case the ionized carbon would be more in equilibrium with the dust at temperatures lower than predicted by current models.

Subject headings: infrared: spectra — interstellar: molecules — nebulae: structure

I. INTRODUCTION

The initiation of star formation in the depths of cold molecular clouds brings about a distinct upheaval in the region. The high UV and optical flux emitted from first-generation stars disturbs the parent molecular material, and the disruptive energetics may trigger the formation of a subsequent generation of stars in the cloud. The interface between the hot, UV-ionized H II region and the colder molecular material is delineated by the presence of both neutral atomic gas and ionized species with ionization potentials less than the 13.6 eV of hydrogen. An important constituent of such photodissociation regions is singly ionized carbon (C II), because carbon is both abundant and has an ionization potential 2.3 eV below that of hydrogen. Models of photodissociation regions, such as those of Glassgold and Langer (1974), Langer (1976), and Tielens and Hollenbach (1985), predict that radiation from the ${}^2P_{3/2}-{}^2P_{1/2}$ fine-structure line of C II at 1900 GHz (158 μ m) will provide the major cooling for intermediate-density regions and consequently should be quite intense. This prediction has been confirmed by observations of the 158 μ m line in several molecular clouds (e.g., Russell *et al.* 1980, 1981; Melnick *et al.* 1986; Crawford *et al.* 1986). However, with the exception of the recent heterodyne observations of Orion (Boreiko, Betz, and Zmuidzinas 1989), previous C II spectra were of limited spectral resolution so that only the integrated intensity and in some cases the approximate line width could be determined, but without any detailed information on the shape of the line profile. Line shapes and resolved peak intensity (T_A^*) measurements are important for determining lower limits to excitation temperature and allow direct comparison with resolved profiles from other species such as CO which trace conditions in the neighboring molecular gas.

In this paper we present the results of observations of the ${}^2P_{3/2}-{}^2P_{1/2}$ line of C II obtained with a laser heterodyne spectrometer operating at 0.8 km s⁻¹ resolution, which is well

matched to the smallest velocity dispersions expected in molecular clouds. For this first study, five sources with ionization fronts observed "edge-on" were selected. By "edge-on" we mean that the source of the ionization is external to the molecular cloud (and not necessarily formed from it) and is angularly separated from the molecular region in the plane of the sky. This geometry is convenient for studying the ionization front and the variation of parameters with distance from the ionizing source without confusion from emission from the front and back parts of an ionized shell. Also, it is the geometry which maximizes the column density for tangential views and hence is most likely to lead to optically thick C II radiation and thereby yield a good estimate for the excitation temperature of the photodissociation region. Some of the objects observed also contain one or more embedded UV-sources and offer the opportunity to compare photodissociation regions formed under different conditions. In these sources with different angles of view available, one might expect a greater C II column density in the side-illuminated regions than in areas foreground to the embedded source. Regardless, in all cases, resolved line profiles for the photodissociation region will give valuable information on the cloud kinematics when compared to line shapes derived independently from the molecular gas (e.g., those of CO).

II. INSTRUMENTATION AND CALIBRATION

The instrument used for the observations discussed here is an airborne far-infrared heterodyne receiver which has been described in detail by Betz and Zmuidzinas (1984). For observations of C II at 1900.5369 GHz (Cooksy, Blake, and Saykally 1986), the local oscillator is an optically pumped CH₂F₂ laser operating at 1891.2743 GHz (Petersen, Scalabrin, and Evenson 1980), thereby yielding an IF centered at 9.3 GHz. The mixer, a GaAs Schottky diode in a corner-reflector mount (Zmuidzinas, Betz, and Boreiko 1989), was operated uncooled in 1987 and

cooled to 77 K in 1988. The "back end" consists of two filter banks in parallel: one with 40 channels of 5 MHz (0.8 km s^{-1}) resolution covering a 32 km s^{-1} range and the other with 64 channels of 20 MHz (3.2 km s^{-1}) resolution spanning 200 km s^{-1} . The wider bandwidth filter bank provides a clear continuum level, while the narrow filter bank gives the high-resolution C II profile.

Since the Earth's atmosphere is essentially opaque from ground level at the C II frequency, the instrument was flown aboard NASA's Kuiper Airborne Observatory at an altitude of 12.5 km, where typically the atmospheric transmission is better than 90%. The telescope beam width was measured from a scan of the lunar limb to be $\sim 43''$ FWHM and the coupling efficiency was measured to be ~ 0.6 for all observations. The telescope secondary was chopped at 2 Hz with an amplitude of $10'$, which is sufficient to prevent significant contamination from line emission in the reference beam for all sources except M17. The direction of chop was perpendicular to the ionization front for all of the edge-illuminated objects.

Most of the observations discussed in this paper were obtained in a single flight on 1987 July 28 with a system noise temperature $T_{\text{sys}} = 30,000 \text{ K}$ (SSB). The sources Cep A and Cep B had also been observed earlier on 1987 February 9 with a 6.5 chopper throw and $T_{\text{sys}} = 35,000 \text{ K}$ (SSB), while S201 was observed later on 1988 February 2 with $T_{\text{sys}} = 26,000 \text{ K}$ (SSB). Calibration in 1987 February and 1988 February was obtained from measurements of the moon, which was assumed to have a physical temperature of 394 K and an emissivity of 0.98 (Linsky 1973). The double- to single-sideband conversion was calculated from the known transmissions of the atmosphere and the aircraft pressure window in the two sidebands. The primary calibration was maintained throughout the flight by periodic observations of a blackbody source which was used as

a secondary standard. The moon was not available for direct calibration during the 1987 July flight, and therefore only the secondary standard was used, and the blackbody temperature was assumed to be the same as for the 1987 February flight. An independent check on this procedure was derived from measurements of the strong C II line in Cep B: the same location was observed in both 1987 July and 1987 February, and the measured antenna temperatures of the resulting spectra were identical to within 5% (which is the statistical uncertainty). The net uncertainty in the calibration for a uniform source filling our beam is estimated to be $\leq 10\%$. Pointing accuracy is $\sim 15''$. The velocity scale, determined from the line and LO frequencies, is accurate to better than 0.4 km s^{-1} .

III. OBSERVATIONS AND ANALYSIS

Two or more locations in five sources having edge-illuminated ionization fronts (S140, S201, NGC 7538, Cep B, and M17) were observed in an attempt to determine the general properties of C II radiation from photodissociation regions at the edges of molecular clouds. The parameters of the observed lines are given in Table 1. The continuum temperature is determined from an average of the data in the $64 \times 20 \text{ MHz}$ filter bank excluding those channels with line radiation, and has been corrected to a SSB value. No significant slope or baseline standing waves were found in any of the spectra. The channel-to-channel variations outside the line profile are consistent with those expected from the quoted system noise temperatures. The antenna temperature of the line has been corrected for the continuum level and, along with V_{LSR} and FWHM, is determined from a fit of a Gaussian line profile to the data. In spectra for which a single Gaussian is not an adequate representation, several Gaussians are fitted, and the parameters for each of the components are listed. The inte-

TABLE 1
OBSERVED C II LINE PARAMETERS

Position	T_A^* (K)	T_B^b (K)	V_{LSR} (km s^{-1})	ΔV_{FWHM} (km s^{-1})	$I_{\text{INT}} \times 10^{-4}$ ($\text{ergs cm}^{-2} \text{ s}^{-1} \text{ sr}^{-1}$)	T_{CON}^c (K)
S140-IRS	8.0(1.0)	36.2(1.7)	-6.8(0.4)	6.5(0.9)	3.6(0.6)	1.05(0.09)
S140-30" SW	17.5(2.0)	50.0(2.6)	-8.3(0.2)	3.5(0.4)	4.6(0.6)	0.67(0.13)
S201-FIR	7.4(0.4)	35.2(0.7)	-38.0(0.2)	7.4(0.5)	4.2(0.4)	0.04(0.05)
S201-1' SW	14.2(1.5)	45.5(2.1)	-37.3(0.2)	3.7(0.4)	4.0(0.5)	0.35(0.11)
NGC 7538-IRS1	11.6(1.0)	41.8(1.5)	-57.5(0.6)	13.7(1.5)	11.6(1.0)	0.42(0.18)
NGC 7538-1' NW	16.1(0.7)	48.1(0.9)	-57.0(0.2)	9.3(0.5)	12.4(0.7)	0.17(0.08)
Cep B-FIR	28.0(0.9)	63.0(1.1)	-13.9(0.1)	4.2(0.1)	9.0(0.5)	0.35(0.08)
Cep B-1' NW	21.3(2.0)	54.8(2.5)	-13.7(0.1)	3.2(0.3)	8.4(0.6)	0.00(0.12)
	5.3(1.5)	31.4(2.9)	-16.5(1.2)	8.7(1.5)		
Cep B-2' NW	5.5(0.9)	31.8(1.7)	-15.8(0.5)	6.7(1.3)	2.1(0.6)	-0.16(0.11)
M17-C II peak	31.2(2.3)	66.7(2.7)	19.4(0.2)	13.0(0.4)	24.4(0.4)	0.80(0.07)
	-10.7(1.9)	40.5(2.9)	21.2(0.1)	1.7(0.3)		
	-11.1(2.2)	41.1(3.3)	17.8(0.4)	5.5(1.1)		
M17-Mid	26.3(1.2)	60.9(1.4)	19.2(0.2)	12.4(0.5)	23.4(0.7)	1.21(0.11)
	-10.6(2.5)	40.3(3.8)	20.8(0.2)	1.8(0.6)		
M17-C I peak	33.1(4.4)	68.9(5.1)	19.3	10.5(0.6)	15.4(0.7)	0.67(0.11)
	-24.0(3.8)	58.2(4.7)	21.2(0.3)	5.9(0.6)		

NOTE.—Values in parentheses represent 1σ statistical uncertainties.

* T_A^* is corrected for the continuum. Negative values of T_A^* represent absorption or reference beam emission; the associated values of T_B^b apply in the case of reference beam emission only.

^b T_B^b is brightness temperature.

^c The continuum temperatures are corrected for transmission of the pressure window in each of the two infrared sidebands, and represent SSB values.

grated intensity is not derived from the fitted parameters and thus represents the total value for all components. In the following sections, the spectra from individual sources are presented and discussed in detail.

a) S140

S140 is a source with an apparently simple geometry which minimizes possible confusion in the interpretation of data. The dense molecular cloud core contains several embedded IR sources, and is surrounded by an extended dark cloud and CO envelope (Blair *et al.* 1978). Toward the SW is an H α rim, and an ionization front exists ~ 2.5 SW of the embedded sources (Hayashi *et al.* 1985). The primary exciting star for the H II region is a B0 star 7' SW of the H α rim, and therefore S140 is a clear-cut example of a source in which the primary ionization front is seen "edge-on". Schematic illustrations of the morphology are given by Blair *et al.* (1978, Fig. 10) and Lester *et al.* (1986, Fig. 1).

Observations in several molecular transitions show that the emission from neutral gas generally peaks near S140 IR, with a sharp cutoff toward the ionization front (CS: Snell *et al.* 1984; Hayashi *et al.* 1985; Mundy *et al.* 1986; CO: Blair *et al.* 1978; Hayashi *et al.* 1987). There is little systematic change of V_{LSR} with position in S140, but the line width shows a general decrease away from the ionization front (Snell *et al.* 1984). LVG modeling of CS data (Snell *et al.* 1984; Mundy *et al.* 1986) indicates that the gas has a maximum density of $\sim 10^6 \text{ cm}^{-3}$ in the SW near the interface with the H II region and decreases toward the NE, and that this gas is clumpy, with the high-density component immersed in a more tenuous extended medium. The foreground or interclump gas has densities of 4×10^3 to $4 \times 10^5 \text{ cm}^{-3}$ (Mundy *et al.* 1987) with a velocity dispersion similar to that of the clumps, since no self-reversals are seen in the profiles. The mean kinetic temperature at S140 IR is $\sim 35 \text{ K}$ as derived from CO (Blair *et al.* 1978) and NH $_3$ (Takano 1986) observations.

We obtained C II spectra of S140 at two locations: the embedded sources (S140 IR) and 30" SW, in the direction toward the ionization front. As can be seen from the parameters listed in Table 1, the C II emission is stronger closer to the ionization front than at S140 IR, as expected. However, the difference in peak T_A^* of the emission at the two nearby locations is accompanied by a compensating factor of ~ 2 change in line width, such that the integrated intensity in the line is very nearly constant. The C II emission from S140 IR probably originates from the ionization region thought to exist around at least two of the embedded sources (Schwartz *et al.* 1983), which are likely to be early B stars. The greater width of the C II line could be due to increased turbulence in the photodissociation region surrounding the embedded sources compared with that in the ionization front. The CO lines show a marked blue asymmetry and increased line width at IRS compared to other locations (Blair *et al.* 1978; Hayashi *et al.* 1987), and the extended wings seen in ^{12}CO and ^{13}CO (Snell *et al.* 1984) have been interpreted as evidence of an outflow. The C II line profile appears quite similar to that of $J = 2-1$ ^{12}CO (see Fig. 1), with the exception of the apparent absence of the extended blue wing in the C II data. Therefore the outflow could be affecting the photodissociated gas to some extent, producing wider lines than at the ionization front. This interpretation is reminiscent of observations of C II in the Orion region (Boreiko, Betz, and Zmuidzinas 1987) which show greater line width toward BN-KL than near the Trapezium, though the C II line wings do not have the large velocity width seen in CO observations.

An alternative interpretation for the width of the C II line might be based on optical depth considerations similar to those used for CO: the ^{13}CO line width is $\sim 60\%$ of that of ^{12}CO , while C ^{18}O produces lines narrower still, suggesting that optical depth may contribute significantly to the observed width. However, given the complicated nature of radiative transfer in an inhomogeneous cloud and the rapid spatial

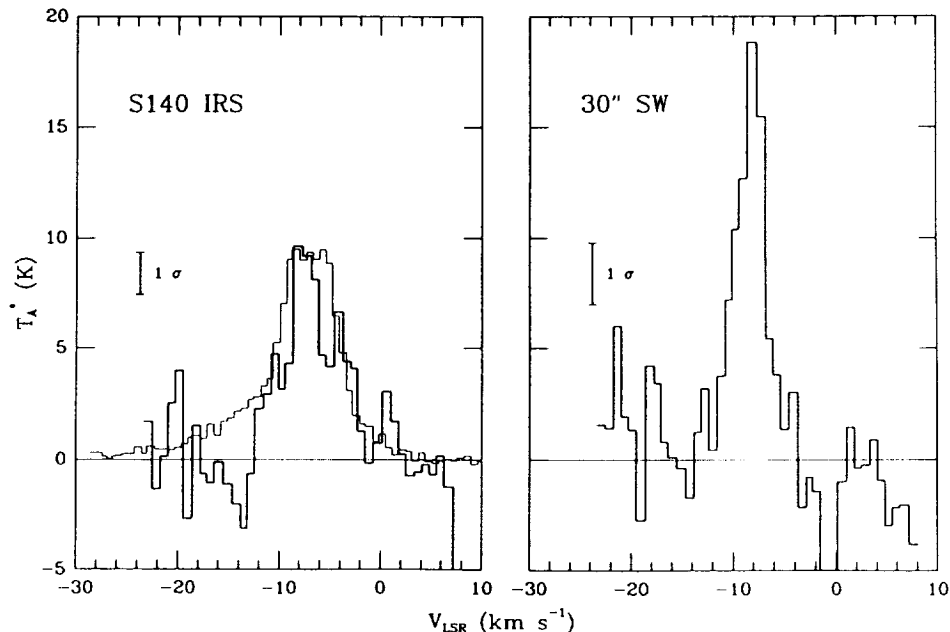


FIG. 1.—C II spectra in the S140 region. *Left panel:* C II at IRS (*heavy line*) compared with CO $J = 2-1$ (*light line*: Plambeck, Snell, and Loren 1983; scaled by 0.5). *Right panel:* C II 30" SW of IRS. Integration times are 8 minutes at IRS and 4 minutes 30" SW. The continuum determined from the wide filter bank has been subtracted from both C II spectra.

variation of line profile seen (and qualitatively expected as the dominant heating changes from an internal source associated with an outflow to an external one), it is impossible to draw any firm conclusions on the role of optical depth in producing the observed line width. Only a 1σ upper limit to τ of ~ 10 (for an assumed isotopic ratio of 60) can be placed by the non-detection of the $^{13}\text{C II}$ hyperfine component at $+11.2 \text{ km s}^{-1}$ relative to the $^{12}\text{C II}$ line.

The C II column density at IRS in the optically thin high temperature ($T > 150 \text{ K}$) limit is $2.3 \times 10^{17} \text{ cm}^{-2}$, a factor of 3–10 smaller than that obtained from photodissociation models for H_2 densities between 10^3 and 10^6 cm^{-3} and UV fluxes between 10^3 and 10^5 times the interstellar flux (Tielens and Hollenbach 1985). Possible beam dilution may be partly responsible for the comparatively low measured value of the integrated intensity and derived column density, since the photodissociated region produced by the embedded sources within the molecular cloud is expected to be compact. In addition, the flux of ionizing radiation is not known at this location, although because of the nearby UV source it is probably within the range quoted above for which the C II column density is not predicted to be very sensitive to UV flux. A lower limit of $36 \pm 2 \text{ K}$ for T_{ex} can be derived from the peak line strength. Partial beam filling would tend to raise this limit.

The C II line profile at the position $30''$ SW of the embedded sources (see Fig. 1) is considerably narrower and brighter than at IRS, but with a similar integrated intensity. The position observed is about midway between IRS and the ridge of heated molecular gas seen in CO inside the ionization front (Hayashi *et al.* 1987), which corresponds with the sharp drop-off in intensity in other species such as CS. The dust temperature reaches a local minimum value of $\sim 40 \text{ K}$ near this location, marking the cross-over point between heating from the embedded sources and the external ionizing star (Lester *et al.* 1986). The brightness temperature of the C II at this position is 50 K , and the minimum column density of C II in the high-temperature limit is $3 \times 10^{17} \text{ cm}^{-2}$, similar to that at IRS. It is likely that the photodissociation in this region is produced by UV from the external star after considerable attenuation by dust and other molecular material. Therefore, the UV flux parameter G_0 will be significantly less than the value of 150 calculated by Keene *et al.* (1985) at the ionization front. Available PDR models do not explicitly predict observable C II intensities for these low values of G_0 , but extrapolation of the trend in integrated intensity with G_0 shown in the model of Tielens and Hollenbach (1985) suggests, as expected, that the observed value could be obtained with an appropriate lower value of G_0 . A stronger C II line would be expected closer to the ionization front, and measurements of the minimum column density and brightness temperature at various points in this direction would be informative for determining the relative roles of the embedded and external sources in C II production.

b) S201

S201 is a small ($\sim 6''$), bright H II region embedded in a molecular cloud extending westward at least $12'$ to the edge of W5. Visually, it has a highly structured and bipolar appearance produced by an E-W lane of obscuration from either foreground material or higher density neutral gas intermixed with the ionized gas. Radio continuum observations (Felli, Hjellming, and Cesaroni 1987) with $6''$ resolution show a bright and almost unresolved ridge at the eastern end of S201, almost

coincident with the brightest optical region. Felli, Hjellming, and Cesaroni modeled the radio continuum data convincingly as a spherical molecular cloud which is illuminated and ionized by an early-type (O9) star that is to the west of the cloud and external to it almost in the plane of the sky. This interpretation is supported by the infrared observations of Mampaso *et al.* (1989). Thus, based on this model, S201 is also a good example of a source in which the ionization front is seen almost edge-on. Only the molecular cloud east of the star shows an ionization front, while the extensive molecular cloud to the west appears to be beyond the Strömgren radius of the ionizing star.

Mapping in CO (Martin and Barret 1978; Wramdemark and Lynga 1987; Snell *et al.* 1988) shows an elongated E-W structure with two distinct peaks in excitation temperature, separated by $\sim 5'$, one on either side of the H II region. The brightest (western) peak has $T_{\text{ex}} \sim 24 \text{ K}$, and the secondary (eastern) peak shows $T_{\text{ex}} \sim 18 \text{ K}$, near but not coincident with the ionization front. The line shape in CO is highly variable spatially and has a weak secondary feature visible at some locations.

Mapping in the far-infrared (FIR) continuum (Thronson *et al.* 1984) shows a single peak near the ionization front with a FWHM $\sim 50''$ and extended lower contours. The dust temperature is $\sim 42 \text{ K}$ at the observed peak, dropping slowly to $30\text{--}35 \text{ K}$ $3'$ to the west. This range of dust temperatures is in good agreement with that predicted by Felli and Harten (1981) under the assumption that the dust is heated by an O9 V star within the positional uncertainty of the infrared source AFGL 416. Densities in the region are fairly low: Martin and Barret (1978) obtained an average density of $2.4 \times 10^3 \text{ cm}^{-3}$, while Thronson *et al.* (1984) calculate a peak density of $\sim 10^4 \text{ cm}^{-3}$ in the east, with possibly slightly higher values at the western CO peak. A schematic representation of S201 is presented by Mampaso *et al.* (1989, Fig. 1).

Our C II observations were made at two locations in the S201 region. The first is at the FIR peak of Thronson *et al.* (1984), where the $43''$ beam size encompasses the ionization front, the location of the proposed ionizing star, and the eastern peak of CO column density, although not the location of peak CO excitation temperature. The second location is $1'$ to the SW along a line joining the two peak positions seen in radio continuum data (Felli, Hjellming, and Cesaroni 1987). At this second location, which is closer to the center of the visible H II region, radio continuum emission is weak, and the ^{13}CO column density is near a local minimum between the eastern and western peaks. The CO excitation temperature at our two observed locations is $\sim 15 \text{ K}$, with the FIR peak being in a high gradient region while the position $1'$ SW is close to the rather extended local minimum between the two CO peaks. The dust temperature is near 40 K at both positions. The C II spectra we observed are shown in Figure 2, and the parameters deduced from Gaussian fits to the data are listed in Table 1.

As shown in Figure 2, the C II line at the FIR peak is symmetric and relatively wide. Its V_{LSR} of $-38.0 \pm 0.2 \text{ km s}^{-1}$ is in fairly good agreement with that of the $J = 1\text{--}0$ line of ^{12}CO , -38.5 km s^{-1} (Snell *et al.* 1988). However, the C II line width of $7.4 \pm 0.5 \text{ km s}^{-1}$ is about a factor of 2 larger than that found for the CO line, which was observed with a similar beam size of $45''$. The difference in line width could be attributed to the greater contribution to the C II emission from the ionization front, where turbulence may be enhanced over that in the molecular cloud. In the model of Felli, Hjellming, and Cesaroni (1987), material in the molecular cloud ionized by the

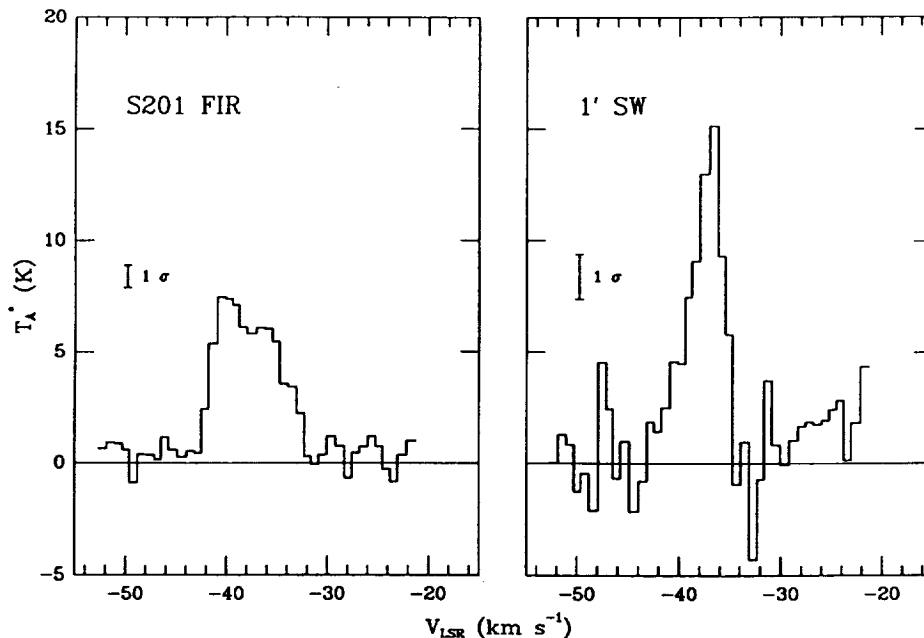


FIG. 2.—C II spectra toward S201: at the FIR peak (*left panel*, 24 minutes integration) and 1' SW of the FIR peak (*right panel*, 6 minutes integration). The continuum determined from the wide filter bank has been subtracted from the spectra. Some residual wing emission may still be present at the limits of the high-resolution spectrum presented here.

stellar UV radiation streams away radially at the speed of sound. A significant fraction of C II line radiation may arise from this newly ionized material and contribute to the apparent width of the line. Because of the geometry of the source, no asymmetry would be expected from the streaming, and none is apparent in the observed C II profile. The brightness temperature of the C II line is ~ 36 K, which is close to the dust temperature at this location but hotter than the CO excitation temperature. The spatial variability of CO line shape and V_{LSR} indicates complex motions within this region, which may account for the striking differences in the C II line profile between the two nearby locations that were observed. The minimum column density of C II at this location in the optically thin high temperature limit is $3 \times 10^{17} \text{ cm}^{-2}$. In the optically thick limit with $T_{\text{ex}} \sim 40$ K, the minimum column density increases to $1 \times 10^{18} \text{ cm}^{-2}$. The source geometry deduced from the model of Felli, Hjellming, and Cesaroni (1987) can be used to estimate G_0 to be 3000 at the ionization front. Thus for S201 the measured integrated intensity and column density are significantly lower than predicted by photodissociation region models for the appropriate conditions, especially for an ionization front oriented along the line of sight. However, beam dilution may be significant for this source which is 2–3 kpc away (Felli, Hjellming, and Cesaroni 1987). Therefore, higher spatial resolution observations are needed before any real discrepancy can be asserted.

The C II line profile 1' SW of the FIR peak is twice as strong and half as wide as that at the FIR peak and appears to have an extended blue wing, although this latter feature is not statistically significant. The high brightness temperature of 45 K at this position is somewhat puzzling, since it is higher than that of C II at the FIR peak, where most of the C II is expected to arise. The C II emission at this location most likely originates from an interface with molecular material located behind the H II region. This interface is viewed more nearly face-on and therefore perhaps has a smaller line-of-sight veloc-

ity gradient than the material at the FIR peak, resulting in a narrower C II line. The possible extended blue wing is consistent with ionized material streaming away from the interface. Furthermore, there might be an additional source of heating in the 1' SW region, perhaps associated with the phenomenon (possibly a shock) responsible for the peculiar CO line shapes seen further SW. Obviously, more complete mapping at high resolution, especially toward the western CO peak and the region of variable and asymmetric line shapes, will be required to understand the complex morphology of S201.

Some of the C II emission may originate from the H II region itself, since in a region ionized by an O9 star, most of the carbon can be expected to be in this ionization state. The integrated intensity of the C II line from this source can be estimated using the electron number density and H II extent deduced from the model of Felli, Hjellming, and Cesaroni (1987), and is found to be $\sim 4 \times 10^{-4} \text{ ergs cm}^{-2} \text{ s}^{-1} \text{ sr}^{-1}$ near the ionization front and $\sim 2 \times 10^{-5} \text{ ergs cm}^{-2} \text{ s}^{-1} \text{ sr}^{-1}$ 1' SW, for a fractional carbon abundance of 10^{-4} . Thus, even taking into account the fact that only about half of the beam at the FIR peak falls on the H II region, a significant part of the observed radiation at this position may arise from the fully ionized hot gas rather than from an ionization front. The greater width of the line at the FIR peak compared with 1' SW could reflect the contribution from the hot ionized gas.

c) NGC 7538

NGC 7538 is an H II region $\sim 5'$ in diameter which is shaped like an incomplete shell; most of the thermal radio emission arises in the western section (Churchwell and Bieging 1982). There are 5 IR sources near the center of the H II region, two of which are mid-O spectral type and at least partly responsible for the ionization of the nebula (Werner *et al.* 1979). Adjacent to the H II region in the south is an extended molecular cloud bounded by the ionization front. Embedded in the cloud $\sim 2'$ SE of the center of the H II region are three closely grouped

(15") infrared sources, IRS 1-3, each accompanied by a compact H II region. Mapping in the FIR continuum (Werner *et al.* 1979) shows that the dust column density is greatest near IRS 1-3, where the derived grain temperature is $T_d \sim 45$ K. The temperature decreases slightly northward, to $T_d \sim 40$ K, before increasing again into the H II region, reaching a value of $T_d \sim 70$ K. The column density of the gas as traced by ^{13}CO also peaks near IRS 1-3, and is extended in the form of an E-W ridge (Dickel, Dickel, and Wilson 1981; Scoville *et al.* 1986). Maps in ^{12}CO and ^{13}CO show a steep gradient in column density, and to a smaller degree excitation temperature, northward from IRS 1-3, with the ridge being coincident with the boundary of the H II region. This morphology (illustrated in Fig. 2 of Dickel, Dickel, and Wilson 1981) suggests that expansion of the ionized region has compressed the molecular cloud (Campbell and Thompson 1984). Emission from vibrationally excited H_2 is also seen over a $\sim 1'$ region between the H II region and the embedded sources and is strongest $\leq 30''$ from IRS 1-3 (Fischer *et al.* 1980). It has been suggested that this emission is from shock-excited gas at the interface between the outflow and the compressed gas at the boundary with the H II region (Fischer *et al.* 1985).

Our C II observations of NGC 7538, shown in Figure 3, were made at two locations: IRS 1-3, and $1'$ NW along a line joining IRS 1-3 with the center of the H II region. This latter position is on the ionization front at the interface between the H II region and the molecular cloud, where the column density and excitation temperature of CO show a steep gradient, and also includes part of the region of vibrationally excited H_2 emission. The excitation temperatures of CO are $T_{\text{ex}} \sim 22$ K and $T_{\text{ex}} \sim 18$ K at IRS 1-3 and $1'$ NW, respectively (Campbell and Thompson 1984), while the dust temperature is $T_d \sim 45$ K at both locations (Werner *et al.* 1979). From Table 1 it can be seen that the brightness temperatures of C II in the two locations, 42 K and 48 K, respectively, are again similar to the dust temperature but somewhat higher than the temperature of the

molecular gas. The $-57 \text{ km s}^{-1} V_{\text{LSR}}$ of the C II line at both locations corresponds to that of the molecular cloud rather than the H II region (-60 km s^{-1} , Churchwell and Bieging 1982).

Figure 3a shows a comparison of our observed C II spectrum (with the continuum subtracted) to the $J = 2-1$ line of CO at IRS 1-3 (G. Stacey, private communication). The agreement between line shapes is good if the different signal-to-noise ratios of the two spectra are taken into account. The extended red wing which is more evident in the CO spectrum may be a contribution from another cloud in the region: Campbell and Thompson (1984) detected at least three additional CO components with more redshifted velocities at various locations in NGC 7538. The asymmetry apparent in the CO spectrum is not obviously present in the C II data, which can be fitted by a single Gaussian component to within statistical uncertainties.

The 13.7 km s^{-1} (FWHM) width of the C II line is similar to that seen in low- J ^{12}CO lines. However, both are wider than the $\Delta V \sim 6 \text{ km s}^{-1}$ line width typical for ^{13}CO (Campbell and Thompson 1984) and C I (Phillips and Huggins 1981), and the $\Delta V \sim 4.5 \text{ km s}^{-1}$ line width observed in species requiring higher densities for excitation (e.g., CN: Churchwell and Bieging 1982; OCS: Goldsmith and Linke 1981). The IRS 1-3 region of NGC 7538 has similar physical characteristics to S140 FIR which also has embedded sources and an outflow seen in CO. Again, it is possible that the outflow in the molecular material also affects the photodissociated region, resulting in a wider line than at the ionization front. However, analogous to ^{12}CO , optical depth effects cannot be ruled out as possible contributors to the observed C II line width.

The 42 K brightness temperature of the C II line at IRS 1-3 is a lower limit to the excitation temperature because both the optical depth and beamfilling factor are unknown. However, beam dilution should be less significant in this case since the three embedded sources are spread over $\sim 15''$. The C II column density, calculated from the physical argument of

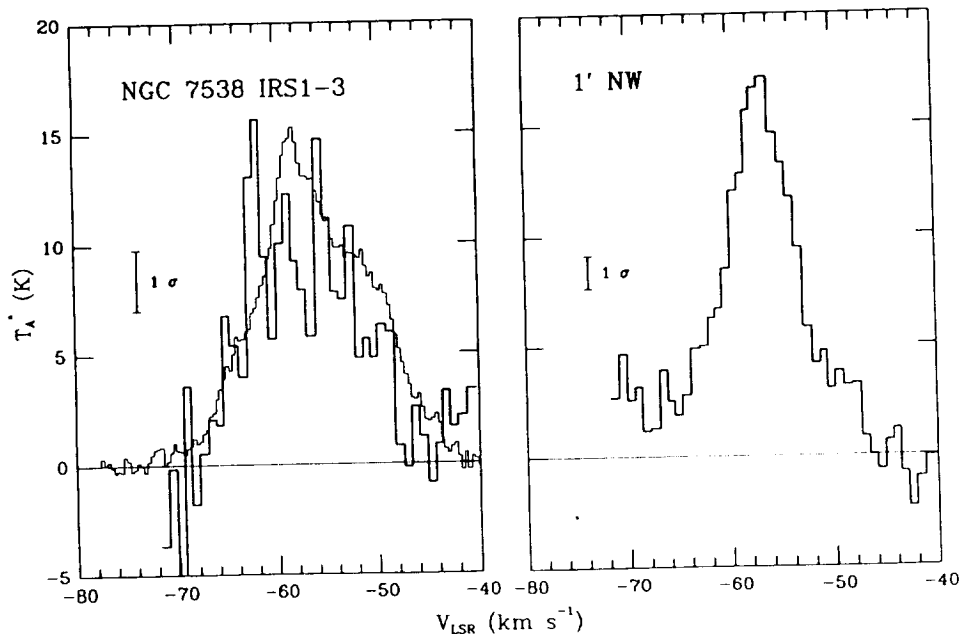


FIG. 3.—C II spectra in the NGC 7538 region. *Left panel:* C II at IRS 1-3 (heavy line) compared with CO $J = 2-1$ (light line; G. Stacey, private communication). *Right panel:* C II $1'$ NW of IRS 1-3, at the ionization front. Integration times are 4 minutes at IRS 1-3 and 14 minutes $1'$ NW. The continuum determined from the wide filter bank has been subtracted from the spectra.

Tielens and Hollenbach (1985) in which the photoionization of C to C⁺ proceeds to a UV penetration depth of $A_v \sim 4$ (or $N_{\text{H II}} = 7.6 \times 10^{21} \text{ cm}^{-2}$), is $\sim 2 \times 10^{18} \text{ cm}^{-2}$ for a single source of ionization when viewed collinear with the direction of ionization, and some factor < 3 greater than this for the net contribution from all three embedded sources. The minimum column density in the optically thin high temperature limit derived from the observed integrated intensity of the C II line at IRS 1-3 is $7.4 \times 10^{17} \text{ cm}^{-2}$. This value is a factor of ~ 4 lower than that expected from the UV-penetration argument, but given the uncertainties such as grain parameters and dust-to-gas ratio implicit in the calculation, as well as the unknown UV flux, is not totally inconsistent with an assumption of optically thin emission. The larger C II integrated intensity in NGC 7538 compared with those from S140 and S201 may simply reflect the number, spatial distribution, and evolutionary stages (UV-output) of the embedded stars responsible for the C II ionization. On the other hand, there is no conclusive evidence to rule out the alternative limiting case of somewhat optically thick C II emission with an excitation temperature $\sim 50 \text{ K}$, close to the dust temperature. Column densities in this latter case would be closer to the values calculated on the basis of UV penetration depths.

Figure 3b shows the C II line at the ionization front. Our beam at this location encompasses a region with H₂ vibrational emission, which has been interpreted as a product of shock excitation. The heating of the gas by the outflow is expected to be localized at this shock front, but should not produce a noticeable increase in line temperature averaged over our beam (Scoville *et al.* 1986). The C II line shape is well represented by a single Gaussian component with no evidence of extended wing emission to within statistical uncertainties. The brightness temperature of the line is higher than at IRS 1-3, but the integrated intensity is very similar because the line width is smaller. Thus calculated column densities in the optically thin high temperature limit are similar to those at IRS 1-3, even though the edge-on view should give a longer projected path through the ionization front at this position.

The UV flux at the ionization front corresponds to $G_0 \sim 1000$ if all the UV is assumed to originate from the O7 star at IRS 6. Column densities from PDR models for this value of G_0 for an interface viewed face-on are similar to the measured value for the approximately edge-on view. However, as in the case of S201, the distance to NGC 7538 ($\sim 3 \text{ kpc}$; Churchwell and Biegging 1982) suggests that beam dilution or pointing uncertainties in the $10''$ - $15''$ range may significantly decrease the measured integrated intensity.

d) Cep B

The molecular cloud in Cepheus is located near the Galactic plane and is elongated parallel to it, extending for over 4° . The cloud consists of several components, as shown by distinct peaks in the spatial distribution of CO radiation (Sargent 1977). The Cep A region contains several embedded sources with at least three compact H II regions within a $5''$ radius (Beichman, Becklin, and Wynn-Williams 1979). Line profiles from this region show the high-velocity wings characteristic of a bipolar outflow (Bally and Lada 1983). Further evidence of energetic activity in this region is provided by emission from vibrationally excited H₂ (Bally and Lane 1982). The millimeter-wave CO lines from Cep A show deep self-absorption at some locations (Sargent 1977; Phillips *et al.* 1981).

The CO radiation of highest excitation arises from a distinct

region in the NW of the molecular cloud, Cep B, which forms an interface with the H II region S155. Observations in the radio continuum (Felli *et al.* 1978) show the presence of a ridge coincident with the optical bright rim at the interface with S155, with a plateau behind the ridge into the molecular cloud. Modeling of the region by Felli and coworkers (1978) indicates that the main source of molecular excitation comes from external stars which are responsible for the ionization of the H II region and are situated such that the ionization front is inclined $\sim 50^\circ$ with respect to the plane of the sky. The far infrared continuum emission is also strongest near the interface between the molecular cloud and H II region S155 (Evans *et al.* 1981; see Fig. 1 for a schematic illustration), with the higher gradient being toward the H II region. Dust temperature appears to decrease away from the photodissociation edge of the cloud, as expected from a morphology in which the source of heating is external.

Our observations of C II in the Cepheus molecular cloud included four positions: Cep A, the FIR peak in Cep B, and locations 1' and 2' NW from the FIR peak in Cep B toward the H II region. Only a single 4 minute integration was obtained at Cep A. No C II emission was seen, with a 2σ upper limit to the integrated intensity of $2.4 \times 10^{-4} \text{ ergs cm}^{-2} \text{ s}^{-1} \text{ sr}^{-1}$. The continuum, however, was quite strong at this location, $1.2 \pm 0.2 \text{ K}$, in good agreement with the 1.1 K expected from the measurements of Evans *et al.* (1981). The reason for the absence of C II emission at this location is not totally clear, since the presence of compact H II regions within the molecular cloud implies a surrounding photodissociation region and a consequent C⁺ envelope. However, beam dilution will be quite severe, since these regions all lie within $\sim 6''$. More significantly, marked reversals are seen in the profiles of CO rotational lines, which raises the possibility that the C II emission could be self-absorbed as well, as seems to be the case in several other molecular clouds (Betz, Boreiko, and Zmuidzinas 1990). With the appropriate velocity, line width, and density or temperature gradients through a cloud, it is possible for C II emission to be completely self-absorbed and for any residuals to be masked by foreground continuum emission from the same cloud. A more definitive conclusion will require more sensitive observations of Cep A at several spatial locations.

The spectra obtained at the three positions in the Cep B-S155 region are shown in Figure 4, and the parameters deduced from Gaussian fits to the spectra are listed in Table 1. At the FIR peak, the C II line has $T_A^* = 28 \text{ K}$, which implies a minimum excitation temperature of 63 K . For comparison, $^{12}\text{CO } J = 1-0$ has $T_A^* \sim 13 \text{ K}$ at this position measured with a $65''$ beam (Sargent 1977), and the dust temperature is $43 \pm 3 \text{ K}$ (Evans *et al.* 1981). The CO velocity structure of the Cep B region is complex, with several components evident. Most of the CO emission from the Cep B region has a V_{LSR} center of approximately -12 km s^{-1} , with a component at -15 km s^{-1} appearing only close to S155. The emission from C II appears at $V_{\text{LSR}} = -13.9 \text{ km s}^{-1}$, and the 4.2 km s^{-1} (FWHM) line width of the C II is similar to the 2 - 4 km s^{-1} seen for CO. The minimum column density of C II at the FIR peak, assuming an optically thin line in the high temperature limit, is $5.7 \times 10^{17} \text{ cm}^{-2}$. Our nondetection of the strongest hyperfine component of the $^{13}\text{C II}$ line places a 3σ upper limit on the optical depth of 11 (assuming $[^{12}\text{C}]/[^{13}\text{C}] = 60$). The $^{12}\text{C II}$ integrated intensity measured at this location is consistent with predictions of PDR models for the geometry of the source and $G_0 \sim 650$, as deduced from the model of Felli *et al.* (1978).

At a position 1' NW of the FIR peak in Cep B, where the

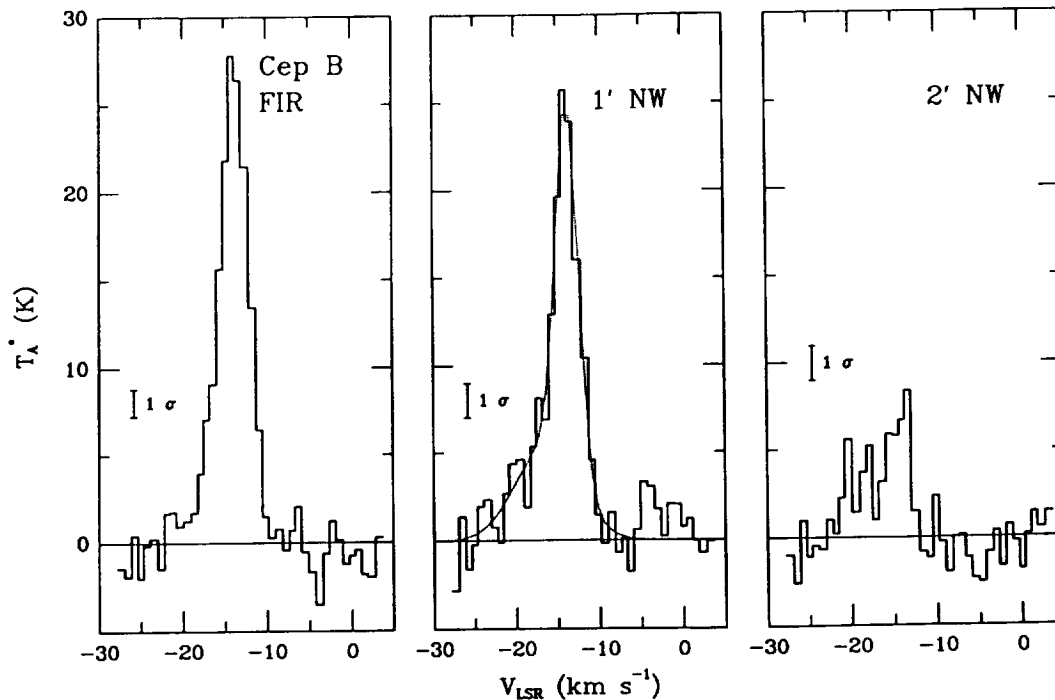


FIG. 4.—C II spectra in the region of Cep B: at the FIR peak (left panel), 1' NW of the FIR peak (middle panel), and 2' NW of the FIR peak (right panel). The dotted line in the central panel shows the fit of two Gaussian components to the spectrum. Integration times are 12 minutes at the FIR peak and 8 minutes for the other positions. The continuum has been subtracted from all spectra.

beam includes the radio peak seen by Felli *et al.* (1978), the integrated intensity of the C II has changed very little from its value at the FIR peak, and T_A^* has decreased only slightly. In contrast, the antenna temperature of the CO emission has decreased to ~ 5 K here, most likely because of the photo-destruction of CO. On the other hand, the dust temperature of ~ 50 K is somewhat higher at this position than at the FIR peak.

The C II line 1' NW of the FIR peak clearly consists of more than one component, and shows an extended blue wing. As shown in Figure 4b, the data are fitted well by two Gaussian components, with V_{LSR} of -13.8 and -16.5 km s^{-1} , and the former component 4 times as bright as the latter. The brighter and narrower component is probably the same as that seen at the FIR peak, while the broader and more blueshifted contribution, if it arises from a single source with a Gaussian line profile rather than asymmetric broadening from gradients within the cloud, represents a component of the photo-dissociated gas heretofore not identified in the molecular gas. Closer examination of the C II line profile from the FIR peak also reveals a slight blue asymmetry, and a fit of two Gaussians rather than one to the profile improves the reduced χ^2 value of the fit by 20%. The additional broad component then has a V_{LSR} of -16.5 ± 0.5 km s^{-1} and a FWHM of 6.0 ± 1.7 km s^{-1} , while the main component shifts to -13.6 ± 0.1 km s^{-1} with a width of 3.8 ± 0.2 km s^{-1} . The component at -16.5 km s^{-1} , obtained from an independent fit to the FIR peak data, is clearly the same as that present 1' to the NW, although its existence could not be certified from just the slight (and statistically, not quite significant) blue asymmetry of the FIR peak spectrum.

Our C II data 2' NW of the FIR peak, well within the H II region, suffer from a low signal-to-noise ratio, since the integrated intensity of the line has decreased more than fourfold from that at the peak. Only one Gaussian component can

justifiably be fitted to the data, at -15.8 ± 0.5 km s^{-1} as shown in Table 1. However, if a second component at -16.5 km s^{-1} with variable amplitude and a FWHM of 7.5 km s^{-1} (deduced from the other two spectra, and fixed in this case) is forced into the fit, then the reduced χ^2 value improves by almost 25%, and the V_{LSR} of the primary component shifts to -13.8 ± 0.3 km s^{-1} , more consistent with that at the other two positions. The FWHM of the main component is 2.1 ± 0.8 km s^{-1} , significantly narrower than that observed closer to the molecular cloud.

Thus, all the data taken together tentatively indicate the presence of two velocity components in the C II emission of Cep B. The strongest component has a velocity of -13.8 km s^{-1} , which is similar to that of CO near the edge of the molecular cloud. The intensity and width of this component both decrease into the H II region. The second component at -16.5 km s^{-1} , whose existence must be considered somewhat tentative, has a more uniform intensity distribution, is more blueshifted, and is significantly wider than the main component. This weaker component may not be associated with the molecular cloud-H II region interface at all, since it does not appear to be peaked there, but may be related to the H II region S155 which shows a similar V_{LSR} in H α emission.

A calculation of the expected C II integrated intensity from the H II region based on the parameters given by Felli *et al.* (1978) yields $\sim 5 \times 10^{-5}$ $\text{ergs cm}^{-2} \text{s}^{-1} \text{sr}^{-1}$, suggesting that some of the observed radiation at the 2' NW position comes from hot, optically thin gas in the H II region. It is possible that the component with V_{LSR} near -16 km s^{-1} at all three locations in Cep B arises from this hot gas.

e) M17

The M17 region can be considered to be an extreme case of the H II region interacting with a molecular cloud, in which everything is on a larger and more intense scale than for the

sources previously discussed. The H II region (M17 or NGC 6618) forms a sharp interface with an extended and massive molecular cloud to the SW (M17 SW), and also with a less dense molecular cloud to the north (Gatley *et al.* 1979). The heating and ionization of the region is dominated by a cluster of up to 100 O and B stars, resulting in a very intense UV field in the region. The CO emission from M17 SW shows a very sharp decrease at the interface with the H II region, and the peak T_A^* is offset toward the ionization front relative to the position of peak CO column density (Lada 1976; Thronson and Lada 1983; Rainey *et al.* 1987). This morphology clearly suggests that the heating of the molecular gas is dominated by UV radiation from the external stars. The conclusion is supported by FIR continuum mapping (Gatley *et al.* 1979), which shows that the color temperature decreases monotonically into the cloud from ~ 85 K near the ionization front. The data also reveal a steep density gradient, with the H_2 density decreasing into the cloud. The FIR mapping suggests that the periphery of the molecular cloud is heated by UV and optical radiation from exciting stars and the nebula, while the core of the cloud is heated by infrared reradiation from embedded dust.

The molecular gas in M17 SW consists of at least two temperature components. The peak T_A^* for several low- J CO transitions which are expected to be optically thick indicate excitation temperatures of ~ 50 K. However, observations in higher- J CO transitions suggest excitation temperatures of up to a few hundred K for some locations (Harris *et al.* 1987). Line profiles in many CO transitions reveal complex structure, with several emission components, possible self-absorption, and significant changes on small spatial scales (Martin, Sanders, and Hills 1984; Rainey *et al.* 1987; Schulz and Krügel 1987; Harris *et al.* 1987). Modeling of the M17 cloud suggests a significant clumpiness both in the molecular and photodissociation regions (Martin, Sanders, and Hills 1984; Snell *et al.* 1984;

Mundy *et al.* 1986, 1987; Genzel *et al.* 1988; Stutzki *et al.* 1988). Figure 1 of this latter reference illustrates the spatial relationship of the various components of M17.

C II in M17 was first observed by Russell *et al.* (1981), who found a uniform halo of emission extending for at least $12'$. Stutzki *et al.* (1988) obtained a strip scan of the integrated intensity of the C II emission at somewhat higher spectral resolution and confirmed the large extent of low-level C II emission. The peak of the C II emission is offset into the molecular cloud relative to the peak in the radio continuum. The emission decreases smoothly to the SW into the bulk of the molecular material, but its distribution is complicated toward the NE because of the existence of a second ionization front/molecular cloud interface. A map of C II emission at $3.7'$ resolution (Matsuhara *et al.* 1989) clearly shows the existence of two peaks in the C II integrated intensity associated with the two interfaces.

Our observations of M17 were performed at three positions: the peak of integrated C II emission observed by Stutzki *et al.* (1988), the C I peak seen by Genzel *et al.* (1988), and halfway between. With respect to the reference position of SAO 161357 at $\alpha(1950) = 18^h 17^m 34.5^s$, $\delta(1950) = -16^\circ 13' 24''$, these three positions are at $(-30, -15)$, $(-90, -45)$, and $(-60, -30)$, respectively, with the values in arcseconds, negative to the W and S. The three positions lie along a line perpendicular to the ionization front. The first position is ~ 1.5 S of the C II peak shown in the map of Matsuhara *et al.* (1989). The last two positions approximately bracket the location of peak T_A^* in low- J CO lines, and the highest column density of CO lies within the beam at the third position. The direction of chop was along our three-position line perpendicular to the ionization front, with an amplitude of 10.5 . The spectra thus obtained are shown in Figure 5.

As can be seen from Figure 5, the line shapes of the C II are

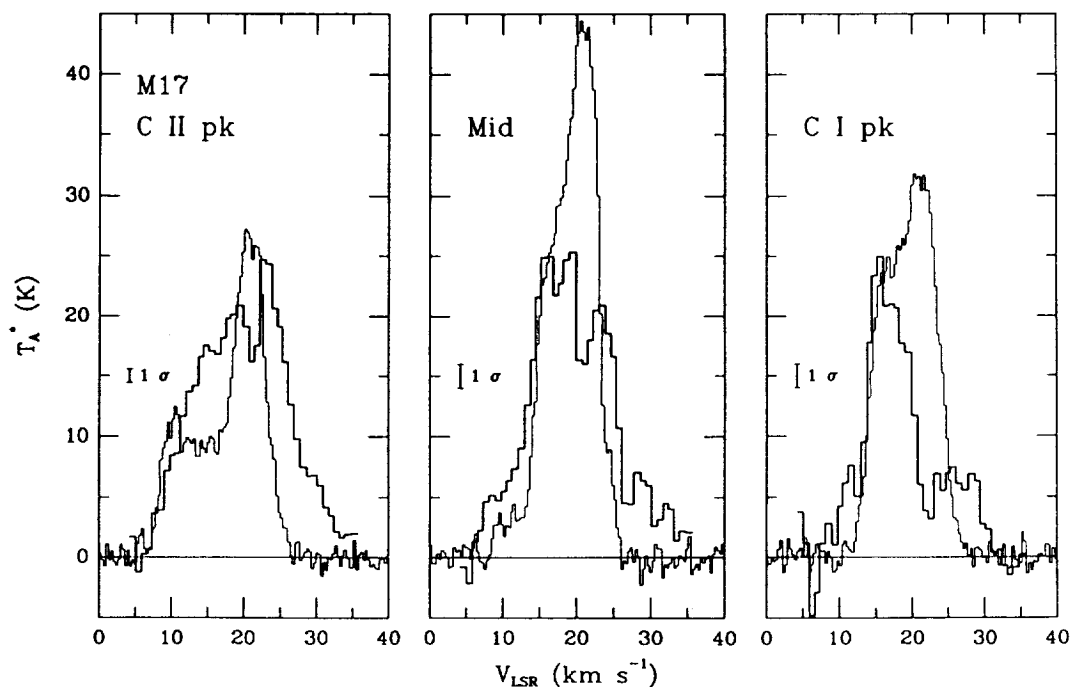


FIG. 5.—C II spectra (heavy lines) compared with CO $J = 2-1$ spectra (light lines: Stutzki *et al.* 1988) at three locations in M17: the C II peak of Stutzki *et al.* (left panel, 24 minutes integration), the C I peak of Genzel *et al.* 1988 (right panel, 8 minutes integration) and midway between (middle panel, 8 minutes integration). The continuum determined from the wide filter banks has been removed from all C II spectra. Some C II emission remains out to the limits of the high-resolution filter bank, as shown here.

complex at all three positions, with features suggesting the existence of at least one emission and one absorption (or "negative emission" from reference beam contamination) component. For comparison, the $^{12}\text{CO } J = 2-1$ spectra at the same locations are also shown. The $^{12}\text{C}^{18}\text{O}$ spectra at the same three positions show relatively simple profiles, with that at the midposition ($-60, -30$) appearing to be a symmetric single Gaussian. The line profile at the C II peak ($-30, -15$) seems to have an extended blue wing, while that at the C I peak ($-90, -45$) shows evidence of an extended red wing. The coincidence of the central dip in the C II spectra with peak emission in the $^{12}\text{CO } J = 2-1$ spectra and the single-peaked profile of the C^{18}O data together suggest that the apparent C II dip may be produced by absorption in cooler or less dense foreground gas rather than the distinction between two separate velocity components.

The observed C II line shapes are probably somewhat complicated by the presence of emission in the "off-source" reference beam position. An estimate of emission in the reference beam can be obtained from the extended C II map of Matsuhara *et al.* (1989). The integrated intensities corrected for reference beam emission are $3.2 \times 10^{-3} \text{ ergs cm}^{-2} \text{ s}^{-1} \text{ sr}^{-1}$, $3.1 \times 10^{-3} \text{ ergs cm}^{-2} \text{ s}^{-1} \text{ sr}^{-1}$, and $2.0 \times 10^{-3} \text{ ergs cm}^{-2} \text{ s}^{-1} \text{ sr}^{-1}$ at ($-30, -15$), ($-60, -30$), and ($-90, -45$), respectively. These values are all consistent with those obtained from the scan of Stutzki *et al.* (1988) and the map of Matsuhara *et al.* (1989) when the larger beam size used for the latter is considered. The calculated minimum column density for optically thin radiation in the high-temperature limit yielding the stated intensities is $\sim 2 \times 10^{18} \text{ cm}^{-2}$.

We have attempted to obtain fits to the observed spectra assuming that they consist of a superposition of Gaussian emission components in both signal and reference beams. The best fits obtained in this manner are shown as the dotted curves in Figure 6, and the parameters of these fits are present-

ed in Table 1. In each case, the fit is $\sim 25\%$ worse than expected from statistical noise alone, indicating that our assumption of the number or shape of the components is probably not quite valid. The V_{LSR} was fixed in the fit to the spectrum in the C I peak ($-90, -45$) location, since the amplitudes of the absorption and emission components are highly coupled in this fit. An increase in the fitted amplitude of the emission component can be compensated by a similar increase in the amplitude of the absorption component, together with a shift to higher V_{LSR} and lower width for emission and to lower V_{LSR} and greater width for absorption, with the net result being fits with comparable values of χ^2 over a range of emission T_A^* of 20–40 K. Therefore the parameters associated with the fit at this particular position should be considered somewhat less certain.

The spectrum at the C II peak ($-30, -15$) with the highest signal-to-noise ratio can be fitted with one emission and two absorption components. There is also evidence in the other two M17 spectra for the existence of the second "absorption" component near $V_{\text{LSR}} = 18 \text{ km s}^{-1}$. This dip (which in Figs. 5 and 6 appears near 16 km s^{-1} because it is superposed upon a sloping wing) is most likely caused by emission in the "off-source" beam located in the molecular cloud, since the $\sim 6 \text{ km s}^{-1}$ width is typical for CO lines within the cloud. For example, the $^{12}\text{CO } J = 2-1$ spectra of Stutzki *et al.* (1988) taken further SW from our source position (although not as far as our reference location) show the existence of a prominent emission at $V_{\text{LSR}} \sim 18 \text{ km s}^{-1}$. Furthermore, the strength of the 18 km s^{-1} C II component decreases toward the SW, as expected from the C II map of Matsuhara *et al.* (1989) if the feature is produced by emission in the "off-source" reference beam in the molecular cloud.

The noticeable negative feature that appears near 21 km s^{-1} V_{LSR} in all three spectra may originate from the other "off-source" reference position near the second ionization front.

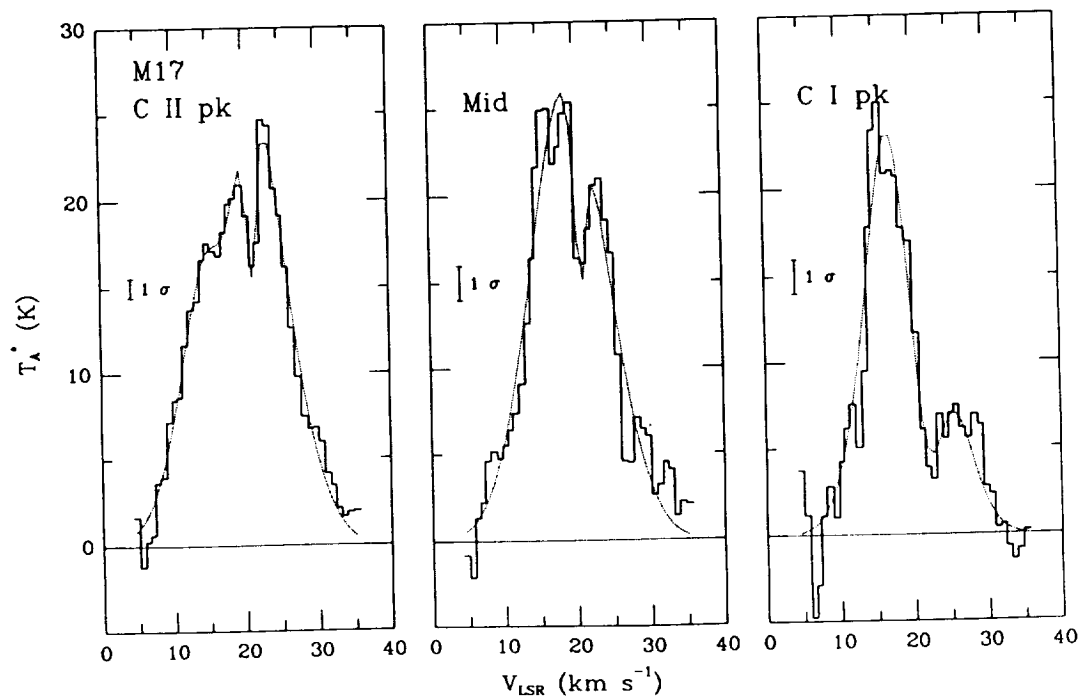


FIG. 6.—C II spectra at three locations in M17, as in Fig. 5. The dotted lines show the fits of a linear combination of Gaussian components to the spectra.

The integrated intensity of this feature increases toward the SW, as expected if this interpretation is valid. One clear conclusion from the C II spectra is that a region exists that produces very narrow C II features, of the order of 1.7 km s^{-1} FWHM, since no linear combination of wider Gaussians can produce the appearance of the sharp-edged absorptions seen in the data. This width is substantially smaller than typical C II line widths observed in other clouds.

The combined integrated intensity in "negative emission" or absorption features is 0.20, 0.06, and 0.41 of that seen in the main Gaussian component at the three positions observed. For comparison, the expected values from the Matsuhara *et al.* (1989) map are all near 0.25. The discrepancy in two of the locations suggests that the line profiles are not approximately Gaussian, that some of the "negative emission" is actually foreground absorption, or that some reference beam emission is not properly identified in the fitting procedure, perhaps because of the interdependence among fitted parameters. For example, we cannot detect the presence of emission in the reference beam with the same V_{LSR} and FWHM as the observed line. The width cannot be greater because of the absence of noticeable signals below continuum level, or much narrower because there are no obvious "absorption" features within the emission, apart from those already discussed.

One alternative interpretation for the narrow feature at 21 km s^{-1} is foreground absorption by cooler or less dense (and hence subthermally excited) material. Fits to the C II spectra under this assumption are equally as good as those obtained assuming reference beam contamination. The minimum optical depth and maximum brightness temperature, respectively, of the foreground absorber indicated by the fits are $\tau_{\text{min}} = 0.41 \pm 0.06$ and $T_{\text{max}} = 53 \pm 2 \text{ K}$ at $(-30, -15)$, $\tau_{\text{min}} = 0.51 \pm 0.15$ and $T_{\text{max}} = 48 \pm 3 \text{ K}$ at $(-60, -30)$, and $\tau_{\text{min}} = 1.7 \pm 0.2$ and $T_{\text{max}} = 31 \pm 2 \text{ K}$ at $(-90, -45)$. Unfortunately, because of our uncertainty of reference beam contamination, we cannot definitively say whether this "self-absorption" interpretation has any physical significance.

The brightness temperature of the main C II emission component deduced from the fit again appears to be similar to the dust temperature in the region, with no strong gradient indicated. As mentioned previously, however, the brightness temperature provides only a lower limit to the excitation temperature, not only because optical depth is unknown but also because reference beam emission with a comparable velocity profile would artificially lower the observed spectrum. The C II lines in M17 are considerably wider than molecular lines such as CO as well as C I observed in the same region, while from the fits the V_{LSR} appears lower by $1\text{--}2 \text{ km s}^{-1}$. The increased width of C II relative to CO could be explained by the turbulence in the photodissociated gas which may be streaming away from its point of origin. Also, given the possibility of line distortion from reference beam contamination and the spatially complex nature of the source, the apparent shift in V_{LSR} between CO and C II may not be real and would need to be confirmed through additional C II observations. Thus, the C II observations are not inconsistent with the clumpy model of Stutzki *et al.* (1988).

IV. SUMMARY AND CONCLUSIONS

We have observed the C II fine-structure line in five sources for which the ionization front/molecular cloud interface is viewed approximately edge-on. For most sources, the C II line has a simple Gaussian profile with a V_{LSR} similar to that seen in

CO, but with a line width greater than that characterizing the molecular gas. Brightness temperatures corresponding to the observed antenna temperature are found to be similar to or somewhat higher than the dust temperature at all locations. The minimum C II column densities calculated by assuming optically thin radiation in the high temperature limit range from $2 \times 10^{17} \text{ cm}^{-2}$ to $2 \times 10^{18} \text{ cm}^{-2}$ for the sources discussed.

In the two sources for which the position of a well-established embedded source was observed (S140 and NGC 7538), the antenna temperature is somewhat lower and the line width is greater at the location of the embedded source than near the ionization front, thereby leading to very similar values of integrated intensity. Both of these sources show outflows in CO, and the wider lines could be due to an interaction of the outflow with the photodissociation region. All of the sources observed at the high resolution of 0.8 km s^{-1} show significant variations in the C II line profile on spatial scales $\leq 1'$, indicating rapid changes in physical conditions and kinematics on smaller scale sizes. Observations with a smaller beam size would be useful for determining the properties of photodissociation regions in more detail.

The sources observed, with the possible exception of M17, appear to have broadly similar characteristics. M17 has a higher brightness temperature, as might be expected from its much more intense UV field. The line shapes in M17 are very complex, with evidence for emission extended over more than $20'$ which does not appear in other sources. There is also a narrow feature at 21 km s^{-1} in the M17 spectra which may be attributed to absorption from foreground gas with a low velocity dispersion. If this is truly absorption rather than "off-source" emission from a second ionization front in the region, then an optical depth of more than 1.7 is indicated.

There is evidence in some of the sources that part of the C II radiation arises from the H II region as well as from the interface with the molecular cloud. It is possible to distinguish between these two contributions to the net integrated intensity due to the side-illuminated geometry and also occasionally by different V_{LSR} , for which the high spectral resolution available with a heterodyne instrument is required. However, in cases of a face-on geometry, it may not be possible to separate the two components, and hence the interpretation of C II line intensities must be approached with caution, recognizing that two regions with greatly different physical characteristics (one hot, leading to very optically thin lines, and the other, considerably cooler, leading to potentially optically thick lines) could contribute to the observed integrated intensity.

The model of photodissociation regions developed by Tielens and Hollenbach (1985) predicts that the column density of C II in a photodissociation region is $\sim 2 \times 10^{18} \text{ cm}^{-2}$ measured along the line of sight from the source of ionization, and that it should not be very sensitive to the UV flux and gas density, since it is determined predominantly by penetration depth of the ionizing UV photons. The column densities derived from our data for embedded sources (i.e., for a face-on view of the ionization front) are consistent with those expected on the basis of the model, given the range of possible UV fluxes, densities, and model parameters such as dust-to-gas ratio. The measured column density should be higher when observed at an angle to the direction of illumination, especially in the case of edge-on ionization fronts. However, column densities we derive for locations at which the ionization front is viewed approximately edge-on are generally very similar to

those derived for face-on ionization regions in the same source, rather than showing a clear increase due to superposition of emission along the line of sight. Unfortunately, the UV fluxes for the two geometries in any single source are significantly different, making meaningful comparisons impossible without more complete knowledge of the source morphology. In addition, the physical extent of the ionization front may be small in several of the observed sources, leading to underestimation of the peak C II column density due to beam dilution and non-optimum pointing.

The C II brightness temperatures are similar to dust temperatures in a variety of sources with line widths ranging from 3 to 14 km s⁻¹. Such a coincidence, resulting just from fortuitous combinations of a high excitation temperature and a low but variable optical depth, while possible, appears somewhat unlikely, and suggests that the C II lines from the edge-illuminated regions may be optically thick. However, there is insufficient dynamic range in the observed C II brightness temperatures to establish a clear relationship with dust temperature, and both temperatures are dependent upon the UV flux.

Whereas the presence of hot gas has been shown via high-*J* emission of CO and other higher excitation lines in sources such as Orion and M17, it should be recognized that these regions are exceptional, with much higher UV fluxes than for most of the sources discussed in this paper. Lower PDR tem-

peratures might be expected for less UV heating, perhaps consistent with the most straightforward interpretation of the present data of optically thick, cool gas. However, if PDRs are intrinsically very clumpy such that beamfilling factors are less than one even for a side-illuminated geometry, then beam dilution could be significant in all of the sources, resulting in higher temperatures even if the lines are optically thick.

A definitive answer to the question of emission optical depth, and hence gas temperature in the photodissociation region, cannot be obtained from the present data. A good approach to the problem would be to observe the hyperfine components of ¹³C II in several of the sources. Also, additional detailed observations of line profile changes across an ionization front and within the molecular clouds would be valuable for drawing more quantitative conclusions on the heating and cooling of photodissociation regions. Also, spectrally resolved observations of the 63 μm O I fine-structure line, which is expected to be somewhat optically thick in PDRs (Tielens and Hollenbach 1985), would be very useful for determining the temperature of these regions.

We are grateful to the staff of the Kuiper Airborne Observatory for their enthusiastic support during the course of these observations. We thank G. Stacey for providing us with access to CO *J* = 2-1 spectra prior to publication. This work was supported by NASA grant NAG 2-254.

REFERENCES

- Bally, J., and Lada, C. J. 1983, *Ap. J.*, **265**, 824.
 Bally, J., and Lane, A. P. 1982, *Ap. J.*, **257**, 612.
 Beichman, C. A., Becklin, E. E., and Wynn-Williams, C. G. 1979, *Ap. J. (Letters)*, **232**, L47.
 Betz, A. L., Boreiko, R. T., and Zmuidzinas, J. 1990, in preparation.
 Betz, A. L., and Zmuidzinas, J. 1984, in *Proc. Airborne Astronomy Symposium*, ed. H. A. Thronson and E. F. Erickson (NASA CP-2353), p. 320.
 Blair, G. N., Evans, II, N. J., Vanden Bout, P. A., and Peters, III, W. L. 1978, *Ap. J.*, **219**, 896.
 Boreiko, R. T., Betz, A. L., and Zmuidzinas, J. 1988, *Ap. J. (Letters)*, **325**, L47.
 Campbell, B., and Thompson, I. 1984, *Ap. J.*, **279**, 650.
 Churchwell, E., and Bieging, J. H. 1982, *Ap. J.*, **258**, 515.
 Cooksy, A. L., Blake, G. A., and Saykally, R. J. 1986, *Ap. J. (Letters)*, **305**, L89.
 Crawford, M. K., Lugten, J. B., Fitelson, W., Genzel, R., and Melnick, G. 1986, *Ap. J. (Letters)*, **303**, L57.
 Dickel, H. R., Dickel, J. R., and Wilson, W. J. 1981, *Ap. J. (Letters)*, **250**, L43.
 Evans, II, N. J., Becklin, E. E., Beichman, C., Gatley, I., Hildebrand, R. H., Keene, J., Slovak, M. H., Werner, M. W., and Whitcomb, S. E. 1981, *Ap. J.*, **244**, 115.
 Felli, M., and Harten, R. H. 1981, *Astr. Ap.*, **100**, 42.
 Felli, M., Hjellming, R. M., and Cesaroni, R. 1987, *Astr. Ap.*, **182**, 313.
 Felli, M., Tofani, G., Harten, R. H., and Panagia, N. 1978, *Astr. Ap.*, **69**, 199.
 Fischer, J., Righini-Cohen, G., Simon, M., Joyce, R. R., and Simon, T. 1980, *Ap. J. (Letters)*, **240**, L95.
 Fischer, J., Sanders, D. B., Simon, M., and Solomon, P. M. 1985, *Ap. J.*, **293**, 508.
 Gatley, I., Becklin, E. E., Sellgren, K., and Werner, M. W. 1979, *Ap. J.*, **233**, 575.
 Genzel, R., Harris, A. I., Jaffe, D. T., and Stutzki, J. 1988, *Ap. J.*, **332**, 1049.
 Glassgold, A. E., and Langer, W. D. 1974, *Ap. J.*, **193**, 73.
 Goldsmith, P. F., and Linke, R. A. 1981, *Ap. J.*, **245**, 482.
 Harris, A. I., Stutzki, J., Genzel, R., Lugten, J. B., Stacey, G. J., and Jaffe, D. T. 1987, *Ap. J. (Letters)*, **322**, L49.
 Hayashi, M., Hasegawa, T., Omodaka, T., Hayashi, S. S., and Miyawaki, R. 1987, *Ap. J.*, **312**, 327.
 Hayashi, M., Omodaka, T., Hasegawa, T., and Suzuki, S. 1985, *Ap. J.*, **288**, 170.
 Keene, J., Blake, G. A., Phillips, T. G., Huggins, P. J., and Beichman, C. A. 1985, *Ap. J.*, **299**, 967.
 Lada, C. J. 1976, *Ap. J. Suppl.*, **32**, 603.
 Langer, W. D. 1976, *Ap. J.*, **206**, 699.
 Lester, D. F., Harvey, P. M., Joy, M., and Ellis, H. B. Jr. 1986, *Ap. J.*, **309**, 80.
 Linsky, J. L. 1973, *Ap. J. Suppl.*, **25**, 163.
 Mampaso, A., Phillips, J. P., Vilchez, J. M., Pismis, P., and Riera, A. 1989, *Astr. Ap.*, **220**, 235.
 Martin, R. N., and Barret, A. H. 1978, *Ap. J. Suppl.*, **36**, 1.
 Martin, H. M., Sanders, D. B., and Hills, R. E. 1984, *M.N.R.A.S.*, **208**, 35.
 Matsuhara, M., et al. 1989, *Ap. J. (Letters)*, **339**, L67.
 Melnick, G., Stacey, G. J., Viscuso, P. J., and Fuller, C. E. 1986, *Ap. J.*, **303**, 638.
 Mundy, L. G., Evans, II, N. J., Snell, R. L., and Goldsmith, P. F. 1987, *Ap. J.*, **318**, 392.
 Mundy, L. G., Snell, R. L., Evans, II, N. J., Goldsmith, P. F., and Bally, J. 1986, *Ap. J.*, **306**, 670.
 Petersen, F. R., Scalabrin, A., and Evenson, K. M. 1980, *Int. J. Infrared Millimeter Waves*, **1**, 111.
 Phillips, T. G., and Huggins, P. J. 1981, *Ap. J.*, **251**, 533.
 Phillips, T. G., Knapp, G. R., Huggins, P. J., Werner, M. W., Wannier, P. G., Neugebauer, G., and Ennis, D. 1981, *Ap. J.*, **245**, 512.
 Plambeck, R. L., Snell, R. L., and Loren, R. B. 1983, *Ap. J.*, **266**, 321.
 Rainey, R., White, G. J., Gatley, I., Hayashi, S. S., Kaifu, N., Griffin, M. J., Monteiro, T. S., Cronin, N. J., and Scivetti, A. 1987, *Astr. Ap.*, **171**, 252.
 Russell, R. W., Melnick, G., Gull, G. E., and Harwit, M. 1980, *Ap. J. (Letters)*, **240**, L99.
 Russell, R. W., Melnick, G., Smyers, S. D., Kurtz, N. T., Gosnell, T. R., Harwit, M., and Werner, M. W. 1981, *Ap. J. (Letters)*, **250**, L35.
 Sargent, A. I. 1977, *Ap. J.*, **218**, 736.
 Schulz, A., and Krügel, E. 1987, *Astr. Ap.*, **171**, 297.
 Schwartz, P. R., Thronson, H. A., Jr., Lada, C. J., Smith, H. A., Glaccum, W., Harper, D. A., and Knowles, S. H. 1983, *Ap. J.*, **271**, 625.
 Scoville, N. Z., Sargent, A. I., Sanders, D. B., Claussen, M. J., Masson, C. R., Lo, K. Y., and Phillips, T. G. 1986, *Ap. J.*, **303**, 416.
 Snell, R. L., Huang, Y.-L., Dickman, R. L., and Claussen, M. J. 1988, *Ap. J.*, **325**, 853.
 Snell, R. L., Mundy, L. G., Goldsmith, P. F., Evans, II, N. J., and Erickson, N. R. 1984, *Ap. J.*, **276**, 625.
 Stutzki, J., Stacey, G. J., Genzel, R., Harris, A. I., Jaffe, D. T., and Lugten, J. B. 1988, *Ap. J.*, **332**, 379.
 Takano, T. 1986, *Ap. J.*, **303**, 349.
 Thronson, H. A., Jr., and Lada, C. J. 1983, *Ap. J.*, **269**, 175.
 Thronson, H. A., Jr., Smith, H. A., Lada, C. J., Glaccum, W., Harper, D. A., Loewenstein, R. F., and Smith, J. 1984, *M.N.R.A.S.*, **207**, 659.
 Tielens, A. G. G. M., and Hollenbach, D. 1985, *Ap. J.*, **291**, 722.
 Werner, M. W., Becklin, E. E., Gatley, I., Matthews, K., and Wynn-Williams, C. G. 1979, *M.N.R.A.S.*, **188**, 463.
 Wramdemark, S., and Lynga, G. 1987, *IAU Symposium 115, Star-Forming Regions*, ed. M. Peimbert and J. Jugaku (Dordrecht: Reidel), p. 211.
 Zmuidzinas, J., Betz, A. L., and Boreiko, R. T. 1989, *Infrared Phys.*, **29**, 119.

A. L. BETZ and R. T. BOREIKO: Space Sciences Laboratory, University of California, Berkeley, CA 94720

J. ZMUIDZINAS: Astronomy Department, University of Illinois, 1011 West Springfield Avenue, Urbana, IL 61801

APPENDIX L

FAR-INFRARED HETERODYNE TECHNOLOGY

A. L. Betz and R. T. Boreiko

Space Sciences Laboratory
University of California, Berkeley

ABSTRACT

The development of laser heterodyne technology over the last five years has extended high resolution spectroscopy to the short submillimeter and far infrared spectral regions. Spectrometers utilizing far infrared lasers as local oscillators and Schottky diodes as mixers are now quite productive in astronomy. In fact, spectrometers of this type are currently the only viable approach for heterodyne spectroscopy at frequencies >800 GHz. Even though sensitivities are still two orders of magnitude worse than the quantum limit, the present generation of receivers has proven capable of making unique scientific measurements. Improvements in diode parameters and laser utility are likely to keep pace with advancements in competing heterodyne technologies, such that airborne spectrometers with laser LOs and Schottky mixers will remain pre-eminent in the far infrared ($\nu > 1000$ GHz) for years to come. The future is less certain for groundbased receivers using Schottky mixers, which are expected to receive increased competition from SIS technology at frequencies below 1000 GHz.

Keywords: heterodyne, far infrared, submillimeter, mixer, local oscillator, laser

1. INTRODUCTION

The submillimeter and far infrared spectral regions are frequently labeled the last frontiers of unexplored spectral territory in astronomy (at least as far as atomic and molecular processes are concerned). Whether this is still true is perhaps debatable. For over a decade spectrometers using incoherent detection techniques have been skimming the spectral cream in the 50-160 μm wavelength region, and already heterodyne technology is well established at the longer submillimeter wavelengths where waveguide techniques are applicable.

Extending heterodyne observations to the more difficult shorter wavelengths requires a different technology. Mixers with open structures, free of the constraints of waveguide dimensioning and thereby manufacturable, are needed. Secondly, local oscillators with powers exceeding a few mW are required to drive the Schottky diode mixing elements. Only Schottkys have been demonstrated to work at frequencies >600 GHz, and only lasers are powerful enough to drive the Schottkys. Therefore, these two technologies - open structure mixers using Schottky diodes and laser local oscillators - form the basis for all current far infrared heterodyne receivers.

This summarized review of short submillimeter and far infrared heterodyne systems will be limited to a discussion of spectrometers using the above-mentioned technology. Receivers of this type are currently the only heterodyne systems doing real astronomy in the wavelength region of interest ($\lambda < 400 \mu\text{m}$). At the longer wavelengths ground-based systems are effective in the atmospheric windows at 450 and 350 μm , while airborne spectrometers are required for the shorter wavelengths ($\lambda < 300 \mu\text{m}$) obscured by water vapor in the atmosphere. Table 1 lists the groups currently active in the field.

Table 1 - Active Groups
Schottky Diode Mixers and Laser Local Oscillators

	Ground-based (MKO)	Airborne (KAO)
GSFC/Greenbelt	---	---
MPI/Bonn	370 μm (UH,IRTF)	370-186 μm
MPI/Garching	440,370 μm (UH,IRTF,JCMT)	---
UC/Berkeley	---	370-119 μm
UT/Austin	370 μm (CSO)	---

The instruments fielded by all these groups are functionally identical. The mixer is a Schottky diode, sometimes cooled to 77 K. The local oscillator (LO) is a fixed-frequency molecular-gas laser capable of oscillating at a frequency near the astronomical line of interest. The IF output signals from the mixer are amplified by a cooled HEMT amplifier whose center frequency is chosen to match the frequency difference between the laser and the astronomical line. Practical IF center frequencies range from 1 to 15 GHz. Doppler corrections are made by fine tuning the frequency of an RF oscillator which drives a second conversion mixer. Spectral processing of the down-converted data is done with filter banks or, more commonly now, an AOS backend. More detailed information regarding the specific characteristics of various instruments may be found in Refs. 1-3. The summary which follows is organized along instrumental lines: first the mixer, then the LO, the performance achievements, and finally some science examples.

2. FAR INFRARED MIXERS

2.1 Corner Reflector Design

The mixer mounts favored at short submillimeter and far infrared wavelengths are all variants of the corner reflector design. The advantage of this type of open structure resonator is that it is easily fabricated even for the shortest wavelengths and yet capable of main beam efficiencies exceeding 50%. (Mixer beam efficiencies are, of course, to be distinguished from telescope main beam efficiencies.) Although the corner reflector principle has been known since its introduction in the 1950's, it wasn't until the work of Kräutle *et al.* two decades later (Refs. 4,5) that the design was introduced to the submillimeter community and verified using laser local oscillators. Shortly thereafter the first astronomical results were achieved with a corner reflector mixer in a laser heterodyne spectrometer. Goldsmith *et al.* in a multi-institutional collaboration put together such a system and used it to detect the J=6-5 line of ^{12}CO in 1980 (Ref. 6). Since then only the corner reflector design has found general acceptance for short submillimeter and far infrared mixers, to the point that all groups active in the field depend on it exclusively. Extensions and refinements to the original design have been introduced by various groups (Refs. 2,3,7,8) but the basic principle remains unchanged.

Basically, a corner reflector mixer consists of a long-wire antenna (several wavelengths long) that is sharpened at the tip and contacted to the anode of a small Schottky diode. The radiation pattern of the long wire consists of multiple lobes, with the principal lobe inclined to the wire axis by the angle:

$$\theta_{pk} = \cos^{-1} \left[1 - 0.37101 \frac{\lambda}{L} \right], \quad (1)$$

where L is the length of the wire. A 90° corner reflector is positioned behind the antenna wire, and forms three images. The spacing s between the apex of the reflector and the antenna is adjusted to satisfy the resonance condition between the antenna wire and the images (Ref. 8):

$$s = \frac{\lambda}{2 \sin \theta_{pk}}. \quad (2)$$

Although most corner reflector mixers use a 4λ antenna and a spacing s of 1.2λ , other antenna lengths are also viable. Figure 1 shows the main beam efficiency of a 90° corner reflector mount as a function of the antenna length (with s adjusted for resonance). Obviously, the shorter lengths will have a lower sidelobe content and higher efficiencies. Grossman (Ref. 9) stresses this point and calculates that an antenna length of $\sim 1.4\lambda$ will be optimum for beam efficiency, given the other constraints of the mixer topology. The high beam divergence (35° FWHM) of such a short antenna, however, requires extra care in the design and fabrication of the coupling optics such that its use may not be practical. Zmuidzinas, Betz, and Boreiko (Ref. 8) take a different tack, and point out the advantages of longer antenna lengths. As shown in Figure 1 the incremental loss in coupling efficiency is rather small for $4\lambda < L < 20\lambda$. Longwire antenna lengths in the $10\text{--}20\lambda$ range are likely the best overall choice for mixers at the shortest wavelengths ($\lambda < 100\mu\text{m}$) for purely practical reasons. The slightly lower main beam efficiencies of these long antennas are more than offset by the increased ease in fabrication.

2.2 Schottky Diodes

The Schottky diodes used in submillimeter and far infrared mixers are GaAs devices with sub-micron anode diameters. The small anode size results in minimum device capaci-

shunt capacitance. All the research groups use diodes developed by the group of Crowe and Mattauch at the Semiconductor Device Laboratory of the University of Virginia (Refs. 10,11). It perhaps goes without saying that the field of submillimeter and far infrared heterodyne spectroscopy owes its existence to this group, which has reliably provided diodes of excellent quality, as it did in years past during the development of millimeter wave astronomy. The smallest devices (UVa type 1T6) have $0.45\mu\text{m}$ diameter anodes, shunt capacitances (C_p) of 0.4 fF , and series resistances (R_s) near $30\ \Omega$. The reactance of the shunt capacitance becomes a problem relative to the $\sim 100\ \Omega$ impedance of the mixer at frequencies above 2 THz . Although there is plenty of room for improvement, especially in the device series resistance R_s , these diodes yield adequate sensitivity in corner reflector mounts to permit a wide variety of astrophysical investigations. The best results at various frequencies are presented later in § 4.2.

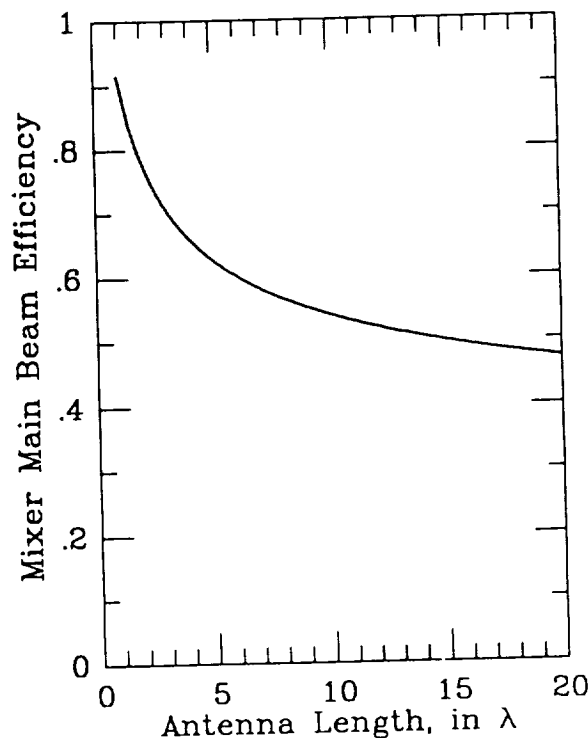


Figure 1: Fraction of power in the main beam of the mixer as a function of antenna length in wavelengths.

3. LASER LOCAL OSCILLATORS

3.1 Requirements

The power requirements of Schottky diodes dictate that the local oscillator (LO) be capable of power outputs exceeding a few mW. Only laser oscillators, specifically optically pumped molecular gas lasers, are compatible with the power requirements of Schottky mixers in the $600\text{--}3000\text{ GHz}$ frequency range of interest. This compatibility is indeed fortunate because lasers are in fact the *ONLY* oscillators available in the FIR.

Aside from adequate power, there are two other major requirements for the laser LO: (1) a frequency coincidence near the astronomical line of interest, and (2) a frequency stability of about 1 part in 10^6 so that profiles of lines as narrow as 0.3 km s^{-1} can be measured accurately. Molecular

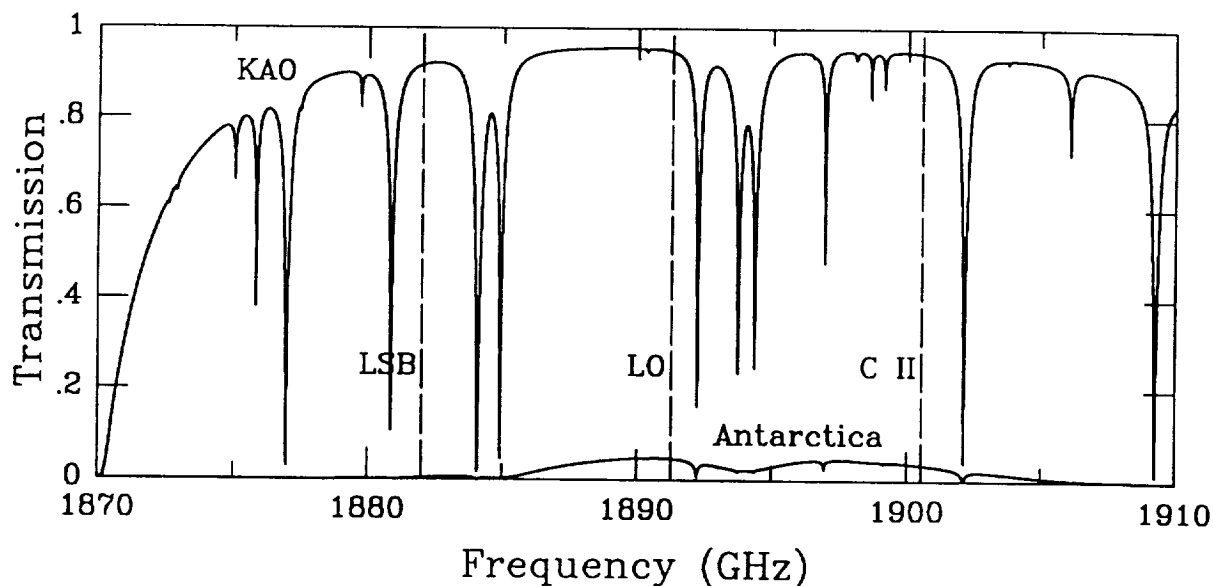


Figure 2: Model calculation of the atmospheric transmission at aircraft altitude (12.5 km) for the spectral region near the C II fine structure line. Line-of-sight water vapor is taken to be 10 μm precipitable. The C II line is in the upper sideband of the LO. Also plotted for comparison is the best transmission expected from a groundbased site: the Soviet Vostok station at 3.5 km altitude with 100 μm prec. H_2O in the line of sight.

gas lasers are fixed-frequency oscillators because they oscillate on the frequency of a molecular rotational transition. Hence, one must search a list of suitable laser lines to find a chance frequency coincidence with the astronomical line of interest. In practice this is usually a relatively simple thing to do, since the coincidence need only be as close as 15-20 GHz (the center frequency of the IF amplifier), and many hundred laser lines are available. Table 2 illustrates this point adequately well for a number of $^{12}\text{C}^{16}\text{O}$ transitions of interest. The second point is the frequency stability of the laser. The linewidths of optically pumped lasers can be exceedingly narrow. For most systems the principal perturber is the stability of the laser cavity, which is controlled by invar spacing rods. In practice, it is easy to maintain the laser frequency stable enough for LO applications in astronomy. The exact LO frequency can be measured with an accuracy exceeding 1 part in 10^9 relative to harmonics of microwave sources, or by beating frequencies with other laser lines which have been so referenced to microwave standards. Because the laser frequencies are molecular resonances, they are quite repeatable, and control circuitry such as the phase-lock systems used with tunable sources are not required. This inherent self-stability of the molecular gas laser frees the user from complexities such as a cumbersome chain of submillimeter harmonic multipliers that might prove difficult to manage at the telescope, especially at 3000 GHz.

One additional factor affecting the choice of LO frequency is the consideration of the image sideband transmission. For accurate calibration of line spectra when a continuum source such as the Moon or some other extraterrestrial object is used for intensity calibration, it is important to know the atmospheric transmissions of both the signal and the image sidebands. Remember that the spectrometer is a double-sideband (DSB) receiver. Ideally the transmissions in both sidebands would be equal (flat) over the spectrum. Figure 2 shows a favorable example: the atmospheric transmission at aircraft altitudes (12.5 km) in the region near the important C II fine-structure line at 1901 GHz. Obviously, for a slightly different LO frequency or large Doppler shift of the astronomical source, the transmission difference between sidebands could become quite large and

thereby introduce additional systematic errors in the intensity calibration of SSB spectra. Of course if the absolute atmospheric transmission in individual sidebands is known exactly, this caveat may be ignored. In practice, however, this is often not the case.

Table 2 - $^{12}\text{C}^{16}\text{O}$ Coincidences

CO Line	ν (GHz)	Laser Gas	I.F. (GHz)
7-6	806.652	$^{15}\text{NH}_3$	3.666
8-7	921.800	$\text{C}_2\text{H}_2\text{F}_2$	3.84
9-8	1036.912	CH_2F_2	-5.238
11-10	1267.014	CH_2F_2	-5.157
12-11	1381.995	CH_2F_2	-15.124
13-12	1496.923	CD_3OH	-11.986
14-13	1611.794	CH_2F_2	-14.809
17-16	1956.018	$^{15}\text{NH}_3$	-6.731
19-18	2185.135	CD_3OD	-3.794
22-21	2528.172	CH_3OH	5.391

3.2 Operation

In an optically pumped FIR laser, polar molecules in the ground vibrational (and thermally populated rotational) state are selectively excited to a rotational level in an upper (usually the first) vibrational state. This pumping process can lead to a population inversion between upper state rotational levels which in turn produces dipole radiation at the difference frequency between the rotational levels. By enclosing the gain medium in a resonant cavity, usually a variant of a Fabry-Perot cavity, a FIR laser is produced which is capable of emitting power levels exceeding tens of mW for the strongest lines. The pump source is usually a CO_2 laser operating on discrete lines in the $\lambda = 10 \mu\text{m}$ bands. The CW CO_2 laser is an effective "optical power supply" for the FIR lasing gas, but only when its pump frequency lies within a Doppler width of the absorbing vibrational transition.

There are obviously a number of parameters that determine the output frequency and power of the FIR laser. In general, the LO frequency increases in a discrete manner for lighter polar molecules and/or higher-J transitions. The FIR power goes up linearly with pump power for a saturated laser, but a nominal pump power of 10 W is needed for FIR power generation at the mW level. Given that the "wallplug" efficiency of the CO₂ laser itself is nominally only 10%, we see that the overall power efficiency of the FIR laser system is low, only 0.0001 at best. Although this inefficiency may hinder some balloon- and space-based applications, it is nevertheless not a problem for ground-based and airborne systems where adequate mains power is available. If one includes the isotopic variants of polar laser molecules, there are hundreds of species suitable for FIR laser applications, and hence a potentially large number of FIR laser lines. Nearly a thousand lines have already been catalogued with accurate frequency measurements (Ref. 12), and many of these are suitable for LO applications.

Typical lasers used in heterodyne receivers are about 1 m in length. This size, although perhaps large by the standards of solid state oscillators used at millimeter wavelengths, is also not a major drawback for spectrometer construction, because the optical beam paths in most FIR heterodyne receivers are of comparable length. Similarly, the HV power supply for the CO₂ pump laser is not the bulky problem it might have been 15-20 yrs ago. Modern HV supplies with up to 500 W output capability occupy only 13 cm of vertical space in a 48 cm relay rack and weigh less than 15 kg. More details on the use of FIR lasers as LOs in astronomical receivers may be found in the review of Chin (Ref. 13).

4. SENSITIVITY

4.1 Requirements

Whether or not a receiver technology is amenable to actual astronomical observations depends on two things: the expected signal strengths and the receiver noise level. Although receiver noise temperatures of 30,000 K, for example, may sound prohibitively high, one should first consider what sensitivity is needed to do useful science, and worry about the ultimate instrumental performance later. For observations of high-J CO in shocked gas, for example, we already knew from earlier Fabry-Perot work the expected signal strengths and upper limits to the line widths. As shown by Figure 3, $T_{\text{sys}} = 31,000$ K (SSB) works very well indeed at 2500 GHz. The strength of heterodyne spectroscopy is apparent. The sensitivity is comparable to that achievable with incoherent techniques (Refs. 14,15), but the achievable resolution is nearly two orders of magnitude higher. FIR line profiles can now be compared to those at millimeter wavelengths with the same high velocity scale resolution and accuracy.

4.2 Achievements

One way of making FIR noise temperatures look more respectable is to compare the current state-of-the-art to the inherent quantum noise level of a coherent receiver: $h\nu/k$. Figure 4 plots the best system noise temperatures of laser heterodyne spectrometers using Schottky diode mixers over the frequency range of 600-3000 GHz. The points are all results achieved in actual astronomical observations unless otherwise noted. The data points can surprisingly be fitted rather well by a straight line with $T_{\text{sys}} = 175$ $h\nu/k$. Although no special significance can be attributed to this empirically derived result, it nevertheless is somewhat interesting because it summarizes the results of three independent groups. On the other hand, perhaps it's not so surprising because all three groups use identical Schottky diodes.

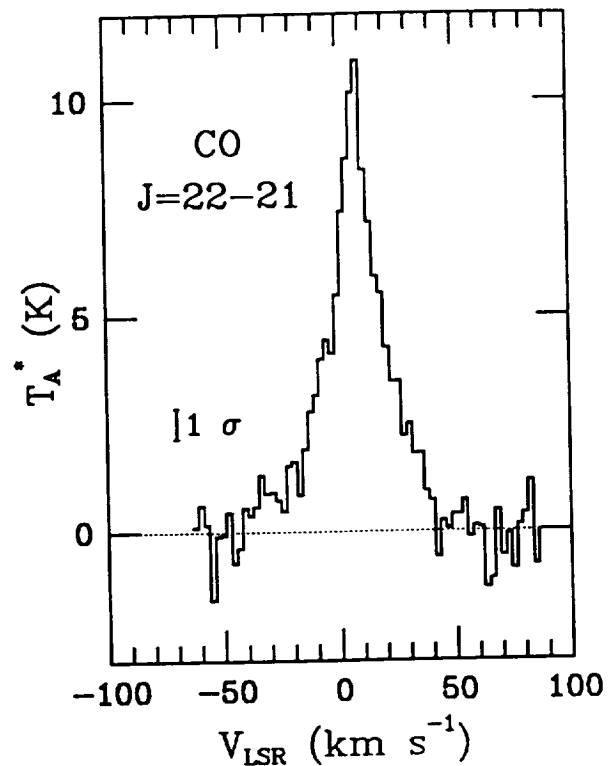


Figure 3: Spectrum of the J=22-21 line of CO in Orion obtained with $T_{\text{sys}} \sim 31,000$ K.

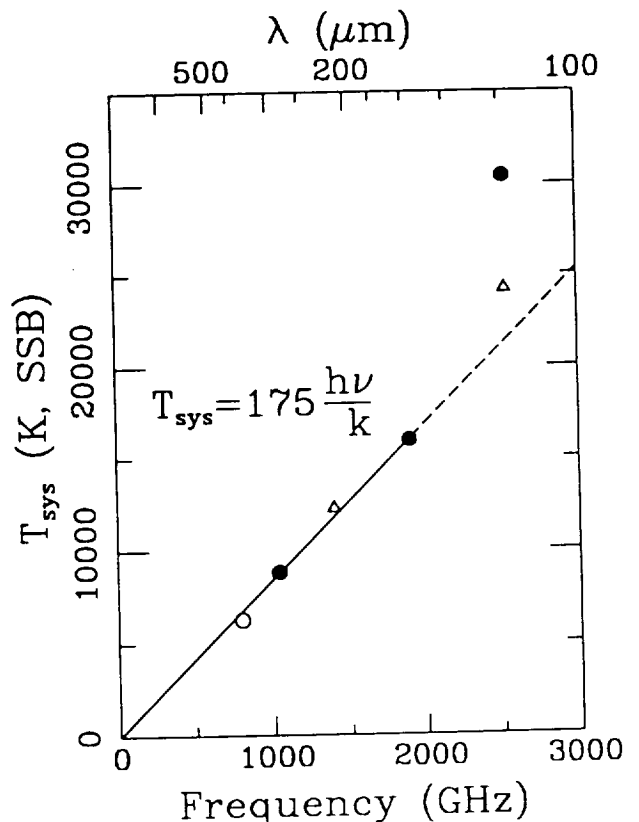


Figure 4. System noise temperature as a function of frequency. Circles represent measurements obtained during astronomical observations while triangles are laboratory data. Filled circles are from our own work aboard the KAO (Ref. 16,17), the open circle is from Ref. 18, and the trian-

The net "quantum efficiency" of existing laser heterodyne systems is on the order of 0.5% (=1/175), with half of the effective loss typically ascribed to optics losses and the fractional noise contribution of the IF amplifier, while the remainder is intrinsic to the mixer. We see that the 1% efficiency of the Schottky mixer leaves what appears to be large room for improvement compared to quantum noise level. Based on progress over the last 5 years, we estimate that over the next 5 years receiver noise temperatures with this technology will continue to come down, at the average rate of 15% per year.

5. FAR-INFRARED OBSERVATIONS

5.1 Published Results

Most observations with submm/FIR heterodyne receivers have concentrated on CO, for reasons much the same as those that make CO the "most favored species" at millimeter wavelengths. As shown in Table 3, the observations with the techniques discussed here span the range from J=6-5 at 625 GHz through J=22-21 at 2528 GHz. The J=6-5 and J=7-6 lines of ^{12}CO can be observed from the best mountaintop site (Mauna Kea), but all the others require a platform above the tropospheric water vapor - to date this means the KAO. Other detections include: HCN at 797 GHz (Ref. 20), CH_3OH at 802 GHz and SO_2 at 797 GHz (Ref. 21), CI at 809 GHz (Refs. 22-25), CII at 1901 GHz (Refs. 26-28), and OH at 2514 GHz (Ref. 29).

Table 3 - Laser Heterodyne Observations of CO

^{12}CO	Reference
J=6-5	[6,30]
J=7-6	[2,31-41]
J=9-8	[17]
J=12-11	[42]
J=14-13	[42]
J=17-16	[43]
J=22-21	[16]
^{13}CO	
J=6-5	[44]
J=9-8	[17]

Figure 3 shows an example of the highest frequency line yet detected with a Schottky-diode receiver: the J=22-21 ^{12}CO line at 2528 GHz. Although T_{sys} was 31,000 K (SSB), the line is well enough detected that profile fitting can be done for comparison with lower-J data (Ref. 16). The OH line at 2514 GHz was also detected at the 3.5 K level (T_A) in Orion with this receiver. Newer diodes made available by the UVa group since these observations were done in 1989 now improve sensitivities by 50% (see Fig. 4).

It is quite evident that the techniques of "radio astronomy" made possible by coherent detection have been extended over the entire submillimeter range ($300 < f < 1000$ GHz) and far into infrared territory ($f > 1000$ GHz). With only modest improvements in the technology of Schottky mixers (meaning that no dramatic breakthroughs are required), lines above 3000 GHz, particularly those of CO, are likely to become observable within the next few years. Of course, only the brightest sources such as Orion will be strong enough for detailed line profile analysis, but nevertheless a good deal of work can be done on the dynamics of shock-heated gas with sub- km s^{-1} velocity resolution. Perhaps even more interesting would be observations of the ground-state fine structure transition of neutral carbon at 4746 GHz

(63 μm), which might eventually be possible with the extra long antennas mentioned earlier.

5.2 Prognosis

In the near future most observations with Schottky receivers will undoubtedly focus on the 1000-2000 GHz region where unique results can be obtained without fear of competition from SIS at the low end or Fabry-Perot spectrometers at the high end. This is not meant to imply that uniqueness necessarily equates with good science, but that within the 1000-2000 GHz band, Schottky receivers will likely provide the only observational capability for the next 5 years or until fundamental breakthroughs occur in the competing technologies. All of this work, of course, depends on the existence of an accessible airborne platform for instrumental and observational tests. NASA's Stratospheric Observatory for Infrared Astronomy (SOFIA), an envisioned 2.5 m telescope in a 747-type aircraft, would be a critically important facility for the development of FIR heterodyne spectroscopy. As the planned successor to the extremely successful Kuiper Airborne Observatory (KAO), SOFIA (Ref. 45) would give FIR spectroscopy the spatial resolution $< 10''$ needed to make the critical observations of the dense cores of molecular clouds. Whether far infrared heterodyne technology ever makes it to space, or deserves to be considered, depends on technical advances that must be demonstrated in the next five years.

This work has been supported in part by the NASA under grant NAG 2-254 and the California Space Institute under grant CS 10-88.

7. REFERENCES

1. Betz, A. L. and Zmuidzinas, J., *Airborne Astronomy Symposium*, NASA CP 2353, 320-329 (1984).
2. Roeser, H. P., Wattenbach, R., Durwen, E. J., and Schultz, G. V., *A. A.*, 165, 287-299 (1986).
3. Harris, A. I., Jaffe, D. T., Stutzki, J., and Genzel, R., *Int. J. Infrared Millimeter Waves*, 8, 857-883 (1987).
4. Kräutle, H., Sauter, E., and Schultz, G. V., *Infrared Phys.*, 17, 477-483 (1977).
5. Kräutle, H., Sauter, E., and Schultz, G. V., *Infrared Phys.*, 18, 705-712 (1978).
6. Goldsmith, P. F., Erickson, N. R., Fetterman, H. R., Clifton, B. J., Peck, D. D., Tannenwald, P. E., Koepf, G. A., Buhl, D., and McAvoy, N., *Ap. J. (Letters)*, 243, L79-L82 (1981).
7. Fetterman, H. R., Tannenwald, P. E., Clifton, B. J., Parker, C. D., Fitzgerald, W. D., and Erickson, N. R., *Appl. Phys. Lett.*, 33, 151-154 (1978).
8. Zmuidzinas, J., Betz, A. L., and Boreiko, R. T., *Infrared Phys.*, 29, 119-131 (1989).
9. Grossman, E. N., *Infrared Phys.*, 29, 875-885 (1989).
10. Mattauch, R. J., and Crowe, T. W., *Int. J. Infrared Millimeter Waves*, 8, 1235-1242 (1987).
11. Crowe, T. W., *Int. J. Infrared Millimeter Waves*, 10, 765-777 (1989).
12. Inguscio, M., Moruzzi, G., Evenson, K. M., and Jennings, D. A., *J. Appl. Phys.*, 60, R161-R192 (1986).
13. Chin, G., *Int. J. Infrared Millimeter Waves*, 8, 1219-1234 (1987).
14. Harris, A. I., these proceedings.
15. Poglitsch, A., these proceedings.

16. Boreiko, R. T. and Betz, A. L., *Ap. J. (Letters)*, 346, L97-L100 (1989).
17. Boreiko, R. T. and Betz, A. L., submitted to *Ap. J.* (1990).
18. Harris, A. I., Stutzki, J., Graf, U. U., and Genzel, R., *Int. J. Infrared Millimeter Waves*, (Nov. 1989).
19. Titz, R. U., Röser, H. P., Schwaab, G. W., Neilson, H. J., Wood, P. A., Crowe, T. W., Peatman, W. C. B., Prince, J., Deaver, B. S., Alius, H., and Dodel, G., *Int. J. Infrared Millimeter Waves*, 11, (1990).
20. Stutzki, J., Genzel, R., Harris, A. I., Herman, J., and Jaffe, D. T., *Ap. J. (Letters)*, 330, L125-L129 (1988).
21. Stutzki, J., Genzel, R., Graf, U. U., Harris, A. I., and Jaffe, D. T., *Ap. J. (Letters)*, 340, L37-L40 (1989).
22. Jaffe, D. T., Harris, A. I., Silber, M., Genzel, R., and Betz, A. L., *Ap. J. (Letters)*, 290, L59-L62 (1985).
23. Zmuidzinis, J., Betz, A. L., and Goldhaber, D. M., *Ap. J. (Letters)*, 307, L75-L79 (1986).
24. Zmuidzinis, J., Betz, A. L., Boreiko, R. T., and Goldhaber, D. M., *Ap. J.*, 335, 774-785 (1988).
25. Genzel, R., Harris, A. I., Jaffe, D. T., and Stutzki, J., *Ap. J.*, 332, 1049-1057 (1988).
26. Boreiko, R. T., Betz, A. L., and Zmuidzinis, J., *Ap. J. (Letters)*, 325, L47-L51 (1988).
27. Betz, A. L., Boreiko, R. T., and Zmuidzinis, J., in *Submillimeter Astronomy*, G. D. Watt and A. S. Webster (eds.), 117-121 (1990).
28. Boreiko, R. T., Betz, A. L., and Zmuidzinis, J., *Ap. J.*, 353, 181-192 (1990).
29. Betz, A. L., and Boreiko, R. T., *Ap. J. (Letters)*, 346, L101-L104 (1989).
30. Koepf, G. A., Buhl, D., Chin, G., Peck, D. D., Fetterman, H. R., Clifton, B. J., and Tannenwald, P. E., *Ap. J.*, 260, 584-589 (1982).
31. Harris, A. I., Jaffe, D. T., Silber, M., and Genzel, R., *Ap. J. (Letters)*, 294, L93-L97 (1985).
32. Schultz, G. V., Durwen, E. J., Röser, H. P., Sherwood, W. A., and Wattenbach, R., *Ap. J. (Letters)*, 291, L59-L61 (1985).
33. Harris, A. I., Stutzki, J., Genzel, R., Lugten, J. B., Stacey, G. J., and Jaffe, D. T., *Ap. J. (Letters)*, 322, L49-L54 (1987).
34. Jaffe, D. T., Harris, A. I., and Genzel, R., *Ap. J.*, 316, 231-242 (1987).
35. Roeser, H. P., Schaefer, F., Schmid-Burgk, J., Schultz, G. V., van der Wal, P., and Wattenbach, R., *Int. J. Infrared Millimeter Waves*, 8, 1541-1556 (1987).
36. Stutzki, J., Stacey, G. J., Genzel, R., Harris, A. I., Jaffe, D. T., and Lugten, J. B., *Ap. J.*, 332, 379-399 (1988).
37. Wattenbach, R., Krügel, E., Röser, H. P., Nett, H., Schwaab, G., and Densing, R., *A. A.*, 202, 133-135 (1988).
38. Jaffe, D. T., Genzel, R., Harris, A. I., Lugten, J. B., Stacey, G. J., and Stutzki, J., *Ap. J.*, 344, 265-276 (1989).
39. Krügel, E., Densing, R., Nett, H., Röser, H. P., Schäfer, F., Schmid-Burgk, J., Schwaab, G., van der Wal, P., and Wattenbach, R., *A. A.*, 211, 419-427 (1989).
40. Schmid-Burgk, J., Densing, R., Krügel, E., Nett, H., Röser, H. P., Schäfer, F., Schwaab, G., van der Wal, P., and Wattenbach, R., *A. A.*, 215, 150-164 (1989).
41. Jaffe, D. T., Genzel, R., Harris, A. I., Howe, J. E., Stacey, G. J., and Stutzki, J., *Ap. J.*, 353, 193-199 (1990).
42. Schwaab, G. W., these proceedings.
43. Boreiko, R. T., Betz, A. L., and Zmuidzinis, J., *Ap. J.*, 337, 332-341 (1989).
44. Graf, U. U., Genzel, R., Harris, A. I., Hills, R. E., Russell, A. P. G., and Stutzki, J., *Ap. J. (Letters)*, 358, L49-L52 (1990).
45. Hildebrand, R., these proceedings.

Discussion - Paper V.2.

Q - J.M. LAMARRE : Do you think possible to use sub-mm lasers in space as local oscillators ?

A - A. BETZ : From a strictly technical viewpoint, a heterodyne spectrometer of the type described here could be space qualified. The far-infrared laser itself is not a problem. The CO₂ pump laser, however, has a power requirement of 300 W, which may exceed the power budget for an orbital system. Given the fixed frequency nature of the laser LO, a space-based spectrometer should concentrate on observing only the most important lines (most likely CII at 158 μm and OI at 63 μm).

OBSERVATIONS OF ^{12}CO and ^{13}CO $J = 9-8$ IN GALACTIC MOLECULAR CLOUDS

R. T. BOREIKO AND A. L. BETZ

Space Sciences Laboratory, University of California, Berkeley, CA 94720

Received 1990 April 30; accepted 1990 August 23

ABSTRACT

We have observed the ^{12}CO and ^{13}CO $J = 9-8$ transitions at a spectral resolution of 1.5 km s^{-1} in four Galactic molecular clouds: W3, DR 21, W51, and M17. The line shapes are generally similar to those of low- J CO lines for each species, with the exception that line reversals produced by less excited foreground gas are not evident. The ratio of ^{12}CO and ^{13}CO intensities shows that for all sources the $J = 9-8$ ^{12}CO line is optically thick with $\tau \sim 5-20$. This high optical depth requires a significant amount of dense ($n_{\text{H}_2} > 10^5 \text{ cm}^{-3}$) gas. The peak brightness temperature of the ^{12}CO $J = 9-8$ line is similar to or less than the dust temperature for all sources, and most of the detected $J = 9-8$ radiation appears to originate in the cool ($T \sim 50 \text{ K}$) molecular gas which comprises the bulk of the clouds. Non-LTE modeling suggests that the gas giving rise to the $J = 9-8$ radiation is clumped on a scale smaller than our $80''$ beam, and that part of the radiation arises from a warmer ($T \geq 100 \text{ K}$) component which is very beam diluted. We do not detect the large amount of hot ($T \sim 200-500 \text{ K}$), spatially extended gas that has been inferred from previous observations of the ^{12}CO $J = 7-6$ line. In addition to a narrow component, the ^{12}CO $J = 9-8$ line shows evidence for a broad emission component ($\Delta V \sim 18 \text{ km s}^{-1}$) in W51 and possibly DR 21. The temperatures and densities of the regions emitting the broader emission appear similar to those producing the dominant quiescent line component in both sources. This suggests that the phenomenon producing the greater velocity dispersion does not significantly heat the molecular material.

Subject headings: infrared: spectra — interstellar: molecules — nebulae: abundances — nebulae: structure

1. INTRODUCTION

The onset of star formation within dense molecular clouds generates a large amount of UV radiation which ionizes the surrounding material, producing an H II region. The boundary of this ionized region forms at the penetration limit of FUV radiation ($E > 13.6 \text{ eV}$), beyond which lies a transition zone from a photodissociation region (PDR) back to the more quiescent conditions prevailing in the parent molecular cloud. The photodissociation region can be studied through far-infrared fine-structure lines of C II and O I which are easily excited under the conditions ascribed to the PDR and hence important for the cooling of the gas. Farther from the star and the PDR, line radiation from molecules, most notably CO which is both abundant and strongly bound, is a significant coolant.

The millimeter rotational transitions of CO have been used as tracers of molecular material in interstellar clouds for over two decades. CO is particularly useful because a number of rotational levels are energetically accessible at the temperatures characteristic of molecular clouds, and also because it is sufficiently abundant that several isotopic variants can be observed. More recently, studies of CO have been extended to the submillimeter and far-infrared spectral regions where, because of higher excitation and critical density requirements, the high- J transitions selectively probe hotter and more dense gas. Multitransitional studies over many rotational levels offer the prospect of examining a wide range of conditions within photodissociated or shock-heated gas. For example, high spectral resolution observations of CO in the IRC2 neighborhood of Orion over the range $J = 1-0$ to $J = 22-21$ have clearly shown the effect of shocks for heating and accelerating the gas. For most other sources, high-resolution data have heretofore only been available up to $J = 7-6$ and, for ^{13}CO , only up to $J = 2-1$. Of particular note are the ^{12}CO $J = 7-6$ data, which

have been interpreted as showing the presence of large amounts of optically thin and hot ($T > 100 \text{ K}$) gas, presumably associated with areas of star formation within the regions observed.

In order to further characterize the physical conditions of this gas, we have obtained high-resolution spectra of the ^{12}CO $J = 9-8$ transition in five Galactic molecular clouds which have previously been observed in the $J = 7-6$ transition: W3, DR 21, W51, M17, and W49. In addition, we have observed the ^{13}CO $J = 9-8$ transition in all sources but W49, with the intent of deriving either the isotopic ratio for the warm gas in the case of optically thin radiation, or conversely the optical depth for the ^{12}CO $J = 9-8$ line for an assumed isotopic ratio. Observing transitions with very similar excitation and critical density in both isotopes ensures that the ratio will be insensitive to excitation provided that the emission for both lines comes from the same region. Detailed comparisons of the line profiles from the two isotopes should allow us to examine that assumption.

The $J = 9$ level lies approximately 250 K above the ground, and thus is not efficiently populated at the temperatures ($T < 50 \text{ K}$) characteristic of the bulk of molecular clouds. Given adequate excitation, the $J = 9-8$ line should be more sensitive to the presence of hot ($T > 100 \text{ K}$) gas than the $J = 7-6$ transition. The complementary observation of the ^{13}CO $J = 9-8$ line at the same locations provides significant additional information on the physical conditions within the emitting region.

2. INSTRUMENTATION AND CALIBRATION

The data were obtained using a far-infrared heterodyne spectrometer (Betz & Zmuidzinas 1984). The local oscillator (LO) was an optically pumped laser and the mixer was a GaAs Schottky diode (University of Virginia types 1T2 and 1T6 for the ^{12}CO and ^{13}CO observations, respectively). The corner

reflector mixer mount (Zmuidzinas, Betz, & Boreiko 1989) was cooled to 77 K. The system noise temperature was measured during flight to be 9000 K (SSB). The IF signals were analyzed in two parallel filter banks, the first with 5 MHz (1.5 km s^{-1}) resolution spanning a bandwidth of 200 MHz (60 km s^{-1}), and the second with 1.2 MHz (0.4 km s^{-1}) resolution covering the central 18 km s^{-1} of the spectrum.

The LO for the $^{12}\text{CO } J = 9-8$ line at 1036.9124 GHz (Nolt et al. 1987) was the 1042.1504 GHz transition of a CH_2F_2 laser (Petersen, Scalabrin, & Evenson 1980), while for the $^{13}\text{CO } J = 9-8$ line, the LO was the 997.7254 GHz line of CH_2F_2 (Golby, Cross & Knight 1986). We measured the frequency difference between the $^{13}\text{CO } J = 9-8$ line and the LO by detecting the line in absorption from a sample cell against a blackbody source. The measured frequency for the $^{13}\text{CO } J = 9-8$ line is 991.330 ± 0.001 GHz. We also measured the difference frequency between the $^{12}\text{CO } J = 9-8$ line and its LO to determine the accuracy with which the laser could be set to its central frequency. The combined uncertainties in the CO and LO frequencies establish our velocity scale accuracy ($\pm 1 \sigma$) as $\pm 0.3 \text{ km s}^{-1}$ for ^{12}CO and $\pm 0.4 \text{ km s}^{-1}$ for ^{13}CO .

From ground level the Earth's atmosphere is completely opaque near 1000 GHz because of absorption primarily from tropospheric water vapor. Therefore the instrument was flown aboard the Kuiper Airborne Observatory (KAO) at an altitude of 12.5 km where the residual atmospheric absorption is greatly reduced. The transmission near the ^{12}CO line frequency is better than 95% at aircraft altitude for normal atmospheric conditions. However, the $^{13}\text{CO } J = 9-8$ line falls on the wing of a strong H_2O line so that the transmission is only $\sim 60\%$ as determined from an atmospheric model and supported by comparison of the lunar spectra at the ^{12}CO and ^{13}CO frequencies. In addition, calibration spectra of the Moon show a weak absorption line at the 10% of continuum level from atmospheric ^{12}CO . Affected source spectra (those with low Doppler shift) have been corrected for this atmospheric feature, which is very narrow ($< 0.8 \text{ km s}^{-1}$ FWZM).

Absolute calibration is based on spectra of the Moon at the subsolar point, for which a temperature of 394 K and emissivity of 0.98 are assumed (Linsky 1973). This primary calibration was maintained by frequent observation of a blackbody source which served as a secondary standard. Conversion from double-sideband to single-sideband was calculated from the transmissions of the atmosphere and anti-reflection-coated pressure window in both sidebands. The net calibration uncertainty for the $^{12}\text{CO } J = 9-8$ line is estimated to be 10% while that for the $^{13}\text{CO } J = 9-8$ line is $\sim 20\%$ because of the poorer atmospheric transmission. These estimates include all sources of systematic uncertainty apart from the unknown coupling of the source to our beam.

The diffraction-limited beam size is $80''$ and $83''$ (FWHM) for the ^{12}CO and ^{13}CO observations, respectively. Pointing accuracy is estimated to be $15''$, and the telescope coupling efficiency is ~ 0.6 . This efficiency is the fractional coupling of the receiver's radiation pattern (essentially a Gaussian) to the sky. The independent determination of the coupling factor is not relevant to the calibration procedure since its value is identical for the primary calibrator (the Moon) and the observed sources. Signal strengths are quoted as corrected antenna temperatures, T_A^* (Kutner & Ulich 1981). The sky chopping frequency was 2 Hz with an amplitude of $9'$ oriented perpendicular to the major axis of each source as delineated by CO. This amplitude is sufficiently large that no emission should be present in the off-source beams.

3. OBSERVATIONS AND ANALYSIS

Our observations of ^{12}CO and $^{13}\text{CO } J = 9-8$ were obtained on 1989 August 17 and August 19. We observed one or two positions in each of the giant molecular clouds W3, DR 21, W51, M17, and W49 in ^{12}CO on the first night. The ^{13}CO observations were limited by the expected low signal as well as the lower atmospheric transmission. For each source, only the position showing the strongest $^{12}\text{CO } J = 9-8$ line was observed in ^{13}CO , with the exception of W49 which was not observed.

Each spectrum was fitted by a continuum plus a single Gaussian, or two Gaussians if a satisfactory (i.e., within statistical uncertainty) fit could not be obtained with only one. The parameters derived from the fits are shown in Table 1. The integrated intensity was obtained by direct integration of the spectra.

As part of the analysis of the ^{12}CO and $^{13}\text{CO } J = 9-8$ data, we have calculated single-component large velocity gradient (LVG) models in the plane-parallel geometry (Scoville & Solomon 1974). Level populations for J up to 15 were calculated using the principle of detailed balance. Collisional cross sections for CO and H_2 were obtained from Flower & Launay (1985) assuming a 3:1 ratio of ortho to para H_2 and were all scaled by a factor of 0.7 to bring the rates into agreement with recent pressure-broadening measurements (Mannucci 1989). Only line radiation was included in the calculations. While this model is clearly an oversimplification of the real situation both in terms of geometry and radiation transfer, it serves to show the most important physical processes contributing to the observed radiation. In the absence of more detailed knowledge of the source kinematics and morphology, the additional complexity entailed in constructing a more realistic model is unwarranted.

For most sources, the optically thick low- J ^{12}CO lines establish the kinetic temperature for the model, and the ^{13}CO data determine both the number density of H_2 and the ^{13}CO column density. Column densities for ^{12}CO are derived using an adopted $^{12}\text{CO}/^{13}\text{CO}$ isotopic ratio of 50. The results are somewhat insensitive to the adopted ratio because for the sources considered all the ^{12}CO lines with $J < 6$ are optically thick. Thus there are only three free parameters in the model: kinetic temperature, H_2 number density, and ^{13}CO column density. In those cases where the simple single-component model discussed above fails to describe the data adequately, other parameters such as beam-filling factor or additional components are added. The relevant modifications, along with all the available CO data, are now discussed for each source individually.

3.1. W3

The W3 core is a region of bright CO emission within a giant molecular cloud. The core itself has an E-W elongation containing two condensations: one associated with IRS 5 and the other $\sim 20''$ S of IRS 4 (Jaffe et al. 1983). The velocity structure of the region is complex, showing both a large-scale E-W gradient and localized N-S gradients near the two condensations. In addition to the two distinct components within the core, there is colder foreground material, probably physically associated with the IRS 5 condensation, which manifests itself through the self-reversals seen in the optically thick low- J ^{12}CO lines.

We observed the ^{12}CO and $^{13}\text{CO } J = 9-8$ lines at W3 IRS 5, and also obtained a spectrum of the $^{12}\text{CO } J = 9-8$ line at W3(OH), $17''$ SE of IRS 5. This latter position is within the

TABLE 1
OBSERVED CO $J = 9-8$ LINE PARAMETERS^a

Position	T_A^{*b} (K)	T_b^c (K)	V_{LSR} (km s^{-1})	Line width (km s^{-1} , FWHM)	Continuum ^d (K)	Integrated Intensity ($\text{ergs s}^{-1} \text{cm}^{-2} \text{sr}^{-1}, \times 10^{-4}$)
¹² CO						
W3 IRS 5	14.0(0.4)	32.8(0.5)	-38.45(0.09)	7.3(0.2)	0.21(0.06)	1.28(0.03)
W3(OH)	4.0(0.4)	19.2(0.6)	-49.81(0.22)	4.2(0.6)	0.15(0.07)	0.20(0.06)
M17(-60, -30)	17.2(0.3)	36.6(0.4)	20.52(0.05)	6.2(0.1)	0.57(0.07)	1.27(0.05)
M17(-100, 0)	18.1(0.3)	37.7(0.4)	20.79(0.05)	7.4(0.2)	0.51(0.08)	1.63(0.04)
W51 Main	{ 4.6(0.6)	20.2(1.0)	61.39(0.18)	6.6(0.7)	0.64(0.09)	1.51(0.04)
	{ 5.7(0.5)	21.9(0.8)	59.11(0.46)	18.2(1.3)		
W51 IRS 2	6.2(0.2)	22.6(0.3)	60.77(0.09)	9.1(0.3)	0.58(0.05)	0.72(0.04)
DR 21 (H II)	7.3(0.2)	24.2(0.3)	-1.37(0.21)	15.7(0.6)	0.38(0.08)	1.40(0.05)
DR 21 (H ₂ peak)	2.3(0.3)	16.0(1.3)	-2.5(1.1)	15.7(2.5)	0.0(0.1)	0.43(0.08)
W 49	{ 5.0(0.2)	20.8(0.3)	3.03(0.23)	7.5(0.5)	0.63(0.05)	1.17(0.04)
	{ 5.2(0.2)	21.2(0.2)	12.35(0.23)	8.7(0.7)		
¹³ CO						
W3 IRS 5	2.4(0.3)	15.7(0.6)	-38.2(0.4)	5.7(1.0)	0.18(0.03)	0.14(0.03)
M17(-100, 0)	1.9(0.4)	14.6(1.0)	21.3(0.8)	6.7(1.9)	0.52(0.04)	0.12(0.04)
W51 Main	1.6(0.2)	13.9(0.5)	60.7(0.6)	11.7(1.9)	0.45(0.04)	0.23(0.04)
DR 21 (H II)	{ 2.6(0.3)	16.1(0.6)	-4.4(0.4)	8.5(1.1)	0.11(0.05)	0.27(0.06)
	{ 0.8(0.3)	11.6(1.1)	9.0(1.2)	6.6(3.3)		

- ^a Values in parentheses represent 1σ statistical uncertainties.
- ^b Corrected for the continuum.
- ^c Brightness temperature.
- ^d SSB value.

cooler molecular cloud, away from the region of foreground absorption. The spectra at the IRS 5 position are shown in Figure 1, and the parameters deduced from Gaussian fits to the

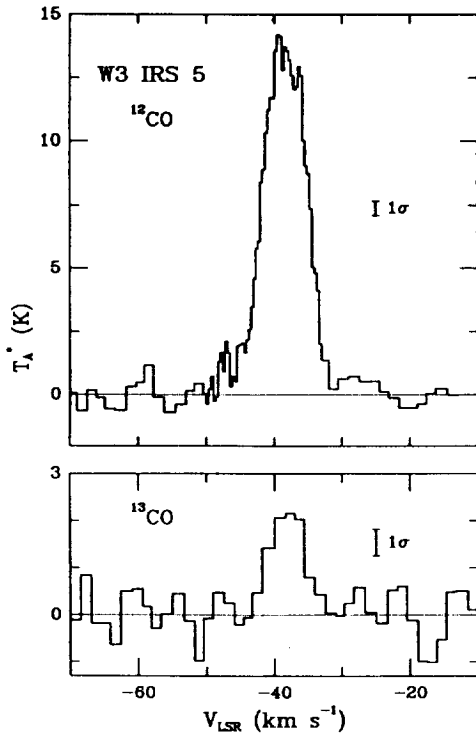


FIG. 1.—Spectra of ¹²CO and ¹³CO $J = 9-8$ at W3 IRS 5. The ¹²CO spectrum is a composite from the two filter banks, with the central section at higher resolution than the edges. The 1σ error bars represent statistical uncertainty for the higher resolution data. Integration times were 28 minutes and 54 minutes for the ¹²CO and ¹³CO data, respectively. The continuum has been subtracted from both spectra.

data are given in Table 1. Both the $J = 9-8$ spectra at IRS 5 are well represented by a single Gaussian centered near a V_{LSR} of -38.5 km s^{-1} which corresponds to the velocity of the IRS 5 condensation. There is no apparent contribution from gas associated with the IRS 4 condensation which is characterized by a V_{LSR} of -43 km s^{-1} . This is somewhat surprising since some of this gas is certainly within our $80''$ beam, and all previous CO observations with equivalent beam sizes, up to the ¹²CO $J = 7-6$ data of Krügel et al. (1989), show more complex line profiles attributable to the additional contribution from this component. The absence of the IRS 4 component in the $J = 9-8$ data suggests that it is cooler or less dense than the IRS 5 component.

Figure 2 shows the available ¹³CO data for all J values obtained at IRS 5 with beam sizes comparable to ours. The inset shows the ¹³CO $J = 1-0$ spectra obtained with a $17''$ beam centered individually on the condensations near IRS 4 and IRS 5 (Hayashi, Kobayashi, & Hasegawa 1989). These spectra clearly show that the two velocity components are intrinsically separate spatially. Fortunately, the small intrinsic line widths of the two components ($\sim 5 \text{ km s}^{-1}$ as deduced from the high spatial resolution data) relative to their 4.5 km s^{-1} velocity separation allow the distinct contributions to the combined line profile to be identified in the larger beam observations.

The -39 km s^{-1} component at IRS 5 is extended at least over $1'$ as shown by the agreement in the T_A^* values for the $17''$ and $66''$ ¹³CO $J = 1-0$ data shown in Figure 2. Therefore beam dilution is unlikely to complicate the interpretation of the data. Although the $J = 1-0$ and $J = 2-1$ ¹³CO lines have similar T_A^* values, they are not likely to be optically thick since the ¹²CO $J = 1-0$ and $J = 2-1$ data show higher T_A^* values even in the most self-absorbed parts of the line (Loren et al. 1981). No single-component model can simultaneously reproduce the measured ¹³CO intensities for the three observed ¹³CO lines. Therefore, assuming that all calibrations are correct, it is likely

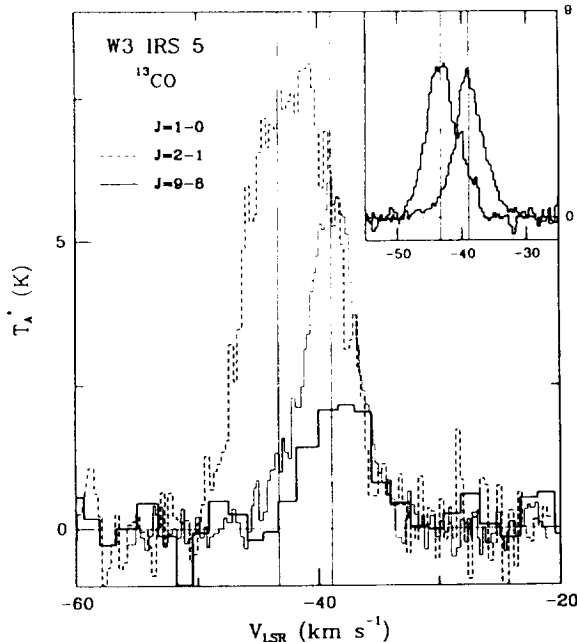


FIG. 2.—Spectra of ^{13}CO at W3 IRS 5 for various J . The vertical lines at -38.8 km s^{-1} and -43.3 km s^{-1} correspond to the approximate velocities of the IRS 5 and IRS 4 condensations, respectively. Beam sizes are $66''$ ($J = 1-0$, Thronson, Lada, & Hewagama 1985), $72''$ ($J = 2-1$, Loren et al. 1981), and $83''$ ($J = 9-8$, this work). The inset shows the $^{13}\text{CO } J = 1-0$ spectra of Hayashi et al. (1989) obtained with a $17''$ beam at the condensations near IRS 4 (left spectrum) and IRS 5 (right spectrum). The continuum has been subtracted from all data.

that at least two different components of gas contribute to the ^{13}CO radiation.

Spectra of $^{12}\text{CO } J = 1-0$ and $2-1$ (Loren et al. 1981) and $3-2$ (Phillips et al. 1988) show deep self-reversals centered near the V_{LSR} of the IRS 5 component. The residual T_A^* values at the center of the absorption dip give an upper limit to the kinetic temperature of the foreground gas of $\sim 17 \text{ K}$ provided that the gas is sufficiently dense to be thermalized in these levels. Consequently, the observed $^{13}\text{CO } J = 9-8$ line must come from the warmer background material and be unaffected by the cold foreground gas.

Interpretation of the ^{12}CO data at W3 IRS 5 is hampered by the significant absorption in the low- J lines. All we can say is that Gaussian reconstruction of the line profiles (a hazardous procedure in the case of several velocity components as in this case) shows that the low- J data are consistent with an optically thick -39 km s^{-1} component at $T_k = 50 \text{ K}$ attenuated by an optically thick foreground cloud at -38 km s^{-1} with $T_k \sim 17 \text{ K}$. The $J = 7-6$ data of Krügel et al. (1989) show the -39 km s^{-1} component as becoming optically thin or somewhat subthermally excited at $T_k = 50 \text{ K}$, and the $J = 9-8$ data continue that trend. Given the uncertainties in the interpretation of the low- J data, we did not construct a detailed model for the CO emission.

Qualitatively, the ratio of peak $^{12}\text{CO}/^{13}\text{CO } J = 9-8$ T_A^* values of 6, together with the low value of T_A^* for the $^{12}\text{CO } J = 9-8$ line relative to that expected from gas in LTE at 50 K (14 K vs. 29 K), suggest that the $^{12}\text{CO } J = 9-8$ line is optically thick but subthermally excited in gas with $n_{\text{H}_2} \leq 4 \times 10^4 \text{ cm}^{-3}$. However, at this low density the ^{13}CO would require a high column density and $\tau \sim 0.5$ to produce the observed emission. As a result, the $^{12}\text{CO } J = 9-8$ line should be so optically

thick that it would be maintained close to LTE by radiation alone. The result is that if gas at $T_k \sim 50 \text{ K}$ uniformly fills our beam, there is no combination of number density and column density for an isotopic ratio greater than 10 which can produce both the ^{12}CO and $^{13}\text{CO } J = 9-8$ lines as observed.

The most likely solution to this apparent discrepancy is an intrinsically clumpy structure for the molecular cloud such that regions with densities large enough to approximately thermalize the $J = 9$ level produce most of the $^{13}\text{CO } J = 9-8$ radiation while filling only a small part of our beam. Somewhat less dense gas filling more of the beam then produces the observed $^{12}\text{CO } J = 9-8$ line. Such a two-component model is discussed in more detail later for M17, a source in which interpretation is more straightforward. The results of the M17 model can be qualitatively applied to W3 to indicate that the two components can indeed give rise to the observed T_A^* values, provided that the additional complication from the colder foreground material is taken into account.

The $^{12}\text{CO } J = 9-8$ spectrum at W3(OH), whose parameters are presented in Table 1, is also adequately represented as a single Gaussian component. However, it is centered near -50 km s^{-1} V_{LSR} and is much less intense than the ^{12}CO line at IRS 5. Previous observations of ^{12}CO and $^{13}\text{CO } J = 1-0$ with a $70''$ beam (Dickel et al. 1980) show that the $^{12}\text{CO } J = 1-0$ line is likely to be optically thick at $T \sim 20 \text{ K}$. However, the column density determined from the observed $^{13}\text{CO } J = 1-0$ intensity is insufficient by more than an order of magnitude to produce the observed $^{12}\text{CO } J = 9-8$ line intensity if the excitation temperature is only 20 K . Therefore at W3(OH) there must be a component of gas warmer than that which produces the low- J radiation. Further observations are required to investigate this hypothesis.

3.2. DR 21

DR 21 consists of four compact H II regions located within a $\sim 20''$ diameter region embedded in a dense molecular cloud. Emissions from various molecules show two distinct velocity components: near -3 km s^{-1} and 9 km s^{-1} (Dickel, Dickel, & Wilson 1978). The spatial distributions of gas characterized by these two velocities are quite different, with the 9 km s^{-1} component most intense near W75 N, north of DR 21, while the -3 km s^{-1} component appears associated with the H II regions. Low- J CO lines show extended wing emission characteristic of an outflow, and H_2 vibrational lines have also been detected (Garden et al. 1986). The CO line shapes are often complex, with a central reversal which has been attributed to dense, cold foreground gas (Jaffe et al. 1989). Thus there are at least four distinct gas components within the region (the outflow, a foreground absorber, and two molecular clouds with different velocities), rendering the interpretation of line profiles a difficult task.

We observed the $^{12}\text{CO } J = 9-8$ and $^{13}\text{CO } J = 9-8$ lines toward the embedded H II region in DR 21. The $^{12}\text{CO } J = 9-8$ line was also observed toward the western peak of vibrational H_2 emission. We estimate that the systematic uncertainty in the ^{12}CO data is 20% (twice our usual estimate) because of the presence of occasional clouds above 12.5 km altitude. The spectra toward the H II region DR 21 are given in Figure 3, and the parameters deduced from Gaussian fits to the data are presented in Table 1.

The first obvious feature of the data is that the shapes of the ^{12}CO and $^{13}\text{CO } J = 9-8$ lines are very different. DR 21 is the only observed source for which this is true. The $^{13}\text{CO } J = 9-8$

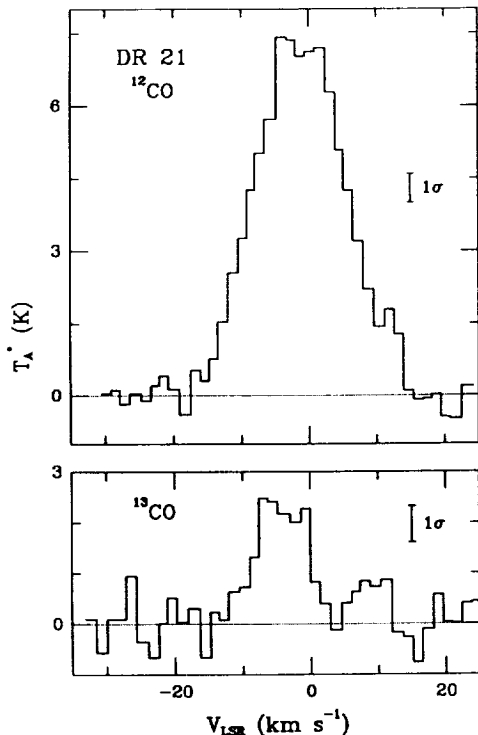


FIG. 3.—Spectra of ^{12}CO and ^{13}CO $J=9-8$ at DR 21. Integration times were 12 minutes and 34 minutes for the ^{12}CO and ^{13}CO data, respectively. The continuum has been subtracted from both spectra.

line traces column density and clearly shows the two distinct clouds mentioned previously. The ^{12}CO $J=9-8$ line is optically thick and therefore its profile is determined by temperature and beam-filling factors rather than by column density. The difference between the two lines illustrates the potential problems of deducing the properties of a molecular cloud on the basis of optically thick lines.

The second notable characteristic of the data shown in Figure 3 is the high optical depth for the ^{12}CO $J=9-8$ line implied by the ratio of ^{12}CO to ^{13}CO intensities, which approaches two in some parts of the line. This, together with the low values for T_A^* in ^{12}CO implies that the gas producing the ^{12}CO $J=9-8$ radiation is cold or has a small beam-filling factor.

Figure 4 shows a comparison of ^{12}CO and ^{13}CO spectra for various J obtained with similar beam sizes. There appear to be at least five velocities with different characteristics evident in the spectra. The first component is that giving rise to the deep central absorption seen in the $J=7-6$ spectra of Jaffe et al. (1989) and also in the $J=3-2$ and $4-3$ spectra of White et al. (1986). The absence of an absorption feature in the $J=9-8$ spectrum is consistent with the interpretation presented by Jaffe et al. (1989), and we will not consider this component further. The other four velocities are indicated by vertical lines in Figure 4. The -3 km s^{-1} and 9 km s^{-1} components correspond to the two clouds mentioned previously. Gas at -6 km s^{-1} produces significant ^{13}CO $J=9-8$ radiation while contributing little in ^{12}CO $J=1-0$ and $2-1$. Finally, the gas at 5 km s^{-1} has very little column density since it appears at or near a minimum in the ^{13}CO spectra but it still produces significant ^{12}CO radiation. We will attempt to deduce some physical properties of each of the regions.

The shapes of the ^{12}CO lines for a wide range of J , when averaged over our $80''$ beam size, are similar except for the different amounts of central reversal caused by the foreground gas. Only the ^{12}CO $J=1-0$ line shows a markedly different profile, being narrower and having a local minimum on the red side of the line distinct from the reversal seen at higher J . This latter feature is due to the low column density at this velocity, as shown by the absence of significant ^{13}CO radiation. The narrower width of the ^{12}CO $J=1-0$ line also appears to be due to decreasing column density in the wings, which makes the line more optically thin away from line center.

Figure 5 shows T_A^* as a function of J for each of the four velocities discussed above, in both ^{12}CO and ^{13}CO . We have calculated T_A^* for the $J=7-6$ spectrum of Jaffe et al. (1989) from the reported T_{mb} by using a geometric main-beam efficiency of 0.8 (Harris 1988). In addition, we have taken the $J=7-6$ spectra mapped with a $30''$ beam size and constructed an approximate $80''$ beam-averaged spectrum. This degradation of spatial resolution of the $J=7-6$ data reduces the T_A^* only by about 30% from the peak value seen in the mapping and should, to first order, eliminate comparative differences with the $J=9-8$ data due to source coupling. We were unable to construct a reasonable model which could simultaneously give rise to the high observed $J=7-6$ intensity and the much lower $J=9-8$ and $J=4-3$ values to within the calibration uncertainties of the various data sets. Observations of the intermediate $J=6-5$ or $8-7$ transitions may shed more light on this problem. For the remainder of the discussion, we will

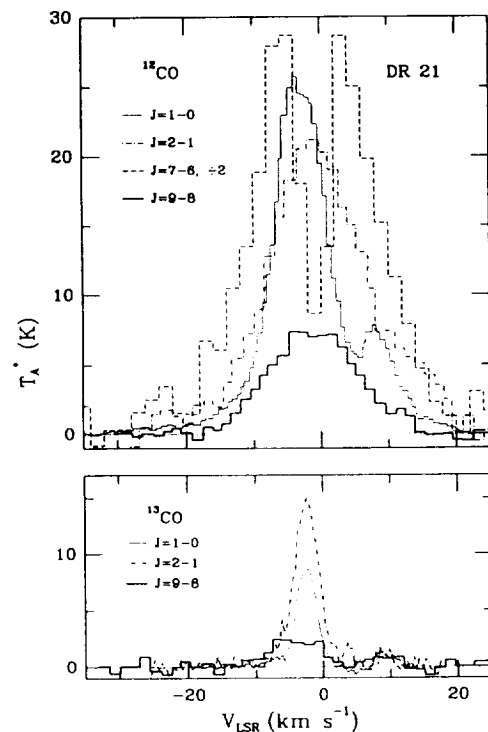


FIG. 4.—Comparison of spectra from DR 21 (see text for details). Top: ^{12}CO : $J=1-0$ (light solid line, Bally & Lada 1983), $J=2-1$ (dotted, White et al. 1986), $J=7-6$ (dashed, beam-averaged and scaled by 0.5, Jaffe et al. 1989), $J=9-8$ (heavy solid line, this work). Bottom: ^{13}CO : $J=1-0$ (light solid line, R. Plambeck, private communication), $J=2-1$ (dashed, R. Plambeck, private communication), $J=9-8$ (heavy solid line, this work). Short vertical lines mark velocities discussed individually in the text.

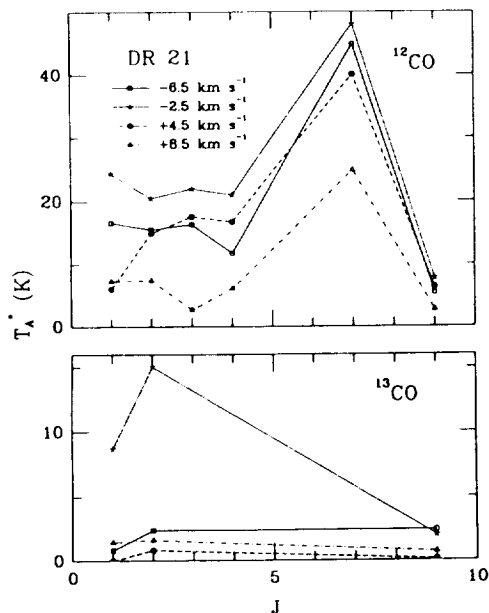


FIG. 5.— T_A^* as a function of J at four selected velocities in DR 21 for ^{12}CO and ^{13}CO .

concentrate only on the $J = 9-8$ data in the context of the lower J ($J < 5$) observations.

The low- J ^{12}CO data for all velocity components except that at the column density minimum are clearly optically thick, as would be expected. Comparison with the ^{13}CO $J = 9-8$ data indicates that the ^{12}CO $J = 9-8$ line also is optically thick but with a lower brightness temperature. Therefore, either the beam-filling factor is smaller for the gas emitting the $J = 9-8$ radiation than for that producing the lower J radiation, or several gas components must selectively contribute to the observed signals from different J values and isotopes.

The relative intensities of the ^{13}CO $J = 1-0$ and $2-1$ lines at the column density peak near -3 km s^{-1} are consistent with $T_k \geq 50 \text{ K}$ (the dust temperature; Harvey, Campbell, & Hoffmann 1977). A lower temperature near 30 K , the peak brightness temperature of the low- J ^{12}CO lines, is inconsistent with the observed ^{13}CO $J = 9-8$ intensity at $V_{\text{LSR}} = -3 \text{ km s}^{-1}$ unless an additional warmer gas component is present. Such a component might be undetectable in the low- J ^{13}CO data. However, it would need to have a small beam-filling factor to yield a low T_A^* while satisfying the joint requirements of a moderate temperature ($T \sim 150 \text{ K}$, for illustrative purposes) and $\tau \sim 10$ in the ^{12}CO $J = 9-8$ line. Subtraction of this warm gas contribution from the observed low- J data leads to an inconsistency between the residual $J = 1-0$ and $2-1$ ^{12}CO T_A^* values and optical depths. Therefore we suggest that the simpler alternative of $T \sim 50 \text{ K}$ gas with a beam-filling factor of ~ 0.6 and $n \sim 10^5 \text{ cm}^{-3}$ is more likely to produce the observed levels of radiation for all lines at the column density peak.

The 5 km s^{-1} and -6 km s^{-1} parts of the line profile could be produced by gas under similar physical conditions but differing column densities. Within the calibration and statistical uncertainties of the data these two components are indistinguishable in the ^{12}CO line profiles except at $J = 1-0$ where the 5 km s^{-1} gas becomes optically thin. Therefore we will assume that radiation at these two velocities arises under the same physical conditions.

Comparison of the ^{12}CO and ^{13}CO intensities at -6 km s^{-1} V_{LSR} shows that the optical depth in ^{12}CO is increasing with J , from $\tau \sim 2$ at $J = 1-0$ to $\tau \sim 6$ at $J = 2-1$ and $\tau \sim 18$ at $J = 9-8$. This trend suggests the presence of highly beam-diluted gas with $T_k > 100 \text{ K}$. All the CO observations can be reproduced to within 20% by a model (not unique) with gas at 50 K having a beam-filling factor of 0.2 and density $n \sim 1 \times 10^5 \text{ cm}^{-3}$ in addition to gas at 150 K with a beam-filling factor ~ 0.04 which is assumed to be sufficiently dense that the $J = 9-8$ transition is thermalized. The column density of the warmer gas is ~ 4 times that in the 50 K component. The data are not consistent with any component with a beam-filling factor near one. Therefore it appears that most of the low- J radiation at -6 km s^{-1} V_{LSR} comes from gas with the same physical characteristics as that at -3 km s^{-1} , while a hotter component also contributes to the $J = 9-8$ data at -6 km s^{-1} . We cannot ascertain the presence of any hot gas at 5 km s^{-1} because of the absence of detectable ^{13}CO radiation. However, the similar dependence of T_A^* on J as at other velocities suggests that the same gas components are present. The column density at 5 km s^{-1} V_{LSR} is much reduced, by at least a factor of 20 in both components, compared to that at the peak of the line profile.

The component at 9 km s^{-1} V_{LSR} is more difficult to interpret since this cloud is spatially distinct from that giving rise to the rest of the line. Consequently, pointing accuracy and beam size are more critical for estimating the beam-filling factor for various rotational transitions. Nevertheless, the data are broadly consistent with a component at $T_k = 50 \text{ K}$, $n = 5 \times 10^5 \text{ cm}^{-3}$, and beam-filling factor ~ 0.15 . Although the gas could be hotter with a smaller beam-filling factor, a significantly lower temperature is ruled out unless an additional warm component is postulated to produce the observed $J = 9-8$ radiation.

Finally, we have also examined the radiation 10 km s^{-1} redward from line center to see whether there is any evidence for shock heating of the higher velocity gas. We find that emission in the near line wing can be explained by the same moderate temperature components of gas that are seen elsewhere in the line, but with lower column densities and beam-filling factors. Higher signal-to-noise ratios, especially in the higher J data, are required before this comparison can be extended farther into the wings.

In summary, we find that the CO radiation in DR 21 arises predominantly from a component with $T \sim 50 \text{ K}$, in apparent equilibrium with the dust. This gas is clumpy at all velocities with a maximum beam-filling factor near 0.6. However, an additional component of warmer gas ($T > 100 \text{ K}$) adds to the emission seen in the $J = 9-8$ line. This component is not obviously present near the velocity of maximum CO column density or at the secondary peak in column density associated with a spatially distinct cloud, as expected if the warm gas is associated with photodissociation regions embedded in the cloud. The warmer gas is either spatially compact (which is likely considering the small sizes of the H II regions) or very clumpy at all velocities with a maximum beam-filling factor less than 0.1 in our $80''$ beam.

3.3. W51

W51 is a very luminous complex of molecular clouds and H II regions located in the Sagittarius spiral arm. Included in the region are several H_2O masers, some associated with bright infrared sources or compact H II regions. CO line obser-

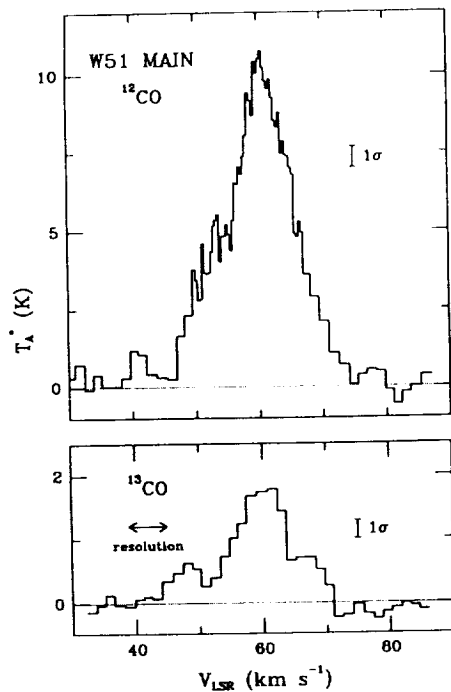


FIG. 6.—Spectra of ^{12}CO and ^{13}CO $J=9-8$ at W51 Main. The ^{12}CO spectrum is a composite from the two filter banks, with the central section at higher resolution than the edges. The 1σ error bar represents statistical uncertainty for the higher resolution data. The ^{13}CO spectrum of W51 is shown as a running mean over four channels. Integration times were 20 minutes and 56 minutes for the ^{12}CO and ^{13}CO spectra, respectively. The continuum has been subtracted from both spectra.

vations show very extended emission with line profiles indicating apparent absorption as well as emission features. Part of the complexity of the spectra arises because the line of sight to W51 is almost tangential to the spiral arm (Mufson & Liszt 1979). Consequently, several spatially distinct molecular clouds contribute to the observed spectra. In addition, SiO observations show a broad component reminiscent of the Orion plateau emission (Downes et al. 1982). A broad component also has been detected in CO $J=7-6$ spectra (Jaffe, Harris & Genzel 1987).

We observed both the ^{12}CO and ^{13}CO $J=9-8$ lines at W51 Main and just the ^{12}CO $J=9-8$ line at IRS 2. Both positions are local peaks of the FIR continuum (Jaffe, Becklin, & Hildebrand 1984) and molecular column density (Schloerb, Snell, & Schwartz 1987). Figures 6 and 7 present the observed spectra, and the parameters deduced from Gaussian fits are given in Table 1.

The ^{12}CO spectrum at W51 Main, shown in Figure 6, clearly shows components with different line widths. Gaussian decomposition of the line profile gives a narrow component with a FWHM of 6.6 km s^{-1} centered near 61 km s^{-1} V_{LSR} and a wide component with a FWHM of 18 km s^{-1} centered at 59 km s^{-1} . The peak T_A^* values of the components are comparable, but the column density of gas in the wide component is about a factor of 3 greater than in the narrow one, provided that both components have similar temperatures and densities. The ^{12}CO $J=9-8$ spectrum at W51 IRS 2, shown in Figure 7, can be fitted to within statistical uncertainties by a single Gaussian, but a slightly better fit can be obtained with the same two components as seen at W51 Main. This result differs from the case of the $J=7-6$ data of Jaffe et al. (1987) for which

the broad component is evident at IRS 2 but not at W51 Main. Unfortunately the signal-to-noise ratio of the ^{13}CO $J=9-8$ spectrum, seen in Figure 6, is too low for more than one Gaussian to be fitted, but the data are consistent with approximately equal T_A^* contributions from wide and narrow features.

The shape of the ^{12}CO $J=9-8$ line is markedly different from that seen in the $J=1-0$ through $4-3$ transitions, all of which are similar and show a deep absorption feature near 65 km s^{-1} . The absorption has been modeled as arising from cold gas, $T_k \sim 10\text{ K}$, with a density $n_{\text{H}_2} \sim 5000\text{ cm}^{-3}$ (White et al. 1986). No absorption from this gas is expected in ^{12}CO $J=7-6$ or $J=9-8$ spectra, consistent with the observations.

The peak T_A^* values of the optically thick low- J lines, extrapolated by assuming that the absorbing feature is intrinsically narrow, suggest for complete beam filling that the excitation temperature is near 35 K , which is significantly lower than the effective temperature of 65 K derived for the dust (Gordon 1987). Our modeling procedure shows that the observed ^{13}CO lines ($J=1-0$, Langer & Penzias 1990; $J=2-1$, R. Plambeck, private communication; $J=9-8$, this work) cannot arise solely from 35 K gas at any density. Alternately, the low- J lines may be affected much more by the absorber than estimated, or the molecular gas may have a small-scale beam-filling factor less than one (as is the case for the dust), so that the gas excitation temperature could be significantly higher than 35 K . The gas producing the CO $J=9-8$ radiation is likely to be kinematically related to that seen in the low- J transitions as shown by the comparable full velocity extents of all the lines.

The profile of the $J=7-6$ line at IRS 2 observed by Jaffe et al. (1989), when spatially averaged over our larger $80''$ beam size, is very similar to our $J=9-8$ profile. The peak spatially averaged T_A^* of the $J=7-6$ data is $\sim 38\text{ K}$ (scaled by a factor of 0.8 from T_{mb} to T_A^*), much higher than the 6 K T_A^* for the $J=9-8$ line. We do not think that source coupling can account for the discrepancy since mapping at $30''$ resolution by Jaffe et al. (1989) shows emission at half the peak observed brightness or higher over an $80''$ region equivalent to our beam

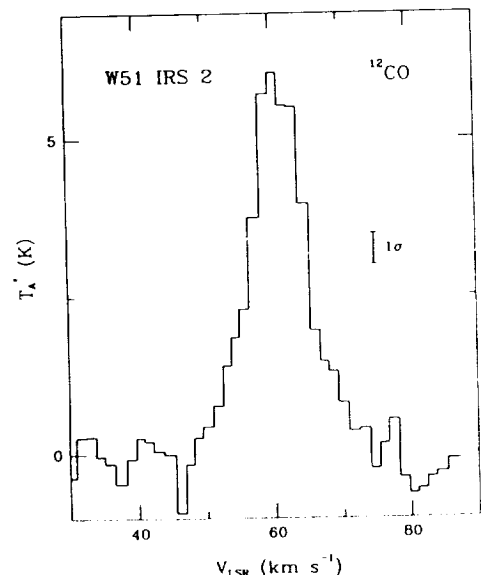


FIG. 7.—Spectrum of ^{12}CO $J=9-8$ at W51 IRS 2 with the continuum subtracted. Integration time was 16 minutes.

size. However, density or temperature gradients could conceivably decrease the beam-filling factor of the higher J emission.

The broad component of the line at W51 IRS 2 was deduced by Jaffe et al. (1987) as arising from hot ($T > 500$ K), dense ($n_{\text{H}_2} > 2 \times 10^4 \text{ cm}^{-3}$) gas with a small filling factor, presumably due to clumping. This conclusion was based on a comparison between the $J = 7-6$ data and the $J = 16-15$ line which was only marginally resolved and was estimated to have a FWHM near 70 km s^{-1} . The new $^{12}\text{CO } J = 9-8$ data do not support this interpretation even with beam-filling factors considered: at temperatures > 500 K, the $J = 9-8$ line should be more intense than the $J = 7-6$ line for optically thin gas, contrary to what is observed. In addition, the widths of the $J = 9-8$ and $J = 7-6$ lines are very similar while that estimated for the $J = 16-15$ line is more than 4 times wider. This difference makes the straightforward comparison of integrated intensities somewhat questionable, since there is little evidence that the lines arise from the same gas. Of course, warm gas must be present to produce the $J = 16-15$ line, but it is not clear that this same gas produces the broad component seen in the $J = 7-6$ and $9-8$ lines. A broad component is also observed in the $v = 0, J = 2-1$ transition of SiO (Downes et al. 1982) with a width similar to that seen in the CO $J = 9-8$ data. Although the SiO-emitting region is compact, the gas giving rise to the broad component in the CO data may be kinematically related to it, analogous to the case in Orion where the SiO plateau emission is compact while the high- J CO emission with the same velocity characteristics is more extended.

At W51 Main the ^{12}CO spectrum of $J = 9-8$, shown in Figure 6, is again quite similar to that obtained from the $J = 7-6$ data of Jaffe et al. (1989) by constructing a spatial average over our beam size. Our $J = 9-8$ spectrum, however, does not resemble an earlier $J = 7-6$ spectrum of Jaffe et al. (1987) which peaks near 54 km s^{-1} (rather than 60 km s^{-1}) and shows no evidence of a broad component. Presumably variations in pointing are the likely explanation for the differences between the two sets of $J = 7-6$ data.

A comparison between the $^{13}\text{CO } J = 9-8$ and $^{12}\text{CO } J = 9-8$ spectra at W51 Main (Fig. 6) shows that the ^{12}CO line is optically thick with $\tau \sim 10$ for an adopted isotopic ratio near 50, given the usual assumption that the lines arise from the same region. If the ^{13}CO line is subthermally excited, then the ^{12}CO optical depth could be somewhat greater, because radiation would then help to maintain the upper state population. The brightness temperature of the ^{12}CO line, ~ 20 K, cannot be the excitation temperature of the gas producing the $^{13}\text{CO } J = 9-8$ radiation, since even in LTE the column density required to give the observed T_{A}^* would make the $^{13}\text{CO } J = 2-1$ line optically thick, contrary to what is observed (R. Plambeck, private communication). Subthermal excitation at higher temperatures also cannot produce the observed emission because the ^{12}CO line has sufficient optical depth to maintain itself near LTE.

The conclusion from the foregoing discussion is that the $J = 9-8$ radiation arises from warm ($T \geq 50$ K) gas which does not fill the beam, most likely because it is clumped. The emitting gas is optically thick in individual clumps in the $^{12}\text{CO } J = 9-8$ line if this radiation arises from the same gas as the $^{13}\text{CO } J = 9-8$ line. Consequently, the $^{12}\text{CO } J = 7-6$ line must also be thick within a clump.

A discrepancy still remains between the T_{A}^* values measured for both lines: ~ 30 K for the $J = 7-6$ line (averaged over our beam size) and ~ 9 K for the $J = 9-8$ line. If both lines are

optically thick and emitted from equivalent regions, their brightness temperatures should be comparable. However, the lines have critical densities which differ by approximately a factor of 2. Therefore, the beam-filling factor of the gas producing the $J = 9-8$ line may be significantly less than that for the $J = 7-6$ line if the medium has density gradients. As an example, the observed T_{A}^* ratio of $J = 7-6$ to $J = 9-8$ could be produced by numerous clumps within the $80''$ beam, each of which has a Gaussian density distribution and a central density near 10^6 cm^{-3} . Even at temperatures greater than 2000 K, though, this (hypothetical) gas would have significant optical depth in individual clumps at $J = 4-3$ and lower. As a result the low- J lines would then have higher T_{A}^* values than are actually observed. Hence, the $J = 7-6/J = 9-8$ intensity discrepancy remains unresolved.

The preceding discussion considered the peak T_{A}^* of the line profiles for simplicity. Since the line profiles of the $J = 9-8$ and $7-6$ lines are similar, it is likely that the physical conditions producing the broad and narrow parts of the emission profile are not too dissimilar, and therefore the above conclusions should be applicable to both. An unambiguous decomposition is not possible for the lower J lines because of the presence of the absorber. As discussed by Jaffe et al. (1987), the temperature of the gas can in principle be estimated from the ratio of two lines such as the $J = 7-6$ and $16-15$ lines. However, given the evidence that the $J = 9-8$ line (and hence, the $7-6$ line) is optically thick and that the beam-filling factor of the gas producing the radiation is less than one (and that it quite possibly varies with J), along with the difficulty of reconciling the observed $J = 7-6$ and $J = 9-8$ intensities and the uncertainty of whether the $J = 16-15$ line has a common origin with the lower J lines, we feel that only a lower limit of 50 K for the temperature of the emitting regions of both the broad and narrow components can be established with any degree of certainty. Further data are obviously required to resolve the apparent inconsistency between the higher T_{A}^* value of the $J = 7-6$ line and the lower T_{A}^* value and moderate optical depth of the $J = 9-8$ line.

3.4. M17

The interface between the H II region M17 and the molecular cloud to the SW has been extensively studied in many transitions, as summarized by Stutzki et al. (1988). Observations in CO transitions for $J < 5$ are consistent with optically thick emission from gas at 50 K, which is also the dust temperature in the interface region (Gatley et al. 1979). However, consideration of the shapes of the low- J CO lines led Martin, Sanders, & Hills (1984) to conclude that the molecular gas in M17 is clumpy and macroturbulent. Subsequent observations in the $J = 7-6$ and $14-13$ transitions of CO by Harris et al. (1987) revealed the existence of a significantly hotter component of gas. The CO observations were modeled by Stutzki et al. (1988) using three components: optically thick clump cores at 50 K with a 70% beam-filling factor which produce most of the low J radiation, warmer (200 K) envelopes with the same filling factor which give rise to the $J = 7-6$ and $14-13$ radiation, and a cool (~ 30 K) extended foreground absorbing layer. The $J = 9-8$ transition is useful for testing the validity of this model (which is underconstrained especially at the high J end) because the warm gas component should dominate the $J = 9-8$ ^{12}CO emission.

We observed $^{12}\text{CO } J = 9-8$ in M17 at two locations corresponding to positions of maximum $J = 7-6$ emission as seen

by Stutzki et al. (1988). These two positions are henceforth referred to as $(-60, -30)$ and $(-100, 0)$, with the numbers representing arcseconds relative to the position of the SAO star at $\alpha = 18^{\text{h}}17^{\text{m}}34^{\text{s}}.5$, $\delta = -16^{\circ}13'24''$ (1950), negative to W and S. The first position is near the ionization front while the second is at the FIR peak. A spectrum of the $^{13}\text{CO } J=9-8$ line was observed at the FIR peak only. The spectra are shown in Figures 8 and 9, and parameters deduced from Gaussian fits to the data are given in Table 1.

As is the case in the other sources, the $^{12}\text{CO } J=9-8$ spectra of M17 show peak T_{A}^* values that are relatively low at both locations. If the gas primarily responsible for the $J=9-8$ emission is distributed similarly to either the molecular material giving rise to the $J=1-0$ and $J=2-1$ emission or that producing the $J=7-6$ emission as shown in the strip maps of Stutzki et al. (1988), then beam dilution will not be significant at the FIR peak $(-100, 0)$. However, a part of the beam at the $(-60, -30)$ location falls on the ionization front where the intensity of CO emission in other transitions decreases rapidly. We estimate that our measured T_{A}^* at this location is 60%–80% of that which would be obtained in a $30''$ beam. (This factor does not constitute a conversion from T_{A}^* to T_{mb} , the main-beam brightness temperature, but includes only the effects of beam dilution.) Thus our data are consistent with the expectation that radiation from warm gas increases toward the ionization front. Unfortunately, beam dilution precludes the determination of gas temperatures in this region from our data. Nevertheless, we do not see a large amount of hot gas, and it appears that most (60%–100%) of the $J=9-8$ radiation can be accounted for by the cooler ($T \sim 50$ K) molecular material which makes up the bulk of the cloud. In particular, the line profile at the $(-60, -30)$ position, shown in Figure 8, is similar to that obtained from low- J CO data for the component near $21 \text{ km s}^{-1} V_{\text{LSR}}$ but is quite dissimilar to the profile of C II at the same location (Boreiko, Betz, & Zmuidzinas 1990). The C II line profile, which should be more characteristic of the warmer

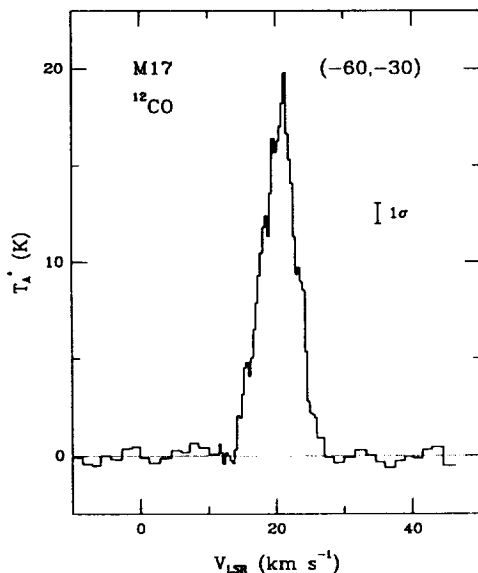


FIG. 8.—Spectrum of $^{12}\text{CO } J=9-8$ at the ionization front in M17. The spectrum is a composite from the two filter banks, with the central section at higher resolution than the edges. The continuum has been subtracted from the spectrum. Integration time was 8 minutes, and the 1σ error bar represents statistical uncertainty for the higher resolution data.

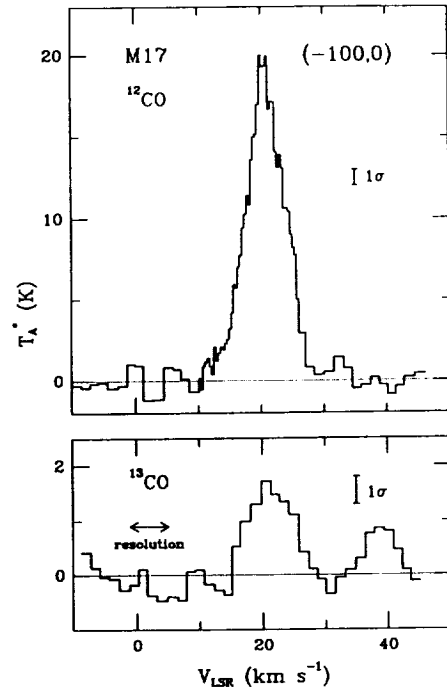


FIG. 9.—Spectra of ^{12}CO and $^{13}\text{CO } J=9-8$ at the FIR peak in M17. The ^{12}CO spectrum is a composite from the two filter banks, with the central section at higher resolution than the edges. The 1σ error bar represents statistical uncertainty for the higher resolution data. The ^{13}CO spectrum of M17 is shown as a running mean over four channels. Integration times were 10 minutes and 28 minutes for the ^{12}CO and ^{13}CO spectra, respectively. The continuum has been subtracted from both spectra.

gas in the PDR, has a FWHM of 12.4 km s^{-1} , approximately twice that of the $J=9-8$ CO line even though it was observed with a smaller ($40''$) beam, and also shows a more complex structure. Therefore, the gas emitting the CO $J=9-8$ radiation is kinematically related much more closely with the molecular cloud material than with that in the photo-dissociation region.

The interpretation of the observations at the $(-100, 0)$ position, shown in Figure 9, is more clear-cut since beam dilution in the cool molecular gas component is expected to be negligible. Also, our detection of the $^{13}\text{CO } J=9-8$ line places additional constraints on conditions in the emitting region. Although the signal-to-noise ratio in this line is quite low, the detection of the line is significant at the 4σ level. The systematic uncertainty in T_{A}^* for the ^{13}CO data is estimated to be 25%, somewhat higher than that for the other sources because of greater amounts of atmospheric water vapor in the line of sight during the M17 observations. As can be seen from Table 1, the V_{LSR} and width of the $^{13}\text{CO } J=9-8$ line are very similar to those of the $^{12}\text{CO } J=9-8$ line, while the integrated intensity and peak T_{A}^* are about a factor of 10 smaller. Since an isotopic ratio this low is unlikely, the $^{12}\text{CO } J=9-8$ line must be somewhat optically thick. If we neglect the effects of sub-thermal excitation, the kinetic temperature of the gas giving rise to the ^{13}CO emission must be near 40 K, the brightness temperature of the $^{12}\text{CO } J=9-8$ line, if the emission uniformly fills our beam.

At $T_{\text{ex}} = 50$ K the optical depth in the $^{13}\text{CO } J=9-8$ transition is approximately the same as that of the $^{13}\text{CO } J=1-0$ transition. Therefore, the weakness of the observed $^{13}\text{CO } J=9-8$ line compared with $T_{\text{A}}^* = 15$ K measured for the ^{13}CO

$J = 1-0$ transition (R. Plambeck, private communication) shows that either subthermal excitation or beam dilution is relevant to the $J = 9-8$ intensity. As a first approach to understanding the data, we have modeled the $V_{\text{LSR}} \sim 21 \text{ km s}^{-1}$ component (derived from Gaussian fits) to available high-resolution ^{12}CO and ^{13}CO data in the LVG approximation described previously.

A comparison between the model with $T_k = 50 \text{ K}$ (as established from the optically thick low- J ^{12}CO lines), $n_{\text{H}_2} = 6 \times 10^4 \text{ cm}^{-3}$, $N_{^{13}\text{CO}} dv^{-1} = 4 \times 10^{16} \text{ cm}^{-2} (\text{km s}^{-1})^{-1}$, and a $^{12}\text{CO}/^{13}\text{CO}$ isotopic ratio of 50 is shown in Figure 10. It should be noted that the uncertainties for all points except the $^{13}\text{CO } J = 9-8$ are almost completely from systematic effects, and thus the larger error bars for the lower- J data simply reflect the higher T_A^* values measured there and not larger statistical uncertainties. The $J = 7-6$ data have been rescaled from the T_{mb} values presented by Harris et al. (1987) to T_A^* using a factor of 0.8 for the geometric main beam efficiency (Harris 1988). Although beam sizes range from $30''$ for $^{12}\text{CO } J = 2-1$ and $7-6$ observations to $80''$ for $J = 9-8$, beam dilution is not likely to be a problem. The $^{12}\text{CO } J = 2-1$ data of Stutzki et al. (1988) and of R. Plambeck (private communication) both show the same peak T_A^* values even though the former data were obtained with a $30''$ beam and the latter with a $75''$ beam.

From Figure 10 it can be seen that the ^{13}CO data are well represented by a single-component model. This is not surprising since ^{13}CO traces predominantly column density and would not be expected to be sensitive to small amounts of gas with different conditions. In contrast, however, the ^{12}CO data would be expected to show greater deviations from the model if several gas components contribute to the emission. In effect, any optically thin gas is more evident in the ^{12}CO data than the ^{13}CO data by a factor equal to the isotopic ratio. In addition, any gas which is subthermally excited will contribute

disproportionately to the observed ^{12}CO radiation because the radiation field will maintain the excitation temperature closer to the kinetic temperature for the dominant isotope.

The low- J ^{12}CO data are moderately well represented by optically thick emission at 50 K . However, the single-component model deduced from the ^{13}CO data overestimates the $^{12}\text{CO } J = 9-8$ radiation significantly. That the $^{12}\text{CO } J = 9-8$ line does not appear to arise in LTE suggests either that (1) the isotopic ratio is much lower than we have assumed, near 10, or (2) that the gas is clumpy or consists of more than one density component, and that these components contribute differently to the ^{12}CO and $^{13}\text{CO } J = 9-8$ radiation.

As an alternative to the single component homogeneous model discussed above, we can apply the relationships developed by Martin et al. (1984) to calculate parameters for a clumpy model. These authors found that the ^{12}CO and $^{13}\text{CO } J = 1-0$ data could arise from a macroturbulent, clumpy medium in which the geometric beam-filling factor at line center is ~ 0.4 and the typical optical depth per clump, modeled with a Gaussian density distribution, is 2 for the $^{13}\text{CO } J = 1-0$ line. Central densities for the clumps are $\sim 6 \times 10^5 \text{ cm}^{-3}$ and, since most of the $^{13}\text{CO } J = 9-8$ radiation should arise from the clump cores, the assumption of LTE for both of our observed transitions should be a valid first approximation. Using just the two $J = 9-8$ lines, we calculate a geometric beam-filling factor of ~ 0.2 and $^{13}\text{CO } J = 9-8$ line center optical depth of ~ 0.3 . Clearly these values are inconsistent with those derived from the $J = 1-0$ observations, and therefore the assumption of LTE (and hence Gaussian clumps with the stated central density) must be abandoned. The clumpy model does, however, have promise for reconciling the low measured T_A^* of the $^{12}\text{CO } J = 9-8$ line with the moderate optical depths implied by the ratio of the $^{12}\text{CO}/^{13}\text{CO } J = 9-8$ data. In the absence of information on the true density distribution within the M17 region, we proceed with a simple model with two discrete density components.

From the subthermal excitation of the $^{13}\text{CO } J = 9-8$ transition we can deduce an average density of $\sim 6 \times 10^4 \text{ cm}^{-3}$. However, observations of molecular species such as CS, C^{34}S , H_2CO , and HCN, which have higher critical densities, clearly show that peak densities are at least an order of magnitude higher than this (Snell et al. 1984; Mundy et al. 1986, 1987; Evans et al. 1987). Given the evidence for dense gas as well as gas with densities insufficient to thermalize the $J = 9-8$ transition of CO, our illustrative model incorporates two density components: the first with $n = 10^6 \text{ cm}^{-3}$, column density of ^{13}CO per velocity interval $N_{^{13}\text{CO}} dv^{-1} = 5 \times 10^{16} \text{ cm}^{-2} (\text{km s}^{-1})^{-1}$, and beam-filling factor $f = 0.2$; and the second with $n = 10^4 \text{ cm}^{-3}$, $N_{^{13}\text{CO}} dv^{-1} = 3 \times 10^{16} \text{ cm}^{-2} (\text{km s}^{-1})^{-1}$, and $f = 0.8$. The values for the parameters are not well constrained by the available data, and hence are merely representative. The beam-filling factor for the dense gas is equal to the minimum value derived by Snell et al. (1984) from CS data. Both components are assumed to have the same kinetic temperature of 50 K and an isotopic ratio of 50. The results of this model are also shown in Figure 10. As can be seen, the two-component model fits the ^{13}CO data equally as well as the single-component model. However, the former predicts significantly less $^{12}\text{CO } J = 9-8$ radiation than does the latter, in better agreement with the observations. This model is, of course, highly simplified because it is based on observations with large beams. As is shown by the small beam data of Stutzki & Güsten (1990), the medium is very clumpy and struc-

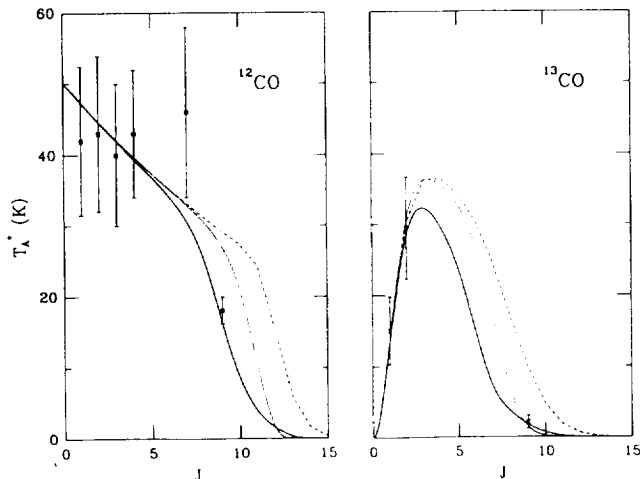


FIG. 10.—Peak T_A^* values for the 21 km s^{-1} component in CO of various J at the FIR peak in M17, compared with the LTE case (*dashed*), a single-density component model (*dotted*), and a model with two density components (*solid*). See text for details of the models. Data are from R. Plambeck (private communication); ^{12}CO and $^{13}\text{CO } J = 1-0$ and $J = 2-1$, Stutzki et al. (1988), $^{12}\text{CO } J = 2-1$, Rainey et al. (1987), $^{12}\text{CO } J = 3-2$, Schulz & Krügel (1987), $^{12}\text{CO } J = 4-3$, Harris et al. (1987), $^{12}\text{CO } J = 7-6$, and the present work (^{12}CO and $^{13}\text{CO } J = 9-8$). The uncertainties are overwhelmingly systematic except for the $^{13}\text{CO } J = 9-8$ data, and are as given in the above references or, if not quoted, assumed to be 25%.

tured both spatially and in velocity. Therefore the model represents only a broad average; further refinements must await the availability of smaller beam observations over a range of J .

Because the low- J ^{12}CO lines are optically thick and only the $J = 9-8$ lines are sensitive to the densities and beam-filling factors of the two components, the model is underconstrained even though there are nine data points and only six free parameters (kinetic temperature, column density, and beam-filling factor for each of the two components—isotopic ratio and number density of each component have been somewhat arbitrarily fixed). We have not included any additional components with different temperatures in the model since the data do not show strong supporting evidence. In particular, the hot ($T \sim 200$ K) gas deduced by Stutzki et al. (1988) from the high T_{mb} of the $J = 7-6$ data is not evident in the $J = 9-8$ data. On the contrary, the $J = 9-8$ line shows evidence for excitation temperature decreasing rather than increasing with J . However, given the systematic uncertainties of all the data, there is no very significant disagreement between the two data sets, only in the interpretation.

Our illustrative model is in qualitative agreement with the conclusion of Mundy et al. (1986) that the total column density of gas with $n \sim 10^4-10^5 \text{ cm}^{-3}$ is less than half of that in the dense gas. Although the $J = 9-8$ data appear to require a clumpy medium, the CO observations to date are insufficient to fully constrain the model, and resolved spectra at other J would be very useful to probe the nature of the clumpy medium of M17.

3.5. W49

The W49 complex is a very active star formation region, and includes several strong masers, a cluster of compact H II regions and newly formed stars, and a large amount of warm dust. The embedded source W49A IRS is thought to be the most luminous region in the galaxy. There are probably two giant molecular clouds associated with the W49A complex: one with $V_{\text{LSR}} = 4 \text{ km s}^{-1}$ and the other with $V_{\text{LSR}} = 12 \text{ km s}^{-1}$, which together give rise to the characteristic double-peaked line profile of this source.

There has been considerable discussion of molecular line profiles in the W49 region. Some authors (e.g., Phillips et al. 1981; Jaffe et al. 1987) suggest that the appearance of two peaks is produced by foreground absorption as is the case in W3 and W51, while others (e.g., Mufson & Liszt 1977; Miyawaki, Hayashi, & Hasegawa 1986) maintain that the profile is caused by the presence of two distinct molecular clouds. The situation is not clear-cut because some isotopic species, such as ^{13}CO and C^{18}O which might be expected to be optically thin, show a fractionally smaller central dip in the composite profile than the optically thick ^{12}CO low- J lines. Furthermore, gas with $V_{\text{LSR}} = 4 \text{ km s}^{-1}$ appears to have a somewhat different spatial distribution than that producing the 12 km s^{-1} peak. The true situation may be a combination of both alternatives, as suggested by Miyawaki et al. (1986): there are two distinct clouds which produce all the radiation in the optically thin isotopes, as well as a foreground cloud which produces the deeper absorption feature in optically thick low-excitation lines.

We observed the $^{12}\text{CO } J = 9-8$ line toward W49 IRS. The spectrum is shown in Figure 11, and parameters deduced from the fit of two Gaussians to the data are given in Table 1. Lack of observing time prevented us from attempting a $^{13}\text{CO } J = 9-8$ detection in this source.

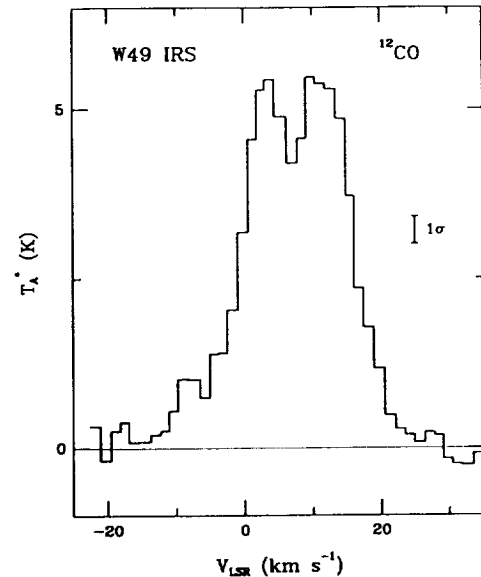


FIG. 11.—Spectrum of $^{12}\text{CO } J = 9-8$ at W49 IRS with the continuum subtracted. Integration time was 24 minutes.

Langer & Penzias (1990) have observed the $^{13}\text{CO } J = 1-0$ and $\text{C}^{18}\text{O } J = 1-0$ and $2-1$ lines with a beam size similar to ours. All their isotopic data show the 12 km s^{-1} component to have a $T_{\text{A}}^* \sim 30\%$ higher than the 4 km s^{-1} component. Their $^{12}\text{CO } J = 1-0$ spectrum shows a similar though less pronounced difference. In our $J = 9-8$ spectrum (Fig. 11), however, the two peaks are essentially identical in intensity. If the $J = 9-8$ line is a tracer predominantly of density rather than temperature, as appears to be the case for the other sources discussed, then the 4 km s^{-1} cloud must have a somewhat higher mean density than the 12 km s^{-1} cloud. A minimum column density of gas required to produce the observed $J = 9-8$ line can be calculated by assuming that the gas is in LTE at approximately 200 K. At lower temperatures, the $J = 9$ level is populated very inefficiently, while at higher temperatures the CO molecules are distributed among more J levels so that the total column density is increased. The minimum column density is $\sim 2 \times 10^{16} \text{ cm}^{-2}$ in each of the two velocity components.

If we adopt a lower temperature of 50 K, as indicated by the dust emission (Gordon 1987), then it is possible to construct a single-component model which agrees with the $^{12}\text{CO } J = 1-0$ and $J = 9-8$ data and also the $^{13}\text{CO } J = 1-0$ line. We cannot, however, in this case explain the $J = 7-6$ data of Jaffe et al. (1987), which shows a T_{A}^* near 35 K. In addition, the $J = 7-6$ line does not show the two characteristic velocity components but instead appears as a single broad ($\Delta V_{\text{FWHM}} \sim 24 \text{ km s}^{-1}$) line centered at $V_{\text{LSR}} = 8 \text{ km s}^{-1}$. Because of these observational differences, we have not attempted to incorporate these data. In our model, the gas producing the 4 km s^{-1} component has a beam-filling factor of 0.3 and density $n_{\text{H}_2} = 5 \times 10^5 \text{ cm}^{-3}$ while that giving rise to the 12 km s^{-1} component has a beam-filling factor of 0.4 and $n_{\text{H}_2} = 2 \times 10^5 \text{ cm}^{-3}$. Both have ^{12}CO column densities of approximately $1 \times 10^{19} \text{ cm}^{-2}$. Part of the beam dilution is likely to arise from the physical source dimensions, since observations with a smaller $45''$ beam (Scoville et al. 1986) show increased T_{A}^* . The increase is proportionally larger in the 4 km s^{-1} component, in qualitative agreement with our relative values for beam dilution. However, this is not

the major contribution to the beam dilution. In our model, the optical depths of the ^{12}CO $J = 9-8$ line are 10 and 7 in the 4 km s^{-1} and 12 km s^{-1} components, respectively, similar to values found in the other sources observed.

The appearance of the two velocity components in ^{12}CO spectra at $J = 1-0$ and $9-8$ as well as in weaker isotopes argues strongly against foreground gas producing the apparent central absorption in all the lines. It would be extremely difficult to envision physical conditions which would produce an absorption with approximately constant relative depth in lines covering such a range of excitation conditions. Nevertheless, it is likely that some foreground gas does produce the deeper and sharper feature seen only in the ^{12}CO $J = 1-0$ spectrum. This gas is likely cold or tenuous, and does not affect the appearance of the $J = 9-8$ line.

4. SUMMARY AND CONCLUSIONS

We have observed the ^{12}CO and ^{13}CO $J = 9-8$ lines in four dense molecular clouds. In all sources the ^{12}CO $J = 9-8$ line is found to be optically thick with $\tau > 5$, provided that both lines arise from similar regions. The brightness temperature of the $J = 9-8$ ^{12}CO line is similar to or less than that of the dust or of low- J CO observed with an equivalent beam size. This suggests that the gas is clumped, with the regions having sufficient density to produce $J = 9-8$ radiation filling only part of our 80" beam. Regions with $n_{\text{H}_2} > 10^5 \text{ cm}^{-3}$ are required to produce the observed ^{13}CO $J = 9-8$ lines, while the optically thick ^{12}CO radiation can arise from somewhat less dense regions. Typical column densities in the emitting gas are $\sim 10^{19} \text{ cm}^{-2}$ in ^{12}CO for an adopted $^{12}\text{CO}/^{13}\text{CO}$ isotopic ratio of 50. Some contribution from gas warmer than that characteristic of the bulk of the molecular cloud is evident in many of the ^{12}CO spectra. This warmer gas may be located near the photodissociation regions in these sources, and be UV-heated. However, most of the $J = 9-8$ emission probably does not arise from this warmer gas, and we do not detect the spatially extended regions of warm gas inferred to explain the $J = 7-6$ emission with measured brightness temperatures $T_b > 50 \text{ K}$. In addition, the profiles of the $J = 9-8$ ^{12}CO lines generally do not resemble the shapes of C II lines which do arise from the photodissociated gas. This result supports the conclusion that the $J = 9-8$ radiation comes predominantly from dense regions of the cooler molecular cloud.

At W3 IRS 5, we find that the low- J ($J < 5$) CO lines arise from gas with $T_k \sim 50 \text{ K}$ attenuated by a foreground cloud with $T_k \sim 15-20 \text{ K}$. The foreground cloud is quite optically thick in the center of the ^{12}CO lines. The ^{12}CO and ^{13}CO $J = 9-8$ lines are also produced in the warmer background gas. However, the regions with sufficient density to populate the $J = 9$ level no longer fill our 80" beam, resulting in lower brightness temperatures even for the optically thick ^{12}CO line. A warmer gas component is not required to explain the observations, although this possibility is not excluded by the data.

The ^{12}CO and ^{13}CO $J = 9-8$ lines in DR 21 show very different shapes, in contrast to the result for the other sources observed. The ^{13}CO line shows two distinct peaks at the known velocities of two clouds present in the region, while the ^{12}CO $J = 9-8$ line is well fitted by a single Gaussian component with a V_{LSR} intermediate to those seen in the ^{13}CO line. However, the much greater apparent width of the ^{12}CO line suggests that a blend of two components is also present. The

^{12}CO optical depth reaches $\tau > 20$ in some parts of the line. Analysis of the intensities as a function of J at several velocities shows that two components, one with $T \sim 50 \text{ K}$ and $n_{\text{H}_2} \sim 10^5 \text{ cm}^{-3}$ and the other thermalized at $T > 100 \text{ K}$, are required to produce the observed lines. The beam-filling factor is less than 1 for both components throughout the line, reaching a maximum of ~ 0.6 for the $T = 50 \text{ K}$ component and no more than 0.1 for the warmer gas. The warmer component is not evident at the velocity of the secondary cloud not associated with H II regions, supporting the identification of this gas with the photodissociation region. Radiation in the line wings can be produced by the same two components seen elsewhere in the line, and hence we see no evidence of shock-heating of the gas.

The ^{12}CO $J = 9-8$ spectrum at W51 Main and also possibly at IRS 2 shows a broad emission component with FWHM $\sim 18 \text{ km s}^{-1}$ in addition to a narrow one. The optical depth at the peak of the ^{12}CO $J = 9-8$ line at W51 Main is about 10. A dense ($n_{\text{H}_2} > 10^5 \text{ cm}^{-3}$) component of gas with $T \geq 50 \text{ K}$ and beam-filling factor less than unity probably produces the observed $J = 9-8$ lines and much of the lower J radiation. There is, however, a discrepancy between the high observed brightness temperatures seen in $J = 7-6$ data and the optically thick $J = 9-8$ line which shows a much lower brightness temperature.

The $J = 9-8$ data from the FIR peak in M17 show evidence for two components of gas with different densities. The ^{13}CO $J = 9-8$ line arises from a region with $n_{\text{H}_2} \sim 10^6 \text{ cm}^{-3}$ and beam-filling factor ~ 0.2 , while some of the ^{12}CO $J = 9-8$ radiation comes from less dense ($n_{\text{H}_2} \sim 10^4 \text{ cm}^{-3}$) gas in the remainder of the beam. The total ^{12}CO column density in the two components is $\sim 3 \times 10^{19} \text{ cm}^{-2}$. While the temperature for both components was assumed to be 50 K in the model, a component with a higher temperature, particularly toward the ionization front, is not excluded by the data.

The ^{12}CO $J = 9-8$ spectrum of W49 IRS shows two velocity components, similar to those seen in ^{13}CO $J = 1-0$. The persistence of these features over a wide range of excitation conditions makes it very unlikely that absorption by foreground gas is responsible for the double-peaked appearance of the spectra. The data are consistent with a model in which 50 K gas with $n_{\text{H}_2} \sim 2-5 \times 10^4 \text{ cm}^{-3}$ and column density $N_{\text{CO}} \sim 10^{19} \text{ cm}^{-2}$ produces the observed radiation in both velocity components. However, once again the presence of warmer gas with a lower beam-filling factor cannot be ruled out by the observations.

In all the sources for which both isotopes were observed, the data require the presence of at least two different density and/or temperature components. However, with the additional free parameters introduced by this requirement, the models are severely underconstrained, and a quantitative determination of the physical conditions in all gas components is not yet possible. Further high-resolution observations, especially at high- J values where the contribution from the cool molecular material becomes very small, are needed to establish the significance of any warmer gas which may be present.

We are grateful to the staff of the KAO for their support during the course of these observations. We thank R. Plambeck for providing us with unpublished ^{12}CO and ^{13}CO $J = 1-0$ and $2-1$ spectra, and A. Harris for useful discussions. This work was supported by NASA grant NAG 2-254.

REFERENCES

- Bally, J., & Lada, C. J. 1983, *ApJ*, 265, 824
 Betz, A., & Zmuidzinas, J. 1984, in *Proc. Airborne Astronomy Symposium (NASA CP-2353)*, 320
 Boreiko, R. T., Betz, A. L., & Zmuidzinas, J. 1990, *ApJ*, 353, 181
 Dickel, J. R., Dickel, H. R., & Wilson, W. J. 1978, *ApJ*, 223, 840
 Dickel, H. R., Dickel, J. R., Wilson, W. J., & Werner, M. W. 1980, *ApJ*, 237, 711
 Downes, D., Genzel, R., Hjalmarsen, A., Nyman, L. A., & Rönnäng, R. 1982, *ApJ*, 252, L29
 Evans N. J., II, Mundy, L. G., Davis, J. H., & Vanden Bout, P. 1987, *ApJ*, 312, 344
 Flower, D. R., & Launay, J. M. 1985, *MNRAS*, 214, 271
 Garden, R., Geballe, T. R., Gatley, I., & Nadeau, D. 1986, *MNRAS*, 220, 203
 Gatley, I., Becklin, E.E., Sellgren, K., & Werner, M. W. 1979, *ApJ*, 233, 375
 Golby, J. A., Cross, N. R., & Knight, D. J. E. 1986, *Internat. J. Infrared Millimeter Waves*, 7, 1309
 Gordon, M. A. 1987, *ApJ*, 316, 258
 Harris, A. I. 1988, *Internat. J. Infrared Millimeter Waves*, 9, 231
 Harris, A. I., Stutzki, J., Genzel, R., Lugten, J. B., Stacey, G. J., & Jaffe, D. T. 1987, *ApJ*, 322, L49
 Harvey, P. M., Campbell, M. F., & Hoffmann, W. M. 1977, *ApJ*, 211, 786
 Hayashi, M., Kobayashi, H., & Hasegawa, T. 1989, *ApJ*, 340, 298
 Jaffe, D. T., Becklin, E. E., & Hildebrand, R. H. 1984, *ApJ*, 279, L51
 Jaffe, D. T., Genzel, R., Harris, A. I., Lugten, J. B., Stacey, G. J., & Stutzki, J. 1989, *ApJ*, 344, 265
 Jaffe, D. T., Harris, A. I., & Genzel, R. 1987, *ApJ*, 316, 231
 Jaffe, D. T., Hildebrand, R. H., Keene, J., & Whitcomb, S. E. 1983, *ApJ*, 273, L89
 Krügel, E., et al. 1989, *A&A*, 211, 419
 Kutner, M. L., & Ulich, B. L. 1981, *ApJ*, 250, 341
 Langer, W. D., & Penzias, A. A. 1990, *ApJ*, 357, 477
 Linsky, J. L. 1973, *ApJS*, 25, 163
 Loren, R. B., Plambeck, R. L., Davis, J. H., & Snell, R. H. 1981, *ApJ*, 245, 495
 Mannucci, A. J. 1989, Ph.D. thesis, University of California, Berkeley
 Martin, H. M., Sanders, D. B., & Hills, R. E. 1984, *MNRAS*, 208, 35
 Miyawaki, R., Hayashi, M., & Hasegawa, T. 1986, *ApJ*, 305, 353
 Mufson, S. L., & Liszt, H. S. 1977, *ApJ*, 212, 664
 ———, 1979, *ApJ*, 232, 451
 Mundy, L. G., Evans, N. J., II, Snell, R. L., & Goldsmith, P. F. 1987, *ApJ*, 318, 392
 Mundy, L. G., Snell, R. L., Evans, N. J., II, Goldsmith, P. F., and Bally, J. 1986, *ApJ*, 306, 670
 Nolt, I. G., et al. 1987, *J. Molec. Spectrosc.*, 125, 274
 Petersen, F. R., Scalabrin, A., & Evenson, K. M. 1980, *Internat. J. Infrared Millimeter Waves*, 1, 111
 Phillips, T. G., Knapp, G. R., Huggins, P. J., Werner, M. W., Wannier, P. G., Neugebauer, G., and Ennis, D. 1981, *ApJ*, 245, 512
 Phillips, J. P., et al. 1988, *A&A*, 190, 289
 Rainey, R., et al. 1987, *A&A*, 171, 252
 Schloerb, F. P., Snell, R. L., & Schwartz, P. R. 1987, *ApJ*, 319, 426
 Schulz, A., and Krügel, E. 1987, *A&A*, 171, 297
 Scoville, N. Z., Sargent, A. I., Sanders, D. B., Claussen, M. J., Masson, C. R., Lo, K. Y., & Phillips, T. G. 1986, *ApJ*, 303, 416
 Scoville, N. Z., & Solomon, P. M. 1974, *ApJ*, 187, L67
 Snell, R. L., Mundy, L. G., Goldsmith, P. F., Evans N. J., II, & Erickson, M. R. 1984, *ApJ*, 276, 625
 Stutzki, J., & Güsten, R. 1990, *ApJ*, 356, 513
 Stutzki, J., Stacey, G. J., Genzel, R., Harris, A. I., Jaffe, D. T., & Lugten, J. B. 1988, *ApJ*, 332, 379
 Thronson, H. A., Jr., Lada, C. J., & Hewagama, T. 1985, *ApJ*, 297, 662
 White, G. J., Phillips, J. P., Richardson, K. J., & Harten, R. H. 1986, *A&A*, 159, 309
 Zmuidzinas, J., Betz, A. L., & Boreiko, R. T. 1989, *Infrared Phys.*, 29, 119

Note added in proof.—The values of intensity and T_{\star}^* quoted for the $J = 9-8$ lines should be increased by a factor of 1.25 in Table 1 and in the text. The only significant effect of this change is to increase the densities used in the models by approximately the same factor.

IONIZED CARBON IN THE LARGE MAGELLANIC CLOUD

R. T. BOREIKO AND A. L. BETZ

Space Sciences Laboratory, University of California, Berkeley, CA 94720

ABSTRACT

We have observed the $158 \mu\text{m } ^2P_{3/2}-^2P_{1/2}$ fine-structure transition of C^+ at selected locations in the Large Magellanic Cloud. The C II emission is most intense toward far-infrared continuum peaks and generally is not seen in positions exhibiting strong $\text{CO } J = 2-1$ radiation. Where both C II and CO emission are detected, the V_{LSR} centroids are similar but the C II line is wider. The differences in spatial distribution and spectral shape suggest a more pronounced physical separation between the predominantly neutral atomic and molecular gas regions than is the case in our Galaxy. In the LMC, the intense and extended C II emission near 30 Dor implies a total amount of C^+ several times greater than that of Galactic molecular cloud complexes.

We also attempted to detect the $289 \mu\text{m } J = 9-8$ transition of ^{12}CO in a few locations. The observed upper intensity limit for N159 implies that moderate density ($n > 4 \times 10^4 \text{ cm}^{-3}$) molecular gas fills less than 5% of our beam and that most of the low J CO emission comes from lower density gas.

Subject headings: galaxies: Magellanic Clouds — infrared: spectra — interstellar: matter — interstellar: molecules

1. INTRODUCTION

The $^2P_{3/2}-^2P_{1/2}$ fine-structure transition of C^+ is widespread in the interface between H II regions and molecular clouds, and is a major coolant for intermediate density, predominantly neutral gas. The $158 \mu\text{m}$ line has been observed in many galactic star-formation regions as well as in numerous galaxies. Generally, the interpretation of extragalactic data can only be done in a statistical sense, since the telescope beam averages over many molecular clouds (see Wolfire, Hollenbach, & Tielens 1989). The Magellanic Clouds present an interesting exception since they are sufficiently close for individual molecular cloud complexes to be resolved. In addition, the Magellanic Clouds have markedly different physical conditions than our Galaxy. Of particular relevance to C II emission are the higher average UV flux, lower metallicity, and higher gas-to-dust ratio.

It is only within the last few years that C II observations with a spectral resolution high enough to determine the line profiles of individual molecular clouds have become feasible. Such data facilitate comparisons with microwave spectra from molecular species and help elucidate the dynamics of photodissociation regions. In order to extend such studies to emission sources with distinctly different physical conditions than those of Galactic clouds, we observed the C II line at 0.8 km s^{-1} resolution in a number of positions in the LMC where molecular linewidths are typically $\sim 10 \text{ km s}^{-1}$. In several of these regions we also attempted to detect the $J = 9-8$ line of CO . By analogy with our Galaxy, the $J = 9-8$ transition would be expected to be strongest in warm ($T > 50 \text{ K}$), moderately dense ($n > 10^5 \text{ cm}^{-3}$) molecular material near interfaces with photodissociation regions.

2. INSTRUMENTATION AND CALIBRATION

The instrument used for the observations is a far-infrared heterodyne receiver (Betz & Zmuidzinas 1984) flown on the Kuiper Airborne Observatory at an altitude of 12.5 km. The local oscillator (LO) is an optically pumped laser, and the mixer is a GaAs Schottky diode (University of Virginia types 1T6 and 1T11) in a corner reflector mount (Zmuidzinas, Betz,

& Boreiko 1989). The system noise temperatures measured in flight were 16,600 K SSB and 7100 K SSB for the 1901 GHz C II and 1037 GHz $J = 9-8$ ^{12}CO observations, respectively. The back end analyzer for the C II data consisted of a 64 channel bank of 20 MHz filters giving 3 km s^{-1} resolution over 200 km s^{-1} and a 40 channel bank of 5 MHz filters which provides 0.8 km s^{-1} resolution over the central 32 km s^{-1} of the spectrum. For the $\text{CO } J = 9-8$ observations, an acousto-optic spectrometer with 400 independent channels of 3.2 MHz (0.9 km s^{-1}) resolution spanning 350 km s^{-1} was used.

Absolute intensity calibration is derived from spectra of the Moon for which a physical temperature of 394 K and emissivity of 0.98 are adopted (Linsky 1973). The conversion from double- to single-sideband intensities uses the relative atmospheric transmissions for the two sidebands calculated from a model atmosphere synthesis. Signal values are quoted as T^* , the antenna temperature corrected for all factors except the coupling of the source to the beam (Kutner & Ulich 1981). The net calibration uncertainty, including all systematic effects apart from the unknown distribution of source radiation, is less than 15%.

The diffraction-limited beam size of the 0.91 cm KAO telescope is $43''$ FWHM for the C II observations at $158 \mu\text{m}$ and $80''$ FWHM for the $\text{CO } J = 9-8$ line at $289 \mu\text{m}$. The absolute pointing accuracy is estimated to be $\sim 15''$. The observations used sky chopping at a frequency of 2 Hz with an amplitude of $10'$ E-W, perpendicular to the major axis of the 30 Dor-N159 complex as delineated by microwave CO and radio continuum observations. The velocity scale accuracy, limited by our knowledge of the line and LO rest frequencies and the stability of the laser LO, is $\pm 0.4 \text{ km s}^{-1}$ ($\pm 1 \sigma$).

3. OBSERVATIONS

The C II spectra were obtained on 1990 May 6 and May 8 toward 17 locations chosen to coincide with far infrared emission peaks or relatively strong $\text{CO } J = 2-1$ detections in the Large Magellanic Cloud. All but two of these locations were within the 30 Dor-N159 region, as shown in Figure 1. Several of the positions were subsequently observed in the $J = 9-8$ line

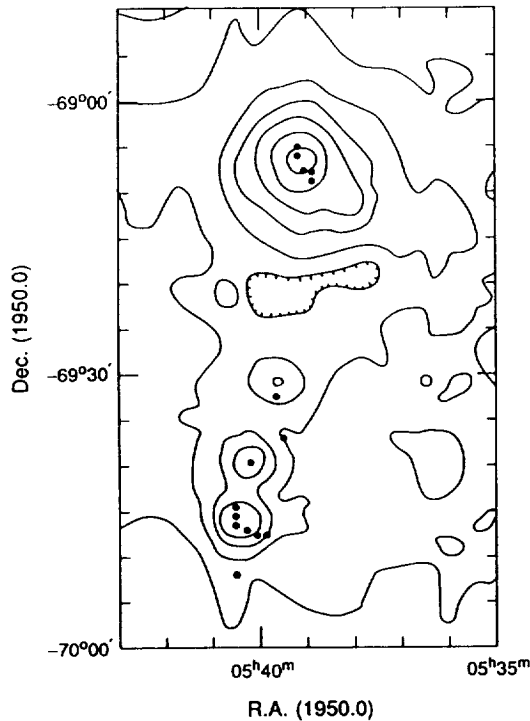


FIG. 1.—Locations of the C II observations are shown superposed on a 5 GHz radio continuum map adapted from McGee et al. (1972). Radio contours are at 0.1, 0.2, 0.5, 1.0, ... K. The dot sizes correspond to the 43'' (FWHM) beam size for the C II data.

of CO on 1991 March 2, and upper limits to the intensity of this transition were obtained. C II emission was detected in over half the locations observed. The measured peak T_r^* values, V_{LSR} , FWHM, and integrated intensities of the spectra are presented in Table 1. No significant continuum was detected in any location, consistent with the previous observations of Werner et al. (1978) and Jones et al. (1986).

The peak value of T_r^* is obtained from an average over several resolution elements near the spectral peak, and the quoted V_{LSR} is the mean velocity within this range. The uncer-

tainties in V_{LSR} and line width are estimates based on the specific appearance of the individual spectra. The velocity limits for the calculation of the C II integrated intensity are typically set to 1 FWHM on either side of line center. For the CO $J = 9-8$ data, the integration was performed over $\pm 7 \text{ km s}^{-1}$ centered on the velocity of the CO $J = 2-1$ line given by Israel et al. (1986). Attempts at fitting the observed spectral shapes to Gaussian profiles produced systematic residuals in almost all cases. In some locations the spectra suggest possible line reversals. In these cases, however, the signal-to-noise ratio is insufficient to establish the hypothesis with any certainty.

4. ANALYSIS AND INTERPRETATION

4.1. C II Observations

The C II emission arises preferentially from warm photodissociated gas in the interface between an H II region and a cooler molecular cloud. Because carbon is abundant in our Galaxy and the excitation conditions are easily met, C II emission at $158 \mu\text{m}$ is intense and widespread. The column density of C II is determined primarily by the penetration depth ($A_v \sim 4$) of carbon-ionizing photons, limited by dust absorption (Tielens & Hollenbach 1985).

The situation in the Large Magellanic Cloud differs from that in our Galaxy in several important respects. The gas-to-dust ratio in the LMC is about a factor of 4 higher (Koornneef 1984) and carbon is relatively depleted by approximately the same factor (Cohen et al. 1988). The UV extinction properties of dust differ from those in our Galaxy (Nandy 1984). The mean UV energy density is 5 times higher, and consequently the dust is generally hotter, than in the Galaxy (Lequeux 1989). In addition, molecules appear to be scarce, and molecular clouds are generally less dense but larger than Galactic clouds (Rubio et al. 1988).

The equivalent decrease in the dust and carbon abundances suggests that, to first order, the column density of C^+ in a photodissociation region should be similar in both the LMC and our Galaxy. The C II line intensities measured for a variety of locations in the LMC (Table 1) are indeed comparable to those seen in Galactic molecular clouds (Boreiko, Betz, & Zmuidzinas 1990). For example, we can calculate the C II inte-

TABLE 1
OBSERVED C II LINE PARAMETERS AND CO $J=9-8$ UPPER LIMITS*

Position	α (1950)	δ (1950)	T_r^* (K)	V_{LSR} (km s^{-1})	FWHM (km s^{-1})	I_{CII} ($10^{-4} \text{ ergs cm}^{-2} \text{ s}^{-1} \text{ sr}^{-1}$)	$I_{CO J=9-8}$ ($10^{-6} \text{ ergs cm}^{-2} \text{ s}^{-1} \text{ sr}^{-1}$)
N11B (CO)	04 ^h 56 ^m 42 ^s	-66°28'32"	1.9 (0.6)	286.4 (1.6)	8.0 (2.0)	1.0 (0.3)	...
N11B (H ₂)	04 57 10	-66 27 54	0.0 (0.6)	...
30 Dor FIR (SW)	05 38 53	-69 07 45	5.1 (0.4)	250.1 (1.6)	15.1 (1.7)	4.9 (0.4)	2.9 (3.5)
30 Dor (1'S)	05 38 53	-69 08 45	2.9 (0.6)	245.0 (1.2)	14.1 (5.0)	2.2 (0.6)	...
30 Dor R136	05 39 03	-69 07 36	0.2 (0.6)	...
30 Dor FIR (NE)	05 39 11	-69 06 00	6.3 (0.6)	247.8 (1.6)	20.5 (1.8)	7.7 (0.6)	4.6 (3.6)
30 Dor (1'N)	05 39 11	-69 05 00	5.2 (0.7)	246.8 (1.2)	13.8 (1.4)	4.0 (0.6)	...
N158 FIR	05 39 39	-69 32 25	0.1 (0.8)	...
N160A CO	05 39 30	-69 37 00	0.9 (0.9)	...
N160A FIR	05 40 12	-69 39 40	6.7 (0.6)	237.1 (1.2)	7.9 (1.4)	6.3 (0.5)	...
N159 (1'W)	05 39 52	-69 47 35	0.6 (0.5)	...
N159 FIR (SW)	05 40 04	-69 47 35	7.7 (0.9)	232.8 (0.8)	9.8 (0.9)	4.3 (0.4)	-14.2(4.0)
N159 MID	05 40 17	-69 47 02	4.6 (0.5)	234.6 (1.2)	11.4 (1.3)	3.3 (0.4)	...
N159 CO	05 40 30	-69 52 00	0.0 (0.5)	-1.5 (8.3)
N159 FIR (NE)	05 40 31	-69 46 30	5.3 (0.5)	237.8 (1.2)	12.1 (0.9)	4.8 (0.4)	4.6 (5.0)
N159 (1'N)	05 40 31	-69 45 30	4.1 (0.6)	236.4 (1.6)	8.6 (1.6)	3.0 (0.4)	...
N159 (2'N)	05 40 31	-69 44 30	0.8 (0.7)	...

* Values in parentheses represent 1σ statistical uncertainties.

grated intensity that would be observed from the Galactic giant molecular cloud complex M17, if it were at the distance of the LMC, to be $\sim 8 \times 10^{-4}$ ergs cm^{-2} sr^{-1} s^{-1} . This value is similar to those measured for several LMC locations. However, the C II map of M17 by Matsuhara et al. (1989) shows that the "extragalactic M17" would be spatially unresolved while several of the LMC cloud complexes are clearly extended. Therefore, the total amount of ionized carbon is several times greater in the large LMC complexes which we observed than in Galactic giant molecular clouds.

There is generally a good spatial correlation between FIR continuum and C II emission, as expected if the dust emission comes from a relatively dense region near an early-type star. Figure 2 shows the spectra observed at the two far-infrared emission peaks (Werner et al. 1978) which straddle the exciting source R136 in 30 Dor. This object (or compact cluster) is extremely bright with a high far-UV luminosity. The nondetection of C II in this area is not surprising, since most of the carbon is expected to be at least doubly ionized in the central region of the nebula where He II is seen. In addition, there is little far infrared or optical emission in this area, suggesting that both the gas and the dust have been largely swept away (Werner et al. 1978).

For the LMC the correlation between locations of strong C II and CO emission is poor, in distinct contrast to the situation in our Galaxy. No C II was detected at the positions in N11 and N160A where CO $J = 2-1$ has been observed (Israel et al. 1986) or in N159 where the CO $J = 1-0$ line has been mapped (Booth et al. 1989). Conversely, no CO $J = 2-1$ emission was detected from the FIR peak of N160A or in 30 Dor at our position 1' N of the NE FIR peak (Israel et al. 1986). The CO $J = 1-0$ line is, however, seen throughout the region and is particularly strong in a ridge extending south from N159 (Cohen et al. 1988). The absence of significant C II emission at the position approximately 5'5 south of N159 FIR (NE) is not unexpected. As has been suggested by several authors (e.g., Israel 1984), star formation in the 30 Doradus complex appears to be propagating southward, with the current activity most intense near N159. Until the activity extends further south, the CO in the region will remain cold, and with no newly formed OB stars, C⁺ will not be abundant.

For our Galaxy a general picture has emerged of clumpy photodissociation regions where a typical density enhancement consists of a cool molecular core, a warm molecular region emitting optically thick low J CO radiation, and a C II envelope (see, e.g., Stutzki et al. 1988). The radiation from warm CO dominates that from cold gas, and hence the locations of maximum CO and C II emission are spatially correlated. This scenario does not hold for the regions we observed in the LMC, however, most likely because of the lower dust abundance. With significantly decreased UV-shielding in the LMC, only large and dense molecular clumps can survive photodissociation. Hence, the lifetimes of neutral clumps are decreased from their equivalent Galactic values. The most probable location for coincident CO and C II radiation would therefore be the youngest star-formation region, N159. The beam filling factor of residual molecular clumps in regions with strong UV would be expected to be low, thereby leading to the small CO line intensities that are observed. Consequently, in galaxies with low dust abundance and high UV flux, most of the low- J CO emission probably comes from cold molecular gas far from the sites of star formation which produce the dominant C II radiation.

Detections of CO $J = 2-1$ (Israel et al. 1982, 1986) and of C II coincided in two of our observed locations: at the 30 Dor FIR (SW) peak and the vicinity of N159 FIR (NE), where the CO $J = 2-1$ line was strongest. Figure 3 shows a comparison between the CO and C II spectra toward N159 FIR (NE). The velocities agree very well for the two transitions, suggesting that the molecular and photodissociated gas components are dynamically linked. The CO data also show a spatially widespread component near $V_{\text{LSR}} = 295$ km s^{-1} . Our nondetection of C II at this velocity supports the conclusion of Israel et al. (1982) that this component is produced by cold clouds not associated with any H II regions.

While the agreement in V_{LSR} between CO and C II spectra is good, the line widths are clearly different, as can be seen for N159 FIR (NE) in Figure 3. The C II line is approximately 50% wider than the CO $J = 2-1$ line even though the C II was observed with a smaller beam (43" vs. 120"). This difference is real, and is widespread: as shown in Table 1, the C II line widths range from 8–20 km s^{-1} FWHM while the CO $J = 2-1$

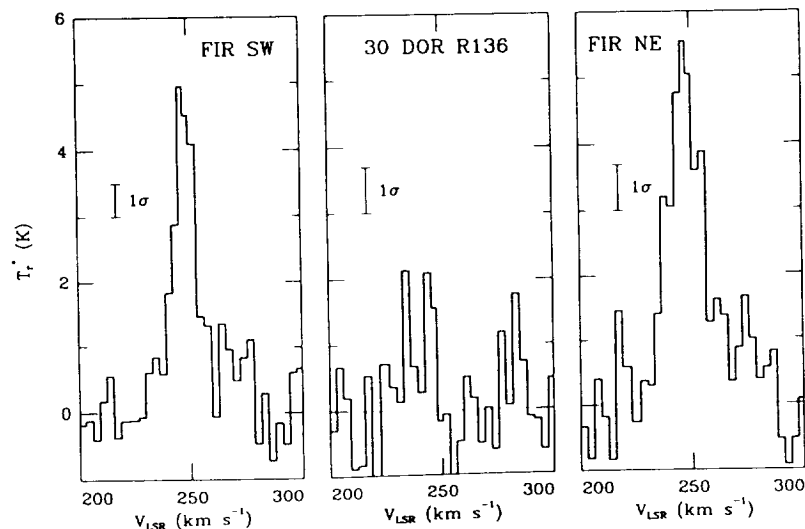


FIG. 2.—Spectra of C II at three positions in 30 Doradus. Integration times were 16 minutes for the SW FIR peak and 8 minutes for the other two locations.

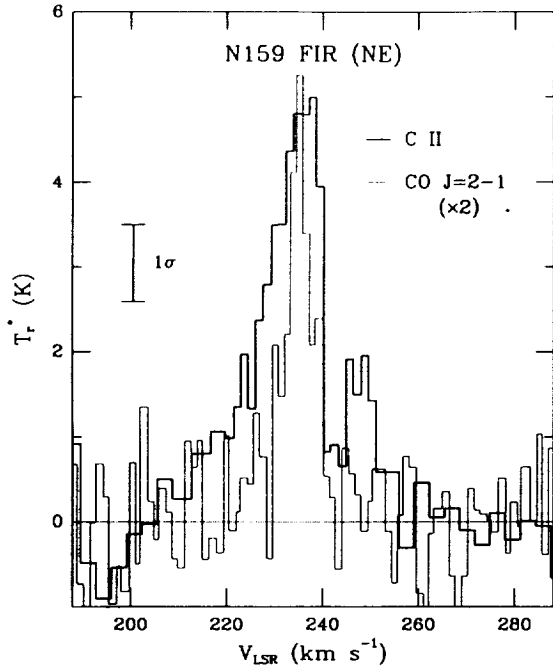


FIG. 3.—C II (heavy line) and $^{12}\text{CO } J=2-1$ (light line) spectra from the NE FIR peak of N159. Integration time for the C II spectrum was 16 minutes. The CO data, from Israel et al. (1982), have been scaled by a factor of 2.

widths are typically $5-7 \text{ km s}^{-1}$ (Israel et al. 1982, 1986). The increased C II line widths are most likely caused by heating of the gas by the UV radiation, which leads to expansion and increased turbulence. In the low-dust environment of the LMC, CO is very susceptible to photodestruction, and therefore exists preferentially deep within molecular clouds where large-scale velocity gradients are limited and conditions are generally more quiescent.

4.2. $^{12}\text{CO } J=9-8$ Observations

The mean density of the N159 molecular cloud can be estimated from the observed upper limit to the $^{12}\text{CO } J=9-8$

integrated intensity (Table 1): $T_r^* < 1.4 \text{ K}$ (2σ) for a 7 km s^{-1} (FWHM) line. Israel et al. (1982) estimated the ^{13}CO column density in this region to be $2.6 \times 10^{17} \text{ cm}^{-2}$ for an excitation temperature of 52 K (Werner et al. 1978), with a clumping factor of ~ 13 . Single-component LVG modeling as described in Boreiko & Betz (1991) shows that the $^{12}\text{CO } J=9-8$ line would have been detectable at our 2σ upper limit for mean H_2 densities greater than $8 \times 10^3 \text{ cm}^{-3}$ within the clumps, if we adopt a $^{12}\text{C}/^{13}\text{C}$ isotopic ratio of ~ 50 . Alternately, the CO $J=9-8$ data can be used to place a lower limit of 20 to the clumping factor of gas with $n_{\text{H}_2} > 4 \times 10^4 \text{ cm}^{-3}$. If there is a warmer component of molecular material (as is seen in several Galactic giant molecular clouds), then the expected intensity of the $^{12}\text{CO } J=9-8$ line will be higher, making the limits on density and beam filling factor more stringent.

The LMC results for CO can be compared with those for Galactic giant molecular clouds. Observations of the ^{12}CO and $^{13}\text{CO } J=9-8$ lines in M17, for example, (Boreiko & Betz 1991) can be explained by a two-component model with dense gas ($n \sim 10^6 \text{ cm}^{-3}$) having a clumping factor of 5 and less dense gas ($n \sim 10^4 \text{ cm}^{-3}$) filling the remainder of the beam. The LMC data are incompatible with a density distribution similar to that suggested by the M17 model even with an overall clumping factor of 13. If 20% of the molecular gas were to have $n_{\text{H}_2} > 10^5 \text{ cm}^{-3}$, then the rest of the material must have $n_{\text{H}_2} < 5 \times 10^3 \text{ cm}^{-3}$ to be consistent with our 2σ upper limit to the $J=9-8$ line intensity. However, dense gas capable of producing the $J=9-8$ line may be prevalent only near the core of the molecular cloud, as is the case in M17 (Snell et al. 1984). Its emission would consequently be considerably beam diluted and hence undetectable in the present observations. Investigations with smaller beams are required to trace the density structure within the LMC star forming regions.

We thank the staff of the KAO for their excellent support during the 1990 and 1991 Southern Skies Expeditions. This work was supported by NASA under grant NAG 2-254.

REFERENCES

- Betz, A., & Zmuidzinas, J. 1984, in Proc. Airborne Astronomy Symposium, ed. H. Thronson & E. Erickson (NASA CP-2353), 320
 Booth, R. S., et al. 1989, *A&A*, 216, 315
 Boreiko, R. T., & Betz, A. L. 1991, *ApJ*, 369, 382
 Boreiko, R. T., Betz, A. L., & Zmuidzinas, J. 1990, *ApJ*, 353, 181
 Cohen, R. S., Dame, T. M., Garay, G., Montani, J., Rubio, M., & Thaddeus, P. 1988, *ApJ*, 331, L95
 Israel, F. P. 1984, in IAU Symp. 108, Structure and Evolution of the Magellanic Clouds, ed. S. van den Bergh & K. S. Boer (Dordrecht: Reidel), 319
 Israel, F. P., de Graauw, T., Lidholm, S., van de Stadt, H., & de Vries, C. 1982, *ApJ*, 262, 100
 Israel, F. P., de Graauw, Th., van de Stadt, H., & de Vries, C. P. 1986, *ApJ*, 303, 186
 Jones, T. J., Hyland, A. R., Straw, S., Harvey, P. M., Wilking, B. A., Joy, M., Gatley, I., & Thomas, J. A. 1986, *MNRAS*, 219, 603
 Koornneef, J. 1984, in IAU Symp. 108, Structure and Evolution of the Magellanic Clouds, ed. S. van den Bergh & K. S. de Boer (Dordrecht: Reidel), 333
 Kutner, M. L., & Ulich, B. L. 1981, *ApJ*, 250, 341
 Lequeux, J. 1989, in Recent Developments of Magellanic Cloud Research, ed. K. S. de Boer, F. Spite, & G. Stasinska (Paris: Obs. Paris), 119
 Linsky, J. L. 1973, *ApJS*, 25, 163
 Matsuhara, H., et al. 1989, *ApJ*, 339, L67
 McGee, R. X., Brooks, J. W., & Batchelor, R. A. 1972, *Australian J. Phys.*, 25, 581
 Nandy, K. 1984, in IAU Symp. 108, Structure and Evolution of the Magellanic Clouds, ed. S. van den Bergh & K. S. de Boer, (Dordrecht: Reidel), 341
 Rubio, M., Garay, G., Dame, T. M., & Thaddeus, P. 1988, in Molecular Clouds in the Milky Way and External Galaxies, ed. R. L. Dickman, R. L. Snell, & J. S. Young (Berlin: Springer), 423
 Snell, R. L., Mundy, L. G., Goldsmith, P. F., Evans II, N. J., & Erickson, M. R. 1984, *ApJ*, 276, 625
 Stutzki, J., Stacey, G. J., Genzel, R., Harris, A. I., Jaffe, D. T., & Lugten, J. B. 1988, *ApJ*, 332, 379
 Tielens, A. G. G. M., & Hollenbach, D. 1985, *ApJ*, 291, 722
 Werner, M. W., Becklin, E. E., Gatley, I., Ellis, M. J., Hyland, A. R., Robinson, G., & Thomas, J. A. 1978, *MNRAS*, 184, 365
 Wolfire, M. G., Hollenbach, D., & Tielens, A. G. G. M. 1989, *ApJ*, 344, 770
 Zmuidzinas, J., Betz, A. L., & Boreiko, R. T. 1989, *Infrared Phys.*, 29, 119

HIGH RESOLUTION FAR INFRARED SPECTROSCOPY

A. L. BETZ and R. T. BOREIKO

Center for Astrophysics & Space Astronomy, University of Colorado, Boulder,
CO 80309

ABSTRACT Spectroscopic observations at far infrared wavelengths between 100 and 400 μm are restricted by the same problem confronting astronomers at all other wavelengths: the need for more photons. This limitation can be partially overcome by improving receiver efficiencies and by increasing the size of the telescope. Currently, heterodyne spectrometers in the FIR are only 1% efficient, primarily because of detector losses, and therefore much can be gained through improvements in existing systems and the introduction of new technologies. Any increase in telescope size will likely come more dearly, however, because observations at FIR wavelengths must be performed above the tropopause. The availability of a telescope like NASA's planned 2.5 m SOFIA facility will significantly enhance the detectability of sources such as external galaxies and the cores of galactic star formation regions that are unresolved by the existing 91 cm Kuiper Airborne Observatory (KAO).

I. INTRODUCTION

Ground-based observations at far-infrared wavelengths are generally impossible because of absorption by water vapor in the Earth's lower atmosphere. Consequently, airborne, balloon, or space-borne platforms above the tropopause are needed to explore this important spectral region. For the shorter FIR wavelengths ($\lambda < 180 \mu\text{m}$) spectrometers using incoherent detection with photoconductors have been quite effective. At the long wavelength end ($\lambda > 500 \mu\text{m}$) receivers using coherent detection with SIS mixers are the leading-edge technology. For the wavelengths between, where neither SIS receivers nor efficient photodetectors are currently available, coherent receivers using Schottky-diode mixers and laser local oscillators have found their spectroscopic niche. In fact the advantages of coherent detection for ultra-high resolution spectroscopy make the laser heterodyne receiver observationally effective at wavelengths as short as 100 μm .

In 1985 we built a laser heterodyne spectrometer to fill the gap in high resolution airborne instrumentation at far-infrared wavelengths. Since its debut with the detection of the C I fine structure line at 370 μm (Zmuidzinas, Betz, & Goldhaber 1986), the capabilities of the instrument have been continually improved and extended to shorter FIR wavelengths. In recent years the observational interest has concentrated on the 158 μm fine structure line of ionized carbon (C II) (e.g., Boreiko and Betz 1990) and the high-J isotopic lines ($9 \leq J \leq 22$) of CO (e.g., Boreiko and Betz 1991). The shapes of the C II line profiles observed at sub- km s^{-1} resolution help us understand the dynamics of gas in "neutral" photodissociation regions (PDR), while the high-J CO emission is an important probe of temperature and density in the cores of molecular clouds supporting star formation.

PRECEDING PAGE BLANK NOT FILMED

More generally, our observational goals with the spectrometer have been to study the energy balance, dynamics, and chemical composition of molecular clouds by detecting line radiation from species which dominate cloud chemistry. In regions of star formation, the temperature of warm dust typically lies between 30 and 100 K. Molecular hydrogen is expected to be approximately in thermal equilibrium with the dust, at least in "quiescent" sources. Densities in the cores are $> 10^4 \text{ cm}^{-3}$. Hence, adequate radiative and collisional excitation is available to support line emission at FIR wavelengths between 100-300 μm because $kT \sim hv$.

With the ultra high resolution capability of the FIR heterodyne spectrometer, we are able to completely resolve the shapes of line profiles, even for the most quiescent sources. Also because we measure the absolute LSR velocities with high accuracy, we can make detailed comparisons with millimeter-wave line data. In this way we can differentiate between the various components of gas present in complex sources. For example, our high resolution observations can distinguish shock- from UV-heated gas, which is critically important for accurate modeling of the conditions extant in star formation regions.

II. INSTRUMENT DESCRIPTION

(A) Overview

A detailed technical description of the instrument has been presented by Betz & Zmuidzinas (1984) and updated by Betz & Boreiko (1990). The spectrometer has the four basic subsystems characteristic of most heterodyne receivers:

- (1) a local oscillator (LO) (an optically-pumped FIR laser),
- (2) a mixer (a Schottky-diode in a corner-reflector mount),
- (3) an intermediate frequency (IF) amplifier and second conversion mixer, and
- (4) an IF signal processor (an acousto-optic spectrometer [AOS]).

Figure 1 illustrates the instrumental layout in schematic form. The monochromatic LO signal is generated by pumping a $10 \mu\text{m}$ vibrational line of an appropriate polar molecule that in turn emits far-infrared rotational quanta in its excited vibrational state. A CO_2 laser excited by a DC electrical discharge generates the pump energy. The signal beam collected by the telescope is combined with the LO beam and focused onto a Schottky-diode mixer. A wire-grid diplexer is used to combine the two beams with nearly 100% efficiency. The IF signal, amplified by a low-noise HEMT amplifier, is directed to a second conversion mixer at microwave frequencies and subsequently processed by an AOS signal analyzer, as shown in Figure 2.

(1) Local Oscillator

Practical considerations dictate that the LO frequency lie within about 20 GHz of the astronomical line of interest. Fortunately, the selection of optically-pumped FIR laser lines is so large that an adequate coincidence can usually (but not always) be found. The accuracy of the LSR velocity scale depends on our knowledge of the LO frequency, which can be measured by various laser/microwave hybrid techniques to about 1 part in 10^8 . The ultimate resolution capability of the spectrometer is governed by the frequency stability of the LO, and this can be as good as 1 part in 10^9 under controlled conditions. In practice, however, it is seldom necessary to exceed a resolution of 1 part in 10^6 , which corresponds to the 0.3 km s^{-1} linewidths found in the most "quiescent" sources.

(2) Mixer/Diplexer/IF Amplifier

The mixer is a 0.9- μm diameter GaAs Schottky-diode installed in our distinct variant of a corner-reflector mount (Zmuidzinas, Betz, & Boreiko 1989). The diodes are fabricated at the Semiconductor Device Laboratory of Crowe and coworkers at the University of Virginia. The mixer and IF amplifier both are cooled in a common dewar to 77 K.

Because the FIR laser frequencies are discrete and non-tunable, the passband of the IF amplifier must be matched to the difference frequency between the laser line and the spectral line of interest. It is important that the bandwidth of this IF system be as wide as possible, so that sources of disparate LSR velocities can be scheduled for the same observing session. Progress in HEMT transistor technology in recent years has dramatically aided our amplifier designs and enabled us to achieve 50% bandwidths and low noise performance ($T_N \sim 30$ K) simultaneously. As a result, without changing cooled "front-ends" we can now observe selected extragalactic and galactic sources on the same flight (e.g., C II in the LMC and galactic sources).

(3) Acousto-Optic Spectrometer

The spectral resolution in a heterodyne spectrometer is determined by the channel widths in the IF signal processor. As mentioned above, the ultimate resolution is limited only by the frequency stability of the local oscillator. In practice, however, linewidths of astronomically important lines are generally greater than 1 km s^{-1} , which corresponds to a resolution of 6 MHz at the C II line frequency of 1900 GHz (158 μm).

We use an acousto-optic spectrometer (AOS) as the IF signal analyzer, as shown in Figure 2. The AOS provides the equivalent of 400 discrete channels each of 3.2 MHz bandwidth to achieve 0.5 km s^{-1} resolution over a range of 200 km s^{-1} in the $\lambda = 150 \mu\text{m}$ region. We are currently building a second AOS with a wider bandwidth of 2000 MHz, but similarly 400 resolution elements. The two AOS analyzers, either in serial or parallel configuration, not only provide increased reliability for the spectrometer, but also give us an extended simultaneous "viewing" range of 3280 MHz that will be especially useful at the shorter infrared wavelengths ($\lambda < 120 \mu\text{m}$) we intend to emphasize in the future.

(B) System Sensitivity

For heterodyne receivers the usual expression of sensitivity is the Rayleigh-Jeans equivalent system noise temperature, T_{sys} , which is independent of bandwidth. The RMS noise level ΔT in a bandwidth B after an integration time t can be computed from T_{sys} as:

$$\Delta T = \frac{1}{\eta_c} \frac{2 T_{\text{sys}}}{(B \cdot t)^{1/2}},$$

where the factor of 2 arises from the 50% duty cycle of beamswitching. Here η_c is the net coupling efficiency between the receiver and the telescope. The noise-equivalent-power (NEP) of the receiver on the telescope can then be readily calculated from ΔT in a 1-second integration:

$$\text{NEP} = 2 k \Delta T \cdot B = \frac{1}{\eta_c} 4 k T_{\text{sys}} B^{1/2} (\text{W Hz}^{-1/2}).$$

An additional factor of 2 loss has been included in the NEP to account for the fact that we detect only one of two available polarizations. This loss is real only for unpolarized sources when we want to compare NEP's with an incoherent type detector. From the equation above, we see that an arbitrarily low (but valid) NEP can be quoted simply by assuming an arbitrarily narrow bandwidth B . For practical observations, however, the resolution need not be much narrower than 1/10 the linewidth.

For comparison purposes we can calculate our NEP at $153\ \mu\text{m}$ (the wavelength for $J=17-16$ CO) where our system noise temperature is 10,000 K (SSB). The corresponding NEP for a bandwidth of 31 MHz equal to a typical linewidth of $5\ \text{km s}^{-1}$ is $5.7 \times 10^{-15}\ \text{W Hz}^{-1/2}$. Within this interval, however, there are ~ 9 3.2-MHz resolution elements, and thus on a per-channel basis an NEP 3 times lower could be quoted. For a single detector system, our heterodyne receiver is as sensitive as a Fabry-Perot spectrometer with an NEP of $9 \times 10^{-16}\ \text{W Hz}^{-1/2}$ and a true resolution of $5\ \text{km s}^{-1}$ which would need to be scanned over the $200\ \text{km s}^{-1}$ bandwidth of our multichannel IF processor. The heterodyne receiver's chief advantage is that at wavelengths $>100\ \mu\text{m}$ this sensitivity has been achieved simultaneously with a spectral resolution (and velocity-scale accuracy) more than an order of magnitude higher than any other FIR spectrometer. Of course, if the emission lines are wide, such as from many extragalactic sources, then the resolution superiority of the heterodyne instrument is less important, unless it is necessary to avoid interfering atmospheric lines, which is often the case even at aircraft altitudes.

The system noise temperature, T_N , increases approximately linearly with frequency with a slope of about 5.5 K/GHz up to 2000 GHz. Although the sensitivity is more than adequate to do good science, it nevertheless is still about 100 times worse than the fundamental quantum limit. Since the average improvement in sensitivity is only $\sim 15\%$ per year, some alternative mixer technology will be required if we are to make any dramatic improvements.

III. RECENT OBSERVATIONS

(A) CO $J=9-8$ Line Radiation

As an example of the capabilities of heterodyne spectroscopy at FIR wavelengths, Figure 3 shows the spectra of the $J=9-8$ lines of ^{12}CO and ^{13}CO toward IRC2 in Orion/KL. The $289\ \mu\text{m}$ $J=9-8$ line shows both the broad plateau emission from the shock-heated outflow and the narrow spectral component associated with more quiescent gas, similar to what is seen in low- J ^{12}CO data. The $304\ \mu\text{m}$ ^{13}CO line, however, shows evidence only of quiescent material. The most straightforward interpretation is that the outflow emission is optically thin, and the quiescent component has an optical depth of ~ 20 in ^{12}CO , if we adopt a $^{12}\text{C}/^{13}\text{C}$ ratio near 60. Combined with CO data of both higher and lower J , the results will help pin down the excitation and abundance of CO in the various dynamical components.

Note that only a modest detection of the ^{13}CO line is needed to establish the ^{12}CO optical depth, and that even in the $J=9-8$ line, significant emission can be expected from relatively cool material ($T \sim 50\ \text{K}$) if the line is optically thick. To unambiguously detect the hotter gas thought to be a significant component of photodissociation regions, we must look for CO lines with $J \geq 11$.

(B) CO J=12-11 and J=14-13 Line Radiation

In August 1991, we observed the J=12-11 and J=14-13 rotational lines of ^{12}CO in W3, M17, W51, DR 21, and W49. We had previously observed the ^{12}CO J=9-8 line in all these sources and the ^{13}CO J=9-8 line in all but W49 (Boreiko & Betz 1991). The higher-J linewidths are typical of those seen in lower-J transitions, and identify the emission as emanating from gas which is not likely shock excited, and therefore presumably the photodissociation component. For W51 our J=14-13 and J=12-11 spectra showed similarly narrow lines, about 10 km s^{-1} (FWHM). No evidence was seen for a broad component of 70 km s^{-1} linewidth in W51 IRS 2 or 90 km s^{-1} linewidth in W51 Main, as reported by Jaffe *et al.* (1987) from Fabry-Perot observations of the J=16-15 transition. The discrepancy is significant, because of the inference of shock activity that broad profiles suggest.

For the 5 sources we observe, the (J=14-13)/(J=12-11) line intensity ratios indicate excitation temperatures $\geq 150\text{ K}$. The lower limit applies to LTE excitation, which is most likely not the case for high-J CO in these sources. Detailed statistical equilibrium calculations are in progress to define the excitation temperature and density of the gas more accurately. Regardless, the temperatures indicated are consistent with the values of 200-300 K predicted for the PDR component by Tielens & Hollenbach (1985). It would be very helpful to have additional data on the weaker ^{13}CO lines in order to estimate column densities of hot gas and to pin down the ^{12}CO optical depths. Supporting observations of this type are planned so that sufficient constraints will be in place to make a definitive interpretation of the data.

IV. DEVELOPMENTS

Recently we have started to evaluate BIB-type photoconductive detectors as high sensitivity heterodyne mixers in the 50-150 μm wavelength region. These photomixers offer the promise of quantum-limited performance with sensitivities initially 10 times better than the best possible with Schottky diodes at 150 μm . Of course this is just speculation until the initial tests have been completed, but the technology is encouraging. Especially significant is the possibility of integrating planar BIB mixers into linear and two dimensional arrays. The capability of line imaging at spectral resolutions exceeding 1 part in 10^6 would be an important breakthrough in receiver technology particularly appropriate for space-based FIR spectrometers.

Another way to get bigger signals is to use a bigger telescope. The dense cores of interest here are usually smaller than the diffraction-limited beam size of the KAO (e.g., 44" at $\lambda = 158\mu\text{m}$). A larger telescope, namely the 2.5 m SOFIA project now under study by NASA, could boost signal levels up to a factor of 10 over the KAO for such unresolved sources. Observations with 10" resolution could be readily compared with millimeter-wave interferometer data of similar spatial acuity. Another important point is that SOFIA would be particularly valuable for spatially resolved observations of FIR line spectra from external galaxies.

This work was supported by NASA under grants NAG2-254 and NAG2-753.

REFERENCES

- Betz, A., & Boreiko, R. T. 1990, in *Proc. 29th Liège International Astrophysical Colloquium: From Ground-Based to Space-Borne Sub-mm Astronomy*, 3-5 July 1990, ESA SP-314, 205
- Betz, A., & Zmuidzinas, J. 1984, in *Proc. Airborne Astronomy Symposium*, 11-13 July 1984, NASA CP-2353, 320
- Boreiko, R. T., & Betz, A. L. 1990, *ApJ*, 353, 181
Boreiko, R. T., & Betz, A. L. 1991, *ApJ*, 369, 382
- Jaffe, D. T., Harris, A. I., & Genzel, R. 1987, *ApJ*, 316, 231
- Tielens, A. G. G. M., & Hollenbach, D. 1985, *ApJ*, 291, 722
- Zmuidzinas, J., Betz, A. L., & Boreiko, R. T. 1989, *Infrared Phys*, 29, 119
- Zmuidzinas, J., Betz, A. L., & Goldhaber, D. M. 1986, *ApJ*, 307, L75

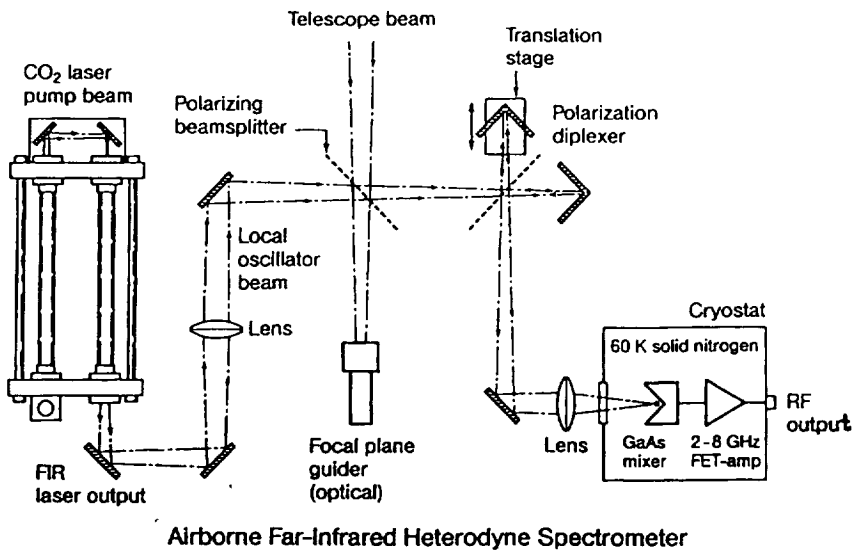


Figure 1

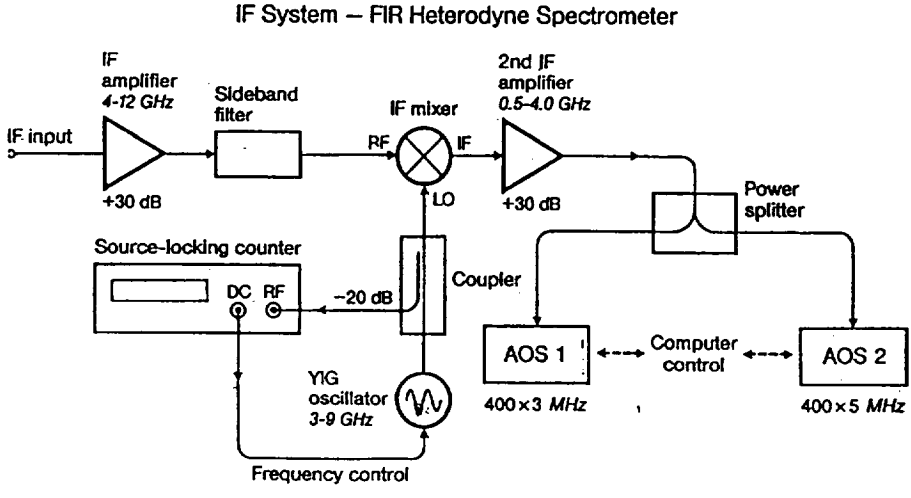


Figure 2

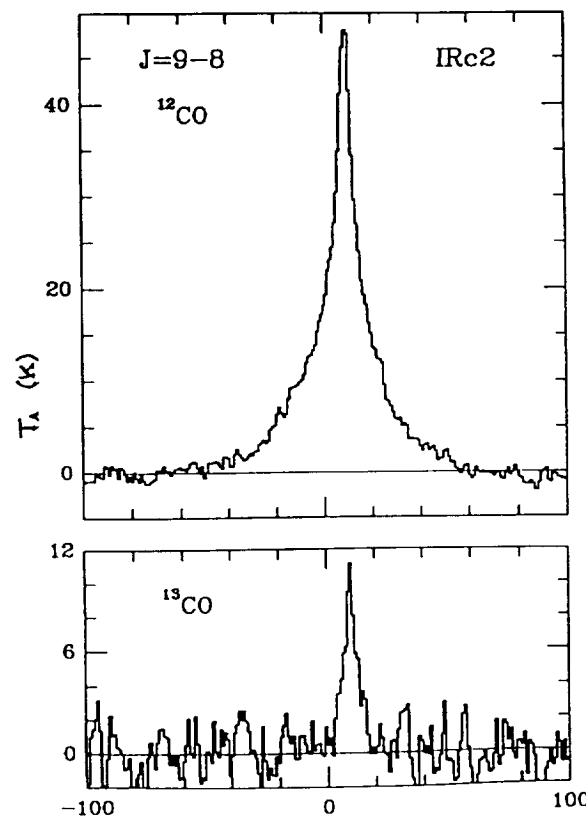


Figure 3

A SEARCH FOR THE ROTATIONAL TRANSITIONS OF H_2D^+ AT 1370 GHz AND H_3O^+ AT 985 GHz

R. T. BOREIKO AND A. L. BETZ

Center for Astrophysics and Space Astronomy, University of Colorado, Boulder, CO 80309

Received 1992 November 6; accepted 1992 December 14

ABSTRACT

We have searched for the 1370 GHz lowest rotational transition of the molecular ion H_2D^+ in NGC 2264, W3, and the IRc2 region of M42. No emission lines were seen from any source, but an absorption feature was detected toward IRc2. If we identify the line as the $1_{01}-0_{00}$ transition of para H_2D^+ , then the total column density is $(6 \pm 3) \times 10^{13} \text{ cm}^{-2}$ for $T \sim 30 \text{ K}$, and the fractional abundance is 3×10^{-11} . The LSR velocity of 3.7 km s^{-1} and the measured line width of 13 km s^{-1} are consistent with the dynamical parameters of the hot core source. However, the physical parameters deduced from the data ($T < 50 \text{ K}$, $n_{\text{H}_2} < 10^6 \text{ cm}^{-3}$, spatial extent $> 25''$) differ from those derived from millimeter-wave observations of the hot core condensation. Our interpretation suggests that significant amounts of low-density gas are associated with this region and that the material is cold enough for enhanced deuterium fractionation to occur. A search was also made for the 985 GHz transition of ortho H_3O^+ in W3 and IRc2 with negative results.

Subject headings: infrared: interstellar: lines — ISM: molecules — ISM: individual: M42

1. INTRODUCTION

The molecular ion H_3^+ is a key species in ion-molecule theories of gas-phase chemistry (Herbst & Klemperer 1973), and therefore measurement of its abundance in molecular clouds represents a valuable test of these theories. The symmetry of the ion precludes permitted rotational transitions; consequently, searches for interstellar H_3^+ have concentrated on the near-infrared rotation-vibration lines which may be detectable in absorption against stellar continua. The observations thus far have provided only upper limits of $\sim 10^{15} \text{ cm}^{-2}$ to the column density of H_3^+ in molecular clouds (Geballe & Oka 1989; Black et al. 1990).

The deuterated form, H_2D^+ , has permitted rotational transitions which may be observable in either emission or absorption. As well as being a tracer for the H_3^+ ion, H_2D^+ is also of intrinsic interest because of its important role in the production of other deuterated species, especially at low temperatures (Millar, Bennett, & Herbst 1989). A tentative detection of the $1_{10}-1_{11}$ transition at 372 GHz was reported by Phillips et al. (1985) in NGC 2264. The result implied an $\text{H}_2\text{D}^+/\text{H}_2$ ratio of $\sim 10^{-10}$ in LTE, within the range expected from ion-molecule chemistry theories. Later observations by Pagani et al. (1992b), however, failed to detect the line at approximately the reported level, and a more sensitive ground-based search by van Dishoeck et al. (1992) set an upper limit to the 372 GHz line intensity in NGC 2264 that was a factor of 2.5 lower. Similar upper limits were determined for several other sources, yielding fractional abundances for H_2D^+ less than a few times 10^{-11} , close to the lower limits expected from ion-molecule chemistry theories.

H_2D^+ is predicted to be most abundant in cold regions ($T < 50 \text{ K}$) where deuterium fractionation is enhanced (Millar et al. 1989). According to the chemical model of Pagani et al. (1992a), the para species is more abundant than the ortho for temperatures between ~ 12 and 40 K . Therefore searches for the 1370 GHz $1_{01}-0_{00}$ para transition appear to be a promising approach for detecting H_2D^+ in the interstellar medium.

An attempt was also made to detect the 985 GHz $0_0^- - 1_0^+$ transition of H_3O^+ .

2. INSTRUMENTATION AND CALIBRATION

The observations of the $1_{01}-0_{00}$ transition of para H_2D^+ and the $0_0^- - 1_0^+$ transition of ortho H_3O^+ were done with a laser heterodyne spectrometer (Betz & Zmuidzinas 1984) flown aboard the NASA Kuiper Airborne Observatory. The local oscillator (LO) for the 1370.0853 GHz line of H_2D^+ (K. Evenson, private communication) was the 1362.4435 GHz transition in $^{13}\text{CH}_3\text{OH}$ discovered in a laboratory search for LO candidates. The LO frequency was measured relative to the strong 1397.1186 GHz line of CH_2F_2 (Inguscio et al. 1986) oscillating in a second laser system. The uncertainty in our LO frequency measurement is estimated to be 1.0 MHz while the long-term stability is better than 2 MHz. For the observations of H_3O^+ at 984.680 GHz, the laser was the 976.5437 GHz transition of $^{13}\text{CH}_2\text{F}_2$ (Inguscio et al. 1986). The V_{LSR} scale accuracy is $\pm 0.5 \text{ km s}^{-1}$. The mixers were GaAs Schottky diodes (University of Virginia types 1T11 and 1T6 for the H_2D^+ and H_3O^+ observations, respectively) in corner-reflector mounts (Zmuidzinas, Betz, & Boreiko 1989) cooled to 77 K. Noise temperatures measured during the flights were 9600 K (SSB) at 1370 GHz and 9800 K (SSB) at 985 GHz. For the first H_2D^+ flight and the H_3O^+ flight, the back end consisted of a 40 channel filterbank with 5 MHz resolution. For the second H_2D^+ flight, an acousto-optic spectrometer (AOS) with 400 independent resolution elements of 3.2 MHz (0.7 km s^{-1}) was used.

The diffraction-limited beam sizes were $60''$ and $84''$ at 1370 and 985 GHz, respectively. Pointing accuracy was better than $15''$ for both observations. Beam switching was performed at 4 Hz with an $8'-10'$ throw oriented NE-SW. Double-sideband calibration was obtained from spectra of the Moon, for which a physical temperature of 394 K and an emissivity of 0.98 were assumed (Linsky 1973). The single-sideband intensity was then obtained from the differential transmission in the two side-

bands derived from an atmospheric synthesis. The accuracy of the intensity calibration for an extended source is estimated to be $\pm 15\%$ for H_2D^+ and $\pm 20\%$ for H_3O^+ .

3. OBSERVATIONS

Spectra of the 1370 GHz $1_{01}-0_{00}$ rotational transition of para H_2D^+ were obtained on 1990 December 5 toward 3 sources: NGC 2264 IRS 1, W3 IRS 5, and IRc2 in Orion. Due to the relatively high dipole moment of 0.6 D for H_2D^+ , the density required to maintain an approximately thermal population in the upper state is greater than 10^8 cm^{-3} . Consequently, the $1_{01}-0_{00}$ line is expected to be difficult to observe in emission, particularly since H_2D^+ is believed to be absent in dense regions. For this transition, a detection in absorption against a strong continuum seems more feasible, and therefore the IRc2 region of Orion was selected as the most likely target. Although no 1370 GHz emission was seen in any source, a promising absorption feature was found in the IRc2 spectrum during the initial flight in 1990 December. This prompted a subsequent observation on 1991 February 21. The combined spectrum is shown in Figure 1.

A search was also made for the 985 GHz $0_0^- - 1_0^+$ transition of the hydronium ion H_3O^+ in W3 and IRc2 on 1990 December 4. The 1_0^+ state is the lowest energy level for ortho H_3O^+ and lies $\sim 8 \text{ K}$ above the lowest para state. No significant emission was seen. Integrated intensities deduced from all the spectra are presented in Table 1.

4. ANALYSIS AND INTERPRETATION

Generally detections of at least two transitions are required to confirm the existence of a new molecule, and therefore the identification of the 1370 GHz line as the $1_{01}-0_{00}$ transition of H_2D^+ cannot be made unambiguously. However, the line was observed on two flights separated by almost 3 months, so that the velocity of the source relative to Earth differed by $\sim 30 \text{ km s}^{-1}$. The absorption appeared at the same V_{LSR} (to within statistical uncertainties) in both sets of data, and thus it is estab-

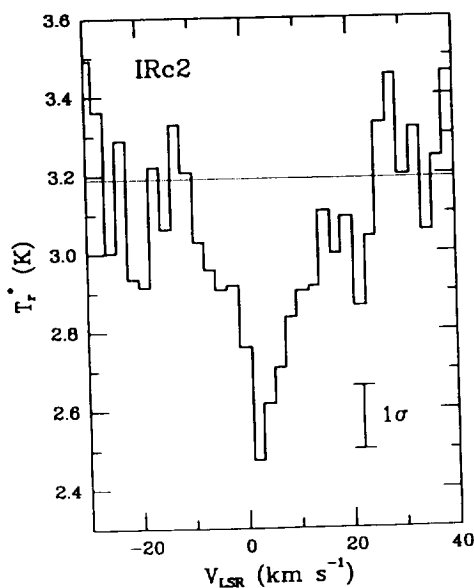


FIG. 1.—IRc2 spectrum at the H_2D^+ frequency from combined AOS and filterbank data at 10 MHz resolution. The 1σ uncertainty applies only to the line; that for the continuum is $\sim 40\%$ larger because of the restricted bandwidth of the filterbank.

TABLE 1
INTEGRATED INTENSITIES*

Source	V_{LSR} range (km s^{-1})	H_2D^+	H_3O^+
M42 IRc2	5 ± 20	$-1.8 (0.4)$	$-1.1 (0.5)$
W3 IRS 5	-40 ± 10	$-0.2 (0.4)$	$0.9 (0.3)$
NGC 2264 IRS 1	7 ± 5	$-0.1 (0.2)$...

* In units of $10^{-5} \text{ ergs cm}^{-2} \text{ s}^{-1} \text{ sr}^{-1}$. Values in parentheses represent 1σ statistical uncertainties.

lished that the feature is at the H_2D^+ frequency rather than in the image sideband. The absorption is statistically significant, and its depth agrees well for both observations. Therefore we believe that the line is a real feature in the IRc2 spectrum. Confusion in the greater than 1000 GHz range is generally not a problem since the line density is much lower than at millimeter wavelengths. Thus, the absorption is most likely due to H_2D^+ , barring an unfortunate (and somewhat unlikely) frequency coincidence with a line from some other light species. The following analysis is based on the assumption that this is the case.

The absorption line shown in Figure 1 can be characterized by a Gaussian shape with an amplitude of $-0.51 \pm 0.13 \text{ K}$, an LSR velocity of $3.7 \pm 1.6 \text{ km s}^{-1}$, and a full width at half-maximum of $13 \pm 4 \text{ km s}^{-1}$. The BN-KL/IRc2 region of Orion is very complicated, with several components of both quiescent and outflowing or shocked gas, as summarized in the review by Genzel & Stutzki (1989). Comparison of the observed line parameters with those characterizing the various gas components suggests that material associated with the hot core is the most likely source of the absorption, with perhaps some contribution from the low-velocity outflow.

It is useful to compare the line profile with that seen from a ground-state transition of another species with comparable excitation (temperature and density) requirements. The H_2D^+ line appears quite similar to an absorption component of the lowest rotational transition of OH at 2514 GHz (Betz & Boreiko 1989), given the rather low signal-to-noise ratios of the data. The absence of any emission component in the H_2D^+ is explained by the high critical density of the transition. One notable feature of the OH data is that material at the hot core velocity absorbs the entire continuum in a $33''$ beam, even though what is usually called the hot core is itself much smaller. Therefore there clearly exists a considerable amount of low-excitation material that is associated with the hot core but is spatially more extended. It is this material that is likely responsible for most of the H_2D^+ feature. A minimum size for the absorbing region can be calculated from the depth of the absorption. If we assume that the continuum fills the beam, then to produce the observed $\sim 16\%$ decrease in intensity would require an optically thick source region of at least $\sim 24''$ in diameter, considerably larger than the hot core as observed in excited NH_3 or HDO emission, for example (Morris, Palmer, & Zuckerman 1980; Plambeck & Wright 1987). Both these latter lines require high densities ($n > 10^6 \text{ cm}^{-3}$) to be excited.

The minimum optical depth (assuming that the source region fills the beam) of the absorption line shown in Figure 1 is 0.16 ± 0.04 at line center, and the integrated intensity is $(-1.8 \pm 0.4) \times 10^{-5} \text{ ergs cm}^{-2} \text{ sr}^{-1} \text{ s}^{-1}$. This corresponds to a minimum column density $N_0 = (4.4 \pm 0.9) \times 10^{13} \text{ cm}^{-2}$ for H_2D^+ in the 0_{00} state.

Submillimeter observations of the I_{10-11} ortho transition of H₂D⁺ in IRC2 at 372 GHz show a possible feature with $V_{LSR} = 0-5 \text{ km s}^{-1}$, $\Delta v(\text{FWHM}) = 5-15 \text{ km s}^{-1}$, and $T_r^* \sim 0.5 \text{ K}$ (E. van Dishoeck, private communication). The excitation model of Black et al. (1990) and van Dishoeck et al. (1992) then can be used to calculate ranges of temperature and density which could produce the lines (assuming that they both are real). The data are consistent with $T_{ex} \sim 30-50 \text{ K}$, $n \sim 10^6 \text{ cm}^{-3}$, and $N(\text{H}_2\text{D}^+) \sim (6 \pm 3) \times 10^{13} \text{ cm}^{-2}$, although higher temperatures and lower densities are not excluded. However, conditions deduced from hot core emission lines ($T \sim 150 \text{ K}$, $n \sim 10^7 \text{ cm}^{-3}$) would produce a much stronger 372 GHz line than observed, for the same 1370 GHz absorption. If the 372 GHz feature is not real (or not H₂D⁺), then the densities and temperatures deduced from the excitation calculation are upper limits: $n < 10^6 \text{ cm}^{-3}$ at 40 K, and $T < 100 \text{ K}$ for $n > 5 \times 10^4 \text{ cm}^{-3}$. It will be difficult to obtain a better constraint from the ortho transition, since observations of Orion near 372 GHz are already badly confused limited at the few-tenths K level (E. van Dishoeck, private communication).

The H₂ column density in the hot core is estimated to be $\sim 2 \times 10^{24} \text{ cm}^{-2}$ (Masson et al. 1985; Wright & Vogel 1985), and therefore the H₂D⁺ fractional abundance is $\sim 3 \times 10^{-11}$. This value is consistent with the predictions of chemical models for $T \sim 30-50 \text{ K}$, but is high for warmer regions (Millar et al. 1989; Pagani et al. 1992a).

The column density of H₃⁺ can be estimated using the theoretical H₂D⁺/H₃⁺ ratios from Pagani et al. (1992a) to be $8 \times 10^{15} \text{ cm}^{-2} - 3 \times 10^{17} \text{ cm}^{-2}$ for temperatures 30-50 K, corresponding to fractional abundances relative to H₂ of $4 \times 10^{-9} - 1.5 \times 10^{-7}$. An even lower estimate for H₃⁺ would be possible if the absorbing gas is $\sim 20 \text{ K}$, the temperature that maximizes the abundance of para H₂D⁺. An upper limit of 5×10^{-9} to the H₃⁺ fractional abundance in the line of sight to BN has been placed by Geballe & Oka (1989). Therefore, unless the chemistry in the hot core region is significantly different than that toward BN, the temperature of the gas containing H₂D⁺ must be low, $\leq 40 \text{ K}$. In any case, H₃⁺ ought to be directly observable in absorption toward IRC2, for most of the range of column densities consistent with the H₂D⁺ data, provided that the absorbing gas is directly in the line of sight to the more compact IRC2 continuum source at 4 μm . Such a measurement would be the best way either to confirm the tentative detection of H₂D⁺ presented here, or if inconclusive, to place stronger constraints on the temperature of the absorbing material.

Limits on the H₃⁺ abundance can also be placed from DCO⁺ and N₂H⁺ observations, as discussed by van Dishoeck et al. (1992). An upper limit to the DCO⁺ $J = 3-2$ and $J = 5-4$ lines is 1 K (E. van Dishoeck, private communication) while the $J = 3-2$ HC¹⁸O⁺ line has $T_r^* \sim 1 \text{ K}$ (Blake et al. 1986). Therefore $[\text{DCO}^+]/[\text{HCO}^+] \leq 0.002$ for $[^{16}\text{O}]/[^{18}\text{O}] = 500$. The resulting H₃⁺ column density is $< 1 \times 10^{16} \text{ cm}^{-2}$, which corresponds to a fractional H₃⁺ abundance of $< 5 \times 10^{-9}$. This value agrees with that derived above from theoretical H₂D⁺/H₃⁺ ratios only for $T \leq 40 \text{ K}$. As discussed by Herbst

(1982), the kinetic temperature derived from the $[\text{DCO}^+]/[\text{HCO}^+]$ ratio under conditions of chemical equilibrium for Orion is low, $\sim 33 \text{ K}$, in agreement with the limit obtained from the H₂D⁺ data.

Finally, the $J = 4-3$ line of N₂H⁺ has been observed to have $T_r^* \sim 0.5-1.5 \text{ K}$ and $\Delta v(\text{FWHM}) \sim 5-15 \text{ km s}^{-1}$ (E. van Dishoeck, private communication), which leads to an inferred column density of $5 \times 10^{12} \text{ cm}^{-2} - 3 \times 10^{13} \text{ cm}^{-2}$. The fractional abundance of N₂H⁺, $3 \times 10^{-12} - 2 \times 10^{-11}$, is also a lower limit to the fractional abundance of H₃⁺. The much higher H₃⁺ abundances derived above would then imply that most of the nitrogen in the IRC2 region is in forms other than N₂.

In summary, the data are consistent with an H₂D⁺ column density of $(6 \pm 3) \times 10^{13} \text{ cm}^{-2}$. A low temperature, $T < 40 \text{ K}$, is implied for the line-forming region both from the relative intensities of the 372 and 1370 GHz lines and from indirect arguments on upper limits to H₃⁺ column density. The density of the absorbing gas is less than 10^6 cm^{-3} , and its spatial extent is at least 25". The velocity and line width of the absorption strongly suggest an association with the hot core source, even though conditions derived from emission-line observations of this multicomponent cloud are incompatible with those deduced here from absorption-line data. Time-dependent chemistry is not a plausible mechanism for enhancing the H₂D⁺ abundance because the $[\text{H}_2\text{D}^+]/[\text{H}_3^+]$ ratio is very quickly equilibrated (Millar et al. 1989). Thus we are led to speculate that there may be a significant amount of colder, less dense gas associated with the hot core which can be seen most easily in absorption.

For NGC 2264 IRS 1 the integrated intensity of the H₂D⁺ line (see Table 1) gives a 2σ upper limit of $T_r^* = 0.3 \text{ K}$ for a 3.8 km s⁻¹ wide line. At 30 K and LTE, this requires that $N(\text{H}_2\text{D}^+) < 7 \times 10^{12} \text{ cm}^{-2}$. However, densities in NGC 2264 are much lower than those required to thermalize the transition, and therefore the nondetection is consistent with the limits determined by van Dishoeck et al. (1992) from the nondetection of the 372 GHz line, without providing any further constraints to the model.

Similarly, the H₃O⁺ nondetections are attributable to sub-thermal excitation: the critical density of the $0_0^- - 1_0^+$ line is greater than 10^9 cm^{-3} (Phillips, van Dishoeck, & Keene 1992). The $\pm 2\sigma$ limits to this line, calculated from the integrated intensities of Table 1, are $-2.1 \text{ K} \leq T_r^* \leq -0.1 \text{ K}$ for a 10 km s⁻¹ wide line in Orion and $0.5 \text{ K} \leq T_r^* \leq 2.5 \text{ K}$ for a 6 km s⁻¹ wide line in W3 IRS 5. These limits are consistent with values expected from the column densities and excitations derived by Phillips et al. (1992) from observations of higher transitions of H₃O⁺.

We are grateful to E. van Dishoeck for providing us with copies of her unpublished data on the 372 GHz H₂D⁺ line and the DCO⁺ and N₂H⁺ results, and for valuable discussions. We thank the staff of the KAO for providing their usual excellent support for the flights. This work was supported by NASA under grants NAG 2-254 and NAG 2-753.

REFERENCES

- Betz, A., & Zmuidzinas, J. 1984, in Proc. Airborne Astronomy Symposium (NASA CP-2353), 320
 Betz, A. L., & Boreiko, R. T. 1989, ApJ, 346, L101
 Black, J. H., van Dishoeck, E. F., Willner, S. P., & Woods, R. C. 1990, ApJ, 358, 459
 Blake, G. A., Sutton, E. C., Masson, C. R., & Phillips, T. G. 1986, ApJS, 60, 357
 Geballe, T. R., & Oka, T. 1989, ApJ, 342, 855
 Genzel, R., & Stutzki, J. 1989, ARA&A, 27, 41
 Herbst, E. 1982, A&A, 111, 76
 Herbst, E., & Klemperer, W. 1973, ApJ, 185, 505
 Inguscio, M., Moruzzi, G., Evenson, K. M., & Jennings, D. A. 1986, J. Appl. Phys., 60, R161

- Linsky, J. L. 1973, ApJS, 25, 163
Masson, C. R., Claussen, M. J., Lo, K. Y., Moffet, A. T., Phillips, T. G., Sargent, A. I., Scott, S. L., & Scoville, N. Z. 1985, ApJ, 295, L47
Millar, T. J., Bennett, A., & Herbst, E. 1989, ApJ, 340, 906
Morris, M., Palmer, P., & Zuckerman, B. 1980, ApJ, 237, 1
Pagani, L., Salez, M., & Wannier, P. G. 1992a, A&A, 258, 479
Pagani, L., et al. 1992b, A&A, 258, 472
Phillips, T. G., Blake, G. A., Keene, J., Woods, R. C., & Churchwell, E. 1985, ApJ, 294, L45
Phillips, T. G., van Dishoeck, E. F., & Keene, J. 1992, ApJ, 399, 533
Plambeck, R. L., & Wright, M. C. H. 1987, ApJ, 317, L101
van Dishoeck, E. F., Phillips, T. G., Keene, J., & Blake, G. A. 1992, A&A, 261, L13
Wright, M. C. H., & Vogel, S. N. 1985, ApJ, 297, L11
Zmuidzinas, J., Betz, A. L., & Boreiko, R. T. 1989, Infrared Phys., 29, 119

